Immobilising biomolecules on amyloid fibrils for biotechnology applications

Thesis submitted in partial fulfilment of the requirements for the degree of

Doctor of Philosophy

at the

University of Canterbury

by

Jared Kenneth Raynes

2012

in memory of my grandfather John Stuart Wilson
who taught me to seek and understand, rather than
be told...

Acknowledgements

First and foremost I must thank my supervisor Juliet Gerrard, your unwavering support, patience, friendship and enthusiasm has enabled me to finish this thesis. I could not ask for more from a supervisor. To Grant, thank you for everything that you have taught me, I am a better scientist because of you. To Susie, thank you for your fantastic support, listening to my problems, and for motivation.

Thanks must go to everyone in the school of biological sciences who helped me during my PhD. In particular, Selwyn, Matt, Dave, Manfred, Arvind and Ashley.

To all past and present members of the purple bubble, thank you for your friendship and help. Particular thanks must go to Andy, Shaggy, and Sophie for the fantastic science you taught me, and the fun that was had outside of university. Coffee breaks have never been the same since you three left. I am extremely grateful to Jackie for the fantastic laboratory support, the many TEM images, and of course for your company.

Laura, I cannot imagine the last four years without your friendship and encouragement. Thank you for making university a fun place to be, and of course, thank you for the many, many, fun times had outside of university.

Moritz, thank you for choosing New Zealand to study so that we got to become great friends. To all of my other friends, thank you for your support, love, and understanding why we have not seen enough of each other, this will change now.

To Rachel, thank you for your love, support, and understanding. You have been incredible, the last three years, the best of my life.

To mum, dad, grandma, and Tiana, I know it has been a long process, but thank you for your love and unparalleled support. Emerson, thank you for being the best cousin and friend anyone could ask for. To Jackie, Paul, and Ollie, thank you for everything.

Table of contents

Abbreviations

Å	Ångström
AFM	atomic force microscopy
amp	ampilcillin
APTS	3-aminopropyltriethoxysilane
Bis-tris	2-[Bis-(2-hydroxyethyl)-amino]-2-hydroxymethyl-propane-1,3 diol
bp	base pair
BSA	bovine serum albumin
°C	degrees Celsius
cam	chloramphenicol
CD	circular dichroism
CLSM	confocal laser scanning microscopy
cm	centimetre
CPR	cytochrome P450 reductase
cryo-EM	cryo-electron microscopy
CR	Congo red
$CYP450_{BM3}$	cytochrome P450 from *Bacillus megaterium*
d	derivative
Da	Daltons
DHDPR	dihydrodipicilonate reductase
DHDPS	dihydrodipicilonate synthase
dH_2O	distilled water
DNA	deoxyribonucleic acid
DSC	*N,N'* – disuccinimidyl carbonate
DSF	differential scanning fluorimetry
DTT	dithiothreitol
ε	extinction coefficient
E. coli	*Escherichia coli*
EDC	1-ethyl-3-(3-dimethylaminopropyl) carbodiimide
EDTA	ethylenediaminetetraacetic acid
eGFP	enhanced green fluorescent protein
EtOH	ethanol

FAD	flavin adenine dinucleotide
FITC	fluorescein isothiocyanate
FMN	flavin mononucleotide
FRET	fluorescence resonance energy transfer
FTIR	Fourier transform infrared spectroscopy
g	gram
GA	glutaraldehyde
GFP	green fluorescent protein
GOD	glucose oxidase
GST	glutathione S-transferase
H_2O	water
HCl	hydrochloric acid
HEPES	N-2-hydroxyethlpiperazine-N'-2-ethane sulphonic acid
His	histidine
HRP	horseradish peroxidase
kan	kanamycin
k_{cat}	catalytic constant
kDa	kiloDalton
K_m	Michaelis-Menton constant
kV	kilovolts
L	litre
LB	Luria-Bertani
M	molar
MBP	maltose-binding protein
MeOH	methanol
µg	microgram
µL	microlitre
mg	milligram
mg/mL	milligram-per-millilitre
min	minute
mL	millilitre
mm	millimetre
mM	millimolar
MOPS	3-(N-morpholino) propanesulfonic acid
M_w	molecular weight

MWCO	molecular weight cut-off
ng	nanogram
nm	nanometre
$NADP^+$	nicotamide adenine dinucleotide phosphate
NADPH	nicotamide adenine dinucleotide phosphate, reduced form
NHS	N-Hydroxysuccinimide
OP	organophosphates
OPH	organophosphate hydrolase
P450	cytochrome P450
$P450_{BM3}$	cytochrome P450 102A1 from *Bacillus megaterium*
PAGE	polyacrylamide gel electrophoresis
PCR	polymerase chain reaction
PDB	protein data bank
PRX3	human peroxiredoxin three
PVOH	poly (vinyl alcohol)
QCM	quartz crystal microbalance
®	registered trademark
RFU	relative fluorescence units
rpm	revolutions per minute
SDS	sodium dodecyl sulfate
sec	second
SEM	scanning electron microscopy
SOB	super optimal broth
SOC	super optimal broth with glucose added
SPR	surface plasmon resonance
ssNMR	solid state nuclear magnetic resonance
SWNT	single walled carbon nanotubes
T	temperature
TAE	tris-acetate-EDTA
TEM	transmission electron microscopy
TEV	tobacco etch virus
TFE	trifluoroethanol
ThT	thioflavin T
TIM	triosephosphate isomerase
T_m	melting temperature

™	trademark
tris	2-Amino-2-hydroxymethyl-propane-1,3-diol
TTR	transthyretin
U	unit
U/g	unit-per-gram
UV	ultraviolet
V	volts
vis	visible
v/v	volume-per-volume
W	tryptophan
w	weight
w/v	weight-per-volume
w/w	weight-per-weight
Y	tyrosine
ZYM-5052	auto-induction medium
%	percent

Abstract

Amyloid fibrils are an insoluble, highly ordered, fibrous protein structure, which have increasingly been recognised as having bionanotechnology applications. Their ability to self-assemble allows a bottom-up approach to material design. Their nanometre dimensions affords them a high surface-to-volume ratio and their proteinaceous building blocks from which they are assembled allow for decoration with biomolecules and chemicals through amino acid residues. Amyloid fibrils are therefore a potential nanoscaffold for immobilisation of biomolecules.

Immobilisation offers a solution to the problems associated with the use of enzymes in *in vitro* applications, by increasing their stability, reusability, and in some cases, enhancing catalytic activity. Nanosupports offer a high surface-to-volume ratio compared to classical planar 2-D supports, potentially affording them dramatic increases in immobilisation capacity.

To investigate the potential of amyloid fibrils as a novel nanoscaffold, organophosphate hydrolase (OPH), cytochrome $P450_{BM3}$ ($P450_{BM3}$), green fluorescent protein (GFP), tobacco etch virus protease (TEV), and glucose oxidase (GOD) were immobilised in solution to the model amyloid fibril forming protein, bovine insulin. Covalently immobilised OPH was found to have a ~300 % increase in relative thermostability at 40 and 50 °C. $P450_{BM3}$ was not successfully immobilised in its active state, most likely due to unfolding of the enzyme on the amyloid fibril surface. Covalently immobilised GFP retained full fluorescence and acted as a fluorescent protein tag. TEV was shown to have a physical interaction with the nanoscaffold and retain activity. GOD was immobilised and retained activity. Although not all proteins retained activity, a range of different protein structures were successfully immobilised onto the insulin amyloid fibril nanoscaffold. Attachment to the crystallin amyloid fibril nanoscaffold remains a work in progress due to the complexities associated with post-translational modifications of these fibrils. Crystallin amyloid fibrils were assembled on a surface for the first time. Their surface assembled structure was found to resemble spherulites, not previously seen before with crystallin amyloid fibrils.

Bovine insulin amyloid fibrils were assembled on the surface of glass beads to increase the available surface area for biomolecule immobilisation. The surface assembled bovine insulin nanoscaffold was first functionalised with GOD, demonstrating that the nanoscaffold provides more surface area for biomolecule immobilisation, although in this case the increase was limited due to high non-specific binding of GOD to the unmodified glass surface. GFP was successfully employed as a fluorescent protein tag to assess the degree of nanoscaffold coverage, confirming the nanoscaffold affords the glass bead a greater surface area. Moreover, a reusable immobilised TEV protease-bead system was developed that was able to sequentially cleave the poly-histidine tags of three different proteins.

In conclusion, bovine insulin amyloid fibrils have been shown to be a versatile nanoscaffold for the immobilisation of a range of biomolecules. The surface characteristics of the nanoscaffold allows for both covalent and physical immobilisation of biomolecules. Thus, amyloid fibrils have exciting potential in the creation of novel bionanotechnologies.

Chapter One

1 Introduction

The aim of this thesis is to investigate the potential of amyloid fibrils as a nanoscaffold for the immobilisation of biomolecules with applications in biotechnology. Amyloid fibrils possess many features which make them ideal candidates for use in bionanomaterials. These include: their nanometre size, giving rise to a high surface to volume ratio; the ability to self-assemble; the potential to be manufactured from waste materials; and the chemical functionality arising from their amino acid composition.

Enzymes are remarkable biocatalysts that can undertake a variety of complex chemical reactions at a range of pHs and temperatures. The use of enzymes at an industrial level is hampered with problems of cost, stability, and reusability. Immobilising enzymes to an amyloid fibril nanoscaffold may overcome some of the limitations of the enzymes. Creating a functional bionanomaterial incorporating enzymatically active amyloid fibrils is the goal of this research.

This chapter will provide background information on amyloid fibrils and the properties that make them useful for bionanotechnology. It will also explore the potential of industrially useful biocatalysts, and uses of immobilised enzymes in biotechnology.

1.1 Amyloid fibril formation

Amyloid fibrils are a type of highly ordered, insoluble, self-assembling protein nanofibre, most notably associated with protein misfolding diseases such as Creutzfeldt-Jakob, Huntington's, Parkinson's, Alzheimer's and type II diabetes (Chiti & Dobson 2006; Harrison *et al.* 2007; Pedersen & Otzen 2008). The defining characteristics of amyloid proteins will be discussed in detail in section 1.2. Whilst associated with 25 human diseases, natural functional amyloid is seen throughout nature in all domains of life (Coustou *et al.* 1997; Vidal *et al.* 1998; Iconomidou *et al.* 2000; Chapman *et al.* 2002; Fowler *et al.* 2005; Sabate *et al.* 2010).

Escherichia coli (*E. coli*) produce surface proteins called curli, which have been found to be amyloid-like (Chapman *et al.* 2002). This functional amyloid is involved in promoting colonisation of surfaces and in the formation of biofilms (Vidal *et al.* 1998). Filamentous fungi such as *Neurospora crassa* produce hydrophobin proteins which can form amyloid-like structures called rodlets (Mackay *et al.* 2001). The hydrophobins self-assemble into amphipathic monolayers on the surface of fungal spores and fruiting bodies at air/water interfaces (Wösten *et al.* 1999). This allows hyphae to penetrate the growth media and gives spores a water-repellent coating to enable aerial dispersion (Wösten *et al.* 1999; Beever & Dempsey 1978). Silkmoths produce chorion proteins which can self-assemble into amyloid fibrils (Iconomidou *et al.* 2000). These amyloid fibrils act as a protective shell around the ooctye and embryo. Melanosomes are cellular organelles found in the mammalian cells, melanocytes, and retinal pigment epithelium, located in the skin and eyes, respectively (Marks & Seabra 2001; Hearing 2000). An amyloid-like forming protein, Pmel17, is found in melanosomes and is required to polymerise into amyloid structures for the manufacture of mature melanin (Fowler *et al.* 2005). Melanin protects cells against toxins, UV radiation, and is required in pigmentation.

1.1.1 Protein folding and misfolding

Proteins are synthesised at the ribosome where the polypeptide chain elongates and starts folding into a thermodynamically stable structure as defined by the amino acid sequence and the particular environment of the protein (Luheshi & Dobson 2009). Protein folding is tightly controlled by the cellular protein quality control systems which include chaperones and proteolytic systems (Koga *et al.* 2011). Chaperones help to increase the rate of folding for proteins and ensure correct folding (Hartl & Hayer-Hartl 2002). The ubiquitin system on the other hand, works to degrade surplus or damaged proteins by breakdown in the proteasome to limit the misfolding of proteins (Hershko & Ciechanover 1998; Glickman & Ciechanover 2002; Ron & Walter 2007). The energy that the cell puts into ensuring correctly folded and functional proteins illustrates how important protein folding is, as misfolded proteins can cause disease (Koga *et al.* 2011).

For a protein to fold into its native conformation it must pass through a number of intermediately folded states as shown in **Figure 1.1** (Tyedmers *et al.* 2010). The kinetics of this process are governed by the environment (protein concentration, pH, temperature, pressure, ionic composition) in which the protein is found (Hamada & Dobson 2002). For amyloid fibrils to form from natively folded globular proteins, a partial unfolding event needs to occur (Uversky *et al.* 2002; Dobson 1999). Partial unfolding can be induced outside the cell by high temperatures, high pressure, low pH or organic solvents (Brange *et al.* 1997). Amyloid fibrils can also form from intrinsically disordered proteins, for example K-casein, allowing them to adopt an ordered folded form (Koudelka *et al.* 2012).

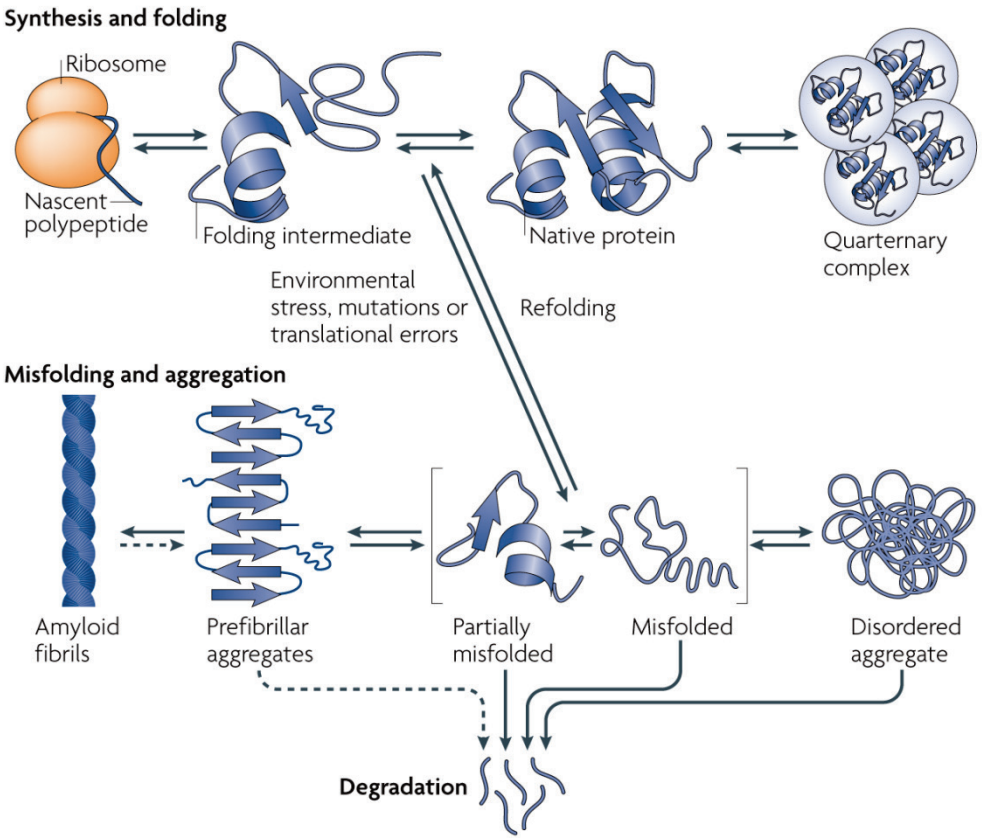

Figure 1.1 *The process of protein folding. Taken from Tyedmers et al. (2010).*

The different conformational states that a protein can adopt are proposed to be driven not only by the environmental conditions the protein is found in, but also by entropy (Mishra & Winter 2008; Jahn & Radford 2008). This process can be illustrated by an energy landscape (**Figure 1.2**), which conceptualises the folding process by taking into account the energy and entropy of all of the protein conformations. Energy landscapes are generally funnel like, where at the high energy, high entropy surface of the funnel there are numerous unfolded conformations the polypeptide can adopt. The polypeptide moves down the energy gradient *via* a series of partially folded intermediates to reach an energetically favourable native state (Onuchic & Wolynes 2004; Wolynes 2005).

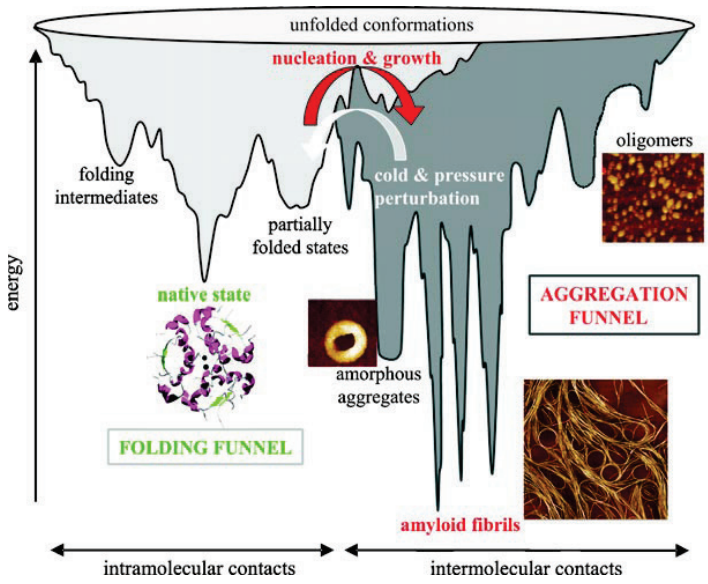

Figure 1.2 *A schematic energy landscape of protein folding and aggregation/amyloid fibril formation. Taken from Mishra & Winter (2008).*

Changes in environmental conditions or polypeptide sequence can influence the topography of the funnel, creating an increase or decrease in the number of energy minima (Mishra & Winter 2008; Jahn & Radford 2005). Changes in the topography can result in the accumulation of partially folded intermediates at the additional energy minima. Under normal protein folding conditions, these states would be transient however; upon perturbation of the physiochemical conditions, these partially folded intermediates can accumulate resulting in non-natural intermolecular interactions. This can result in folding pathways in which the polypeptide chain has access to entropically lower energy states such as amorphous aggregates or amyloid fibrils (Jahn & Radford 2008).

1.1.2 Amyloid fibrils - A generic protein structure?

It is widely thought that amyloid fibril formation is a universal property of most, if not all proteins (Chiti *et al.* 1999). The lack of sequence similarity of the known amyloid-forming proteins and the existence of non-disease forming amyloid proteins which are beneficial to organisms (section 1.1) suggests that the amyloid structure is possibly a generic protein fold of all polypeptide chains (Nerelius *et al.* 2010). However, specific sequences are also known to promote or reduce the tendency of the protein to adopt the amyloid form (Giraldo 2007; Nerelius *et al.* 2010).

Amyloid fibril formation is thought to occur through a nucleated-polymerisation mechanism (Liang *et al.* 2010). Examining the time-course of the transition of peptides and proteins into amyloid fibrils using techniques such as Thioflavin T (ThT) fluorescence and light scattering, generally shows a pronounced lag phase, followed by an exponential growth phase (Naiki *et al.* 1997; Serio *et al.* 2000; Uversky *et al.* 2002; Beck *et al.* 2004). The observed lag phase is thought to be due to the formation of nuclei. Once formed, fibril growth proceeds rapidly through the association of monomers or oligomers. Schmit *et al.* (2011) have developed a theory to describe the nucleation process. They hypothesised that there are three states of equilibrium for amyloid peptides: the monomer, oligomer, and the fibril (**Figure 1.3**). As with other nucleation dependent mechanisms this equilibrium can be shifted with the addition of preformed fibrils or 'seeds' where the lag phase can be shortened or eliminated completely (Naiki *et al.* 1997; Serio *et al.* 2000).

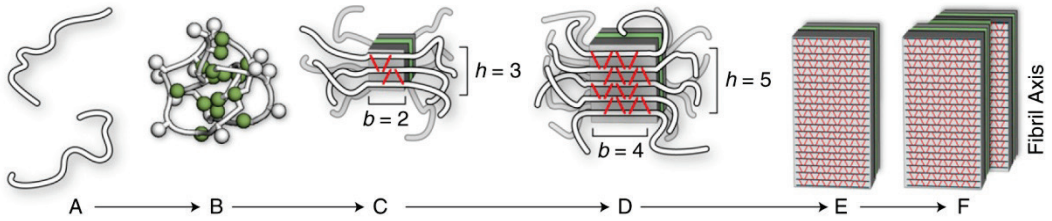

Figure 1.3 *A model process of amyloid fibril formation via a nucleated growth mechanism. Taken from Schmit et al. (2011). "(State A) Isolated peptide monomers in solution. (State B) Oligomeric assembly of a few peptide chains. (State C) Nucleus of β-sheet structure. The peptide backbone runs perpendicular to the fibre axis. (State D) Postcritical nucleus structure showing more β-structure. (State E) A protofilament is a single long thread of β-structure consisting of a β-sandwich and two face-to-face β-sheet planes. (State F) The full fibril, a bundle of protofilaments shown here to contain p = 2 protofilament threads."*

1.2 Amyloid fibril structure

Identifying the atomic-level structure of amyloid fibrils has been a goal of numerous research groups worldwide. These elusive atomic structures have been extremely difficult to determine because of the non-crystalline and insoluble nature of amyloid fibrils. The first atomic-level structural model of an amyloid-like cross-β spine, which is a signature of all amyloid fibrils, was only published in 2005 (Nelson *et al.* 2005). This X-ray crystal structure came from a yeast prion-derived peptide. The crystal structure of the entire amyloid forming protein has yet to be achieved. Other techniques have been used to gain an understanding of the structure of amyloid fibrils including cryo-electron microscopy (cryo-EM), X-ray fibre diffraction, transmission electron microscopy (TEM), atomic force microscopy (AFM), and most recently, solid-state nuclear magnetic resonance (ssNMR).

The first structures of amyloid fibrils came from TEM, X-ray fibre diffraction, and later AFM (Chiti & Dobson 2006). These techniques gave vital information about the size, unbranched morphology, the presence of a core structure made up of protofilaments and the repeating nature of the characteristic cross-β spine (section 1.1) (Sunde & Blake 1997; Serpell *et al.* 2000; Serpell & Smith 2000). More recently cryo-EM, together with 3D reconstruction software, have provided highly detailed models of amyloid fibrils at resolutions of up to 8 Å (**Figure 1.4**) (Schmidt *et al.* 2009). Mass-per-length measurements have allowed for the number of peptides (~ 2.5) per cross-β repeat per protofilament for the Aβ(1-42) and Aβ(1-40) peptide fibrils to be modelled (Schmidt *et al.* 2009).

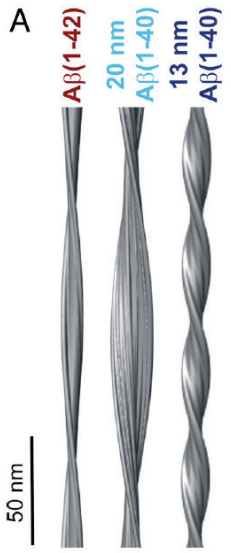

Figure 1.4 *Side views of reconstructions of $A\beta_{1-42}$ and $A\beta_{1-40}$ amyloid fibrils. Taken from Schmidt et al. (2009).*

Since the first atomic level structure of amyloid-like fibrils in 2005 (Nelson *et al.* 2005), X-ray crystallography has provided a great deal of knowledge about the structure of peptide derived amyloid fibrils. When these structures are used in combination with ssNMR (Tycko 2011), a detailed understanding of amyloid structures was elucidated. Supplementation of ssNMR data with constraints from lower resolution structures, such as those from electron microscopy, makes it possible to develop full molecular models for amyloid fibrils (Tycko 2011).

ssNMR has shown that whilst amyloid fibrils and amyloid-like fibrils all share the common cross-β structure, the way in which polypeptide chains adopt the β-sheet structure can be variable. For example, amylin fibrils are comprised of parallel β-sheets, whilst the $A\beta_{11-25}$ fibrils are comprised of antiparallel β-sheets (Tycko 2006). A new high resolution structural model of mature $A\beta_{1-40}$ amyloid fibrils (**Figure 1.5**) obtained using ssNMR, highlights the polymorphism of amyloid fibrils by having a different fold for the mature fibrils (Bertini *et al.* 2011). This model was obtained using highly homogeneous isotopically-labelled amyloid fibrils which generated a very accurate model compared other models which used heterogeneous samples.

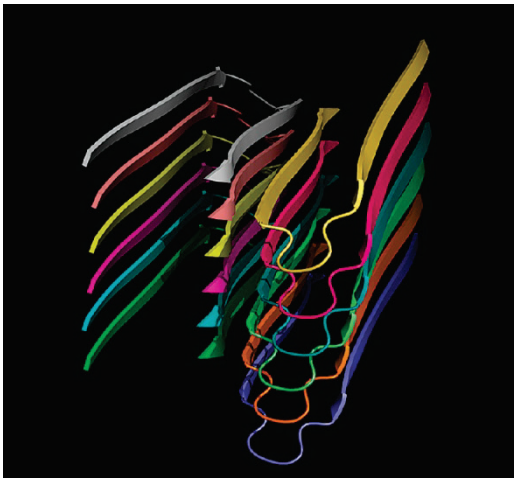

Figure 1.5 *Structural model of mature $A\beta_{1-40}$ amyloid fibrils. Taken from Bertini et al. (2011).*

Structural polymorphisms occur not only between different amyloid forming proteins, but within the same amyloid forming protein are diverse. A single structural model is unlikely to be accurate for all amyloid forming proteins. This needs to be taken into account when producing amyloid structures for use in nanotechnology. Changing the conditions under which the amyloid fibrils are formed can result in structural diversity and therefore non-reproducibility. However, polymorphism could also be advantageous in that the morphology of amyloid forming proteins could be tailored to suit particular applications (Rao *et al.* 2011).

1.2.1 Defining characteristics

The generally recognised criteria of amyloid or amyloid like fibrils include: the binding of the histological dyes Congo red (CR) and ThT; fibrillar morphology by AFM, and TEM; and β-sheet secondary structure as measured by Fourier transform infrared (FTIR) spectroscopy and X-ray fibre diffraction (Nilsson 2004; Hatters & Griffin 2011; Gras *et al.* 2011; Gras & Squires 2011). X-ray fibre diffraction is the 'gold standard' method for amyloid fibril characterisation, where the amyloid structures give characteristic diffraction patterns (**Figure 1.6**) with ~4.7 Å meridional reflections and ~10 Å equatorial reflections (Eanes & Glenner 1968). This diffraction pattern reflects the highly ordered repeating structural units within the fibrils corresponding to a structure containing a cross-β spine, with β-strands perpendicular to the fibrils axis (Kirschner *et al.* 1986; Sunde & Blake 1997; Sunde *et al.* 1997).

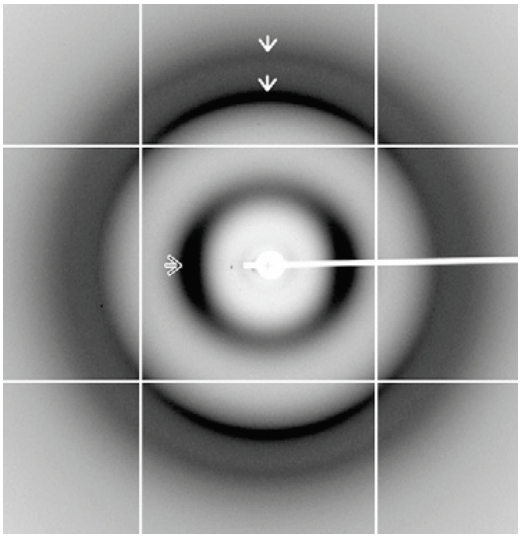

Figure 1.6 *X-ray fibre diffraction pattern of semi hydrated MetO-apoA-1 fibrils. Figure taken from Wong* et al. *(2010). Meridional reflections of 4.64 and 3.57 Å are shown with the white arrows. An equatorial reflection of 9.94 Å is shown by the outlined arrows.*

CR is a widely used diazo dye used to test for the presence of amyloid fibrils (Howie & Brewer 2009). The structure of CR is shown in **Figure 1.7**. Once stained with CR, the dye binds perpendicular to the fibril axis and so when viewed under cross-polarised light an apple-green birefringence is observed (Westermark *et al.* 1999; Nilsson 2004; Hatters & Griffin 2011).

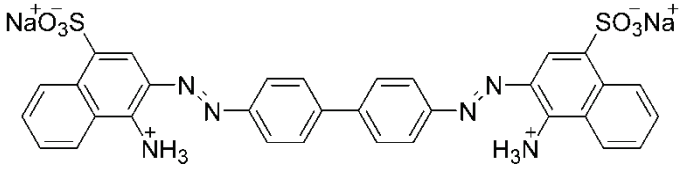

Figure 1.7 *The structure of Congo red (Nilsson 2004).*

ThT is a benzothiazole dye that selectively binds to amyloid fibrils and has a structure as shown in **Figure 1.8**. Amyloid fibrils can be detected using ThT through excitation at 450 nm and recording the emission at 485 nm (LeVine III 1999). ThT is thought to bind to the cavities running parallel to the fibril axis, between the protofilaments of the amyloid fibrils (Groenning 2010). Other fluorescent dyes such as amino derivatives of benzanthrone are being investigated as potential amyloid-binding dyes because they can potentially offer greater sensitivity and lower background protein fluorescence (Gorbenko *et al.* 2010).

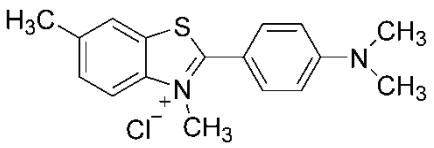

Figure 1.8 *The structure of Thioflavin T (Biancalana & Koide 2010).*

TEM is one of the most effective ways of distinguishing amyloid fibrils from other types of protein aggregates because of their fibrillar morphology (Nilsson 2004). Under the TEM amyloid fibrils generally have an unbranched twisted appearance with dimensions of 6-20 nm wide and up to several microns in length (Goldsbury *et al.* 2011).

In this thesis, the histological dye ThT was used extensively as well as TEM, and SEM. ThT was chosen because it is widely used to test for the presence of amyloid fibrils and because it is known to work reliably with the model amyloid forming protein, insulin (section 1.3) (Groenning *et al.* 2007).

1.3 Bovine insulin – a model amyloid forming protein

Bovine insulin in its native form is a ~5.7 kDa protein composed of two polypeptide chains connected by two inter-chain and one intra-chain disulfide bonds (**Figure 1.9**) (Baker *et al.* 1988). Insulin is a small, globular, predominantly α-helical protein that exists as a hexamer at physiological pH (Baker *et al.* 1988). The role of this anabolic hormone protein is to regulate the metabolism of carbohydrates and fats in the body (Saltiel & Kahn 2001).

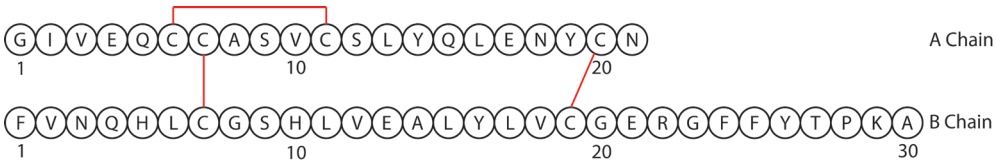

Figure 1.9 *Primary structure of bovine insulin. Adapted from Hong & Fink (2005).*

Bovine insulin is commonly used as a model amyloid-forming protein because it readily forms amyloid fibrils *in vitro* at high temperatures and low pH, but also because it is extremely well characterised (Waugh 1946; Ortiz *et al.* 2007). Many other conditions influence the formation of amyloid fibrils from bovine insulin, for example, insulin concentration, salt concentration, seeding, agitation and the presence/concentration of ThT (Nielsen *et al.* 2001). Insulin is also studied because it can cause amyloidosis in patients with type II diabetes by amyloid formation during the production, storage and transport of insulin (Nielsen *et al.* 2001; Nayak *et al.* 2009).

Bovine insulin was therefore selected as the model amyloid forming protein for this research because the protocols for ThT staining, high throughput 96 well spectrophotometer experiments, TEM and SEM are very well established. The amino acid sequence of bovine insulin is known (**Figure 1.9**). There is one lysine residue and two N-terminal residues per insulin molecule that can be potentially available for protein-protein cross-linking using the homo-bifunctional cross-linker glutaraldehyde (Shi 2006).

1.4 Crystallin proteins – the industrially relevant amyloid forming protein

Crystallins constitute about 90 % of the proteins in vertebrate eye lenses (Bloemendal 1977). α-, β-, and γ-crystallins are the main structural proteins (Meehan *et al.* 2004). The function of the lens is to focus the light onto the retina of the eye. This requires transparency and stability from the lens proteins which is gained from the β-sheet rich secondary structure of the crystallins (Harding 1991). The crystallin proteins contained within the lens fibre cells are kept for the entire life of a vertebrate and therefore need to be extremely stable. The stability is in part provided by the β-sheet rich structure of the crystallins, as well as the intrinsic chaperone ability of the α-crystallins (Reddy *et al.* 2002; Horwitz 2003; Ecroyd & Carver 2009).

α-Crystallin is a member of the small heat-shock protein (sHSP) family in which the 'α-crystallin domain' has a consensus sequence common to all members of the sHSP super family (de Jong *et al.* 1998). Jakob *et al.* (1993) demonstrated that sHSP can act as chaperones by investigating the unfolding and refolding of citrate synthase and α-glucosidase. The chaperone activity of α-crystallin has also now been well established *in vitro*, demonstrating the ability to inhibit amyloid fibrillation of many different amyloid forming proteins (Ecroyd & Carver 2009). These proteins include: α-synuclein (Rekas *et al.* 2007; Wang *et al.* 2008; Rekas *et al.* 2004), β2-microglobulin (Raman *et al.* 2005), κ-casein (Ecroyd *et al.* 2007; Ecroyd & Carver 2008), ccβ-Trp peptide (Ecroyd *et al.* 2007), apoC-II protein (Hatters *et al.* 2001) and Aβ (Shammas *et al.* 2011).

With the progression of age, older proteins undergo major post-translational modifications and in normal aging there is known to be an increase in the 'high molecular weight' protein fraction (Derham & Harding 1999; Meehan *et al.* 2004). These changes can occur in the lens without compromising the transparency of the lens. The protein aggregation that occurs in the centre of the lens is, for the most part, controlled, but when uncontrolled aggregation takes place cataract can occur, interfering with vision (Meehan *et al.* 2004; Horwitz 2003). α-Crystallin's chaperone ability comes into play by selectively binding partially unfolded proteins and controlling the non-specific aggregation (Horwitz 2003).

Crystallin proteins make an ideal candidate for the economic production of amyloid fibrils on an industrial scale (Garvey *et al.* 2009). Crystallin proteins can be sourced from eye lenses which are waste products from marine and agricultural industries. They exist in high concentration and have known ability to form amyloid fibrils both *in vivo* and *in vitro* (Garvey *et al.* 2009; Ecroyd & Carver 2009). Recently, Healy *et al.* (2012) have shown that a variety of protein nanofibre structures can be formed from crude mixtures of fish lens crystallins.

1.5 Enzymes as biocatalysts

Enzymes, which have been optimised by evolution, exhibit major advantages over classical chemical catalysts. Advantages include an extremely high level of catalytic efficiency and a range of specificities including substrate specificity, regio-specificity and even stereo-specificity (Krajewska 2004). Their remarkable properties stem from their primary amino acid sequence and the resulting three dimensional structures that a particular enzyme adopts (Rubenwolf *et al.* 2011).

There is enormous interest in the use of enzymes in an industrial setting. Enzymes, unlike many traditional chemical catalysts, can work in mild processing (low pressure, temperature, aqueous medium) conditions, and produce high yields of desired products. They are thought of as 'green chemistry' (Fernandez-Lafuente 2009), as they are energy efficient, environmentally benign, biodegradable, and are capable of functioning at low temperatures (Krajewska 2004; Sheldon & Rantwijk 2004).

Enzymes are used in many industries, ranging from the production of high value pharmaceuticals, to the manufacture of commodity chemicals such as fructose and aspartic acids (Aleksey 2001). When an enzyme cannot be found to catalyse the reaction of choice, *in silico* enzyme design provides a method to develop entirely new enzymes with completely unique catalytic reactions can be created. Sigel *et al.* (2010) showed this by the *de novo* computational design of an enzyme capable of catalysing Diels-Alder reactions, a reaction that has not been found in naturally occurring enzymes (Siegel *et al.* 2010). This provides the possibility of creating enzymes to undertake potentially any reaction of choice.

Whilst there are numerous advantages in utilising enzymes as biocatalysts, there are also some disadvantages which need to be overcome for their practical use. Firstly, the use of enzymes generally requires isolation and purification to homogeneity, which can be time consuming and expensive. Once enzymes are isolated from their natural cellular environment, there stability is typically reduced (Fágáin 1995). This is due to enzymes naturally possessing optimal catalytic activity under relatively mild conditions, for example, mild temperatures, pH and usually in aqueous media (Tran & Balkus 2011). Because many enzymes are soluble in an aqueous environment, they may require separation from the product after the enzymatic reaction has taken place (D'Souza 1999). Enzymes are also very sensitive to trace levels of certain chemicals which can inactivate or inhibit their activity. Inhibition can also occur from side and end products of the enzyme's own reaction (Krajewska 2004). Many of the problems associated with enzymes are currently being addressed by enzyme engineering, and immobilisation of the enzymes onto insoluble supports (Cao 2005a; Keasling 2008).

1.5.1 Enzyme engineering

Enzyme engineering is the process of altering the natural amino sequence of an enzyme to suit a combination of altered catalytic function, increased stability and optimal catalytic activity (Quin & Schmidt-Dannert 2011). There are two main approaches to engineering enzymes, directed evolution, and rational design (Quin & Schmidt-Dannert 2011). Directed evolution is based on the process of natural evolution selection. Large mutant libraries are generated, which are then monitored for changes in thermostability, substrate specificity, or increases in catalysis, using high-throughput methods (Labrou 2010). Error-prone polymerase chain reaction (PCR) is the most commonly used method to make these libraries (Parajuli & Williams 2011). This method uses the *Taq* polymerase, which lacks 3'-5' exonuclease proofreading activity, and so can randomly insert mutations along the sequence. Ni *et al.* (2011) recently used error-prone PCR to improve the specific activity of an arginine deaminase ~20 fold, and shift the pH optimum. Arginine deaminase is a potential anti-cancer agent for inhibiting arginine-auxotrophic tumors.

The rational design of enzymes is based on making informed changes to the enzyme by studying the enzyme's structure and/or catalytic mechanism, then applying computational design to make selective mutations to enhance the properties of the enzyme (Lutz 2010). This method generates much smaller mutant libraries, but, does rely on prior knowledge of the enzyme's, structure or catalytic mechanism. Saab-Rincón *et al.* (2012) used a combination of rational design and random mutagenesis to change a triosephosphate isomerase to a thiamin phosphate synthase. This example worked well because both enzymes share the same $(\alpha/\beta)_8$ barrel fold. The generated enzyme had a K_m similar to a native thiamin phosphate synthase, but with a k_{cat} four orders of magnitude lower (Saab-Rincón *et al.* 2012).

Other examples of enzymes that have undergone successful enzyme engineering include members of the cytochrome P450 (P450) family of enzymes. This family of enzymes catalyse a very large diversity of reactions ranging from carbon hydroxylation to dealkylation and C-C bond cleavage (Urlacher & Eiben 2006). Substrate size also varies, ranging from ethylene (M_w 28) to cyclosporin A (M_w 1201) (Isin & Guengerich 2007). The large diversity in reactions catalysed, and substrate range, has made them attractive biocatalysts (Gideon 2011). These unique features of P450s have meant that they been subjected to both directed evolution and rational design. Li *et al.* (2001) generated a triple mutant of cytochrome $P450_{BM3}$ ($P450_{BM3}$) using directed evolution that afforded it the ability to oxidise polycyclic aromatic hydrocarbons, instead of the native long-chain fatty acid substrates (Li *et al.* 2001). Dietrich *et al.* (2009) altered the regioselectivity of cytochrome $P450_{BM3}$ using rational design, so that the fatty acid substrates were hydroxylated in a stereospecific manner (Dietrich *et al.* 2009). $P450_{BM3}$ will be discussed in detail in section 2.3.

1.5.2 Enzyme immobilisation

Immobilisation of enzymes is the other major method of improving the properties of biocatalysts. Immobilisation can be used on any natural or engineered enzyme to further stabilise an enzyme, thus, enzyme engineering and immobilisation can be used in tandem. **Table 1.1** is a selected list of industrially important enzymes which are used in their immobilised form. The products produced from these immobilised enzymes are commercially important products, such as high-fructose corn syrup.

Table 1.1 *Selection of important immobilised enzymes used in industry. Adapted from Krajewska (2004).*

Enzyme (EC number)	Substrate	Product
Aminoacylase (3.5.1.14)	D,L-Amino acids	L-Amino acids (methionine, alanine, phenylalanine, tryptophan, valine)
Aspartate ammonia-lyase (4.3.1.1)	Ammonia + fumaric acid	L-Aspartic acid (used for production of synthetic sweetener aspartame)
β-Galactosidase (3.2.1.23)	Lactose	Glucose and galactose (lactose-free milk and whey)
Glucoamylase (3.2.1.3)	Starch	D-Glucose
Glucose isomerase (5.3.1.5)	Glucose	Fructose (high-fructose corn syrup)
Hydantoinase (3.5.2.2)	D,L-Amino acid hydantoins	D,L-Amino acids
Invertase (3.2.1.26)	Sucrose	Glucose/fructose mixture (invert sugar)
Lipase (3.1.1.3)	Triglycerides	Cocoa butter substitutes
Nitrile hydratase (4.2.1.84)	Acrylonitrile	Acrylamide
	Adiponitrile	5-Cyanovaleramide
	3-Cyanopyridine	Nicotinamide
Papain (3.4.22.2)	Proteins	Removal of "chill haze" in beers
Penicillin amidase (3.5.1.11)	Penicillins G and V	6-Aminopenicillanic acid (precursor of semi-synthetic penicillins, e.g. ampicillin)
Raffinase (3.2.1.22)	Raffinose	Galactose and sucrose (raffinose-free solutions)
Thermolysin (3.4.24.27)	Peptides	Aspartame
β-Tyrosinase (4.1.99.2)	Pyrocatechol	L-3,4-dihydroxyphenylalanine

Enzyme immobilisation overcomes many of the limitations of enzymes because it confers not only stability, but allows the separation and reuse of the biocatalyst to improve the economic viability of the process (Polizzi *et al.* 2007). Immobilising enzymes also allows for their use in multienzyme cascades (Sheldon 2007). Crestini *et al.* (2011) provide a good example of an immobilised multienzyme cascade, in which laccase and horseradish peroxidase were co-immobilised in a layer-by-layer coating process for the oxidation of lignin. A range of enzymes will be investigated as immobilised biocatalysts in this thesis, including, organophosphate hydrolase (OPH), $P450_{BM3}$, glucose oxidase (GOD), and tobacco etch virus (TEV) protease.

Immobilising enzymes started around the second half of the last century when the advantages of separation and reusability were the main driving force of the research (Silman & Katchalski 1966). Enzyme immobilisation is generally a process of trial and error to retain enzymatic activity, stability and selectivity, and is often called an art as much as a science (Cao 2005b). When planning the immobilising of an enzyme there are many factors to be considered, as shown in **Table 1.2** (Cao 2005a). All of these factors can influence the outcome of enzyme immobilisation and need to be considered when selecting appropriate immobilisation conditions.

Table 1.2 *Factors to be taken into consideration when planning the immobilisation of an enzyme. Adapted from Hanefeld et al. (2009).*

Immobilisation technique	**Factors to be taken into account**
General	Additives in the enzyme preparation that might interfere
	Stability of the enzyme under immobilisation conditions
	Stability of the carrier
	Protein leaching
	Non-specific carrier-substrate interactions
	Cost and availability of the carrier
Adsorption	
- Hydrophobic carrier	Presence of hydrophobic regions on the enzyme
	Ionic strength of the immobilisation buffer to favour protein adsorption
- Hydrophilic carrier	Presence of hydrophilic regions on enzyme/glycosylation
- Ionic interactions	pI of the enzyme
	Charged residues on the enzyme surface
	pH and ionic strength of the immobilisation buffer
Cross-linking	Location of the enzyme's residues needed for linking
	pH of the immobilisation step suitable for nucleophilic attack
	Conformational flexibility required by the enzyme's catalytic activity
Entrapment/encapsulation	Size of the enzyme
	Synthesis conditions of the polymer

There are a range of methods to immobilise enzymes. There are three generally recognised categories: adsorption, entrapment/encapsulation and cross-linking, as shown in **Figure 1.10** (Sheldon 2007; Moehlenbrock & Minteer 2011).

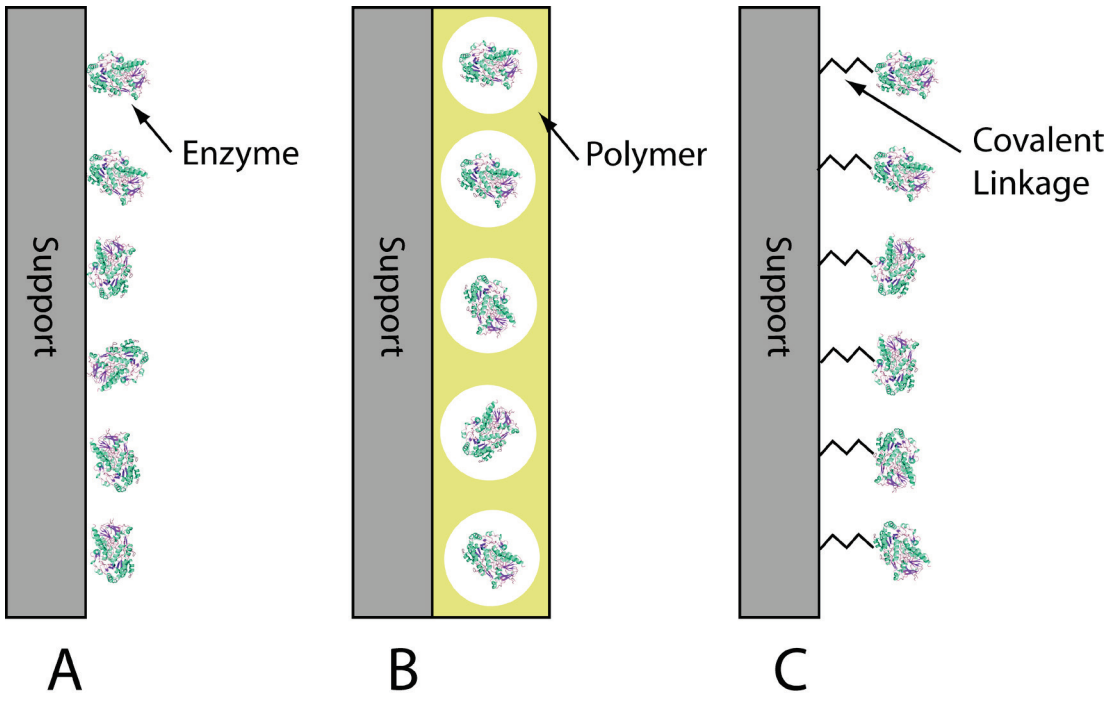

Figure 1.10 *Schematics of three main types of enzyme immobilisation: (A) physical adsorption, (B) entrapment/encapsulation, and (C) cross-linking. Adapted from Spahn & Minteer (2008).*

1.5.3 Adsorption enzyme immobilisation

Adsorption is where the enzyme is accumulated on a solid surface by either hydrophobic, van der Waals or ionic interactions (Spahn & Minteer 2008). This method is the simplest of the immobilisation methods because it generally only requires bathing the chosen support in a solution of enzyme for a given period of time to allow the adsorption to occur (Hanefeld *et al.* 2009). The benefits of the adsorption method are that the physical nature of the carrier can be modified so the enzyme can be recovered if needed and it can allow for very high retention of enzyme activity because there is no chemical modification (Sharma & Yamazaki 1984). Because of the simplicity of the adsorption method there is a tendency to lose immobilised enzyme through leaching. This can be caused by changes in ionic strength and pH (Moehlenbrock & Minteer 2011). Chloroperoxidase was recently immobilised *via* the adsorption method onto nanostructured silica with promising results (Águila *et al.* 2011). The adsorbed enzyme showed improvements in turnover numbers of up to 54,000 times higher than the free enzyme and because they used nanostructured silica with nanopores, the leaching of the enzyme was minimal.

1.5.4 Entrapment/encapsulation enzyme immobilisation

Entrapment and encapsulation differ slightly from each other but are under the same branch of immobilisation. Entrapment of an enzyme refers to an enzyme within the confines of a matrix, whereas encapsulation refers to the formation of a membrane-like physical barrier around the enzyme (Cao 2005a).

Entrapment is another simple immobilisation technique whereby the enzyme solution and the matrix solution are mixed together before a solidification (e.g. cross-linking, polymerisation or gelation) process occurs to immobilise the enzyme in the insoluble matrix (Sheldon 2007). Benefits are simplicity, ability to co-immobilise more than one enzyme, and stabilisation *via* confinement effects (Cao 2005a). Depending on whether cross-linking is used during the immobilisation procedure, enzyme leakage can be problematic as well as the possibility of severe limitations on diffusion of substrates and products because of the enzyme confinement (D'Urso & Fortier 1996). Mushroom tyrosinase exhibits rapid inactivation, therefore it was investigated whether entrapment of the enzyme would increase its stability (Jahangiri *et al.* 2012). The tyrosinase was immobilised within sol-gels and hybrid silica sol-gels but showed no activity, and was therefore immobilised within cross-linked polyacrylamide, where it retained ~25 % of its activity. This highlights the downfalls of entrapment due to diffusional limitations and the need to optimise the immobilisation media.

Encapsulation works on the principle of having enzymes inside a carrier with pore sizes smaller than the enzyme so that only substrates and products can diffuse in and out, but the enzyme cannot (Jen *et al.* 1996). Again, this is a mild immobilisation method allowing the enzyme to remain chemically unmodified and therefore potentially avoiding deactivation. It also permits the immobilisation of more than one enzyme at a time (Cousineau & Chang 1977). This method can suffer from the substrate/product diffusional problems, depending on the pore size of the membrane. A good example of enzyme encapsulation is the work of Wu *et al.* (2011) in which they emulsified solutions of a lipase A, lipase B, and a benzaldehyde lyase inside hydrophobic SiO_2 for use in organic media. This showed that the enzymes remained active, but the activity was lowered because of diffusion problems. This example demonstrates the potential of encapsulation because it allows the use of enzymes in environments where they would normally be fully inactivated.

1.5.5 Cross-linking enzyme immobilisation

Cross-linking is where the enzyme is immobilised to a support *via* a covalent bond (Betancor *et al.* 2006). This covalent bond provides the most stable type of immobilisation compared to the other non-covalent and adsorption methods (Zaborsky 1973). The covalent bond formation typically occurs between amino acid residues found on the surface of the enzyme and active functional groups found on the support (Twyman 2005). Cross-linking of enzymes is widely used because it generally results in an increase in enzyme stability and very low enzyme leakage (Spahn & Minteer 2008). The gain in stability is associated with the decrease in movement of the enzyme due to the buttressing effect of the multipoint covalent attachment (Sheldon 2007). The buttressing effect can have negative side effects because it commonly results in some loss of enzymatic activity due to the conformation restrictions (Sheldon 2007). Loss of activity can also be due to the uncontrolled reaction of essential active site residues with the cross-linking reagent or if cross-linked enzyme aggregates have formed, diffusional effects can again come into play (Cao 2005a).

Typically used supports for cross-linking enzymes include Eupergit C and Eupergit C 250 L. These contain reactive epoxy groups available for the cross-linking of enzymes through their amine and thio groups (Boller *et al.* 2002). Others include Sepabeads®, which can be functionalised with either epoxy or amino groups (Basso *et al.* 2007), and agarose and glyoxyl agarose (Mateo *et al.* 2007).

In this thesis two types of enzyme immobilisation were used, cross-linking and adsorption. Cross-linking was selected because of the potential increase in thermal stability and low enzyme leakage from the amyloid fibrils. Adsorption was employed when cross-linking induced inactivation, or if a strong interaction between the enzyme and amyloid fibrils was observed.

1.6 Nanosupports for enzyme immobilisation

There are many different types of nanosupports that have been used to immobilise enzymes, including, nanoporous media, nanoparticles, carbon nanotubes, and nanofibres (Kim *et al.* 2008). Each of these nanosupports has benefits and limitations depending on the applications to which they are applied. Nanosupports offer advantages because they possess very large surface area, permitting greater enzyme loading per unit mass of material compared to conventional materials (Ping 2006).

1.6.1 Nanoporous media

Nanoporous media are materials with pore sizes ranging in size from 2-50 nm (Kim *et al.* 2008). Nanoporous media has been investigated as a nanosupport because of their controlled porosity and high surface area. Adsorption of enzymes into nanoporous media has been the main method of enzyme immobilisation, but this method suffered from the serious drawback of enzyme leaching from the media (Kim *et al.* 2008). Pore size also has major consequences for enzymatic adsorption and activity. Depending on the size of the enzyme, it may or may not be able to enter the pores, and if it does enter the pores, then diffusional effects can play a part in lowering the activity of the material (Kim *et al.* 2006). A well used example of a nanoporous material is mesoporous silica developed by Mobil research group (Beck *et al.* 1992).

1.6.2 Nanoparticles

There are a huge number of different types of nanoparticles: ranging from metals such as gold; magnetic nanoparticles using iron and silica; and polymers such as polystyrene (Ping 2006). Nanoparticles overcome the diffusional limitations of nanoporous media and still provide the large surface area for enzyme immobilisation, but they are disadvantaged by dispersion in reaction media, and problems with recovery after the reaction due to their size and distribution (Jia *et al.* 2002).

1.6.3 Carbon nanotubes

Carbon nanotubes have attracted a lot of attention as a nanoscaffold because of their nanometre size, high electrical conductivity, chemical stability, and exceptional mechanical strength (Wang & Lin 2008). Single-walled carbon nanotubes (SWNTs) have been shown to increase the stabilisation of immobilised enzymes over flat surfaces due to their curvature (Asuri *et al.* 2006). The curvature of the SWNTs is thought to stop unfavourable lateral protein-protein interactions and therefore can afford the immobilised enzymes greater activity and stability.

All manner of enzyme immobilisation methods have been used to immobilise enzymes to carbon nanotubes. Non-covalent immobilisation methods such as physical adsorption have been the main focus of the immobilisation methods so as to limit the disruption to the enzyme structure and activity (Feng & Ji 2011). For example, Nejadnik *et al.* (2011) used 3-D scaffolds of carbon nanotubes for the immobilisation of GOD *via* physical adsorption for use in analytical sensing of glucose. Whilst this method does preserve the integrity of the immobilised enzymes, it does suffer the problem of enzyme leaching and the lack of reusability over time (Wang & Lin 2008).

Covalent enzyme immobilisation has also been achieved with carbon nanotubes, but this method requires chemical derivitisation of the surface first (Tasis *et al.* 2006). Bogner *et al.* (2010) created a glucose powered bio-fuel-cell by covalently immobilising glucose dehydrogenase and bilirubin oxidase using 1-ethyl-3-(3-dimethylaminopropyl) carbodiimide (EDC) to multi-walled carbon nanotubes which had been oxidised to yield surface carboxyl groups. The immobilised enzymes gave an operation time of more than four hours showing the potential of enzymes covalently immobilised to carbon nanotubes.

1.6.4 Protein nanofibres

Protein nanofibres such as amyloid fibrils offer an exciting alternative to the currently used nanoscaffolds for enzyme immobilisation. They offer the large surface area from their nanometre size range (Waterhouse & Gerrard 2004), intrinsic side chain chemistry from their amino acid composition (Fágáin 1995), strength comparable to steel (Smith *et al.* 2006), a protein environment beneficial to enzyme stability and activity (Wang 2006), and the ability to self-assemble providing a bottom-up approach to material design (Gras 2007). Amyloid fibrils will be used as the nanoscaffold for enzyme immobilisation in this thesis.

1.7 Amyloid fibrils in bionanotechnology

Amyloid fibril containing bionanomaterials have potential applications in a wide range of fields, including biosensing and bioremediation (Gras 2007; Waterhouse & Gerrard 2004). Amyloid fibrils are highly suited to incorporation within biomaterials because of their ability to self-assemble, their high surface to volume ratio, and their nanoscaffold capability (Gras *et al.* 2008; Scanlon & Aggeli 2008). Amyloid fibrils can act as a nanoscaffold by the addition of functional groups through the side chain chemistry gained from an amino acid such as lysine, which will be discussed in detail in section 3.3 (Fágáin 1995).

The self-assembling nature of amyloid fibrils allows for the potential of bottom-up approaches to the design of novel materials (Gras 2007; Paparcone *et al.* 2011). Bottom-up material design offers potential for the delicate fine-tuning of a material, and in the case of protein structures such as amyloid fibrils, there is the potential to make single amino acid substitutions one at a time *via* mutagenesis until the material has the desired properties (Hauser & Zhang 2010).

Nature employs the bottom-up design approach to solve the problems of assembling highly sophisticated molecular machines and structures in the form of enzymes and protein structures such as microtubules and microfilaments (Seeman 2002). Mimicking nature on the nanoscale may provide a means of designing 'smart' self-assembling materials, and amyloid fibrils fulfil these requirements (Zhang 2003; Tu & Tirrell 2004; Knowles & Buehler 2011). The potential use of amyloid fibrils in bionanotechnology has only recently been recognised (Gras 2007; MacPhee & Dobson 2000; MacPhee & Woolfson 2004). In the past ten years amyloid fibrils have been explored for a multitude of different bionanotechnology applications, some of which are summarised by **Table 1.3** (Waterhouse & Gerrard 2004).

Table 1.3 *Summary of papers utilising amyloid fibrils in bionanotechnology*

Amyloid fibril forming protein	Technology	Reference
ApoA1	Glutathione S-transferase (GST) fusion	(Guglielmi *et al.* 2009)
Insulin	Cell adhesion	(Sakono *et al.* 2011)
Insulin & α-lactalbumin	Coaggregation with hyrolases	(Kim *et al.* 2012)
Insulin	Hybrid bioinorganic fibrils	(Tang *et al.* 2010)
Insulin	Nanocomposite	(Rao *et al.* 2012)
Insulin	Nanoscaffold for glucose oxidase immobilisation	(Pilkington *et al.* 2010)
Insulin	Phosphorescent amyloid-like protein fibrils	(Rizzo *et al.* 2010)
Insulin	Surface assembly	(Ha & Park 2005)
N-terminal & middle region of Sup35p	Conducting nanowires	(Scheibel *et al.* 2003)
α-synuclein	Amyloid hydrogel for enzyme entrapment	(Bhak *et al.* 2010)
Transthyretin (TTR)	Biological cell adhesion sequence fusion	(Gras *et al.* 2008)
$TTR_{105-115}$-cycloRGDfK	Cell adhesion	(Bongiovanni *et al.* 2011)
Tandem repeat of the SH3 domain	*b*-Type cytochrome fusion	(Baldwin *et al.* 2006)
Ure2 prion protein	Barnase fusion	(Baxa *et al.* 2002)
Ure2 prion protein	Carbonic anhydrase fusion	(Baxa *et al.* 2002)
Ure2 prion protein	GFP fusion	(Baxa *et al.* 2002)
Ure2 prion protein	GST fusion	(Baxa *et al.* 2002)

Of the few available research papers utilising amyloid fibrils to create self-assembling structures with enzymatic activity, the enzymatically active amyloid fibrils are based around fusing the gene of a particular enzyme with an amyloid forming component peptide (**Figure 1.11**) (Woolfson & Mahmoud 2010). The amyloid forming peptide component can either be derived from the sequence of an amyloid forming protein such as transthyretin (Gras *et al.* 2008), or can be a synthesised peptide (Channon & MacPhee 2008).

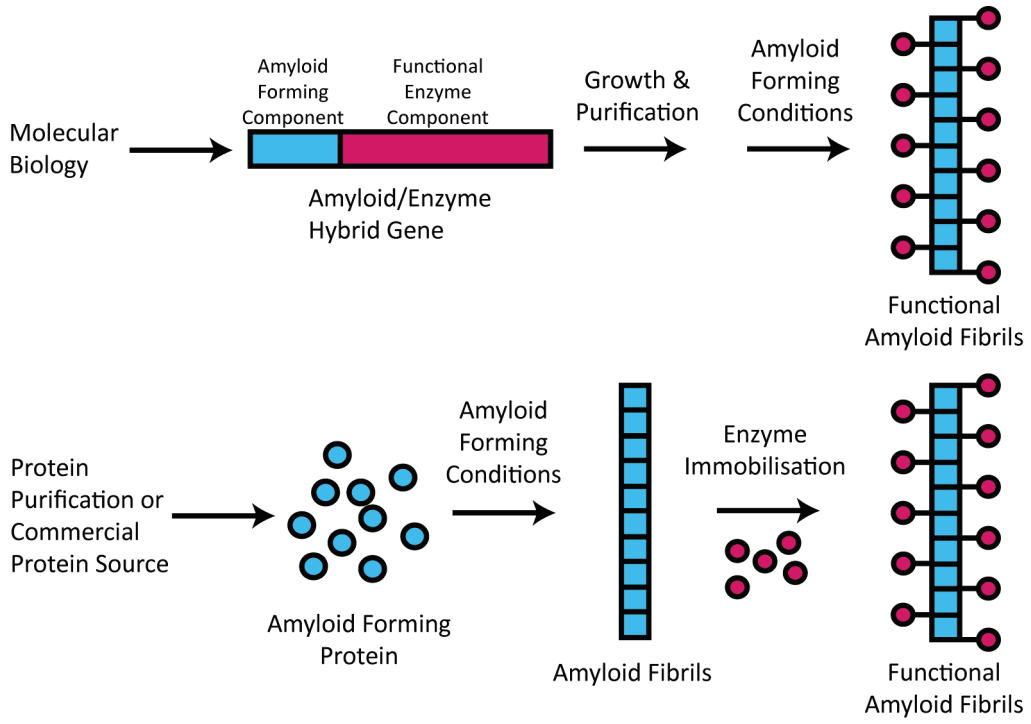

Figure 1.11 *Formation of functional amyloid fibrils by: (top) gene fusion of an amyloid forming peptide/protein sequence with a functional enzyme/protein sequence, or (bottom) enzyme immobilisation post-amyloid formation.*

Baxa *et al.* (2002) fused the URE2 prion domain with four proteins, carbonic anhydrase, barnase, GST, and GFP. The four proteins were chosen to create amyloid fusions because of their small substrates, to minimise the possible steric hindrance from the aggregates formed. Subsequent activity assays revealed that only the GST and GFP amyloid fusion aggregates retained significant activity, ~80 % and ~ 130 %, respectively. By contrast, the barnase and carbonic anhydrase amyloid fusion aggregates had minimal activity. The reduction in barnase and carbonic anhydrase activity was surmised to be from diffusional limitations because both of these enzymes are near-diffusion-limited enzymes (Jönsson & Wennerström 1978; Day *et al.* 1992).

Guglielmi *et al.* (2009) created a similar amyloid fusion protein with GST, but, instead of the URE2 prion domain, they used a 93 residue polypeptide derived from the amyloidogenic domain of apolipoprotein A-I. In this research the amyloid fusion enzyme had to be incubated for 3 weeks to generate amyloid fibrils. This is an extremely long time if this technology were to be used industrially. The resulting GST amyloid fusion aggregates were again shown to be active and were able to be stored for up to two weeks without loss of activity.

Baldwin *et al.* (2006) generated a *b*-type cytochrome amyloid fusion by constructing a gene which has a cytochrome domain and an amyloid forming domain derived from a tandem repeat of a SH3 domain. The fusion amyloid fibrils were shown to be able to bind metalloporphyrins and from TEM experiments it was estimated that the density of metalloporphyrins was 2.6 per nm. The authors reason that at this concentration rapid electron transfer would be able to occur and that this technology could be used to create self-assembling molecular wires.

Gras *et al.* (2008) and Bongiovanni *et al.* (2011) use an 11 amino acid sequence corresponding to residues 105-115 from the amyloidogenic protein transthyretin as the amyloid forming component of their fusion peptides for the creation of functional amyloid fibrils for cell adhesion. Gras *et al.* (2008) fused a biological cell adhesion sequence (RGD) to the amyloid forming component and created amyloid fibrils capable of promoting cell adhesion, whereas, Bongiovanni *et al.* (2011) fused a cycloRGDfk peptide to target mammalian cell surface $\alpha_v\beta_3$ integrin receptors, and again showed that the fusion amyloid fibrils were capable of promoting cell adhesion and spreading. Peptide synthesis was used in the creation of both the fusion peptides, demonstrating the applications of being able to modify one amino acid at a time to create a desired sequence.

The above examples create fusion proteins, either at the gene level, or synthetically using standard solid phase peptide synthesis chemistry. The fusion method could have great potential when creating small peptide fusion amyloid fibrils such as the $TTR_{105-115}$-RGD amyloid fibrils because they can be completely synthetically made. The gene level fusion amyloid fibrils would be more difficult to produce because of the molecular biology involved in creating the genes, but with many companies now specialising in these methods, these problems are becoming less of a hindrance. The major obstacle for the gene based fusions could be in the protein growth and purification because of the intrinsic aggregation potential of the gene product, therefore, the bacterial host may produce low yields. Generating gene based fusions could also be time consuming if the active enzyme component of the fusion amyloid fibrils turns out to have a low activity or be inactivated, as was the case for the barnase and carbonic anhydrase (Baxa *et al.* 2002).

Immobilising enzymes post amyloid formation is an alternative method of creating nanostructures with enzymatic activity (**Figure 1.11**). Pilkington *et al.* (2010) proved this to be a valid approach when immobilising glucose oxidase to insulin amyloid fibrils by cross-linking with glutaraldehyde. Recently, Kim *et al.* (2012) immobilised an SGNH esterase to insulin and α-lactalbumin amyloid fibrils by first coaggregating the amyloid fibrils and enzyme using high concentrations of ammonium sulfate, followed by cross-linking with glutaraldehyde. This method also proved successful, but adds an extra step to the immobilisation procedure. The advantages of post-assembly modification include the opportunity to create a more general material that can be readily modified with any desired enzyme or other decoration (Woolfson & Mahmoud 2010). Immobilising enzymes post amyloid formation is the method used to create functional amyloid fibrils in this thesis, with a long term aim to develop a commercially scalable process.

1.8 Functionalising surfaces for enzyme immobilisation

Most surfaces require some type of modification before enzymes can be immobilised to them. The type of modification depends on what type of immobilisation method will be used and what the starting surface chemistry is. For example, the surface of gold is readily functionalised with alkanethiols to create an environment beneficial to enzyme adsorption (Halling *et al.* 2005), or gold surfaces can be functionalised with aminoethanethiol for the covalent immobilisation of enzymes (Stine *et al.* 2011).

The use of nanoscaffolds such as carbon nanotubes or amyloid fibrils for enzyme immobilisation provides a large surface area for enzyme immobilisation, but due to their size, can still be difficult to handle and recover from reaction media. Modifying surfaces by assembling amyloid fibrils could provide an easy method for the handling and recovery of the nanoscaffold, whilst retaining the benefits of an increase in surface area (Ha & Park 2005). Carbon nanotubes can also be self-assembled on surfaces such as gold, but, the surface used for the self-assembly must be able to tolerate high temperature (>700 °C) because of the process used to create the nanotubes (Lin *et al.* 2010). The high temperatures required for the manufacture of carbon nanotubes place limitations on the choice of surfaces available for self-assembly. Amyloid fibrils on the other hand, can be assembled at lower temperatures, for example, 60 °C for bovine insulin (Nielsen *et al.* 2001). The lower amyloid fibril assembly temperatures potentially allows more surfaces to be modified because the process is not limited by the self-assembly temperature. The functionalisation of surfaces with amyloid fibrils will be discussed in detail in chapters three and five. Bovine insulin and fish eye lens crystallin amyloid fibrils will be used in this thesis to functionalise glass and cellulose surfaces. The surface assembled insulin amyloid fibrils will then be used to immobilise biomolecules, creating active bionanomaterials.

1.9 Thesis objectives

This introduction has given an overview of amyloid fibrils and their defining characteristics. It has also introduced the use of enzymes as biocatalysts and how they can be immobilised to insoluble supports using different techniques.

The initial part of this thesis investigates the potential of the model amyloid forming protein, bovine insulin, to act as a nanoscaffold for the immobilisation of a range of biotechnologically important biomolecules, to establish whether the simple methodology developed by Pilkington *et al.* (2010) is applicable to a wider range of biomolecules.

Amyloid fibrils are then assembled on glass and cellulose surfaces to create materials with surface assembled nanoscaffolds. These surfaces are characterised by a range of methods, then the surface assembled insulin amyloid fibril nanoscaffold is functionalised with biotechnologically important biocatalysts for the generation of active bionanomaterials.

1.10 References

Águila, S., Vazquez-Duhalt, R., Covarrubias, C., Pecchi, G. & Alderete, J.B., 2011. Enhancing oxidation activity and stability of iso-1-cytochrome c and chloroperoxidase by immobilization in nanostructured supports. *Journal of Molecular Catalysis B: Enzymatic*, 70(3-4), pp.81–87.

Aleksey, Z., 2001. Industrial biocatalysis. *Current Opinion in Chemical Biology*, 5(2), pp.130–136.

Asuri, P., Karajanagi, S.S., Yang, H., Yim, T.-J., Kane, R.S. & Dordick, J.S., 2006. Increasing protein stability through control of the nanoscale environment. *Langmuir*, 22(13), pp.5833–5836.

Baker, E.N., Blundell, T.L., Cutfield, J.F., Cutfield, S.M., Dodson, E.J., Dodson, G.G., Hodgkin, D.M., Hubbard, R.E., Isaacs, N.W. & Reynolds, C.D., 1988. The structure of 2Zn pig insulin crystals at 1.5 Å resolution. *Philosophical transactions of the Royal Society of London. Series B: Biological sciences*, 319(1195), pp.369–456.

Baldwin, A.J., Bader, R., Christodoulou, J., MacPhee, C.E., Dobson, C.M. & Barker, P.D., 2006. Cytochrome display on amyloid fibrils. *Journal of the American Chemical Society*, 128(7), pp.2162–2163.

Basso, A., Braiuca, P., Cantone, S., Ebert, C., Linda, P., Spizzo, P., Caimi, P., Hanefeld, U., Degrassi, G. & Gardossi, L., 2007. *In silico* analysis of enzyme surface and glycosylation effect as a tool for efficient covalent immobilisation of calB and PGA on Sepabeads®. *Advanced Synthesis & Catalysis*, 349(6), pp.877–886.

Baxa, U., Speransky, V., Steven, A.C. & Wickner, R.B., 2002. Mechanism of inactivation on prion conversion of the Saccharomyces cerevisiae Ure2 protein. *Proceedings of the National Academy of Sciences of the United States of America*, 99(8), pp.5253 –5260.

Beck, J.S., Christensen, G. & Otzen, D.E., 2004. Modulation of S6 fibrillation by unfolding rates and gatekeeper residues. *Journal of Molecular Biology*, 341(2), pp.575–588.

Beck, J.S., Vartuli, J.C., Roth, W.J., Leonowicz, M.E., Kresge, C.T., Schmitt, K.D., Chu, C.T.W., Olson, D.H. & Sheppard, E.W., 1992. A new family of mesoporous molecular sieves prepared with liquid crystal templates. *Journal of the American Chemical Society*, 114(27), pp.10834–10843.

Beever, R.E. & Dempsey, G.P., 1978. Function of rodlets on the surface of fungal spores. *Nature*, 272(5654), pp.608–610.

Bertini, I., Gonnelli, L., Luchinat, C., Mao, J. & Nesi, A., 2011. A new structural model of Aβ40 fibrils. *Journal of the American Chemical Society*, 133(40), pp.16013–16022.

Betancor, L., López-Gallego, F., Hidalgo, A., Alonso-Morales, N., Mateo, C., Fernández-Lafuente, R. & Guisán, J.M., 2006. Different mechanisms of protein immobilization on glutaraldehyde activated supports: Effect of support activation and immobilization conditions. *Enzyme and Microbial Technology*, 39(4), pp.877–882.

Bhak, G., Lee, S., Park, J.W., Cho, S. & Paik, S.R., 2010. Amyloid hydrogel derived from curly protein fibrils of α-synuclein. *Biomaterials*, 31(23), pp.5986–5995.

Biancalana, M. & Koide, S., 2010. Molecular mechanism of Thioflavin-T binding to amyloid fibrils. *Biochimica et Biophysica Acta (BBA) - Proteins & Proteomics*, 1804(7), pp.1405–1412.

Bloemendal, H., 1977. The vertebrate eye lens. *Science*, 197(4299), pp.127–138.

Bogner, M., Schnaithmann, M., Sägebarth, J. & Sandmaier, H., 2010. Bio-fuel cell based on modified carbon nanotubes with immobilized enzymes. *Procedia Engineering*, 5(Eurosensor XXlV Conference), pp.1047–1050.

Boller, T., Meier, C. & Menzler, S., 2002. Eupergit oxirane acrylic beads: How to make enzymes fit for biocatalysis. *Organic Process Research & Development*, 6, pp.509–519.

Bongiovanni, M.N., Scanlon, D.B. & Gras, S.L., 2011. Functional fibrils derived from the peptide TTR1-cycloRGDfK that target cell adhesion and spreading. *Biomaterials*, 32(26), pp.6099–6110.

Brange, J., Andersen, L., Laursen, E.D., Meyn, G. & Rasmussen, E., 1997. Toward understanding insulin fibrillation. *Journal of Pharmaceutical Sciences*, 86(5), pp.517–525.

Cao, L., 2005a. *Carrier-bound Immobilized Enzymes: Principles, Applications and Design*, Weinheim, FRG: Wiley-VCH Verlag GmbH & Co. KGaA.

Cao, L., 2005b. Immobilised enzymes: Science or art? *Current Opinion in Chemical Biology*, 9(2), pp.217–226.

Channon, K. & MacPhee, C.E., 2008. Possibilities for "smart" materials exploiting the self-assembly of polypeptides into fibrils. *Soft Matter*, 4(4), pp.647-652.

Chapman, M.R., Robinson, L.S., Pinkner, J.S., Roth, R., Heuser, J., Hammar, M., Normark, S. & Hultgren, S.J., 2002. Role of Escherichia coli curli operons in directing amyloid fiber formation. *Science*, 295(5556), pp.851–855.

Chiti, F. & Dobson, C.M., 2006. Protein misfolding, functional amyloid, and human disease. *Annual Review of Biochemistry*, 75, pp.333–366.

Chiti, F., Webster, P., Taddei, N., Clark, A., Stefani, M., Ramponi, G. & Dobson, C.M., 1999. Designing conditions for in vitro formation of amyloid protofilaments and fibrils. *Proceedings of the National Academy of Sciences of the United States of America*, 96(7), pp.3590-3594.

Cousineau, J. & Chang, T.M.S., 1977. Formation of amino acid from urea and ammonia by sequential enzyme reaction using a microencapsulated multi-enzyme system. *Biochemical and Biophysical Research Communications*, 79(1), pp.24–31.

Coustou, V., Deleu, C., Saupe, S. & Begueret, J., 1997. The protein product of the het-s heterokaryon incompatibility gene of the fungus *Podospora anserina* behaves as a prion analog. *Proceedings of the National Academy of Sciences of the United States of America*, 94(18), pp.9773–9778.

Crestini, C., Melone, F. & Saladino, R., 2011. Novel multienzyme oxidative biocatalyst for lignin bioprocessing. *Bioorganic & Medicinal Chemistry*, 19(16), pp.5071–5078.

D'Souza, S.F., 1999. Immobilized enzymes in bioprocess. *Current Science*, 77(1), pp.69–79.

D'Urso, E.M. & Fortier, G., 1996. Albumin-poly(ethylene glycol) hydrogel as matrix for enzyme immobilization: Biochemical characterization of crosslinked acid phosphatase. *Enzyme and Microbial Technology*, 18(7), pp.482–488.

Day, A.G., Parsonage, D., Ebel, S., Brown, T. & Fersht, A.R., 1992. Barnase has subsites that give rise to large rate enhancements. *Biochemistry*, 31(28), pp.6390–6395.

Derham, B.K. & Harding, J.J., 1999. α-Crystallin as a molecular chaperone. *Progress in Retinal and Eye Research*, 18(4), pp.463–509.

Dietrich, M., Do, T.A., Schmid, R.D., Pleiss, J. & Urlacher, V.B., 2009. Altering the regioselectivity of the subterminal fatty acid hydroxylase P450 BM-3 towards γ- and δ-positions. *Journal of Biotechnology*, 139(1), pp.115–117.

Dobson, C.M., 1999. Protein misfolding, evolution and disease. *Trends in Biochemical Sciences*, 24(9), pp.329–332.

Eanes, E.D. & Glenner, G.G., 1968. X-ray diffraction studies on amyloid filaments. *Journal of Histochemistry and Cytochemistry*, 16(11), pp.673–677.

Ecroyd, H. & Carver, J.A., 2009. Crystallin proteins and amyloid fibrils. *Cellular and Molecular Life Sciences*, 66(1), pp.62–81.

Ecroyd, H. & Carver, J.A., 2008. The effect of small molecules in modulating the chaperone activity of αB-crystallin against ordered and disordered protein aggregation. *The Federation of European Biochemical Societies Journal*, 275(5), pp.935–947.

Ecroyd, H., Meehan, S., Horwitz, J., Aquilina, J.A., Benesch, J.L.P., Robinson, C.V., Macphee, C.E. & Carver, J.A., 2007. Mimicking phosphorylation of αB-crystallin affects its chaperone activity. *Biochemical Journal*, 401(1), pp.129-141.

Fágáin, C.Ó., 1995. Understanding and increasing protein stability. *Biochimica et Biophysica Acta (BBA) - Protein Structure and Molecular Enzymology*, 1252(1), pp.1–14.

Feng, W. & Ji, P., 2011. Enzymes immobilized on carbon nanotubes. *Biotechnology Advances*, 29(6), pp.889–895.

Fernandez-Lafuente, R., 2009. Stabilization of multimeric enzymes: Strategies to prevent subunit dissociation. *Enzyme and Microbial Technology*, 45(6-7), pp.405–418.

Fowler, D.M., Koulov, A.V., Alory-Jost, C., Marks, M.S., Balch, W.E. & Kelly, J.W., 2005. Functional amyloid formation within mammalian tissue. *PLoS Biology*, 4(1), pp.100-107.

Garvey, M., Gras, S.L., Meehan, S., Meade, S.J., Carver, J.A. & Gerrard, J.A., 2009. Protein nanofibres of defined morphology prepared from mixtures of crude crystallins. *International Journal of Nanotechnology*, 6(3-4), pp.258–273.

Gideon, G., 2011. Cytochromes P450: Exploiting diversity and enabling application as biocatalysts. *Current Opinion in Chemical Biology*, 15(2), pp.241–248.

Giraldo, R., 2007. Defined DNA sequences promote the assembly of a bacterial protein into distinct amyloid nanostructures. *Proceedings of the National Academy of Sciences of the United States of America*, 104(44), pp.17388–17393.

Glickman, M.H. & Ciechanover, A., 2002. The ubiquitin-proteasome proteolytic pathway: Destruction for the sake of construction. *Physiological Reviews*, 82(2), pp.373–428.

Goldsbury, C., Baxa, U., Simon, M.N., Steven, A.C., Engel, A., Wall, J.S., Aebi, U. & Müller, S.A., 2011. Amyloid structure and assembly: Insights from scanning transmission electron microscopy. *Journal of Structural Biology*, 173(1), pp.1–13.

Gorbenko, G., Trusova, V., Kirilova, E., Kirilov, G., Kalnina, I., Vasilev, A., Kaloyanova, S. & Deligeorgiev, T., 2010. New fluorescent probes for detection and characterization of amyloid fibrils. *Chemical Physics Letters*, 495(4-6), pp.275–279.

Gras, S.L., 2007. Amyloid fibrils: From disease to design. New biomaterial applications for self-assembling cross-β fibrils. *Australian Journal of Chemistry*, 60(5), pp.333–342.

Gras, S.L. & Squires, A.M., 2011. Dried and hydrated X-ray scattering analysis of amyloid fibrils. In A. F. Hill, K. J. Barnham, S. P. Bottomley, & R. Cappai, eds. *Protein Folding, Misfolding, and Disease*. Totowa, NJ: Humana Press, pp. 147–163.

Gras, S.L., Tickler, A.K., Squires, A.M., Devlin, G.L., Horton, M.A., Dobson, C.M. & MacPhee, C.E., 2008. Functionalised amyloid fibrils for roles in cell adhesion. *Biomaterials*, 29(11), pp.1553–1562.

Gras, S.L., Waddington, L.J. & Goldie, K.N., 2011. Transmission electron microscopy of amyloid fibrils. In A. F. Hill, K. J. Barnham, S. P. Bottomley, & R. Cappai, eds. *Protein Folding, Misfolding, and Disease*. Totowa, NJ: Humana Press, pp. 197–214.

Groenning, M., 2010. Binding mode of Thioflavin T and other molecular probes in the context of amyloid fibrils-current status. *Journal of Chemical Biology*, 3(1), pp.1–18.

Groenning, M., Norrman, M., Flink, J.M., van de Weert, M., Bukrinsky, J.T., Schluckebier, G. & Frokjaer, S., 2007. Binding mode of Thioflavin T in insulin amyloid fibrils. *Journal of Structural Biology*, 159(3), pp.483–497.

Guglielmi, F., Monti, D.M., Arciello, A., Torrassa, S., Cozzolino, F., Pucci, P., Relini, A. & Piccoli, R., 2009. Enzymatically active fibrils generated by the self-assembly of the ApoA-I fibrillogenic domain functionalized with a catalytic moiety. *Biomaterials*, 30(5), pp.829–835.

Ha, C. & Park, C.B., 2005. Template-directed self-assembly and growth of insulin amyloid fibrils. *Biotechnology and Bioengineering*, 90(7), pp.848–855.

Halling, P.J., Ulijn, R.V. & Flitsch, S.L., 2005. Understanding enzyme action on immobilised substrates. *Current Opinion in Biotechnology*, 16(4), pp.385–392.

Hamada, D. & Dobson, C.M., 2002. A kinetic study of β-lactoglobulin amyloid fibril formation promoted by urea. *Protein Science*, 11(10), pp.2417–2426.

Hanefeld, U., Gardossi, L. & Magner, E., 2009. Understanding enzyme immobilisation. *Chemical Society Reviews*, 38, pp.453-468.

Harding, J., 1991. *Cataract — Biochemistry, epidemiology and pharmacology* 1st ed., London: Chapman and Hall.

Harrison, R.S., Sharpe, P.C., Singh, Y. & Fairlie, D.P., 2007. Amyloid peptides and proteins in review. *Reviews of Physiology, Biochemistry & Pharmacology*, 159, pp.1–77.

Hartl, F.U. & Hayer-Hartl, M., 2002. Protein folding. Molecular chaperones in the cytosol: From nascent chain to folded protein. *Science*, 295(5561), pp.1852–1858.

Hatters, D.M. & Griffin, M.D.W., 2011. Diagnostics for amyloid fibril formation: Where to begin? In A. F. Hill, K. J. Barnham, S. P. Bottomley, & R. Cappai, eds. *Protein Folding, Misfolding, and Disease*. Totowa, NJ: Humana Press, pp. 121–136.

Hatters, D.M., Lindner, R.A., Carver, J.A. & Howlett, G.J., 2001. The molecular chaperone, α-crystallin, inhibits amyloid formation by apolipoprotein C-II. *Journal of Biological Chemistry*, 276(36), pp.33755–33761.

Hauser, C.A.E. & Zhang, S., 2010. Designer self-assembling peptide nanofiber biological materials. *Chemical Society Reviews*, 39(8), pp.2780-2790.

Healy, J., Wong, K., Roux, C., Domigan, L., Sunde, M., Gerrard, J.A. & Vasudevamurthy, M., 2012. Polymorphism and higher ordered structures of protein nanofibres from crude mixtures of fish lens crystallins: Towards useful materials. *Accepted to Biopolymers*.

Hearing, V.J., 2000. The melanosome: the perfect model for cellular responses to the environment. *Pigment Cell Research / Sponsored by the European Society for Pigment Cell Research and the International Pigment Cell Society*, 13(Suppl 8), pp.23–34.

Hershko, A. & Ciechanover, A., 1998. The ubiquitin system. *Annual Review of Biochemistry*, 67(1), pp.425–479.

Hong, D.-P. & Fink, A.L., 2005. Independent heterologous fibrillation of insulin and its B-chain peptide. *Biochemistry*, 44(50), pp.16701–16709.

Horwitz, J., 2003. Alpha-crystallin. *Experimental Eye Research*, 76(2), pp.145–153.

Howie, A.J. & Brewer, D.B., 2009. Optical properties of amyloid stained by Congo red: History and mechanisms. *Micron*, 40(3), pp.285–301.

Iconomidou, V.A., Vriend, G. & Hamodrakas, S.J., 2000. Amyloids protect the silkmoth oocyte and embryo. *FEBS Letters*, 479(3), pp.141–145.

Isin, E.M. & Guengerich, F.P., 2007. Complex reactions catalyzed by cytochrome P450 enzymes. *Biochimica Et Biophysica Acta*, 1770(3), pp.314–329.

Jahangiri, E., Agharafeie, R., Kaiser, H.-J., Tahmasbi, Y., Legge, R.L. & Haghbeen, K., 2012. Medium engineering to enhance mushroom tyrosinase stability. *Biochemical Engineering Journal*, 60, pp.99–105.

Jahn, T.R. & Radford, S.E., 2008. Folding versus aggregation: Polypeptide conformations on competing pathways. *Archives of Biochemistry and Biophysics*, 469(1), pp.100–117.

Jahn, T.R. & Radford, S.E., 2005. The yin and yang of protein folding. *FEBS Journal*, 272(23), pp.5962–5970.

Jakob, U., Gaestel, M., Engel, K. & Buchner, J., 1993. Small heat shock proteins are molecular chaperones. *Journal of Biological Chemistry*, 268(3), pp.1517–1520.

Jen, A.C., Wake, M.C. & Mikos, A.G., 1996. Review: Hydrogels for cell immobilization. *Biotechnology and Bioengineering*, 50(4), pp.357–364.

Jia, H., Zhu, G., Vugrinovich, B., Kataphinan, W., Reneker, D.H. & Wang, P., 2002. Enzyme-carrying polymeric nanofibers prepared *via* electrospinning for use as unique biocatalysts. *Biotechnology Progress*, 18(5), pp.1027–1032.

de Jong, W.W., Caspers, G.-J. & Leunissen, J.A.M., 1998. Genealogy of the α-crystallin small heat-shock protein superfamily. *International Journal of Biological Macromolecules*, 22(3-4), pp.151–162.

Jönsson, B. & Wennerström, H., 1978. Diffusion control in reversible enzyme reactions. Applications to carbonic anhydrase. *Biophysical Chemistry*, 7(4), pp.285–292.

Keasling, J.D., 2008. Synthetic biology for synthetic chemistry. *Chemical Biology*, 3(1), pp.64–76.

Kim, J., Grate, J.W. & Wang, P., 2008. Nanobiocatalysis and its potential applications. *Trends in Biotechnology*, 26(11), pp.639–646.

Kim, J., Grate, J.W. & Wang, P., 2006. Nanostructures for enzyme stabilization. *Chemical Engineering Science*, 61(3), pp.1017–1026.

Kim, S., Bae, S.Y., Lee, B.Y. & Kim, T.D., 2012. Coaggregation of amyloid fibrils for the preparation of stable and immobilized enzymes. *Analytical Biochemistry*, 421(2), pp.776–778.

Kirschner, D.A., Abraham, C. & Selkoe, D.J., 1986. X-ray diffraction from intraneuronal paired helical filaments and extraneuronal amyloid fibers in Alzheimer disease indicates cross-β conformation. *Proceedings of the National Academy of Sciences of the United States of America*, 83(2), pp.503–507.

Knowles, T.P.J. & Buehler, M.J., 2011. Nanomechanics of functional and pathological amyloid materials. *Nature Nanotechnology*, 6(8), pp.469–479.

Koga, H., Kaushik, S. & Cuervo, A.M., 2011. Protein homeostasis and aging: The importance of exquisite quality control. *Ageing Research Reviews*, 10(2), pp.205–215.

Koudelka, T., Dehle, F.C., Musgrave, I.F., Hoffmann, P. & Carver, J.A., 2012. Methionine Oxidation Enhances κ-Casein Amyloid Fibril Formation. *Journal of Agricultural and Food Chemistry*, 60(16), pp.4144–4155.

Krajewska, B., 2004. Application of chitin-and chitosan-based materials for enzyme immobilizations: A review. *Enzyme and Microbial Technology*, 35(2-3), pp.126–139.

Labrou, N.E., 2010. Random mutagenesis methods for *in vitro* directed enzyme evolution. *Current Protein & Peptide Science*, 11(1), pp.91–100.

LeVine III, H., 1999. Quantification of β-sheet amyloid fibril structures with thioflavin T. *Methods in Enzymology*, 309, pp.274–284.

Li, Q.S., Ogawa, J., Schmid, R.D. & Shimizu, S., 2001. Engineering cytochrome P450 BM-3 for oxidation of polycyclic aromatic hydrocarbons. *Applied and Environmental Microbiology*, 67(12), pp.5735–5739.

Liang, Y., Lynn, D.G. & Berland, K.M., 2010. Direct observation of nucleation and growth in amyloid self-assembly. *Journal of the American Chemical Society*, 132(18), pp.6306–6308.

Lin, J.-H., Chen, C.-S., Rümmeli, M.H. & Zeng, Z.-Y., 2010. Self-assembly formation of multi-walled carbon nanotubes on gold surfaces. *Nanoscale*, 2(12), pp.2835–2840.

Luheshi, L.M. & Dobson, C.M., 2009. Bridging the gap: From protein misfolding to protein misfolding diseases. *FEBS Letters*, 583(16), pp.2581–2586.

Lutz, S., 2010. Beyond directed evolution—semi-rational protein engineering and design. *Current Opinion in Biotechnology*, 21(6), pp.734–743.

Mackay, J.P., Matthews, J.M., Winefield, R.D., Mackay, L.G., Haverkamp, R.G. & Templeton, M.D., 2001. The hydrophobin EAS is largely unstructured in solution and functions by forming amyloid-like structures. *Structure*, 9(2), pp.83–91.

MacPhee, C.E. & Dobson, C.M., 2000. Formation of mixed fibrils demonstrates the generic nature and potential utility of amyloid nanostructures. *Journal of the American Chemical Society*, 122(51), pp.12707–12713.

MacPhee, C.E. & Woolfson, D.N., 2004. Engineered and designed peptide-based fibrous biomaterials. *Current Opinion in Solid State and Materials Science*, 8(2), pp.141–149.

Marks, M.S. & Seabra, M.C., 2001. The melanosome: Membrane dynamics in black and white. *Nature Reviews Molecular Cell Biology*, 2(10), pp.738–748.

Mateo, C., Palomo, J.M., Fernandez-Lorente, G., Guisan, J.M. & Fernandez-Lafuente, R., 2007. Improvement of enzyme activity, stability and selectivity *via* immobilization techniques. *Enzyme and Microbial Technology*, 40(6), pp.1451–1463.

Meehan, S., Berry, Y., Luisi, B., Dobson, C.M., Carver, J.A. & MacPhee, C.E., 2004. Amyloid fibril formation by lens crystallin proteins and its implications for cataract formation. *Journal of Biological Chemistry*, 279(5), pp.3413–3419.

Mishra, R. & Winter, R., 2008. Cold- and pressure-induced dissociation of protein aggregates and amyloid fibrils. *Angewandte Chemie (International ed. in English)*, 47(35), pp.6518–6521.

Moehlenbrock, M.. J. & Minteer, S.D., 2011. Introduction to the field of enzyme immobilization and stabilization. *Methods in Molecular Biology*, 679, pp.1–7.

Naiki, H., Hashimoto, N., Suzuki, S., Kimura, H., Nakakuki, K. & Gejyo, F., 1997. Establishment of a kinetic model of dialysis-related amyloid fibril extension in vitro. *Amyloid*, 4(4), pp.223–232.

Nayak, A., Sorci, M., Krueger, S. & Belfort, G., 2009. A universal pathway for amyloid nucleus and precursor formation for insulin. *Proteins: Structure, Function, and Bioinformatics*, 74(3), pp.556–565.

Nejadnik, M.R., Deepak, F.L. & Garcia, C.D., 2011. Adsorption of glucose oxidase to 3-D scaffolds of carbon nanotubes: Analytical applications. *Electroanalysis*, 23(6), pp.1462–1469.

Nelson, R., Sawaya, M.R., Balbirnie, M., Madsen, A.O., Riekel, C., Grothe, R. & Eisenberg, D., 2005. Structure of the cross-β spine of amyloid-like fibrils. *Nature*, 435(7043), pp.773–778.

Nerelius, C., Fitzen, M. & Johansson, J., 2010. Amino acid sequence determinants and molecular chaperones in amyloid fibril formation. *Biochemical and Biophysical Research Communications*, 396(1), pp.2–6.

Ni, Y., Liu, Y., Schwaneberg, U., Zhu, L., Li, N., Li, L. & Sun, Z., 2011. Rapid evolution of arginine deiminase for improved anti-tumor activity. *Applied Microbiology and Biotechnology*, 90(1), pp.193–201.

Nielsen, L., Khurana, R., Coats, A., Frokjaer, S., Brange, J., Vyas, S., Uversky, V.N. & Fink, A.L., 2001. Effect of environmental factors on the kinetics of insulin fibril formation: Elucidation of the molecular mechanism. *Biochemistry*, 40(20), pp.6036–6046.

Nilsson, M.R., 2004. Techniques to study amyloid fibril formation in vitro. *Methods*, 34(1), pp.151–160.

Onuchic, J.N. & Wolynes, P.G., 2004. Theory of protein folding. *Current Opinion in Structural Biology*, 14(1), pp.70–75.

Ortiz, C., Zhang, D., Ribbe, A.E., Xie, Y. & Ben-Amotz, D., 2007. Analysis of insulin amyloid fibrils by Raman spectroscopy. *Biophysical Chemistry*, 128(2-3), pp.150–155.

Paparcone, R., Cranford, S.W. & Buehler, M.J., 2011. Self-folding and aggregation of amyloid nanofibrils. *Nanoscale*, 3(4), pp.1748–1755.

Parajuli, N. & Williams, G.J., 2011. A high-throughput screen for directed evolution of aminocoumarin amide synthetases. *Analytical Biochemistry*, 419(1), pp.61–66.

Pedersen, J.S. & Otzen, D.E., 2008. Amyloid - A state in many guises: Survival of the fittest fibril fold. *Protein Science*, 17(1), pp.2–10.

Pilkington, S.M., Roberts, S.J., Meade, S.J. & Gerrard, J.A., 2010. Amyloid fibrils as a nanoscaffold for enzyme immobilization. *Biotechnology Progress*, 26(1), pp.93–100.

Ping, W., 2006. Nanoscale biocatalyst systems. *Current Opinion in Biotechnology*, 17(6), pp.574–579.

Polizzi, K.M., Bommarius, A.S., Broering, J.M. & Chaparro-Riggers, J.F., 2007. Stability of biocatalysts. *Current Opinion in Chemical Biology*, 11(2), pp.220–225.

Quin, M.B. & Schmidt-Dannert, C., 2011. Engineering of biocatalysts: From evolution to creation. *Catalysis*, 1(9), pp.1017–1021.

Raman, B., Ban, T., Sakai, M., Pasta, S.Y., Ramakrishna, T., Naiki, H., Goto, Y. & Rao, C.M., 2005. αB-crystallin, a small heat-shock protein, prevents the amyloid fibril growth of an amyloid β-peptide and β2-microglobulin. *Biochemical Journal*, 392(3), p.573.

Rao, S.P., Meade, S.J., Healy, J.P., Sutton, K.H., Larsen, N.G., Staiger, M.P. & Gerrard, J.A., 2012. Amyloid fibrils as functionalizable components of nanocomposite materials. *Biotechnology Progress*, 28(1), pp.248–256.

Rao, S.P., Meade, S.J., Joyce, N.I., Healy, J.P., Sutton, K.H., Larsen, N.G. & Gerrard, J.A., 2011. Amyloid fibril formation from crude protein mixtures. *Biotechnology Progress*, 27(6), pp.1768–1776.

Reddy, G.B., Reddy, P.Y., Vijayalakshmi, A., Kumar, M.S., Suryanarayana, P. & Sesikeran, B., 2002. Effect of long-term dietary manipulation on the aggregation of rat lens crystallins: Role of alpha-crystallin chaperone function. *Molecular Vision*, 8, pp.298–305.

Rekas, A., Adda, C.G., Andrew Aquilina, J., Barnham, K.J., Sunde, M., Galatis, D., Williamson, N.A., Masters, C.L., Anders, R.F., Robinson, C.V., Cappai, R. & Carver, J.A., 2004. Interaction of the molecular chaperone αB-crystallin with α-synuclein: Effects on amyloid fibril formation and chaperone activity. *Journal of Molecular Biology*, 340(5), pp.1167–1183.

Rekas, A., Jankova, L., Thorn, D.C., Cappai, R. & Carver, J.A., 2007. Monitoring the prevention of amyloid fibril formation by α-crystallin. *FEBS Journal*, 274(24), pp.6290–6304.

Rizzo, A., Solin, N., Lindgren, L.J., Andersson, M.R. & Inganäs, O., 2010. White light with phosphorescent protein fibrils in OLEDs. *Nano Letters*, 10(6), pp.2225–2230.

Ron, D. & Walter, P., 2007. Signal integration in the endoplasmic reticulum unfolded protein response. *Nature Reviews Molecular Cell Biology*, 8(7), pp.519–529.

Rubenwolf, S., Kerzenmacher, S., Zengerle, R. & von Stetten, F., 2011. Strategies to extend the lifetime of bioelectrochemical enzyme electrodes for biosensing and biofuel cell applications. *Applied Microbiology and Biotechnology*, 89(5), pp.1315–1322.

Saab-Rincón, G., Olvera, L., Olvera, M., Rudiño-Piñera, E., Benites, E., Soberón, X. & Morett, E., 2012. Evolutionary walk between $(\beta/\alpha)_8$ barrels: Catalytic migration from triosephosphate isomerase to thiamin phosphate synthase. *Journal of Molecular Biology*, 416(2), pp.255–270.

Sabate, R., De Groot, N.S. & Ventura, S., 2010. Protein folding and aggregation in bacteria. *Cellular and Molecular Life Sciences*, 67(16), pp.2695–2715.

Sakono, M., Akiyama, S., Zako, T., Sakaki, S., Waku, T., Tanaka, N. & Maeda, M., 2011. Application of two morphologically different fibrillar and filamentous insulin amyloids as a biomaterial for cell culture surfaces. *Reactive and Functional Polymers*, 71(3), pp.324–328.

Saltiel, A.R. & Kahn, C.R., 2001. Insulin signalling and the regulation of glucose and lipid metabolism. *Nature*, 414(6865), pp.799–806.

Scanlon, S. & Aggeli, A., 2008. Self-assembling peptide nanotubes. *Nano Today*, 3(3-4), pp.22–30.

Scheibel, T., Parthasarathy, R., Sawicki, G., Lin, X.-M., Jaeger, H. & Lindquist, S.L., 2003. Conducting nanowires built by controlled self-assembly of amyloid fibers and selective metal deposition. *Proceedings of the National Academy of Sciences*, 100(8), pp.4527–4532.

Schmidt, M., Sachse, C., Richter, W., Xu, C., Fändrich, M. & Grigorieff, N., 2009. Comparison of Alzheimer Aβ(1–40) and Aβ(1–42) amyloid fibrils reveals similar protofilament structures. *Proceedings of the National Academy of Sciences*, 106(47), pp.19813–19818.

Schmit, J.D., Ghosh, K. & Dill, K., 2011. What drives amyloid molecules to assemble into oligomers and fibrils? *Biophysical Journal*, 100(2), pp.450–458.

Seeman, N.C., 2002. Emulating biology: Building nanostructures from the bottom up. *Proceedings of the National Academy of Sciences*, 99(2), pp.6451–6455.

Serio, T.R., Cashikar, A.G., Kowal, A.S., Sawicki, G.J., Moslehi, J.J., Serpell, L.C., Arnsdorf, M.F. & Lindquist, S.L., 2000. Nucleated conformational conversion and the replication of conformational information by a prion determinant. *Science*, 289(5483), pp.1317–1321.

Serpell, L.C. & Smith, J.M., 2000. Direct visualisation of the β-sheet structure of synthetic Alzheimer's amyloid. *Journal of Molecular Biology*, 299(1), pp.225–231.

Serpell, L.C., Sunde, M., Benson, M.D., Tennent, G.A., Pepys, M.B. & Fraser, P.E., 2000. The protofilament substructure of amyloid fibrils. *Journal of Molecular Biology*, 300(5), pp.1033–1039.

Shammas, S.L., Waudby, C.A., Wang, S., Buell, A.K., Knowles, T.P.J., Ecroyd, H., Welland, M.E., Carver, J.A., Dobson, C.M. & Meehan, S., 2011. Binding of the molecular chaperone αB-crystallin to Aβ amyloid fibrils inhibits fibril elongation. *Biophysical Journal*, 101(7), pp.1681–1689.

Sharma, S. & Yamazaki, H., 1984. Preparation of hydrophobic cotton cloth. *Biotechnology Letters*, 6(5), pp.301–306.

Sheldon, R.A., 2007. Enzyme immobilization: The quest for optimum performance. *Advanced Synthesis & Catalysis*, 349(8-9), pp.1289–1307.

Sheldon, R.A. & Rantwijk, F. van, 2004. Biocatalysis for sustainable organic synthesis. *Australian Journal of Chemistry*, 57(4), pp.281–289.

Shi, D., 2006. *Introduction to Biomaterials*, Beijing, China: World Scientific Publishing Company.

Siegel, J.B., Zanghellini, A., Lovick, H.M., Kiss, G., Lambert, A.R., St.Clair, J.L., Gallaher, J.L., Hilvert, D., Gelb, M.H., Stoddard, B.L., Houk, K.N., Michael, F.E. & Baker, D., 2010. Computational design of an enzyme catalyst for a stereoselective bimolecular Diels-Alder reaction. *Science*, 329(5989), pp.309–313.

Silman, I.H. & Katchalski, E., 1966. Water-insoluble derivatives of enzymes, antigens, and antibodies. *Annual Review of Biochemistry*, 35(1), pp.873–908.

Smith, J.F., Knowles, T.P.J., Dobson, C.M., MacPhee, C.E. & Welland, M.E., 2006. Characterization of the nanoscale properties of individual amyloid fibrils. *Proceedings of the National Academy of Sciences*, 103(43), pp.15806–15811.

Spahn, C. & Minteer, S.D., 2008. Enzyme immobilization in biotechnology. *Recent Patents on Engineering*, 2(3), pp.195–200.

Stine, K.J., Jefferson, K. & Shulga, O.V., 2011. Nanoporous gold for enzyme immobilization. *Methods in Molecular Biology (Clifton, N.J.)*, 679, pp.67–83.

Sunde, M. & Blake, C.C.F., 1997. The structure of amyloid fibrils by electron microscopy and X-ray diffraction. *Advances in Protein Chemistry*, Volume 50, pp.123–159.

Sunde, M., Serpell, L.C., Bartlam, M., Fraser, P.E., Pepys, M.B. & Blake, C.C.F., 1997. Common core structure of amyloid fibrils by synchrotron X-ray diffraction. *Journal of Molecular Biology*, 273(3), pp.729–739.

Tang, Q., Solin, N., Lu, J. & Inganäs, O., 2010. Hybrid bioinorganic insulin amyloid fibrils. *Chemical Communications*, 46(23), pp.4157–4159.

Tasis, D., Tagmatarchis, N., Bianco, A. & Prato, M., 2006. Chemistry of carbon nanotubes. *Chemical Reviews*, 106(3), pp.1105–1136.

Tran, D.N. & Balkus, K.J., 2011. Perspective of recent progress in immobilization of enzymes. *ACS Catalysis*, 1(8), pp.956–968.

Tu, R.S. & Tirrell, M., 2004. Bottom-up design of biomimetic assemblies. *Advanced Drug Delivery Reviews*, 56(11), pp.1537–1563.

Twyman, R.M., 2005. Immobilized enzymes. In *Encyclopedia of Analytical Science*. London, UK: Elsevier Science, pp. 523–529.

Tycko, R., 2006. Molecular structure of amyloid fibrils: Insights from solid-state NMR. *Quarterly Reviews of Biophysics*, 39(01), pp.1–55.

Tycko, R., 2011. Solid-state NMR studies of amyloid fibril structure. *Annual Review of Physical Chemistry*, 62(1), pp.279–299.

Tyedmers, J., Mogk, A. & Bukau, B., 2010. Cellular strategies for controlling protein aggregation. *Nature Reviews Molecular Cell Biology*, 11(11), pp.777–788.

Urlacher, V.B. & Eiben, S., 2006. Cytochrome P450 monooxygenases: Perspectives for synthetic application. *Trends in Biotechnology*, 24(7), pp.324–330.

Uversky, V.N., Li, J., Souillac, P., Millett, I.S., Doniach, S., Jakes, R., Goedert, M. & Fink, A.L., 2002. Biophysical properties of the synucleins and their propensities to fibrillate. *Journal of Biological Chemistry*, 277(14), pp.11970–11978.

Vidal, O., Longin, R., Prigent-Combaret, C., Dorel, C., Hooreman, M. & Lejeune, P., 1998. Isolation of an Escherichia coli K-12 mutant strain able to form biofilms on inert surfaces: Involvement of a new ompR allele that increases curli expression. *Journal of Bacteriology*, 180(9), pp.2442–2449.

Wang, J. & Lin, Y., 2008. Functionalized carbon nanotubes and nanofibers for biosensing applications. *Trends in Analytical Chemistry*, 27(7), pp.619–626.

Wang, J., Martin, E., Gonzales, V., Borchelt, D.R. & Lee, M.K., 2008. Differential regulation of small heat shock proteins in transgenic mouse models of neurodegenerative diseases. *Neurobiology of Aging*, 29(4), pp.586–597.

Wang, P., 2006. Nanoscale biocatalyst systems. *Current Opinion in Biotechnology*, 17(6), pp.574–579.

Waterhouse, S.H. & Gerrard, J.A., 2004. Amyloid fibrils in bionanotechnology. *Australian Journal of Chemistry*, 57(6), pp.519–523.

Waugh, D.F., 1946. A fibrous modification of insulin. I. The heat precipitate of insulin. *Journal of the American Chemical Society*, 68(2), pp.247–250.

Westermark, G., Johnson, K.H. & Westermark, P., 1999. Amyloid, prions, and other protein aggregates R. Wetzel, ed. *Staining methods for identification of amyloid in tissue*, 309(1922), pp.3–25.

Wolynes, P.G., 2005. Energy landscapes and solved protein-folding problems. *Philosophical Transactions. Series A, Mathematical, Physical, and Engineering Sciences*, 363(1827), pp.453–464; discussion 464–467.

Wong, Y.Q., Binger, K.J., Howlett, G.J. & Griffin, M.D.W., 2010. Methionine oxidation induces amyloid fibril formation by full-length apolipoprotein A-I. *Proceedings of the National Academy of Sciences of the United States of America*, 107(5), pp.1977–1982.

Woolfson, D.N. & Mahmoud, Z.N., 2010. More than just bare scaffolds: Towards multi-component and decorated fibrous biomaterials. *Chemical Society Reviews*, 39(9), pp.3464–3479.

Wösten, H.A.B., van Wetter, M.-A., Lugones, L.G., van der Mei, H.C., Busscher, H.J. & Wessels, J.G.H., 1999. How a fungus escapes the water to grow into the air. *Current Biology*, 9(2), pp.85–88.

Wu, C., Bai, S., Ansorge-Schumacher, M.B. & Wang, D., 2011. Nanoparticle cages for enzyme catalysis in organic media. *Advanced Materials*, 23(47), pp.5694–5699.

Zaborsky, O.R., 1973. *Immobilized enzymes* 3rd ed., The University of Michigan: CRC Press.

Zhang, S., 2003. Fabrication of novel biomaterials through molecular self-assembly. *Nature Biotechnology*, 21(10), pp.1171–1178.

Chapter Two

2 Purification and characterisation of proteins

2.1 Introduction

The biomolecules employed in this thesis were organophosphate hydrolase, cytochrome $P450_{BM3}$, glucose oxidase, green fluorescent protein, and tobacco etch virus protease. All of the above proteins required recombinant expression and purification, apart from glucose oxidase, which was purchased commerically as a lyophilised powder from Sigma-Aldrich.

The proteins purified ranged in size from ~27-175 kDa, included monomeric and dimeric quaternary structures, and are made up of a hydrolase, hydroxylase, oxido-reductase and a cysteine protease. Utilising a diverse range of proteins was an important requirement in this research to be able to stringently test amyloid fibrils as a versatile nanoscaffold for biomolecule immobilisation. The results of the biomolecule immobilisation to the amyloid fibril nanoscaffold will be covered in chapters three and five.

2.2 Organophosphate hydrolase (OPH)

OPH (EC number 3.1.8.1) catalyses the hydrolysis of organophosphates (OP), including the pesticide, paraoxon and the nerve agents Soman, Sarin and VX (Dumas *et al.* 1989; Hill *et al.* 2003). OP are among the most toxic compounds synthesised to date (Mulchandani *et al.* 1998a). Their toxicity to humans relates to their ability to irreversibly inhibit acetylcholinesterase, a key enzyme required for a proper functioning nervous system (Ghanem & Raushel 2005).

Accidental exposure to OP pesticide compounds is responsible for an estimated 200,000 deaths annually in developing countries (Eddleston 2000). There is also evidence to suggest that chronic exposure to OP pesticides can cause long-term health problems (De Silva *et al.* 2006). Additionally, OP remain potential chemical warfare agents (Rebmann *et al.* 2009), thus methods to eliminate OP from the environment, and decontaminate in the event of a chemical attack, are urgently needed.

OPH is a homodimer with a 'TIM' (α/β_8)-barrel structure containing a binuclear metal binding site located at the C-terminus (Benning *et al.* 1994; Yang *et al.* 2003). OPH natively contains two zinc ions linked by a bridging hydroxide ion and the side-chain oxygens of a carboxylated Lys169 (Omburo *et al.* 1992). The reaction mechanism of OPH has been extensively studied and the proposed mechanism by Kim *et al.* (2008) as supported by crystallography using a bound product analogue, and density function theory, show strong evidence that the bridging hydroxide acts as a direct nucleophile for the hydrolysis of organophosphates (Kim *et al.* 2008). The zinc ions can be replaced with nickel, cobalt, manganese and cadmium, with Co^{2+}/Co^{2+}-OPH giving the highest activity, whilst Zn^{2+}/Zn^{2+}-OPH being the most stable (Rochu *et al.* 2004). Due to the stability problems associated with recombinantly expressed proteins the Zn^{2+}/Zn^{2+}-OPH was used in this research.

OPH was used in this research because it is an enzyme that has enormous potential applications in the bioremediation, biosensing and detoxification of OP warfare agents and pesticides (Ghanem & Raushel 2005; Yair *et al.* 2008; Mulchandani *et al.* 1998b). The problem with OPH is that it suffers from stability and reusability issues for use in industrial applications (Kanugula *et al.* 2011), and could therefore potentially benefit from being immobilised to an amyloid fibril nanoscaffold.

In this thesis the S5 mutant of OPH is used. The S5 mutant contains three active point mutants, R319S, K185R, D208G, and four silent mutations (Roodveldt & Tawfik 2005). The S5 mutant was chosen because of the 20-fold increase in functional expression it provides compared to the wild-type enzyme. The increase in functional expression was found to be because of stabilisation of the apo-enzyme. The S5 mutant was a kind gift from Dan Tawfik, Weizmann Institute.

2.2.1 OPH purification

E. coli XL-1 blue competent cells were transformed (section 7.3.4) with the pMAL-c2x plasmid containing the gene for S5-OPH for amplification. Once it was established *via* restriction digest (section 7.3.3) that the correct construct was present (**Figure 2.1**), *E. coli* BL21 (DE3) star competent cells were transformed (section 7.3.5) with the pMAL-c2x plasmid for overexpression of the recombinant protein.

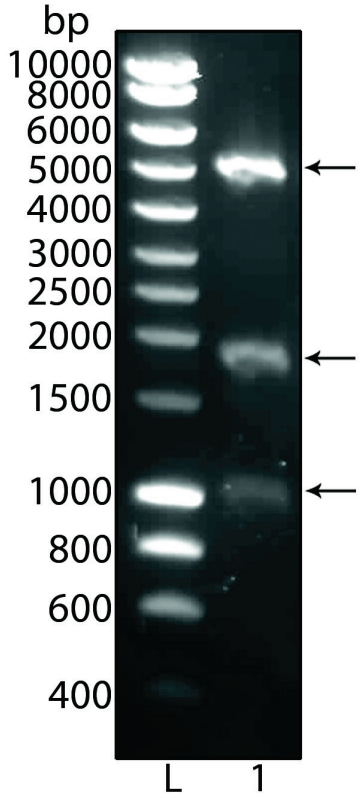

Figure 2.1 *Agarose gel of the restriction digest of pMAL-c2x-S5 by Hind III, Eco RI, and Eco RV. L – ladder, lane 1 – digest fragments. The arrows are pointing to the digest bands which are of the predicted 1 kb, 1.9 ka, and 5 ka sizes for the pMAL-c2x-S5 plasmid.*

Purification was based on the methods of Roodveldt & Tawfik (2005) which took advantage of the C-terminal maltose binding protein (MBP) (section 7.4.2). MBP is a fusion protein which is highly soluble and acts as a molecular chaperone accumulating the fusion protein in the periplasm (Kapust & Waugh 1999; Nikaido 1994). MBP allows an easy one-step affinity chromatography purification method using an amylose resin (Hennig & Schäfer 1998). Initially it was decided not to cleave the MBP from OPH because it had previously been shown that the fusion enzyme had similar activity to the wild type enzyme, and the MBP offered more potential binding sites for immobilisation to the amyloid fibril scaffold (section 4.3) (Roodveldt & Tawfik 2005).

Figure 2.2 shows an SDS-PAGE gel of the purification procedure, with the eluted OPH (~77 kDa) the major protein in the extract. The average quantity of OPH attained from each litre was ~30 mg. The specific activity of the protein was 0.013 µmol/sec/mg for the hydrolysis of paraoxon, measured by monitoring the initial rate of reaction as discussed in sections 2.2.2 and 7.9.1.

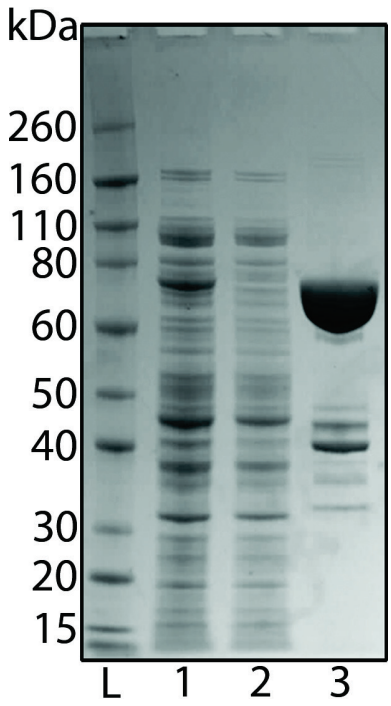

Figure 2.2 *SDS-PAGE gel of a typical OPH preparation. L – ladder, lane 1 – crude cell free extract, lane 2 – wash fraction, lane 3 – eluted protein.*

Cleavage of the MBP used factor Xa protease. The cleavage reaction was carried out as stated in the Novagen® factor Xa kit instructions (section 7.4.3). **Figure 2.3** shows the cleavage of the MBP-OPH fusion protein. The expected M_w of OPH-MBP is ~77 kDa, and once cleaved, MBP has an expected M_w of ~42 kDa, and OPH has an expected M_w of ~35 kDa. The SDS-PAGE gel shows that full cleavage of the MBP-OPH fusion protein occurs (lanes 5 and 6). Lane 1 is the cleavage control reaction that is done to ensure the factor Xa is active. Factor Xa is active if the control protein with a M_w ~53 kDa is cleaved into two bands of M_w ~17 kDa and ~35 kDa. These two bands are faintly visible in lane one. The control OPH solution (lane 2) shows that there is already a small amount of cleavage occurring in the protein solution in the absence of factor Xa. This could be attributed to a small amount of protease present. The protein band at ~40 kDa is regularly seen when using a MBP tag (Nallamsetty *et al.* 2005), and is thought to be a proteolytic MBP product due to the elution with MBP from the amylose column (lane 7).

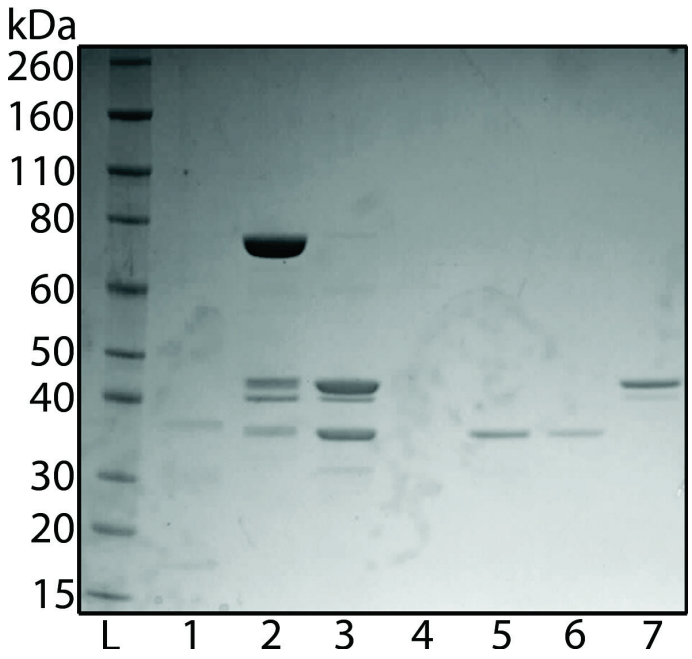

Figure 2.3 *SDS-PAGE gel showing the cleavage of OPH-MBP. L – ladder, lane 1 – cleavage control reaction from factor Xa kit, lane 2 – OPH-MBP pre cleavage, lane 3 – OPH and MBP post cleavage, lane 4 – peak one (Factor Xa) from purification with the amylose column, lane 5 – peak two (OPH) from purification with the amylose column, lane 6 – OPH after using Xarrest™ agarose to bind Factor Xa, lane 7 – eluted MBP from amylose column.*

2.2.2 OPH characterisation

The substrate specificity of OPH is very broad. The best substrate identified thus far is paraoxon, which OPH can catalyse at rates approaching the limits of diffusion (Caldwell *et al.* 1991). The hydrolysis of paraoxon is shown in **Figure 2.4**. The enzymatic hydrolysis of paraoxon to form diethyl phosphate and *p*-nitrophenol can be assayed by monitoring the absorbance of *p*-nitrophenol at 405 nm (section 7.9.1) (Donarski *et al.* 1989). This assay was routinely used in this research for the accurate measurement of initial rates of samples containing OPH.

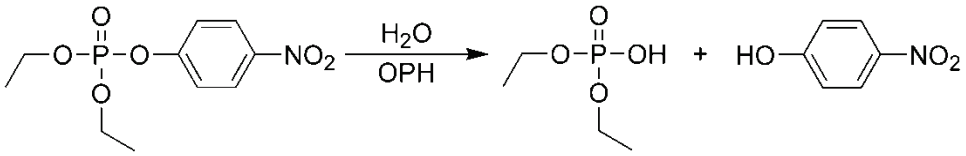

Figure 2.4 *The hydrolysis of paraoxon to diethyl phosphate and p-nitrophenol, as catalysed by OPH. Adapted from Donarski et al. (1989).*

Table 2.1 shows the published and experimentally determined kinetic parameters for wild-type OPH, S5-OPH-MBP, and S5-OPH. The experimental steady-state kinetic parameters were investigated by measurement of initial rates at varied paraoxon concentration, using the paraoxon assay described in section 7.9.1 (Dumas *et al.* 1989). The resulting data were analysed by non-linear curve fitting using the EnzFitter program (Biosoft, Cambrige), allowing determination of K_m and k_{cat} values. The published and experimental data correspond nicely, and show that the MBP fusion tag does not have any significant effect on the catalytic properties of OPH. Because the MPB was not hindering the activity of OPH, it was initially not cleaved from OPH.

Table 2.1 *Literature and experimental kinetic values for OPH hydrolysis of paraoxon.*

Sample	K_m (µM)	k_{cat} (s^{-1})
Wild-type OPH[a]	35	2280
S5-MPB-OPH[b]	54 ± 6	2150 ± 217
S5-MPB-OPH experimental	39 ± 5	2310 ± 146
S5-OPH experimental	98 ± 25	3465 ± 579

[a] Kinetic parameters for wild-type were determined by Hong & Raushel (1999)
[b] Kinetic parameters for S5-MBP-OPH were determined by Roodveldt & Tawfik (2005)

The thermostability of MBP-OPH and OPH was determined by differential scanning fluorimetry (DSF) (section 7.2.7). As can be seen in **Table 2.2** the T_m (°C) of the cleaved OPH was 2 °C higher than the MBP-OPH fusion protein. This information will be relevant when OPH is immobilised to amyloid fibrils and tested for changes in the thermostability of immobilised and in-solution OPH (section 4.4).

Table 2.2 *Melting temperature of OPH-MBP and OPH using DSF. The melting temperature was determined as the point of maximum inflection of the -dRFU/dT curve. Each sample was measured in triplicate and the error is the standard deviation of the mean.*

Sample	T_m (°C)	error
MBP-OPH	51.8	± 0.3
OPH	53.8	± 0.3

2.3 Cytochrome $P450_{BM3}$ (P450BM3)

Cytochrome P450s (EC number 1.14.14.1) are a hugely diverse super family found throughout all classes of life. P450s derive their name from the absorption maximum at 450 nm due to a Fe(II)-CO complex and an axial ligation with the cysteine thiolate of the enzyme (Omura & Sato 1964; Guengerich 1991).

Collectively, P450s catalyse a very diverse range of chemical reactions (Guengerich 2001). They recognise a broad range of both endogenous and exogenous substrates, such as steroid hormones in mammals, and herbicides in plants (Whitehouse *et al.* 2012). The substrate specificity of any given P450 largely depends on its primary function. For example, a P450 involved in steroid anabolism will have strict substrate specificity, whilst one that is involved in the oxidation of xenobiotics will have a broad substrate specificity, to protect an organism from as many different xenobiotics as possible (Guengerich 1991).

$$NAD(P)H + H^+ + O_2 + RH \rightarrow NADP^+ + H_2O + ROH \quad (1)$$

Collectively, P450s catalyse the reaction shown in reaction 1. This reaction uses molecular oxygen to incorporate one oxygen atom onto a substrate (R) and reduces the second oxygen to a water molecule (Furge & Guengerich 2006). The two electrons required are supplied by NAD(P)H *via* an electron transfer partner. There are two classes of P450s. The first class is the bacterial/mitochondrial P450s, which acquire the electrons required for the reaction from a NADH-dependent FAD-containing reductase *via* an iron-sulfur cluster of the [2Fe-2S] type. The second class are the microsomal P450s, which accept electrons from a microsomal NADPH-cytochrome P450 reductase (CPR), which contains FAD and FMN (McLean *et al.* 2005). There are non-microsomal examples of class two P450s such as $P450_{BM3}$ from *Bacillus megaterium.* $P450_{BM3}$ is a P450 fusion protein, containing both a CPR domain and oxygenase domain on the same polypeptide sequence and therefore is placed in the second class (Yun *et al.* 2007).

$P450_{BM3}$ is a 119 kDa fatty acid hydroxylase derived from *Bacillus megaterium.* It catalyses the sub-terminal hydroxylation of medium and long-chain fatty acids at the ω-1, ω-2 and ω-3 (Schwaneberg *et al.* 1999). $P450_{BM3}$ is a class two P450, containing both its reductase, and oxygenase domains on the same polypeptide. This fusion of the domains is accredited with affording the enzyme with the highest k_{cat} (285 s^{-1}, determined for NADPH oxidation) for the oxidation of arachidonic acid, out of any of the P450s discovered thus far (Noble *et al.* 1999). $P450_{BM3}$ also has the highest recombinant expression levels for any P450 reported for *E. coli* (12500 nmol L^{-1}) (Pflug *et al.* 2007). Combining these features with the large body of research already undertaken, make $P450_{BM3}$ one of the more attractive P450s for potential research applications (Munro *et al.* 2002).

Whilst the native reactions catalysed by $P450_{BM3}$ are not of any real research or commercial benefit, it has provided a very exciting template enzyme for the creation of variants that can catalyse more interesting chemical reactions (Julsing *et al.* 2008). One of the major uses of mutant $P450_{BM3}$ is in the creation of pharmaceutical metabolites to study the potential breakdown-products created from pharmaceuticals metabolised in humans (Vottero *et al.* 2011; van Vugt-Lussenburg *et al.* 2007). Kille *et al.* (2011) also created a mutant $P450_{BM3}$ capable of the regio- and stereo-selective oxidative hydroxylation of testosterone, a substrate not accepted by wild-type $P450_{BM3}$, a reaction that is very difficult to achieve by conventional synthetic organic chemistry (Newhouse & Baran 2011).

$P450_{BM3}$ was selected for use in this research, because of the potential applications of the enzyme in a range of biocatalytic applications, including: xenobiotic metabolism, pharmaceutical and chemical synthesis, and chemical detoxification (Gillam 2008). $P450_{BM3}$ is also the 'model' P450, being the most studied of the enzyme family, therefore is the logical choice when trying to employ any P450s for research purposes (Munro *et al.* 2002). Again, like OPH, $P450_{BM3}$ suffers from stability and reusability issues so could potentially benefit from immobilisation to an amyloid fibril nanoscaffold (Maurer *et al.* 2003).

2.3.1 $P450_{BM3}$ purification

E. coli BL21 (DE3) star competent cells were transformed with the pET28-BM3 plasmid containing the $P450_{BM3}$ gene for protein overexpression (section 7.3.5). The protocol employed for the purification of $P450_{BM3}$ was modified from the procedure published by Maurer *et al.* (2003) (section 7.5). The purification used a one step procedure, taking advantage of the poly-histidine tag, using nickel affinity chromatography. The protocol in section 7.5.2 resulted in the production of reasonably homogenous $P450_{BM3}$, as judged by SDS-PAGE (**Figure 2.5**). The protein band at ~119 kDa is the full $P450_{BM3}$ fusion, containing both the oxygenase and reductase domains. The protein band at ~55 kDa may be the oxygenase domain of $P450_{BM3}$ (Miles *et al.* 1992) that has been subjected to proteolytic cleavage. The poly-histidine tag is located on the oxygenase domain of $P450_{BM3}$, and this could explain why the domain eluted with the full length poly-histidine tagged $P450_{BM3}$. The yield for each purification was ~40 mg/L of culture, as judged by the NanoDrop (section 7.2.2).

To monitor the enzymatic activity of $P450_{BM3}$ a modified method based on Neeli *et al.* (2005) was used (section 7.9.2). Enzymatic activity of $P450_{BM3}$ toward the substrate lauric acid, was monitored by the rate of oxidation of NADPH (ε_{340} = 6220 M^{-1} cm^{-1}) (scheme 1), which strongly absorbs at 340 nm. Near saturating concentrations of NADPH (160 μM) and lauric acid (500 μM) were used in conjunction with ~45 nM of $P450_{BM3}$ to determine the initial rate of reaction. The initial rate of reaction for the purified protein was determined to be 0.79 μM NADPH/s^{-1} with a specific activity of 0.014 μmol $s^{-1}mg^{-1}$.

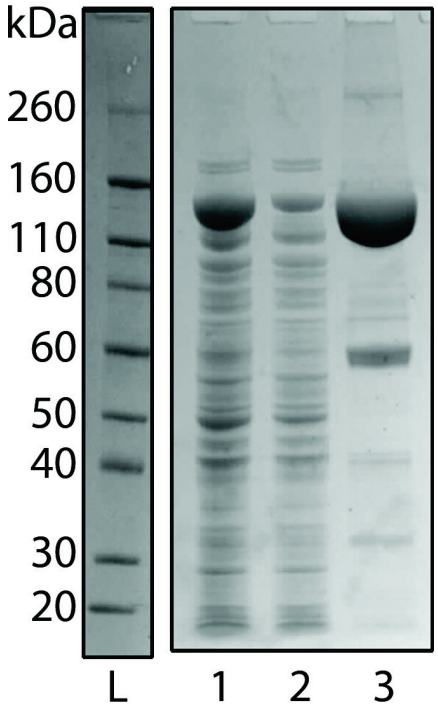

Figure 2.5 *SDS-PAGE gel of a typical $P450_{BM3}$ preparation. L – ladder, lane 1 – crude cell free extract, lane 2 – flow through when loading on the nickel affinity column, lane 3 – eluted protein.*

2.3.2 $P450_{BM3}$ characterisation

$P450_{BM3}$ secondary structure was characterised by circular dichroism (CD) spectroscopy to ensure correctly folded protein (section 7.2.15). The CD spectrum of purified $P450_{BM3}$ is shown in **Figure 2.6**, demonstrating that $P450_{BM3}$ does have a folded secondary structure in solution and that there is a double minima at approximately 208 and 222 nm, characteristic of a predominantly α-helical structure, and consistent with the literature (Munro *et al.* 1995).

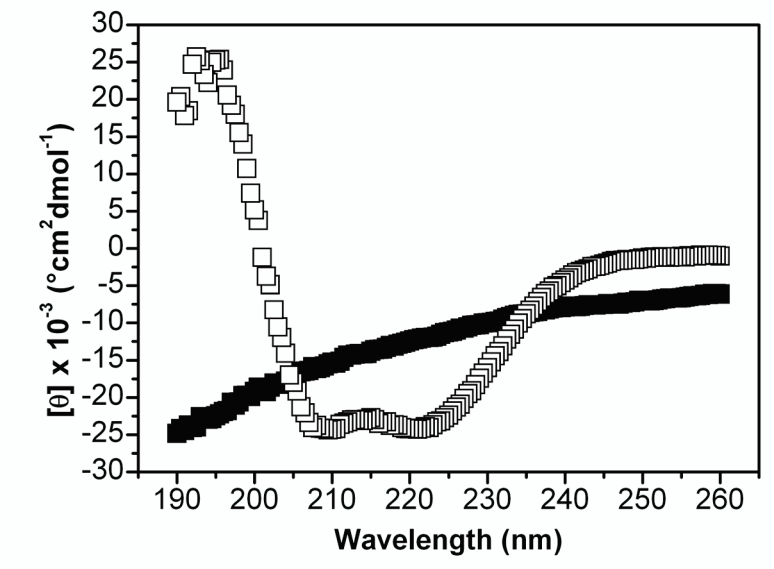

Figure 2.6 *Circular dichroism spectroscopy of $P450_{BM3}$ (□) and buffer control (■). The measurements were the average of three scans of each sample.*

2.4 Green fluorescent protein (GFP)

GFP from the jelly fish *Aequorea victoria* is a 238 amino acid, 27 kDa monomeric protein with intrinsic fluorescence (Prasher *et al.* 1992; Yang *et al.* 1996). The intrinsic fluorescence is derived from the primary amino acid sequence, through the cyclisation of a serine-dehydrotyrosine-glycine tri-peptide, to create a natural chromophore (Cody *et al.* 1993). GFP was used in this research to act as a fluorescent protein tag, to aid in the visualisation of the amyloid fibril nanoscaffold.

The biological function of GFP is thought to be a light induced electron donor (Bogdanov *et al.* 2009). GFP is co-expressed with aequorin, a protein that produces calcium triggered blue chemiluminescence, which can subsequently be absorbed by GFP and released as green fluorescent light (Morise *et al.* 1974). Wild-type GFP has an absorbance/excitation maximum at 398 nm with a smaller peak at 470 nm, and a fluorescence emission spectrum maximum at 509 nm, with a shoulder at 540 nm (Morise *et al.* 1974).

In this research, a red-shifted GFP mutant, enhanced GFP (eGFP), was used. eGFP contains two mutations in the chromophore region, F64L, and S65T, which give it a single absorbance/excitation peak at 488 nm and the same fluorescence emission spectrum maximum at 509 nm, but with a ~35 fold increase in the fluorescent intensity (Cormack *et al.* 1996). The mutations also give eGFP a much greater folding efficiency when produced recombinantly in *E. coli*.

2.4.1 Purification and characterisation of GFP

E. coli DH5α containing the pGEM GFP plasmid showed good expression levels of GFP, therefore this bacterium was used for the growth and recombinant expression of GFP. There was no fusion tag present to aid in purification, therefore, one step ion-exchange chromatography based on the methods of Yang *et al.* (1996) (section 7.6.2) was used. **Figure 2.7** shows a typical GFP purification analysed by SDS-PAGE. As can be seen in lane 1, most of the GFP was in the insoluble crude extract, but the yield (~7 mg/L culture) and purity of GFP (lane 8) was enough for the applications needed in this thesis.

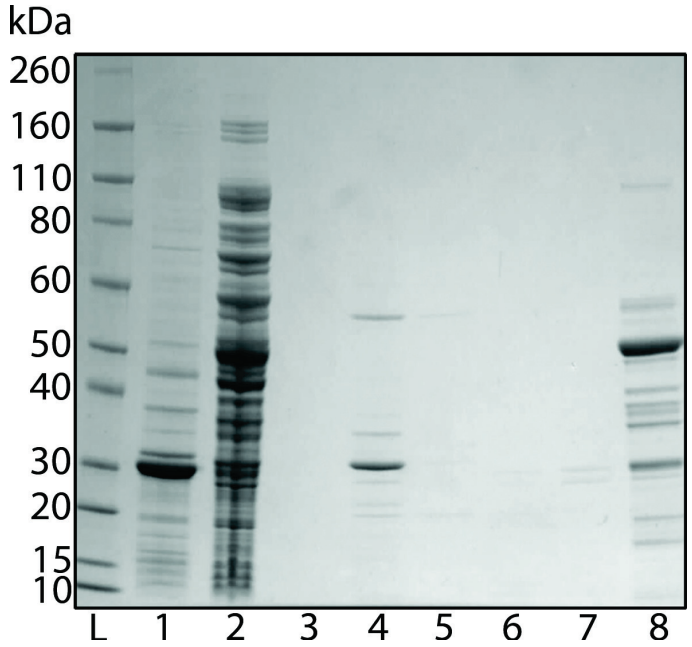

Figure 2.7 *SDS-PAGE gel of a typical GFP preparation. L – ladder, lane 1 – insoluble crude extract, lane 2 – soluble crude cell free extract, lanes 3-7 – wash fractions, lane 8 – pooled fluorescent eluted fractions.*

GFP is intrinsically fluorescent, therefore, only eluted fractions that displayed fluorescence were pooled, giving a good protein yield (~7 mg/L culture) for a single step ion-exchange chromatography purification. The intrinsic fluorescence allows for easy characterisation of GFP due to only correctly folded protein retaining fluorescence. Thus, the purified GFP was correctly folded.

2.5 Tobacco etch virus (TEV) protease

TEV protease (EC number 3.4.22.44) recognises the linear epitope sequence E-Xaa-Xaa-Y-X_{aa}-Q-(G/S), with cleavage occurring between the Q and the G/S amino acid residues (Stols *et al.* 2002). The optimal recognition site of TEV protease was shown to be ENLYFQG (Kapust *et al.* 2002), which is the sequence present in all of the cleavable His-tagged proteins used in this research.

The S219V TEV protease with an N-terminal poly histidine tag was used in this research. This mutant stops self-cleavage which produces a truncated enzyme with greatly reduced activity. The mutation also increases the catalytic efficiency and has a MBP to aid in solubilising the protein in *E. coli* (Kapust *et al.* 2001; Blommel & Fox 2007). TEV protease was used in this research as an example of a commercially relevant biomolecule that could benefit enormously from immobilisation to an amyloid fibril nanoscaffold. TEV protease could benefit from immobilisation due to its instability outside of the cellular environment (Puhl *et al.* 2009), and so that it could potentially be reused multiple times, saving on production costs.

2.5.1 Purification and characterisation of TEV protease

TEV protease purification was based on the methods of Blommel & Fox (2007). This method (section 7.7.2) took advantage of the N-terminal poly-histidine tag, by using nickel affinity chromatography purification, followed by a self-cleaving step, to cleave the MBP, then another nickel affinity purification. The purification procedure can be seen in **Figure 2.8**, and shows the protocol resulted in homogenous pure TEV protease. The predicted mass of the TEV protease-MBP fusion is ~69 kDa, ~27 kDa for TEV protease and ~42 kDa for MBP. From the gel in **Figure 2.8**, it can be seen that the self-cleavage of the MBP by TEV protease occurs very rapidly inside the cell, because there is virtually no TEV protease-MBP fusion protein present in the crude cell free extract (lane 2) and therefore this step could be bypassed in subsequent purifications. The yield for each purification was ~10 mg per litre of culture.

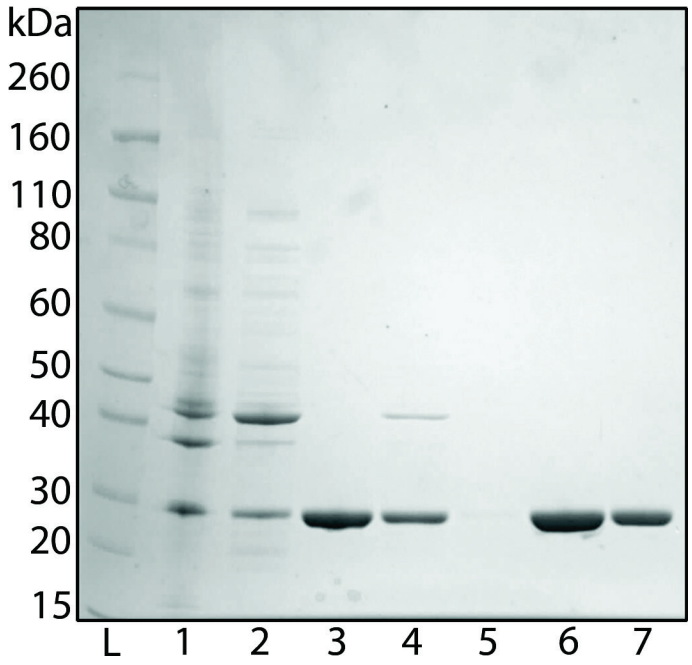

Figure 2.8 *SDS-PAGE gel of a typical MBP-TEV protease preparation. L – ladder, lane 1 – insoluble crude extract, lane 2 – crude cell free extract, lane 3 – eluted TEV protease, lane 4 – MBP cleaving, lane 5 - flow through when loading the nickel affinity column with the cleaved protein, lane 6 – eluted cleaved TEV protease, lane 7 – desalted TEV protease.*

For the characterisation of TEV protease, a cleavage control reaction was undertaken to assess the activity of the purified TEV protease for its ability to cleave the poly-histidine tag from wild-type *E. coli* dihydrodipicolinate synthase (DHDPS). DHDPS is an enzyme that is readily available in our laboratory, which has been shown previously to contain a cleavable poly-histidine tag. As can be seen in **Figure 2.9**, the purified TEV protease does show the ability to cleave the poly-histidine tag of the DHDPS. The cleavage reaction was only run for 2 hours with a 1:100 TEV protease to DHDPS ratio, to ensure that cleavage could occur. Subsequent cleavage reactions were generally run overnight with more TEV protease in the reaction.

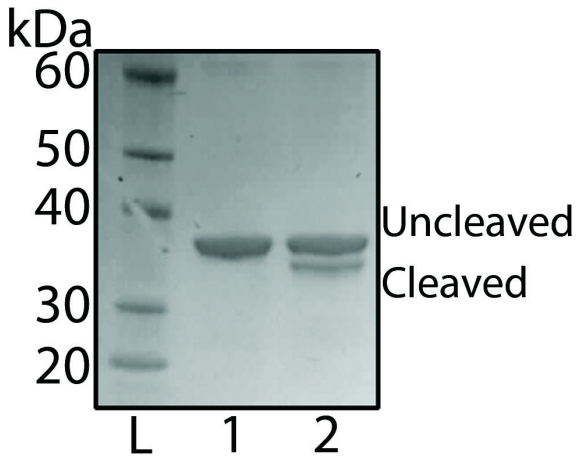

Figure 2.9 *Poly-histidine tag cleavage of wild-type E. coli DHDPS by TEV protease. L – ladder, lane 1 – DHDPS pre cleavage, lane 2 – DHDPS post cleavage with TEV protease for 2 hours at 4 °C.*

2.6 Glucose oxidase (GOD)

Glucose oxidase (GOD) (EC 1.1.3.4) from *Aspergillus niger*, is an oxido-reductase enzyme that catalyses the oxidation of β-D-glucose and oxygen to form hydrogen peroxide and glucono-1,5-lactone, which spontaneously hydrolyses to gluconic acid (**Figure 2.10**) (Fuglsang *et al.* 1995; Leskovac *et al.* 2005). GOD is a homodimeric glycoprotein with a molecular weight of ~130-175 kDa depending on the carbohydrate content of the carbohydrate shell (Kalisz *et al.* 1997). Each dimer contains a strongly bound flavin adenine dinucleotide (FAD) as a cofactor for the reaction (Wohlfahrt *et al.* 1999).

GOD was selected as the model enzyme for immobilisation to the surface assembled amyloid fibrils because Pilkington *et al.* (2010) had previous shown that GOD can be immobilised to insulin amyloid fibrils in solution. GOD was also used because it is extremely stable under a variety of condition (Wilson & Turner 1992), can be purchased commercially, and has many commercial applications (Bankar *et al.* 2009). In addition, numerous research groups utilise GOD as the model enzyme for immobilisation (Shi *et al.* 2011).

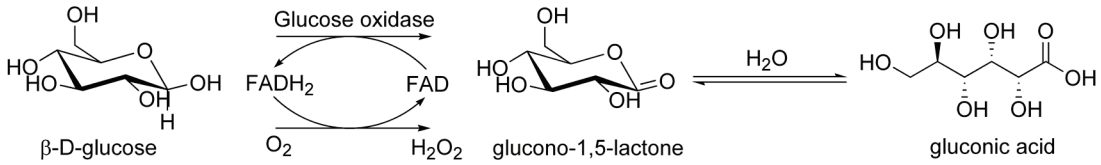

Figure 2.10 *The reaction catalysed by GOD. The oxidation of glucose by molecular oxygen to glucono-1,5-lactone, which spontaneously hydrolyses to gluconic acid. During the oxidation reaction, FAD is reduced to $FADH_2$ and molecular oxygen is reduced to hydrogen peroxide. Adapted from Witt et al. (2000) and Leskovac et al. (2005).*

2.6.1 GOD characterisation

The GOD catalysed reaction can be monitored using a fluorescent coupled assay containing horseradish peroxidase (HRP) and Resorufin (**Figure 2.11**) (section 7.9.3) (Zhang *et al.* 2004). This method was routinely used to monitor GOD activity.

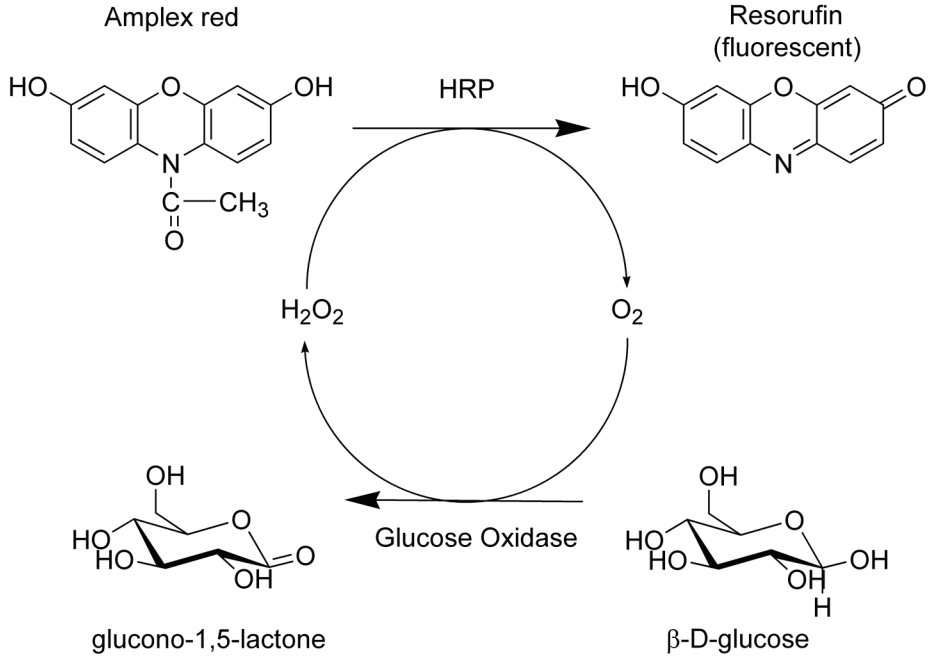

Figure 2.11 *GOD and HRP fluorescent coupled assay to monitor the reaction catalysed by GOD, adapted from Mohanty et al. (1997).*

Employing the fluorescent coupled assay, a standard curve was created (**Figure 2.12**) using between 1 and 21 mU of GOD, as stated in the Invitrogen Amplex® red glucose/glucose oxidase assay kit (Invitrogen 2006). 1 U is defined as the ability to oxidise 1.0 μM of β-D-glucose to D-gluconolactone and H_2O_2 per min at pH 5.1 at 35 °C, equivalent to an O_2 uptake of 22.4 μL per min.

The coupled assay has a 1:1 stoichiometry. It is extremely sensitive so samples had to be diluted by ~10,000 to be in the correct range of the standard curve. The coupled assay is a continuous reaction, therefore an incubation time of 4 min was selected, as this generated a very accurate standard curve, and allowed the assay to be performed on many samples quickly.

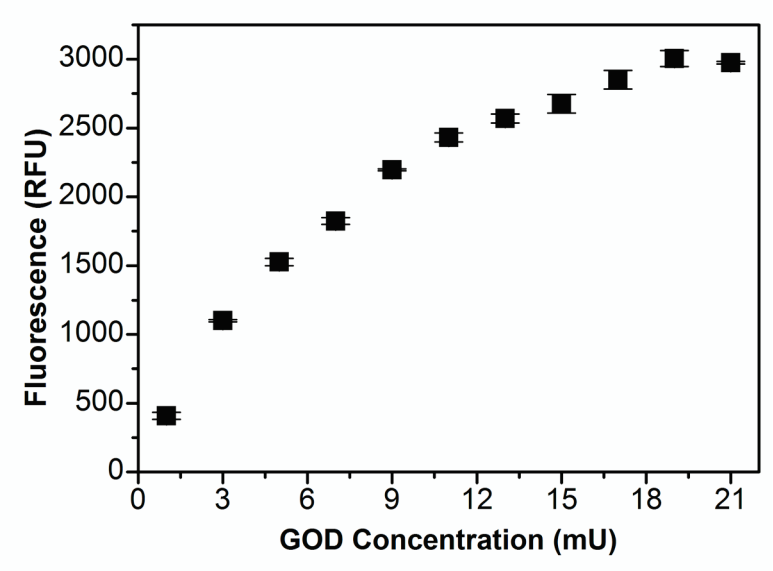

Figure 2.12 *Glucose oxidase standard curve. Each sample contained the appropriate concentration of glucose oxidase, 0.1 U/mL horse radish peroxidase, 50 mM D-glucose, 50 µM Amplex® red and was incubated for 4 min. The average of 3 replicates of each sample was used and the error is the standard deviation of the mean.*

2.7 Summary

The proteins OPH, $P450_{BM3}$, GFP, and TEV protease have been overexpressed in *E. coli* and purified to the required purity for this research. The characterisation of the proteins used different approaches depending on which protein was being characterised, and what was relevant to the experimental process needed to demonstrate the immobilisation of the protein on the amyloid fibril nanoscaffold. All of the biomolecules mentioned in this chapter will be immobilised to insulin amyloid fibrils in solution (chapter 4), and GOD, GFP, and TEV protease will be immobilised to surface assembled insulin amyloid fibrils as described in chapter 5.

2.8 References

Bankar, S.B., Bule, M.V., Singhal, R.S. & Ananthanarayan, L., 2009. Glucose oxidase-an overview. *Biotechnology Advances*, 27(4), pp.489–501.

Benning, M.M., Kuo, J.M., Raushel, F.M. & Holden, H.M., 1994. Three-dimensional structure of phosphotriesterase: An enzyme capable of detoxifying organophosphate nerve agents. *Biochemistry*, 33(50), pp.15001–15007.

Blommel, P.G. & Fox, B.G., 2007. A combined approach to improving large-scale production of tobacco etch virus protease. *Protein Expression and Purification*, 55(1), pp.53–68.

Bogdanov, A.M., Mishin, A.S., Yampolsky, I.V., Belousov, V.V., Chudakov, D.M., Subach, F.V., Verkhusha, V.V., Lukyanov, S. & Lukyanov, K.A., 2009. Green fluorescent proteins are light-induced electron donors. *Nature Chemical Biology*, 5(7), pp.459–461.

Caldwell, S.R., Newcomb, J.R., Schlecht, K.A. & Raushel, F.M., 1991. Limits of diffusion in the hydrolysis of substrates by the phosphotriesterase from Pseudomonas diminuta. *Biochemistry*, 30(30), pp.7438–7444.

Cody, C.W., Prasher, D.C., Westler, W.M., Prendergast, F.G. & Ward, W.W., 1993. Chemical structure of the hexapeptide chromophore of the *Aequorea* green-fluorescent protein. *Biochemistry*, 32(5), pp.1212–1218.

Cormack, B.P., Valdivia, R.H. & Falkow, S., 1996. FACS-optimized mutants of the green fluorescent protein (GFP). *Gene*, 173(1), pp.33–38.

Donarski, W.J., Dumas, D.P., Heitmeyer, D.P., Lewis, V.E. & Raushel, F.M., 1989. Structure-activity relationships in the hydrolysis of substrates by the phosphotriesterase from *Pseudomonas diminuta*. *Biochemistry*, 28(11), pp.4650–4655.

Dumas, D.P., Caldwell, S.R., Wild, J.R. & Raushel, F.M., 1989. Purification and properties of the phosphotriesterase from *Pseudomonas diminuta*. *Journal of Biological Chemistry*, 264(33), pp.19659–19665.

Eddleston, M., 2000. Patterns and problems of deliberate self-poisoning in the developing world. *QJM: An International Journal of Medicine*, 93(11), pp.715–731.

Fuglsang, C.C., Johansen, C., Christgau, S. & Adler-Nissen, J., 1995. Antimicrobial enzymes: Applications and future potential in the food industry. *Trends in Food Science & Technology*, 6(12), pp.390–396.

Furge, L.L. & Guengerich, F.P., 2006. Cytochrome P450 enzymes in drug metabolism and chemical toxicology. *Biochemistry and Molecular Biology Education*, 34(2), pp.66–74.

Ghanem, E. & Raushel, F.M., 2005. Detoxification of organophosphate nerve agents by bacterial phosphotriesterase. *Toxicology and Applied Pharmacology*, 207(2, Supplement 1), pp.459–470.

Gillam, E.M.J., 2008. Engineering cytochrome P450 enzymes. *Chemical Research in Toxicology*, 21(1), pp.220–231.

Guengerich, F.P., 2001. Common and uncommon cytochrome P450 reactions related to metabolism and chemical toxicity. *Chemical Research in Toxicology*, 14(6), pp.611–650.

Guengerich, F.P., 1991. Reactions and significance of cytochrome P-450 enzymes. *The Journal of Biological Chemistry*, 266(16), pp.10019–10022.

Hennig, L. & Schäfer, E., 1998. Protein purification with C-terminal fusion of maltose binding protein. *Protein Expression and Purification*, 14(3), pp.367–370.

Hill, C.M., Li, W.-S., Thoden, J.B., Holden, H.M. & Raushel, F.M., 2003. Enhanced degradation of chemical warfare agents through molecular engineering of the phosphotriesterase active site. *Journal of the American Chemical Society*, 125(30), pp.8990–8991.

Hong, S.-B. & Raushel, F.M., 1999. Stereochemical constraints on the substrate specificity of phosphotriesterase. *Biochemistry*, 38(4), pp.1159–1165.

Invitrogen, 2006. Amplex® red glucose/glucose oxidase assay kit. Available at: www.probes.invitrogen.com/media/pis/mp22189.pdf.

Julsing, M.K., Cornelissen, S., Bühler, B. & Schmid, A., 2008. Heme-iron oxygenases: Powerful industrial biocatalysts? *Current Opinion in Chemical Biology*, 12(2), pp.177–186.

Kalisz, H.M., Hendle, J. & Schmid, R.D., 1997. Structural and biochemical properties of glycosylated and deglycosylated glucose oxidase from *Penicillium amagasakiense*. *Applied Microbiology and Biotechnology*, 47(5), pp.502–507.

Kanugula, A.K., Repalle, E.R., Pandey, J.P., Sripad, G., Mitra, C.K., Dubey, D.K. & Siddavattam, D., 2011. Immobilization of organophosphate hydrolase on biocompatible gelatin pads and its use in removal of organophosphate compounds and nerve agents. *Indian Journal of Biochemistry & Biophysics*, 48(1), pp.29–34.

Kapust, R.B., Tözsér, J., Copeland, T.D. & Waugh, D.S., 2002. The P1' specificity of tobacco etch virus protease. *Biochemical and Biophysical Research Communications*, 294(5), pp.949–955.

Kapust, R.B., Tözsér, J., Fox, J.D., Anderson, D.E., Cherry, S., Copeland, T.D. & Waugh, D.S., 2001. Tobacco etch virus protease: Mechanism of autolysis and rational design of stable mutants with wild-type catalytic proficiency. *Protein Engineering*, 14(12), pp.993–1000.

Kapust, R.B. & Waugh, D.S., 1999. *Escherichia coli* maltose-binding protein is uncommonly effective at promoting the solubility of polypeptides to which it is fused. *Protein Science*, 8(8), pp.1668–1674.

Kille, S., Zilly, F.E., Acevedo, J.P. & Reetz, M.T., 2011. Regio- and stereoselectivity of P450-catalysed hydroxylation of steroids controlled by laboratory evolution. *Nature Chemistry*, 3(9), pp.738–743.

Kim, J., Tsai, P.-C., Chen, S.-L., Himo, F., Almo, S.C. & Raushel, F.M., 2008. Structure of diethyl phosphate bound to the binuclear metal center of phosphodiesterase. *Biochemistry*, 47(36), pp.9497–9504.

Leskovac, V., Trivic, S., Wohlfahrt, G., Kandrac, J. & Pericin, D., 2005. Glucose oxidase from *Aspergillus niger*: The mechanism of action with molecular oxygen, quinones, and one-electron acceptors. *The International Journal of Biochemistry & Cell Biology*, 37(4), pp.731–750.

Maurer, S.C., Schulze, H., Schmid, R.D. & Urlacher, V., 2003. Immobilisation of P 450 BM-3 and an NADP cofactor recycling system: Towards technical application of hemecontaining monooxygenases in fine chemical synthesis. *Advanced Synthesis & Catalysis*, 345(6-7), pp.802–810.

McLean, K.J., Sabri, M., Marshall, K.R., Lawson, R.J., Lewis, D.G., Clift, D., Balding, P.R., Dunford, A.J., Warman, A.J. & McVey, J.P., 2005. Biodiversity of cytochrome P450 redox systems. *Biochemical Society Transactions*, 33(4), pp.796-801

Miles, J.S., Munro, A.W., Rospendowski, B.N., Smith, W.E., Mcknight, J. & Thomson, A.J., 1992. Domains of the catalytically self-sufficient cytochrome p-450 BM-3. Genetic construction, overexpression, purification and spectroscopic characterization. *Biochemical Journal*, 288(2), pp.503–509.

Mohanty, J.G., Jaffe, J.S., Schulman, E.S. & Raible, D.G., 1997. A highly sensitive fluorescent micro-assay of H_2O_2 release from activated human leukocytes using a dihydroxyphenoxazine derivative. *Journal of Immunological Methods*, 202(2), pp.133–141.

Morise, H., Shimomura, O., Johnson, F.H. & Winant, J., 1974. Intermolecular energy transfer in the bioluminescent system of *Aequorea*. *Biochemistry*, 13(12), pp.2656–2662.

Mulchandani, A., Mulchandani, P. & Chen, W., 1998a. Enzyme biosensor for determination of organophosphates. *Field Analytical Chemistry and Technology*, 2(6), pp.363–369.

Mulchandani, A., Mulchandani, P., Kaneva, I. & Chen, W., 1998b. Biosensor for direct determination of organophosphate nerve agents using recombinant *Escherichia coli* with surface-expressed organophosphorus hydrolase. 1. Potentiometric microbial electrode. *Analytical Chemistry*, 70(19), pp.4140–4145.

Munro, A.W., Leys, D.G., McLean, K.J., Marshall, K.R., Ost, T.W.B., Daff, S., Miles, C.S., Chapman, S.K., Lysek, D.A. & Moser, C.C., 2002. P450 BM3: The very model of a modern flavocytochrome. *Trends in Biochemical Sciences*, 27(5), pp.250–257.

Munro, A.W., Lindsay, J.G., Coggins, J.R., Kelly, S.M. & Price, N.C., 1995. NADPH oxidase activity of cytochrome P-450 BM3 and its constituent reductase domain. *Biochimica et Biophysica Acta (BBA) - Bioenergetics*, 1231(3), pp.255–264.

Nallamsetty, S., Austin, B.P., Penrose, K.J. & Waugh, D.S., 2005. Gateway vectors for the production of combinatorially-tagged His6-MBP fusion proteins in the cytoplasm and periplasm of *Escherichia coli*. *Protein Science: A Publication of the Protein Society*, 14(12), pp.2964–2971.

Neeli, R., Girvan, H.M., Lawrence, A., Warren, M.J., Leys, D., Scrutton, N.S. & Munro, A.W., 2005. The dimeric form of flavocytochrome P450 BM3 is catalytically functional as a fatty acid hydroxylase. *FEBS Letters*, 579(25), pp.5582–5588.

Newhouse, T. & Baran, P.S., 2011. If C-H bonds could talk: Selective C-H bond oxidation. *Angewandte Chemie International Edition*, 50(15), pp.3362–3374.

Nikaido, H., 1994. Maltose transport system of *Escherichia coli*: An ABC-type transporter. *FEBS Letters*, 346(1), pp.55–58.

Noble, M.A., Miles, C.S., Chapman, S.K., Lysek, D.A., MacKay, A.C., Reid, G.A., Hanzlik, R.P. & Munro, A.W., 1999. Roles of key active-site residues in flavocytochrome P450 BM3. *Biochemical Journal*, 339(2), pp.371–379.

Omburo, G.A., Kuo, J.M., Mullins, L.S. & Raushel, F.M., 1992. Characterization of the zinc binding site of bacterial phosphotriesterase. *Journal of Biological Chemistry*, 267(19), pp.13278–13283.

Omura, T. & Sato, R., 1964. The carbon monoxide-binding pigment of liver microsomes I. Evidence for its hemoprotein nature. *Journal of Biological Chemistry*, 239(7), pp.2370–2378.

Pflug, S., Richter, S.M. & Urlacher, V.B., 2007. Development of a fed-batch process for the production of the cytochrome P450 monooxygenase CYP102A1 from *Bacillus megaterium* in *E. coli*. *Journal of Biotechnology*, 129(3), pp.481–488.

Prasher, D.C., Eckenrode, V.K., Ward, W.W., Prendergast, F.G. & Cormier, M.J., 1992. Primary structure of the *Aequorea victoria* green-fluorescent protein. *Gene*, 111(2), pp.229–233.

Puhl, A.C., Giacomini, C., Irazoqui, G., Batista-Viera, F., Villarino, A. & Terenzi, H., 2009. Covalent immobilization of tobacco-etch-virus NIa protease: A useful tool for cleavage of the histidine tag of recombinant proteins. *Biotechnology and Applied Biochemistry*, 53(Pt 3), pp.165–174.

Rebmann, T., Clements, B.W., Bailey, J.A. & Evans, R.G., 2009. Organophosphate antidote auto-injectors vs. traditional administration: A time motion study. *The Journal of Emergency Medicine*, 37(2), pp.139–143.

Rochu, D., Viguié, N., Renault, F., Crouzier, D., Froment, M.-T. & Masson, P., 2004. Contribution of the active-site metal cation to the catalytic activity and to the conformational stability of phosphotriesterase: Temperature- and pH-dependence. *Biochemical Journal*, 380(3), pp.627–633.

Roodveldt, C. & Tawfik, D.S., 2005. Directed evolution of phosphotriesterase from Pseudomonas diminuta for heterologous expression in *Escherichia coli* results in stabilization of the metal-free state. *Protein Engineering, Design and Selection*, 18(1), pp.51–58.

Schwaneberg, U., Schmidt-Dannert, C., Schmitt, J. & Schmid, R.D., 1999. A continuous spectrophotometric assay for P450 BM-3, a fatty acid hydroxylating enzyme, and its mutant F87A. *Analytical Biochemistry*, 269(2), pp.359–366.

Shi, J., Claussen, J.C., McLamore, E.S., ul Haque, A., Jaroch, D., Diggs, A.R., Calvo-Marzal, P., Rickus, J.L. & Marshall Porterfield, D., 2011. A comparative study of enzyme immobilization strategies for multi-walled carbon nanotube glucose biosensors. *Nanotechnology*, 22(35), p.355502.

De Silva, H.J., Samarawickrema, N.A. & Wickremasinghe, A.R., 2006. Toxicity due to organophosphorus compounds: what about chronic exposure? *Transactions of the Royal Society of Tropical Medicine and Hygiene*, 100(9), pp.803–806.

Stols, L., Gu, M., Dieckman, L., Raffen, R., Collart, F.R. & Donnelly, M.I., 2002. A new vector for high-throughput, ligation-independent cloning encoding a tobacco etch virus protease cleavage site. *Protein Expression and Purification*, 25(1), pp.8–15.

Vottero, E., Rea, V., Lastdrager, J., Honing, M., Vermeulen, N.P.E. & Commandeur, J.N.M., 2011. Role of residue 87 in substrate selectivity and regioselectivity of drug-metabolizing cytochrome P450 CYP102A1 M11. *Journal of Biological Inorganic Chemistry*, 16(6), pp.899–912.

van Vugt-Lussenburg, B.M.A., Stjernschantz, E., Lastdrager, J., Oostenbrink, C., Vermeulen, N.P.E. & Commandeur, J.N.M., 2007. Identification of critical residues in novel drug metabolizing mutants of cytochrome P450 BM3 using random mutagenesis. *Journal of Medicinal Chemistry*, 50(3), pp.455–461.

Whitehouse, C.J.C., Bell, S.G. & Wong, L.-L., 2012. P450BM3 (CYP102A1): Connecting the dots. *Chemical Society Reviews*, Advanced Article.

Wilson, R. & Turner, A.P.F., 1992. Glucose oxidase: An ideal enzyme. *Biosensors and Bioelectronics*, 7(3), pp.165–185.

Witt, S., Wohlfahrt, G., Schomburg, D., Hecht, H.J. & Kalisz, H.M., 2000. Conserved arginine-516 of *Penicillium amagasakiense* glucose oxidase is essential for the efficient binding of β-D-glucose. *Biochemical Journal*, 347(Pt 2), pp.553–559.

Wohlfahrt, G., Witt, S., Hendle, J., Schomburg, D., Kalisz, H.M. & Hecht, H.J., 1999. 1.8 and 1.9 A resolution structures of the Penicillium amagasakiense and *Aspergillus niger* glucose oxidases as a basis for modelling substrate complexes. *Acta Crystallographica. Section D, Biological Crystallography*, 55(Pt 5), pp.969–977.

Yair, S., Ofer, B., Arik, E., Shai, S., Yossi, R., Tzvika, D. & Amir, K., 2008. Organophosphate degrading microorganisms and enzymes as biocatalysts in environmental and personal decontamination applications. *Critical Reviews in Biotechnology*, 28(4), pp.265–275.

Yang, F., Moss, L.G. & Phillips, G.N., Jr, 1996. The molecular structure of green fluorescent protein. *Nature Biotechnology*, 14(10), pp.1246–1251.

Yang, H., Carr, P.D., McLoughlin, S.Y., Liu, J.W., Horne, I., Qiu, X., Jeffries, C.M.J., Russell, R.J., Oakeshott, J.G. & Ollis, D.L., 2003. Evolution of an organophosphate-degrading enzyme: A comparison of natural and directed evolution. *Protein Engineering*, 16(2), pp.135–145.

Yun, C.H., Kim, K.H., Kim, D.H., Jung, H.C. & Pan, J.G., 2007. The bacterial P450 BM3: A prototype for a biocatalyst with human P450 activities. *Trends in Biotechnology*, 25(7), pp.289–298.

Zhang, W., Huang, Y., Dai, H., Wang, X., Fan, C. & Li, G., 2004. Tuning the redox and enzymatic activity of glucose oxidase in layered organic films and its application in glucose biosensors. *Analytical Biochemistry*, 329(1), pp.85–90.

Chapter Three

3 Characterisation of amyloid fibril nanoscaffolds

3.1 Introduction

Many different supports exist for enzyme immobilisation, as outlined in chapter one, and the aim of this thesis was to investigate the ability of amyloid fibrils to act as a biomolecule nanoscaffold. The intrinsic features of amyloid fibrils such as their nanometre size, chemical functionality arising from amino acid side chains and the ability to self-assemble, make amyloid fibrils an ideal candidate as a nanoscaffold.

This chapter will explore the use of bovine insulin and fish eye lens crystallin proteins as building blocks for amyloid fibril nanoscaffolds in solution, and assembled on glass and cellulose surfaces. To realise the full potential of amyloid fibrils as a nanoscaffold, easy methods to collect, reuse, and functionalise them are needed. Surface assembly of the nanoscaffolds was therefore investigated. The characterisation of the amyloid fibril nanoscaffolds in this research used the methods: fluorescein isothiocyanate fluorescence (FITC), ThT fluorescence, CD, TEM, SEM, and FTIR. Investigations into the functionalisation of the solution and surface assembled amyloid fibril nanoscaffolds with a range of biomolecules will be covered in chapters four and five.

3.2 Solution assembled amyloid fibril nanoscaffold characterisation

3.2.1 Bovine insulin

The routine self-assembly of bovine insulin amyloid fibrils (section 7.10.1) was based on an in-house method modified from Nielsen *et al.* (2001). This method relies on the fact that insulin can form amyloid fibrils at pH 1.6 and high (60 °C) temperature (Waugh 1946; Ortiz *et al.* 2007). The formation of bovine insulin amyloid fibrils can be detected by monitoring the increase in ThT fluorescence upon binding to the forming amyloid fibrils (section 7.2.8). ThT is thought to bind to cavities running parallel to the fibril axis of the amyloid fibrils (section 1.2.1) (Groenning 2010). The time-course monitoring of the formation of bovine insulin amyloid fibrils using ThT is shown in **Figure 3.1**. As can be seen, there is a pronounced lag phase preceding an exponential growth phase, characteristic of amyloid fibril formation occurring by a nucleated growth mechanism (Schmit *et al.* 2011).

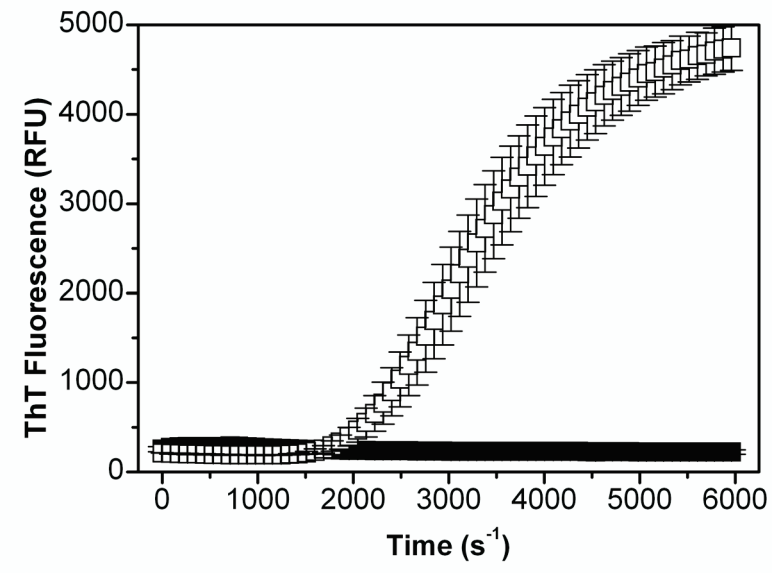

Figure 3.1 *Time course profile of 5.8 mg/mL bovine insulin (□) dissolved in 25 mM HCl, 100 mM NaCl, pH 1.6 amyloid fibril formation and a buffer control (■) at 60 °C, as monitored by ThT fluorescence. Each sample was measured in triplicate, and the error bars are the standard deviation of the mean.*

This transition from a predominantly α-helical protein to a β-sheet protein structure can also be characterised by CD (section 7.2.15) (Bouchard *et al.* 2000). **Figure 3.2** shows the change in secondary structure for the native insulin protein and the resulting insulin amyloid fibrils formed at pH 1.6 and heating at 60 °C. The CD spectrum confirms that native insulin has a predominantly α-helical structure in solution with double minima present at approximately 208 and 222 nm (Greenfield & Fasman 1969), and that the insulin amyloid fibrils have a β-sheet rich structure characterised by a minimum at 216 nm (Greenfield & Fasman 1969), which is in agreement with previous studies (Bouchard *et al.* 2000).

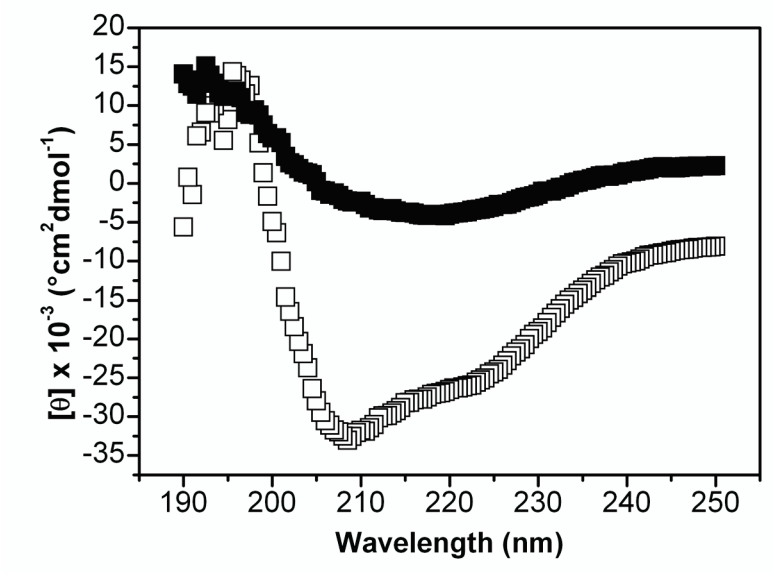

Figure 3.2 *CD spectroscopy of 0.2 mg/mL native insulin (□) in 20 mM NaPi, and 0.2 mg/mL insulin amyloid fibrils (■) in 20 mM NaPi. The measurements were based on triplicate scans of each sample.*

The formed amyloid fibrils can be characterised by negatively staining with uranyl acetate and viewing using TEM (section 7.2.11) (Whittingham *et al.* 2002). An electron micrograph of bovine insulin amyloid fibrils is shown in **Figure 3.3**. As can be seen, the bovine insulin amyloid fibrils have the characteristic unbranched, twisted, fibrillar morphology that is diagnostic of amyloid fibrils (Nilsson 2004).

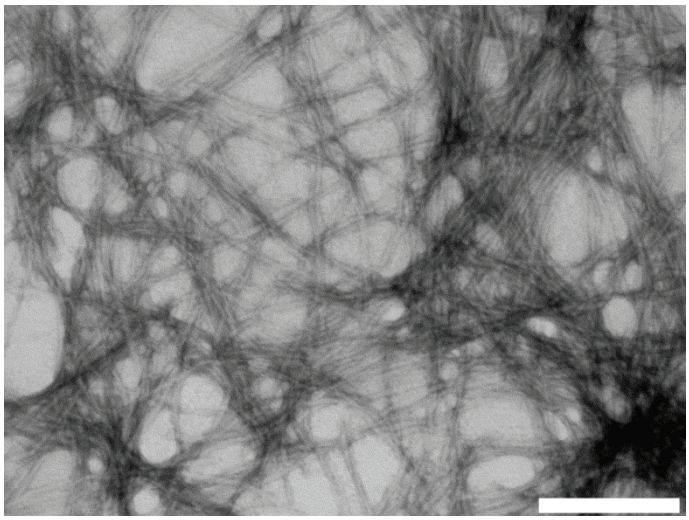

Figure 3.3 *Representative TEM micrograph of 1.45 mg/mL insulin amyloid fibrils viewed at 89,000 x magnification. The scale bar = 200 nm.*

FITC (**Figure 3.4**) is an isothiocyanate derivative of fluorescein. FITC can react and form a stable product with amine nucleophiles such as the ε- and N-terminal amine groups of proteins (Jobbágy & Király 1966). FITC has an excitation absorbance maximum at 494 nm, and an emission wavelength of 520 nm (Hermanson 1996). FITC was used in this research to estimate the number of potential amino binding sites for biomolecule immobilisation. FITC has previously been used for the fluorescent labelling of β-amyloid peptides (Fülöp *et al.* 2001), therefore should be applicable to insulin amyloid fibrils.

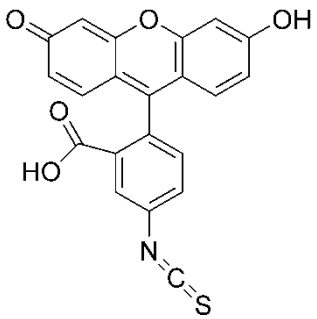

Figure 3.4 *Structure of FITC (Hermanson 1996).*

Estimation of the number of bound FITC molecules to the insulin amyloid fibrils was based on the methods of Thermo Scientific (2011), and used the assumption that the extinction coefficient for insulin fibrils is the same as insulin (ε_{280} = 5800 $M^{-1}cm^{-1}$). The extinction coefficient used for FITC was ε_{494} = 68000 $M^{-1}cm^{-1}$. Three 1 mg/mL (0.17 mM) solutions of insulin amyloid fibrils were formed (section 7.10.1), followed by centrifugation to pellet the amyloid fibrils. The supernatants were then discarded, and the pellets resuspended in 1 mL of FITC (2.6 mM) (section 7.10.4), followed by incubation at 25 °C for 1 hour. The solutions were then centrifuged, the pellet washed and resuspended in FITC buffer, followed by centrifugation. The washing steps were done five times to ensure only FITC bound to the amyloid fibrils was present. The concentration of insulin amyloid fibrils was determined, and bound FITC concentration was then determined. These parameters were then put into equation 1 to work out the ratio of dye to amyloid fibrils. The average number of moles dye per mole of amyloid fibrils was 1.3 ± 0.2, meaning that ~1 in 3 amine groups had bound FITC.

$$Moles\ dye\ per\ mole\ protein = \frac{A_{max}\ of\ labeled\ protein}{68000 \times protein\ conc.} \times dil.factor \qquad (1)$$

Employing the techniques of ThT binding, CD, and TEM, the routinely manufactured bovine insulin amyloid fibrils were thus shown to have the characteristic features of amyloid fibrils: ThT binding, a β-sheet secondary structure, and an unbranched and fibrillar morphology. Binding of FITC to the bovine insulin amyloid fibrils estimated that 1 in 3 amine groups of the amyloid fibrils are potentially available for biomolecule immobilisation. The estimate of the available amine groups will ensure that an excess of cross-linker will be present in the immobilisation conditions to maximise immobilisation of biomolecules to the bovine insulin amyloid fibrils.

3.2.2 Fish lens crystallins

The manufacture of amyloid fibrils from the crude protein source, fish eye lenses, used in-house methods modified from Garvey *et al.* (2009) (section 7.9.5). Crystallin amyloid fibrils were harder to characterise because of their native β-sheet secondary structure. The method used for the manufacture of the crystallin amyloid fibrils had previously been shown to produce validated amyloid fibrils *via* X-ray fibre diffraction (Garvey *et al.* 2009; Healy *et al.* 2012). The β-sheet crystallin structure meant that the protein natively bound ThT and therefore the formation of amyloid fibrils could not be monitored by an increase in ThT fluorescence (Meehan *et al.* 2007). Because of the native structure, CD could not be used either. Therefore, TEM (section 7.2.11) was the main method with which the crystallin amyloid fibrils were characterised. **Figure 3.5** shows a representative micrograph of crystallin amyloid fibrils viewed using TEM.

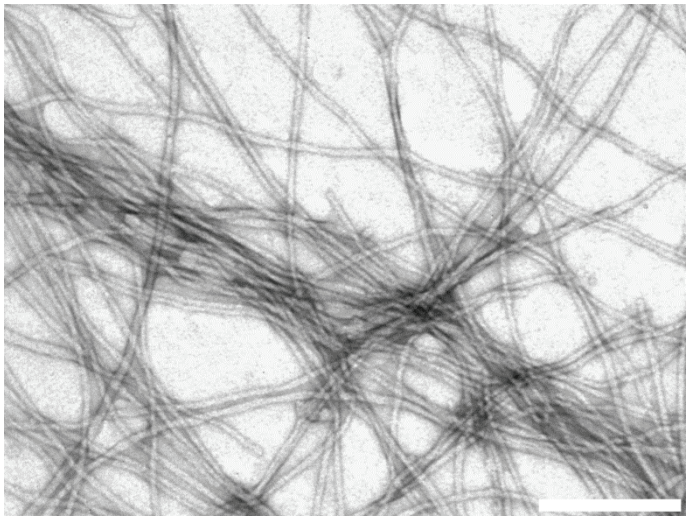

Figure 3.5 *Representative TEM of crystallin amyloid fibrils viewed at 89,000 x magnification. The scale bar = 200 nm.*

Like the insulin amyloid fibrils, the crystallin amyloid fibrils have a characteristic unbranched, twisted, fibrillar morphology. The morphology of the crystallin amyloid fibrils differs slightly though, being wider (18 nm ± 3 compared to 12 nm ± 2) and considerably longer. This is apparent in **Figure 3.6**, which is a micrograph of the crystallin amyloid fibrils at 14,000 x magnification. As can be seen, the crystallin amyloid fibrils are very long, with some being >10 μm in length compared to an average of ~2 μm for bovine insulin amyloid fibrils (Domigan *et al.* 2012). The crystallin amyloid fibrils also seem to have a tendency to come together and form much larger bundle-type structures with a twisted morphology (Healy *et al.* 2012). The longer length of the crystallin amyloid fibrils could prove to be beneficial for surface assembly (section 3.4.3), by providing even more active surface area for potential biomolecule immobilisation.

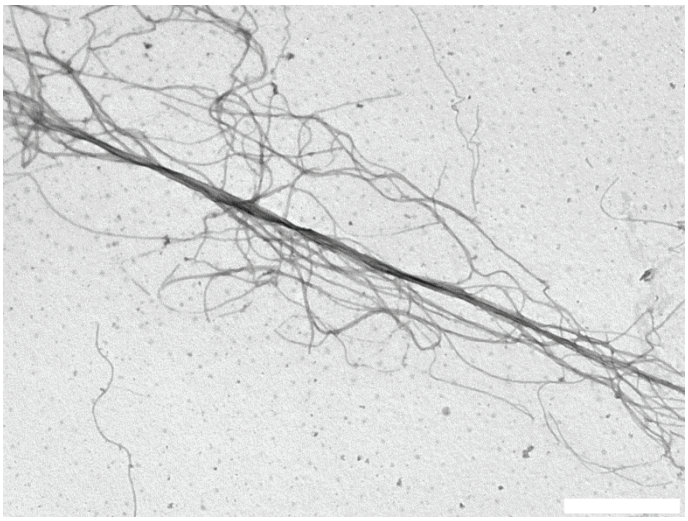

Figure 3.6 *Representative TEM micrograph of crystallin amyloid fibrils viewed at 14,000 x magnification. The scale bar = 1 μm.*

3.3 Surface assembled amyloid fibril nanoscaffold characterisation

The method to assemble the amyloid fibril nanoscaffold relies on the fact that amyloid fibril formation occurs by a nucleated growth mechanism (Schmit *et al.* 2011). With this in mind, the surface assembly process is based around covalent immobilisation of seed amyloid fibrils to the surfaces, from which mature amyloid fibrils can assemble (Ha & Park 2005).

Amyloid fibrils have previously been incorporated into materials to create bionanomaterials, but not by self-assembly on surfaces with the view to be functionalised with biomolecules. Oppenheim *et al.* (2010) created a lysozyme amyloid fibril-elastomer composite containing a 10 % amyloid fibril filling ratio which was shown to be a minimum of 2 times stiffer than a carbon nanotube-elastomer composition with the same fill ratio. Rao *et al.* (2012) incorporated pre-manufactured insulin amyloid fibrils into poly (vinyl alcohol) (PVOH), creating a bionanocomposite. The mechanical properties of the resulting bionanocomposite were evaluated, and a PVOH film containing 0.6 % w/w insulin amyloid fibrils was 15 % stiffer than the control. Pilkington *et al.* (2010) extended the creation of bovine insulin amyloid fibril-PVOH bionanocomposites by incorporating GOD functionalised bovine insulin amyloid fibrils into PVOH (Pilkington *et al.* 2010). The bionanocomposite was shown to retain GOD activity, and be able to function as an antimicrobial material by inhibiting the growth of *E. coli* when supplemented with glucose. The creation of bionanocomposite materials with amyloid fibrils has shown that amyloid fibrils can provide benefits to the materials in terms of increases in mechanical strength and by acting as a scaffold for enzyme immobilisation. Complementing amyloid fibril bionanocomposites with amyloid fibril surface assembly could create new nanomaterials with enhanced mechanical properties and large increases in surface area for biomolecule immobilisation.

The self-assembly of insulin amyloid fibrils on glass surfaces has shown to be possible *via* the covalent attachment of amyloid seeds to the glass surface (Ha & Park 2005). The covalently attached seeds provide the base to which mature amyloid fibrils assemble. Surface assembled amyloid fibrils offer many potential applications for highly active surfaces by increasing the surface area of the surface to which the amyloid fibrils are assembled. Assembling the amyloid fibrils on surfaces could also provide a method of collecting the amyloid fibrils, and potentially allow for a bottom-up approach to functional bionanomaterial design (Williams *et al.* 2010).

Glass (SiO_2) was chosen as a model surface because bovine insulin amyloid fibrils have previously been self-assembled from the surface of micro cover glasses (Ha & Park 2005), and because the transparency of glass allows for spectrophotometric assays to be used. Initially glass microscope slides were used for the surface assembly of bovine insulin amyloid fibrils, but this method only allowed one sample at a time to be analysed. Therefore, 5 mm glass beads (**Figure 3.7**) were used in a 96 well sample plate to allow for high throughput sample analysis.

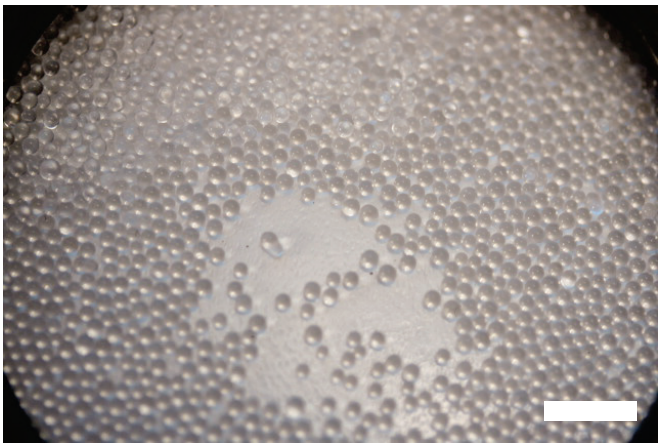

Figure 3.7 *5 mm diameter borosilicate glass beads. The scale bar = 3 cm. The image was taken from sigmaaldrich.com.*

To ensure the glass beads did not interfere with ThT fluorescence measurements, a solution of mature insulin amyloid fibrils was produced (section 7.10.1), and the fluorescence was measured with and without a glass bead in the wells of the 96 well plate (section 7.12.5). **Table 3.1** shows that glass beads placed in an insulin amyloid fibril/ThT solution decreases the ThT fluorescence by ~15 %. This confirms the glass beads only hinder ThT fluorescence slightly, and that ThT fluorescence measurements in the 96 well plates will be able to be used for verification of surface assembled insulin amyloid fibrils.

Table 3.1 *ThT fluorescence of samples with and without glass beads. Measurements are the average of three replicates of each sample and the error is the standard deviation of the mean.*

Bead	Fibrils	ThT (RFU)	Error
+	-	198	2
-	-	187	1
+	+	1764	17
-	+	2090	82

Figure 3.8 provides an overview of the surface assembled amyloid fibril process. First, the surface is chemically derivatised to yield an aminated surface which amyloid seeds can be covalently attached to through their ε-amino lysine or N-terminal α-amino groups (Brady & Jordaan 2009). As stated in section 1.1.2, amyloid fibril formation proceeds *via* a nucleated growth mechanism which allows the assembly of mature amyloid fibrils from the covalently bound amyloid seeds when the seeded surface is placed in a solution of native protein, and heated at low pH.

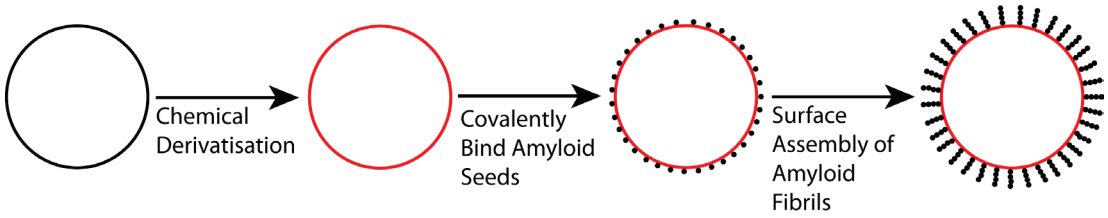

Figure 3.8 *Overview of the amyloid fibril surface assembly process. First the surface is chemically derivatised, covalent binding of the seeds can then occur, followed by assembly of the mature amyloid fibrils from the bound seeds.*

3-aminopropyltriethoxysilane (APTS) is an organo-functional silane that has a non-hydrolysable amino group, and three ethoxy groups which can react with the hydroxyl groups of glass and cellulose, and can undergo a condensation reaction with itself to create an aminated surface coating (Howarter & Youngblood 2006). The chemical derivation of glass and cellulose with APTS (**Figure 3.9**), and subsequent activation with *N, N'* – disuccinimidyl carbonate (DSC), is a straight forward procedure allowing the covalent immobilisation of proteins through amide coupling chemistry (Morpurgo *et al.* 1999). This surface chemistry is readily applicable to other types of materials such as polyesters, polyamides and polycarbonates, where silanes have been used as coatings for many different applications (Howarter & Youngblood 2007).

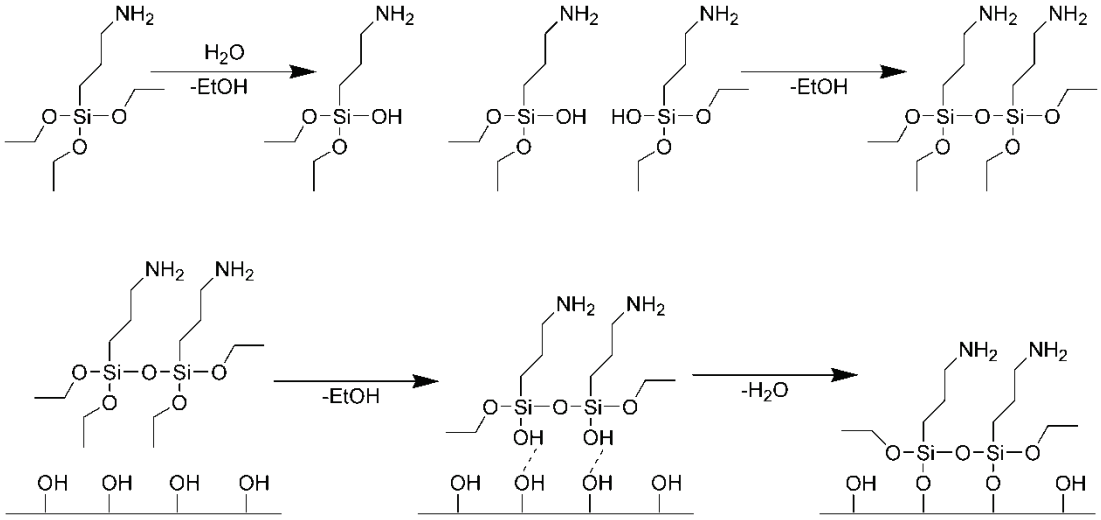

Figure 3.9 *Reaction scheme of APTS hydrolysis, followed by condensation (top). Reaction scheme of APTS hydrolysis, followed by condensation to a surface containing hydroxyl groups such as glass or cellulose (bottom). Adapted from Howarter & Youngblood (2006).*

Two cellulose based materials, cotton, and 20 μm microcrystalline cellulose powder, were used in this research. Cellulose is the most abundant natural polymer on earth, therefore, cellulose is an inexhaustible environmentally friendly resource for the manufacture of products (Klemm *et al.* 2005; Kim *et al.* 2006). Cellulose based materials have wide use in industry including: clothing, coatings, films, membranes, building materials, pharmaceuticals, and foodstuffs (Klemm *et al.* 2005).

The aim of template directed amyloid fibril growth from surfaces is to increase the available surface area for enzyme immobilisation, and to create an environment that is advantageous towards enzyme activity and stability. The use of other nanosupports such as nanoparticles, nanotubes, electrospun nanofibers and nanoporous matrices (section 1.6) have shown the ability to increase the available surface area for enzyme immobilisation, whilst lowering mass transfer resistance (Jia *et al.* 2002; Wang 2006). Template directed amyloid fibril growth allows the creation of self-assembling nanomaterials, provides a means to collect amyloid fibrils, and if the surface assembled amyloid fibrils are functionalised with biomolecules, the biomolecules can be easily reused due to their surface attachment.

3.4 Silicon oxide (glass) surfaces

5 mm diameter borosilicate glass beads (**Figure 3.7**) were utilised for the majority of the research into surface assembly. Glass beads were chosen because of their ability to fit into the wells of a 96 well plate for use in a plate reader. The plate reader allows for high throughput of multiple samples with triplicates of each sample to ensure accuracy and reproducibility of results.

3.4.1 Derivatisation of glass surfaces

The reaction between APTS and a glass surface (**Figure 3.9**) (section 7.12.1) firstly involves a hydrolysis and condensation step of APTS, followed by a hydrolysis and condensation step with the glass surface. The reaction produces an aminated surface that can then be activated with DSC *via* the formation of a succinimido carbamate to yield a surface that is able to spontaneously react with proteins through their ε - amino group of lysine residues and the N-terminal α-amino group (Nimura *et al.* 1986; Hermanson 2008; Edwards *et al.* 2011).

3.4.2 Template directed self-assembly of insulin amyloid fibrils

The first step in template directed amyloid fibril growth is the covalent immobilisation of the template to the surface of the glass bead. The template directed self-assembly is illustrated in **Figure 3.10**.

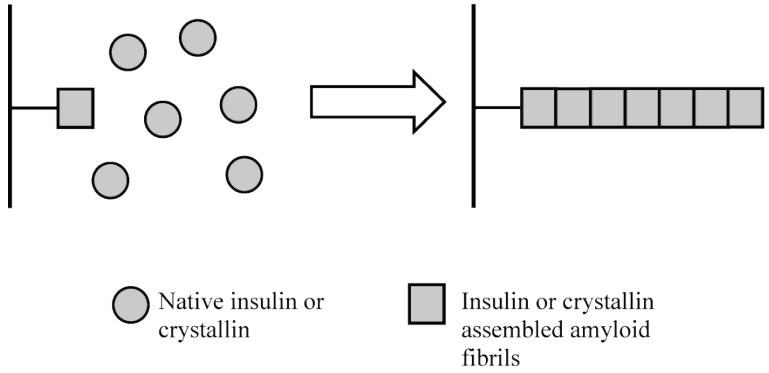

Figure 3.10 *Schematic of a possible mechanism for the template directed self-assembly of insulin and crystallin amyloid fibrils on surfaces. Adapted from Ha & Park (2005).*

Ha & Park (2005) used insulin seeds as their template for the surface assembly of insulin amyloid fibrils. The seeds were created by incubating a fresh solution of insulin and heating it until the end of the lag phase, which is characteristic of a nucleated-polymerisation mechanism (section 1.1.2). The protein species formed just before the exponential growth phase are classed as seeds if they are able to eliminate the lag phase in a fresh solution of the same amyloid forming protein (Jarrett & Lansbury 1992). In this research insulin amyloid fragments were used as the template for the surface assembly of insulin amyloid fibrils. Fragments are mature amyloid fibrils that have been fragmented usually by mechanical means to produce shorter amyloid fibrils (Xue *et al.* 2009). Insulin amyloid fibril fragments were produced by a freeze-fracture method (section 7.10.2), whereby mature insulin amyloid fibrils were subjected to freezing at -20 °C overnight, then thawing (Domigan *et al.* 2012). The thawed amyloid fibril samples were then assessed for the presence of fragments using TEM (section 7.2.11) before use as a template. **Figure 3.11** shows the electron micrographs of mature insulin amyloid fibrils before freezing (A), and after freezing (B). As can be seen, the freeze-fracture method yields shorter (40 nm ± 17) fragmented amyloid fibrils than the mature control sample (207 nm ± 66), confirming the method can produce amyloid fragments.

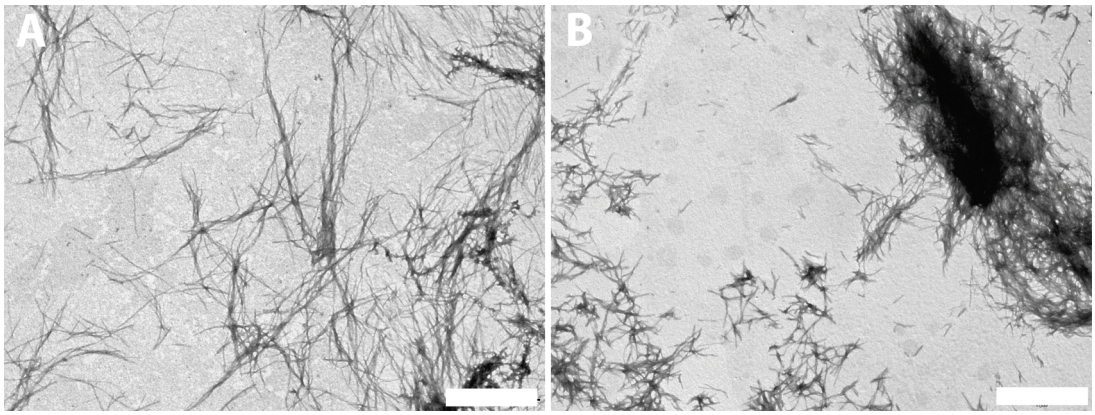

Figure 3.11 *Representative TEM micrographs of insulin amyloid fibrils. A – Pre freezing, B – post freezing. The scale bar represents 1 μm.*

Insulin amyloid fragments were chosen over insulin amyloid seeds (section 7.10.3) because fragments seeded the formation of mature amyloid fibrils faster than seeds (**Figure 3.12**). Fragmentation of the amyloid fibrils also gave more reproducible template directed amyloid fibril formation. This was because the incubation time to produce seeds before the exponential growth phase occurred varied between repetitions. **Figure 3.12** shows that when insulin amyloid fragments or fragments buffer exchanged into 50 mM HEPES pH 9 are added at 5 % v/v, both fragment types induce amyloid fibril formation faster, starting from time 0 when incubated at 60 °C. Insulin seeds added at 5 % v/v induced amyloid fibril formation at ~40 min, only slightly faster than not adding seeds. The fragments were buffer exchanged into 50 mM HEPES pH 9 to allow the amide coupling chemistry to proceed (Hermanson 2008). **Figure 3.12** shows that exchanging the buffer had almost no consequence on the ability of the fragments to seed the formation of insulin amyloid fibrils.

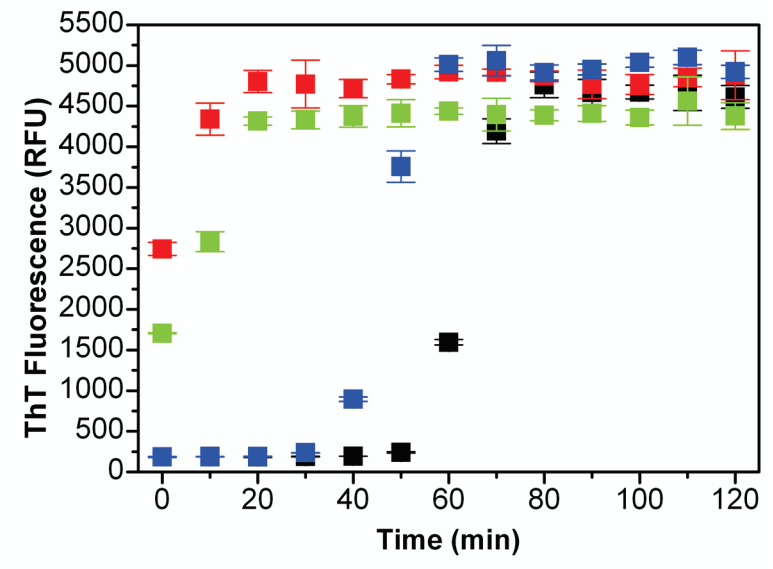

Figure 3.12 *Time course profile of insulin (1 mg/mL) amyloid fibril formation at 60 °C with either 5 % insulin seeds (■), 5 % insulin fragments (■), 5 % insulin fragments buffer exchanged (■), or insulin only (■), as monitored by ThT fluorescence. Measurements are the average of 3 replicates of each sample and the error is the standard deviation of the mean.*

The surface-activated glass beads were placed in a solution of buffer exchanged insulin amyloid fragments to covalently bond them to the glass surface *via* the amide coupling chemistry (Hermanson 2008). The beads with the covalently bound insulin amyloid fragments were then placed into a solution containing dissolved insulin at pH 1.6. By heating the insulin solution at 50 °C for 5 hours, insulin amyloid fibrils will self-assemble from the surface bound fragments (section 7.12.2). This process was monitored using ThT fluorescence in the 96 well plate reader (**Figure 3.13**) (section 7.2.8). As can be seen, the glass beads which had been seeded with the fragments, then amyloid fibrils assembled, had the shortest lag phase for amyloid fibril formation. This implies that by seeding the surface of the glass beads with the fragments, template directed amyloid fibril assembly can occur. The slower amyloid formation seen with the beads can be attributed to the lower amyloid formation temperature of 50 °C, and because the native insulin has to interact with surface immobilised amyloid seeds slowing the formation process due to diffusion.

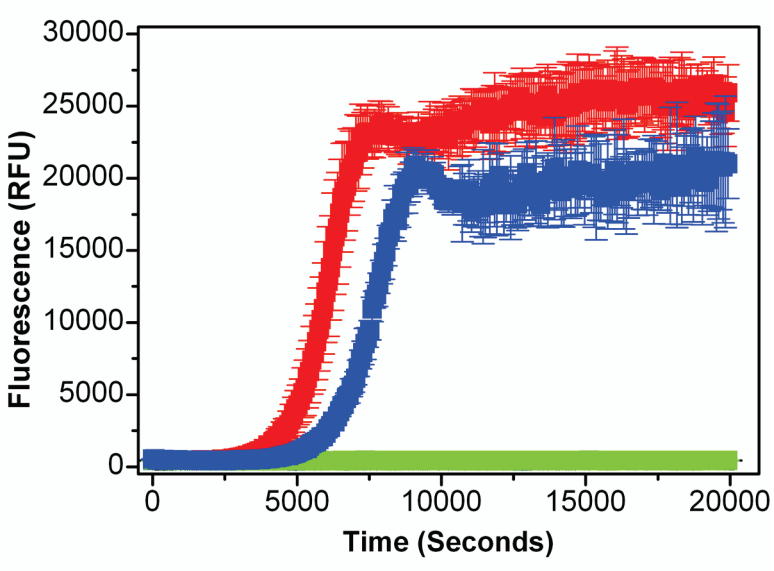

Figure 3.13 *Time course profile of template directed assembly of 1 mg/mL insulin amyloid fibrils in 25 mM HCl, 100 mM NaCl, pH 1.6 at 50 °C for 5 hours, as monitored by ThT fluorescence. (■) – seeded with fragments, fibrils assembled, (■) – not seeded, fibrils assembled, (■) – seeded, no fibrils, (■) (behind ■) – not seeded, no fibrils. Measurements are the average of 3 replicates of each sample and the error is the standard deviation of the mean.*

The beads which are not seeded with fragments still show mature amyloid fibrils are produced, but, after washing the beads and testing ThT fluorescence (**Table 3.2**), only the beads which were seeded with fragments retain significant fluorescence, compared to the control without fragments or amyloid fibrils. This implies that only the seeded beads have the template directed amyloid fibrils present and that the fibrils formed in the non-seeded sample were free in solution.

Table 3.2 *ThT fluorescence of 1 mg/mL insulin amyloid fibril samples assembled on glass beads after washing to remove amyloid fibrils from the solution phase. Measurements are the average of 3 replicates of each sample and the error is the standard deviation of the mean.*

Sample	ThT (RFU)	Error
Not seeded, no fibril	207	17
Not seeded, fibrils	228	19
Seeded, no fibrils	218	18
Seeded, fibrils	1145	228

Experimentation was carried out to ensure full surface derivatisation was necessary for maximum surface assembly of the insulin amyloid fibrils. This was achieved by measuring ThT fluorescence (section 7.2.9) on a variety of controls (**Table 3.3**). As shown by sample 9, the beads which had the full surface derivatisation, seeded with fragments, and mature amyloid fibrils assembled, did indeed have the highest ThT fluorescence and therefore the most surface assembled insulin amyloid fibrils. Sample 1, which is identical to sample 9 but without surface derivatisation, also shows a relatively high ThT fluorescence, suggesting there could be a relatively strong intrinsic association between the glass beads and the amyloid fragments.

Table 3.3 *ThT fluorescence (RFU) of glass bead controls with or without 1 mg/mL insulin fibrils assembled. Measurements are the average of 3 replicates of each sample and the error is the standard deviation of the mean.*

Sample	APTS	DSC	Seeded	Fibrils	ThT	Error
1	-	-	+	+	1054	151
2	-	-	+	-	545	32
3	-	-	-	+	535	61
4	-	-	-	-	612	156
5	+	-	+	+	594	170
6	+	-	+	-	278	12
7	+	-	-	+	310	32
8	+	-	-	-	296	31
9	+	+	+	+	1513	238
10	+	+	+	-	301	10
11	+	+	-	+	293	17
12	+	+	-	-	275	24

3.4.3 Template directed self-assembly of crystallin amyloid fibrils

Insulin amyloid fibrils are relatively short, therefore if crystallin amyloid fibrils, which were shown to be much longer (section 3.2.2), were able to be assembled on a surface, a larger surface area would result, and may allow for greater biomolecule immobilisation. The same protocol for the derivatisation of the glass beads (section 7.12.1) used with the insulin template directed amyloid self-assembly was used for the crystallin template directed amyloid self-assembly. Crude crystallin amyloid fibrils were prepared as in section 7.10.5, and verified by TEM (section 7.2.11). Initially, production of crystallin fragments by the freeze-thaw method implemented with the insulin amyloid fibrils was trialled. TEM revealed that the freeze-thaw method did not produce fragmented crystallin amyloid fibrils, therefore another method for the production of the fragments was needed. Freeze-thawing of proteins has long been known to induce denaturation of proteins (Chang *et al.* 1996), hence the inability of freeze-thawing to fracture the crystallin amyloid fibrils was unexpected, and could be due to the fibril forming buffer containing 10 % trifluoroethanol, because other alcohols such as ethanol are known cyroprotectants (Arakawa *et al.* 2001). Sonication has previously been shown to cause the fragmentation of insulin amyloid fibrils (Huang *et al.* 2009), and was therefore investigated as a method to produce crystallin amyloid fibril fragments. Mature crystallin amyloid fibrils were subjected to a range of sonication times (0-60 sec) (section 7.10.6). The resulting solutions were assessed for fragmentation by TEM, and found that a sonication time of 10 sec was needed to fragment the crystallin amyloid fibrils. **Figure 3.14** shows the before and after sonication electron micrographs of the crystallin amyloid fibrils. As can be seen, the sonication successfully fragmented the crystallin amyloid fibrils. Analysing the average length of the control crystallin amyloid fibrils (755 nm ± 200) versus the sonicated crystallin amyloid fragments (75 nm ± 48) revealed the extent of the fragmentation. The fragments were then covalently immobilised to the surface of the glass beads using the same method as for the insulin fragments, and subsequently used to seed the growth of crystallin amyloid fibrils (section 7.12.3).

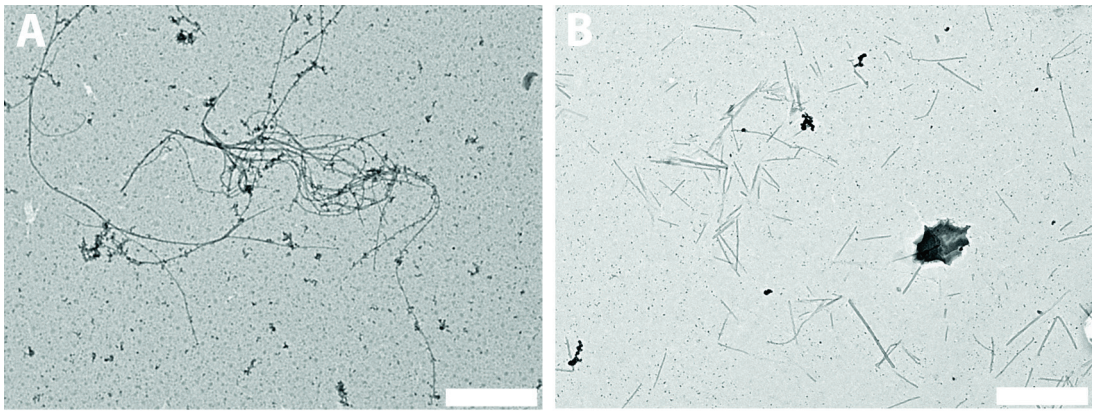

Figure 3.14 *Representative TEM micrographs of crystallin amyloid fibrils. A – Pre sonication, B – post sonication. The scale bar represents 1 μm.*

For the formation of the template directed crystallin amyloid fibrils, glass beads with covalently bound crystallin were placed in a solution of crystallin protein extracted from fish eye lenses (section 7.10.5), and heated for 24 h at 80 °C. The beads were then left in the crystallin solution at room temperature for at least 2 days. As it had previously been shown that ThT could not be used to detect crystallin amyloid fibrils (section 3.2.2), SEM (section 7.2.12) was therefore used as an alternative method to investigate the presence of crystallin amyloid fibrils on the surface of the glass beads. SEM was previously attempted on the surface assembled insulin amyloid fibrils but, no amyloid structures were able to be seen. This was probably due to the gold coating needed for SEM being too thick and making the insulin amyloid fibrils not viewable.

The crystallin amyloid fibrils were able to be viewed with SEM because of their larger size, and tendency to bundle together to form larger structures (Healy *et al.* 2012). **Figure 3.15** shows electron micrographs of the surface of the four template directed crystallin amyloid fibril glass bead samples. As can be seen, the blank glass bead (B) surface appears relatively smooth, whilst seeded only (C) and fibrils only (A) both have a more crater-like surface. The only bead sample (D) which had amyloid fibril structures on the surface were the beads which had been seeded with crystallin amyloid fibril fragments, then crystallin amyloid fibrils assembled from the surface bound fragments. The surface assembled crystallin amyloid fibrils appear as spherulitic structures very similar to those previously seen with amyloid β fibril surface assembly (Ban *et al.* 2006). The coverage of the crystallin amyloid fibrils on the glass surface is reasonably regular, although fine-tuning of the crystallin seeding and assembly process may be able to increase the density and distribution of the amyloid fibrils to provide more surface area. The electron micrograph results provide evidence that crystallin amyloid fibrils can be assembled on the surface of glass beads, and that the surface needs to be seeded for surface assembled amyloid fibril formation to occur. This is thought to be the first time that crystallin amyloid fibrils have been assembled from a surface, and provides a proof of principle for the surface assembly of crystallin amyloid fibrils. It is also thought to be the first time that crystallin amyloid fibrils have been shown to form spherulitic structures.

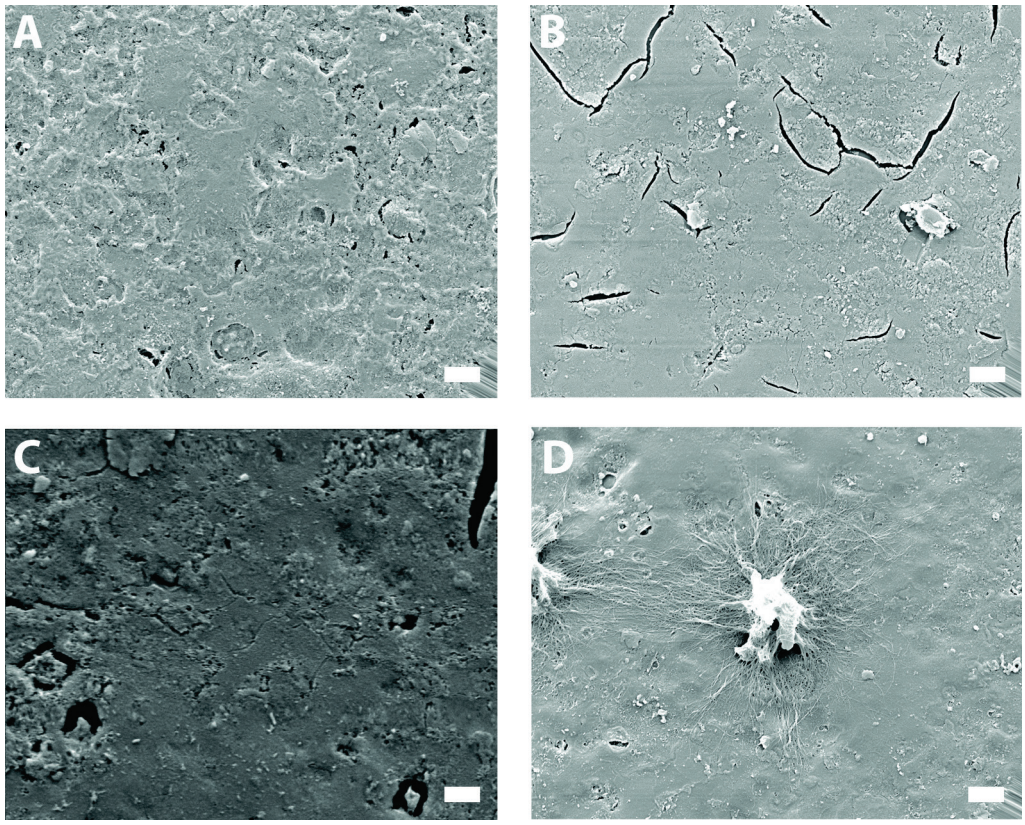

Figure 3.15 *Representative SEM micrographs of the surface of glass beads. A – Not seeded, plus crystallin fibrils, B – not seeded, no fibrils (blank), C – seeded, no fibrils, D – seeded, plus crystallin fibrils. The scale bar = 1 μm.*

3.5 Cellulose based surfaces

Cellulose is manufactured by plants, bacteria and a group of animals called tunicates *via* the condensation polymerisation of glucose (Klemm & Heinze 1998). The native state of cellulose in plant cell walls is of a crystalline nature, held together by hydrogen bonding (Kamel 2008). The structure of cellulose is shown in **Figure 3.16** (A) and consists of long chains of anhydro-D-glucopyranose units, with each cellulose molecule containing three hydroxyl groups (Klemm *et al.* 2005).

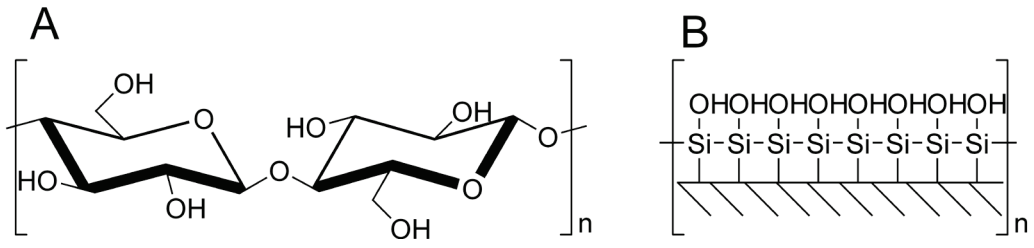

Figure 3.16 *Chemical structure of cellulose (A) (Klemm* et al. *2005), and glass (B) (Howarter & Youngblood 2006).*

Cellulose is used in many different applications, but due to its relative inertness and insolubility in water, chemical modifications to the surface are often required before cellulose can be used (Doheny *et al.* 1999). Chemical modification of cellulose is employed to change the properties of cellulose to suit desired applications. There are many different types of chemical modifications that are applied to cellulose including: esterifications, etherifications, ionic and radical grafting, acetylation, deoxyhalogenation, and oxidation (Kamel 2008). Pahimanolis *et al.* (2011) used click-chemistry to functionalise the surface of nanofibrillated cellulose *via* the etherification of 1-azido-2,3-epoxypropane introducing reactive azide groups, which were subsequently reacted with propargyl amine using copper catalysed azide-alkyne cycloaddition, creating a pH-responsive material.

Many enzymes have been immobilised to cellulose based materials such as: glucoamylase (Bryjak *et al.* 2007), and invertase (Bryjak *et al.* 2008). In most cases of enzyme immobilisation, the cellulose surfaces are first functionalised to yield an active amine group, to which the enzyme can covalently bind to. Recently, Edwards *et al.* (2011) immobilised lysozyme to cotton, first by functionalising the cotton with APTS, then activating the amine group with a carbodiimide. This method is similar to how the amyloid fibril fragments will be covalently bound to cellulose based materials in this research, and how they were attached to the glass bead surface.

The surface chemistry used on the glass is readily adaptable to cellulose because of the similar surface chemistry in the form of the hydroxyl groups (**Figure 3.16**) (Aslam & Dent 1998). Silanes have been extensively used to treat cellulose based materials not only for enzyme immobilisation but also, for example, to change properties such as the wettability and hydrophobicity of the material (Abdelmouleh *et al.* 2004; Yu *et al.* 2007). The application of APTS and the subsequent template directed amyloid fibril self-assembly was therefore expected to be applicable to cellulose based materials.

Two types of cellulose material were used in this research: unbleached, untreated, starched cotton; and 20 μm microcrystalline cellulose powder. Cotton was selected as a material to investigate the ability to assemble insulin amyloid fibrils because of its wide use in many industries, including the textile industry (Klemm *et al.* 2005). The potential to create cotton materials with increased surface area that may subsequently be able to be functionalised with biomolecules, could provide a new type of surface treatment for the creation of bionanomaterials. Microcrystalline cellulose was utilised to aid in the analysis of surface chemistry when the cotton fibres were too large. The dry weight of cotton is made up of ~95 % cellulose (Kim & Triplett 2001), therefore a direct comparison can be made between cotton and microcrystalline cellulose.

3.5.1 Derivatisation and analysis of cellulose surfaces

The derivatisation of the microcrystalline cellulose (section 7.14.2) and the cotton (section 7.14.1) used very similar methods as were used on the glass beads (section 3.4.1). The surface chemistry of the cotton and glass beads was not able to be analysed with FTIR because of their size not been compatible with the spectrophotomer. Microcrystalline cellulose was used because of the similarities of the surface chemistry present in the form of hydroxyl groups. In-depth analysis of the surface derivatisation of cellulose using FTIR was possible because of the size of the microcrystalline cellulose used.

FTIR (section 7.2.9) is a technique commonly used when studying chemical treatments of cellulose based materials (Yang *et al.* 1987). FTIR was used to assess whether APTS surface derivatisation had been successful in modifying the surface of the cellulose, and to confirm the presence of the template directed insulin amyloid fibrils on the microcrystalline cellulose. FTIR can be used to assess differences in secondary structure of proteins by the amide I peptide band (~1600-1700 cm^{-1}) arising from the carbonyl vibrations (Arrondo *et al.* 1993).

The 20 μm microcrystalline cellulose samples were treated with APTS (section 7.14.2) using the same protocol as with the glass beads (section 3.4.1). The samples were then analysed by FTIR. **Figure 3.17** shows the FTIR spectra of the cellulose with and without treatment of APTS, and also pre-heating and post-heating at 110 °C of APTS cellulose. Heating at 110 °C causes the condensation reaction to proceed, therefore, a reduction in the number of hydroxyl groups should be seen. The appearance of a peak at ~ 1575 cm^{-1} in the APTS treated cellulose samples is indicative of an amine group which arises from the amine moiety in APTS (Chiang *et al.* 1980), confirming APTS is present on the cellulose. Chiang *et al.* (1980) were able to analyse APTS on the surface of glass because the glass was a fine powder glass, similar in size to the microcrystalline cellulose.

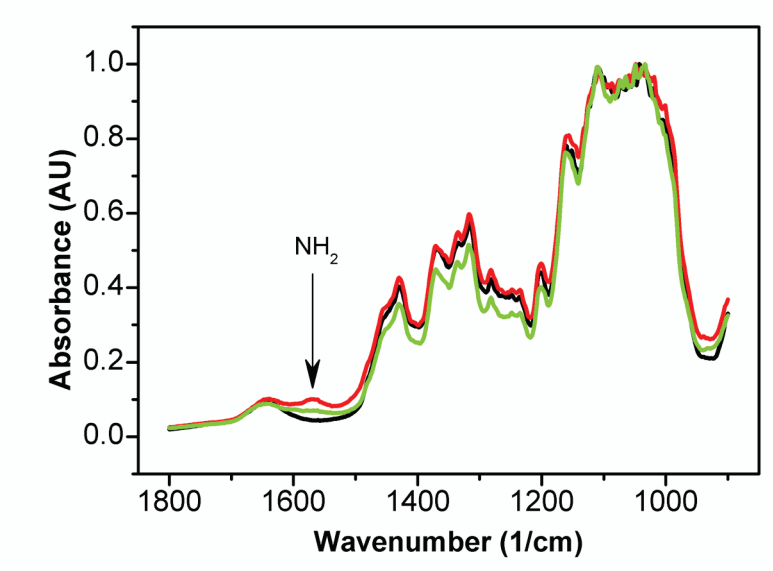

Figure 3.17 *FTIR of untreated cellulose powder (black), cellulose treated with APTS pre-heating (green), and cellulose treated with APTS post-heating (red). The arrow points towards the amide peak 1575 cm. Measurements are the average of 40 scans of each sample.*

To investigate whether the condensation reaction between APTS and cellulose took place after heating of the sample, subtraction spectra corresponding to the cellulose samples treated with APTS, before and after heating were analysed. **Figure 3.18** shows a peak around 1017 cm^{-1} on the FTIR spectrum of the pre-heated sample, which was attributed to Si-OH groups (Abdelmouleh *et al.* 2004). This peak decreases after heating and a new peak around 1035 cm^{-1} increases, characteristic of Si-O-Si groups (Lu *et al.* 2008). These peak assignments are in accordance with the literature (Chiang *et al.* 1980), confirming APTS has successfully derivatised the surface of the cellulose.

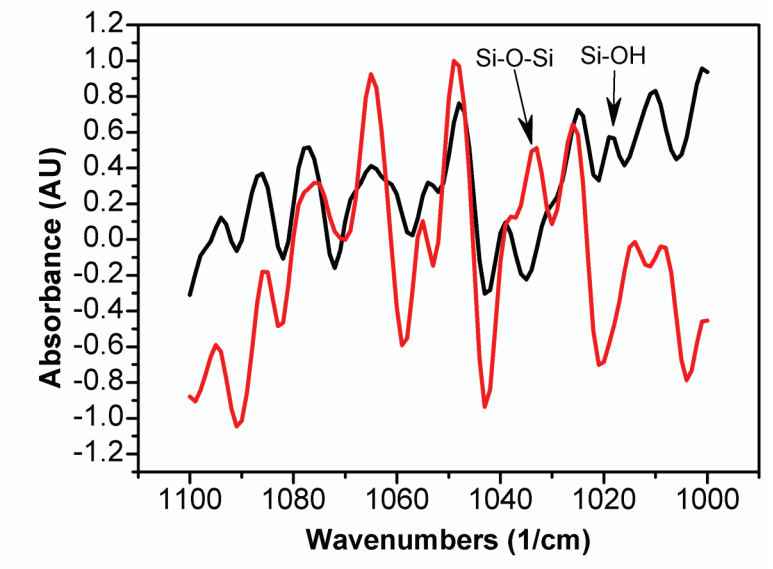

Figure 3.18 *FTIR subtraction spectra of cellulose powder treated with APTS pre-heating (black) and post-heating (red). The baseline of the cellulose powder only has been subtracted from the two samples. Measurements are the average of 40 scans of each sample.*

3.5.2 Template directed self-assembly of insulin amyloid fibrils on cellulose surfaces

An almost identical method to that used on the glass beads for template directed self-assembly of insulin amyloid fibrils was used for the cellulose surfaces (section 7.14.3 and 7.14.4). When using the microcrystalline cellulose, extra care was needed when washing the cellulose due to its size and the possibility of decanting the cellulose during the wash steps. The cotton also required extra drying because of the absorptive nature of cotton.

To assess the presence of insulin amyloid fibrils on the surface of the cellulose based materials, ThT fluorescence of the materials was investigated. ThT fluorescence of the microcrystalline cellulose samples used the 96 well plate reader (section 7.2.8). This method proved unsuitable due to the extreme high background fluorescence of the cellulose only sample. ThT has been shown to bind to cellulose (Raj & Ramaraj 2001) and the fact that microcrystalline cellulose was used may have increased the background fluorescence due to its high binding capacity compared to the cotton material. A surface fluorescence spectrophotometer was used to assess the ThT fluorescence of the cotton samples (section 7.2.9). The cotton samples were placed between two microscope cover slips and the surface fluorescence measured at an angle of 90 °. **Figure 3.19** shows the ThT fluorescence of the template directed insulin amyloid fibril cotton samples. As can be seen, the cotton samples which had been seeded with insulin amyloid fragments, then mature insulin amyloid fibrils assembled had the highest ThT fluorescence. This confirms for the first time that template directed insulin amyloid fibril formation can occur on cellulose based materials as well as glass surfaces.

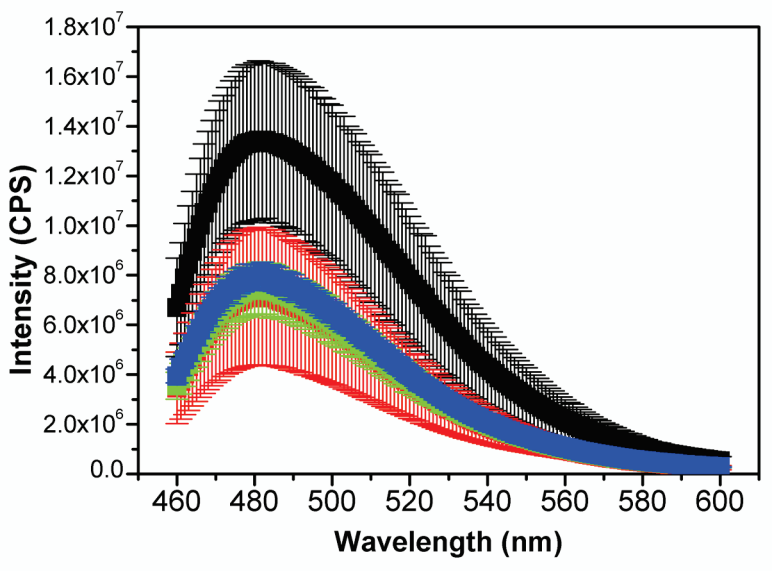

Figure 3.19 *ThT fluorescence of cotton samples. (■) – Seeded and fibrils assembled, (■) – Seeded and fibrils not assembled, (■) – Not seeded, and fibrils assembled, (■) – Not seeded and fibrils not assembled. Measurements are the average of 3 replicates of each sample and the error is the standard deviation of the mean.*

Because the ThT assay could not be used on the microcrystalline cellulose, FTIR was employed to monitor the insulin amyloid fibril secondary structure. FTIR requires dried samples to minimise background noise from H_2O, therefore the surface assembled microcrystalline cellulose samples were first thoroughly dried at 37 °C for 1 week. **Figure 3.20** shows the second derivative FTIR spectrum of cellulose powder which had either been seeded with insulin fragments or not seeded, then mature amyloid fibrils assembled or not assembled. There is the appearance of a shoulder at about ~1630 cm^{-1} in the samples that contain amyloid fibrils, which reveals the presence of a parallel β-sheet hydrogen bond networks (Bouchard *et al.* 2000). The sample that was not seeded, but had amyloid fibrils assembled also has the ~1630 cm^{-1} shoulder, therefore must contain amyloid structures as well. This result would agree with results previously seen in which insulin amyloid fibril formation was monitored in solution by FTIR (Bouchard *et al.* 2000). This provides good evidence that insulin amyloid fibrils can be assembled on the surface of microcrystalline cellulose.

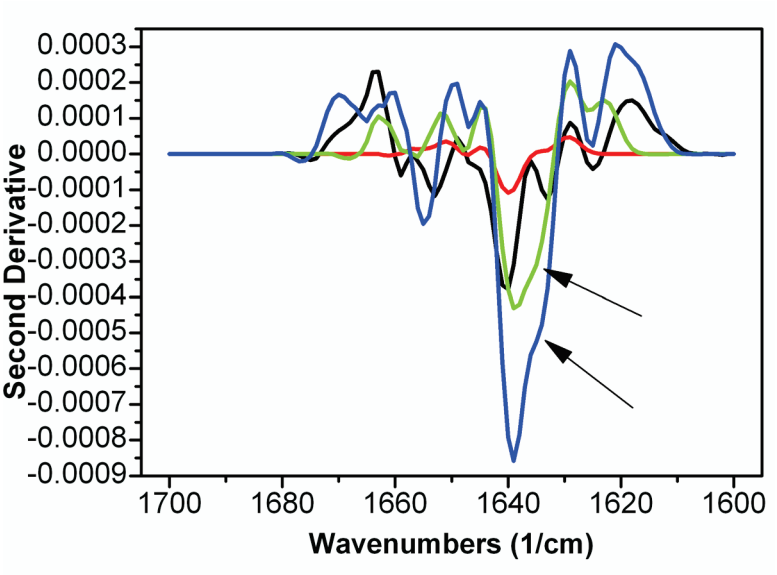

Figure 3.20 *FTIR of APTS treated cellulose powder. All spectra had their second derivative taken. (Black) is not seeded and no fibrils assembled, (red) is seeded, no fibrils assembled, (green) is not seeded, but fibrils assembled, and (blue) is seeded, and fibrils assembled. The arrows point to the shoulder corresponding to the presence of a β-sheet secondary protein structure. Measurements are the average of 40 scans of each sample.*

3.6 Summary

Bovine insulin and fish eye lens crystallin amyloid fibrils have been successfully manufactured and characterised in solution. Both the solution assembled amyloid fibrils showed the unbranched, twisted, fibrillar morphology, characteristic of amyloid fibrils. The crystallin amyloid fibrils were slightly wider and considerably longer than the insulin amyloid fibrils. Highly reproducible template directed self-assembly of bovine insulin amyloid fibrils was shown to be possible on the surface of glass beads, and for the first time the methodology was shown to be applicable to crystallin amyloid fibrils. This could imply that surface assembly may be applicable to any amyloid forming protein. The surface assembled crystallin amyloid fibrils had a spherulite appearance when viewed with SEM. This is thought to be the first time a spherulite structure has been seen for crystallin amyloid fibrils. Template directed self-assembly of bovine insulin amyloid fibrils has also been confirmed on cellulose based surfaces for the first time. Demonstrating surface assembly of insulin amyloid fibrils on cellulose based materials suggests that they could be assembled on other surfaces as well, although more work is needed to establish if insulin amyloid fibril surface assembly is a property of other surfaces.

3.7 References

Abdelmouleh, M., Boufi, S., Belgacem, M.N., Duarte, A.P., Ben Salah, A. & Gandini, A., 2004. Modification of cellulosic fibres with functionalised silanes: Development of surface properties. *International Journal of Adhesion and Adhesives*, 24(1), pp.43–54.

Arakawa, T., Prestrelski, S.J., Kenney, W.C. & Carpenter, J.F., 2001. Factors affecting short-term and long-term stabilities of proteins. *Advanced Drug Delivery Reviews*, 46(1–3), pp.307–326.

Arrondo, J.L.R., Muga, A., Castresana, J. & Goñi, F.M., 1993. Quantitative studies of the structure of proteins in solution by fourier-transform infrared spectroscopy. *Progress in Biophysics and Molecular Biology*, 59(1), pp.23–56.

Aslam, M. & Dent, A., 1998. *Bioconjugation: Protein Coupling for the Biomedical Sciences* 1st ed., United Kingdom: Stockton Press.

Ban, T., Morigaki, K., Yagi, H., Kawasaki, T., Kobayashi, A., Yuba, S., Naiki, H. & Goto, Y., 2006. Real-time and single fibril observation of the formation of amyloid β spherulitic structures. *Journal of Biological Chemistry*, 281(44), pp.33677–33683.

Bouchard, M., Zurdo, J., Nettleton, E.J., Dobson, C.M. & Robinson, C.V., 2000. Formation of insulin amyloid fibrils followed by FTIR simultaneously with CD and electron microscopy. *Protein Science*, 9(10), pp.1960–1967.

Brady, D. & Jordaan, J., 2009. Advances in enzyme immobilisation. *Biotechnology Letters*, 31, pp.1639–1650.

Bryjak, J., Aniulyte, J. & Liesiene, J., 2007. Evaluation of man-tailored cellulose-based carriers in glucoamylase immobilization. *Carbohydrate Research*, 342(8), pp.1105–1109.

Bryjak, J., Liesiene, J. & Štefuca, V., 2008. Man-tailored cellulose-based carriers for invertase immobilization. *Cellulose*, 15(4), pp.631–640.

Chang, B.S., Kendrick, B.S. & Carpenter, J.F., 1996. Surface-induced denaturation of proteins during freezing and its inhibition by surfactants. *Journal of Pharmaceutical Sciences*, 85(12), pp.1325–1330.

Chiang, C.-H., Ishida, H. & Koenig, J.L., 1980. The structure of γ-aminopropyltriethoxysilane on glass surfaces. *Journal of Colloid and Interface Science*, 74(2), pp.396–404.

Doheny, J.G., Jervis, E.J., Guarna, M.M., Humphries, R.K., Warren, R.A. & Kilburn, D.G., 1999. Cellulose as an inert matrix for presenting cytokines to target cells: production and properties of a stem cell factor-cellulose-binding domain fusion protein. *Biochemical Journal*, 339(Pt 2), pp.429–434.

Domigan, L.J., Healy, J.P., Meade, S.J., Blaikie, R.J. & Gerrard, J.A., 2012. Controlling the dimensions of amyloid fibrils: Toward homogenous components for bionanotechnology. *Biopolymers*, 97(2), pp.123–133.

Edwards, J.V., Prevost, N.T., Condon, B. & French, A., 2011. Covalent attachment of lysozyme to cotton/cellulose materials: Protein verses solid support activation. *Cellulose*, 18(5), pp.1239–1249.

Fülöp, L., Penke, B. & Zarándi, M., 2001. Synthesis and fluorescent labeling of beta-amyloid peptides. *Journal of Peptide Science: An Official Publication of the European Peptide Society*, 7(8), pp.397–401.

Garvey, M., Gras, S.L., Meehan, S., Meade, S.J., Carver, J.A. & Gerrard, J.A., 2009. Protein nanofibres of defined morphology prepared from mixtures of crude crystallins. *International Journal of Nanotechnology*, 6(3-4), pp.258–273.

Greenfield, N.J. & Fasman, G.D., 1969. Computed circular dichroism spectra for the evaluation of protein conformation. *Biochemistry*, 8(10), pp.4108–4116.

Groenning, M., 2010. Binding mode of Thioflavin T and other molecular probes in the context of amyloid fibrils-current status. *Journal of Chemical Biology*, 3(1), pp.1–18.

Ha, C. & Park, C.B., 2005. Template-directed self-assembly and growth of insulin amyloid fibrils. *Biotechnology and Bioengineering*, 90(7), pp.848–855.

Healy, J., Wong, K., Roux, C., Domigan, L., Sunde, M., Gerrard, J.A. & Vasudevamurthy, M., 2012. Polymorphism and higher ordered structures of protein nanofibres from crude mixtures of fish lens crystallins: Towards useful materials. *Accepted to Biopolymers*.

Hermanson, G.T., 1996. *Bioconjugate Techniques* 1st ed., Rockford, IL USA: Academic Press.

Hermanson, G.T., 2008. *Bioconjugate Techniques* 2nd ed., Rockford, IL USA: Academic Press.

Howarter, J.A. & Youngblood, J.P., 2006. Optimization of silica silanization by 3-aminopropyltriethoxysilane. *Langmuir*, 22(26), pp.11142–11147.

Howarter, J.A. & Youngblood, J.P., 2007. Surface modification of polymers with 3-aminopropyltriethoxysilane as a general pretreatment for controlled wettability. *Macromolecules*, 40(4), pp.1128–1132.

Huang, Y.Y., Knowles, T.P.J. & Terentjev, E.M., 2009. Strength of nanotubes, filaments, and nanowires from sonication-induced scission. *Advanced Materials*, 21(38-39), pp.3945–3948.

Jarrett, J.T. & Lansbury, P.T., 1992. Amyloid fibril formation requires a chemically discriminating nucleation event: studies of an amyloidogenic sequence from the bacterial protein OsmB. *Biochemistry*, 31(49), pp.12345–12352.

Jia, H., Zhu, G., Vugrinovich, B., Kataphinan, W., Reneker, D.H. & Wang, P., 2002. Enzyme-carrying polymeric nanofibers prepared *via* electrospinning for use as unique biocatalysts. *Biotechnology Progress*, 18(5), pp.1027–1032.

Jobbágy, A. & Király, K., 1966. Chemical characterization of fluorescein isothiocyanate-protein conjugates. *Biochimica Et Biophysica Acta*, 124(1), pp.166–175.

Kamel, S., 2008. Pharmaceutical significance of cellulose: A review. *eXPRESS Polymer Letters*, 2(11), pp.758–778.

Kim, H.J. & Triplett, B.A., 2001. Cotton fiber growth *in planta* and *in vitro*. Models for plant cell elongation and cell wall biogenesis. *Plant Physiology*, 127(4), pp.1361–1366.

Kim, J., Yun, S. & Ounaies, Z., 2006. Discovery of cellulose as a smart material. *Macromolecules*, 39(12), pp.4202–4206.

Klemm, D. & Heinze, T., 1998. *Comprehensive Cellulose Chemistry: Fundamentals and analytical methods*, New York: Wiley-VCH.

Klemm, D., Heublein, B., Fink, H.-P. & Bohn, A., 2005. Cellulose: Fascinating biopolymer and sustainable raw material. *Angewandte Chemie International Edition*, 44(22), pp.3358–3393.

Lu, J., Askeland, P. & Drzal, L.T., 2008. Surface modification of microfibrillated cellulose for epoxy composite applications. *Polymer*, 49(5), pp.1285–1296.

Meehan, S., Knowles, T.P.J., Baldwin, A.J., Smith, J.F., Squires, A.M., Clements, P., Treweek, T.M., Ecroyd, H., Tartaglia, G.G., Vendruscolo, M., MacPhee, C.E., Dobson, C.M. & Carver, J.A., 2007. Characterisation of amyloid fibril formation by small heat-shock chaperone proteins human αA-, αB- and R120G αB-crystallins. *Journal of Molecular Biology*, 372(2), pp.470–484.

Morpurgo, M., Bayer, E.A. & Wilchek, M., 1999. N-hydroxysuccinimide carbonates and carbamates are useful reactive reagents for coupling ligands to lysines on proteins. *Journal of Biochemical and Biophysical Methods*, 38(1), pp.17–28.

Nielsen, L., Khurana, R., Coats, A., Frokjaer, S., Brange, J., Vyas, S., Uversky, V.N. & Fink, A.L., 2001. Effect of environmental factors on the kinetics of insulin fibril formation: Elucidation of the molecular mechanism. *Biochemistry*, 40(20), pp.6036–6046.

Nilsson, M.R., 2004. Techniques to study amyloid fibril formation *in vitro*. *Methods*, 34(1), pp.151–160.

Nimura, N., Iwaki, K., Kinoshita, T., Takeda, K. & Ogura, H., 1986. Activated carbamate reagent as derivatizing agent for amino compounds in high-performance liquid chromatography. *Analytical Chemistry*, 58(12), pp.2372–2375.

Oppenheim, T., Knowles, T.P.J., Lacour, S.P. & Welland, M.E., 2010. Fabrication and characterisation of protein fibril–elastomer composites. *Acta Biomaterialia*, 6(4), pp.1337–1341.

Ortiz, C., Zhang, D., Ribbe, A.E., Xie, Y. & Ben-Amotz, D., 2007. Analysis of insulin amyloid fibrils by Raman spectroscopy. *Biophysical Chemistry*, 128(2-3), pp.150–155.

Pahimanolis, N., Hippi, U., Johansson, L.-S., Saarinen, T., Houbenov, N., Ruokolainen, J. & Seppälä, J., 2011. Surface functionalization of nanofibrillated cellulose using click-chemistry approach in aqueous media. *Cellulose*, 18(5), pp.1201–1212.

Pilkington, S.M., Roberts, S.J., Meade, S.J. & Gerrard, J.A., 2010. Amyloid fibrils as a nanoscaffold for enzyme immobilization. *Biotechnology Progress*, 26(1), pp.93–100.

Raj, C.R. & Ramaraj, R., 2001. Emission of Thioflavin T and its off–on control in polymer membranes. *Photochemistry and Photobiology*, 74(6), pp.752–759.

Rao, S.P., Meade, S.J., Healy, J.P., Sutton, K.H., Larsen, N.G., Staiger, M.P. & Gerrard, J.A., 2012. Amyloid fibrils as functionalizable components of nanocomposite materials. *Biotechnology Progress*, 28(1), pp.248–256.

Schmit, J.D., Ghosh, K. & Dill, K., 2011. What drives amyloid molecules to assemble into oligomers and fibrils? *Biophysical Journal*, 100(2), pp.450–458.

Thermo Scientific, 2011. Calculate dye:protein (F/P) molar ratios. Available at: http://www.piercenet.com/files/TR0031-Calc-FP-ratios.pdf.

Wang, P., 2006. Nanoscale biocatalyst systems. *Current Opinion in Biotechnology*, 17(6), pp.574–579.

Waugh, D.F., 1946. A fibrous modification of insulin. I. The heat precipitate of insulin. *Journal of the American Chemical Society*, 68(2), pp.247–250.

Whittingham, J.L., Scott, D.J., Chance, K., Wilson, A., Finch, J., Brange, J. & Guy Dodson, G., 2002. Insulin at pH 2: Structural analysis of the conditions promoting insulin fibre formation. *Journal of Molecular Biology*, 318(2), pp.479–490.

Williams, R.J., Mart, R.J. & Ulijn, R.V., 2010. Exploiting biocatalysis in peptide self-assembly. *Peptide Science*, 94(1), pp.107–117.

Xue, W.F., Hellewell, A.L., Gosal, W.S., Homans, S.W., Hewitt, E.W. & Radford, S.E., 2009. Fibril fragmentation enhances amyloid cytotoxicity. *The Journal of biological chemistry*.

Yang, C.Q., Bresee, R.R., Fateley, W.G. & Perenich, T.A., 1987. Cellulose textile materials studied by using Fourier transform infrared photoacoustic spectroscopy. In *ACS Symposium series - American Chemical Society*. pp. 214–232.

Yu, M., Gu, G., Meng, W.-D. & Qing, F.-L., 2007. Superhydrophobic cotton fabric coating based on a complex layer of silica nanoparticles and perfluorooctylated quaternary ammonium silane coupling agent. *Applied Surface Science*, 253(7), pp.3669–3673.

Chapter Four

4 Amyloid fibrils as a biomolecule nanoscaffold in solution

4.1 Introduction

This chapter will explore the use of bovine insulin and fish eye lens crystallin protein nanoscaffolds in solution, to which the enzymes purified and characterised in chapter two will be immobilised using the model cross-linker glutaraldehyde. Specifically, OPH was thoroughly investigated to determine immobilisation conditions that can then potentially be applied to $P450_{BM3}$, GFP, TEV protease and GOD. The diversity of biomolecule immobilisation should help with understanding if insulin amyloid fibrils can act as a versatile nanoscaffold.

4.2 Glutaraldehyde cross-linking

Glutaraldehyde (GA) is a homo-bifunctional cross-linking agent containing two aldehyde groups on a five carbon chain (**Figure 4.1**). GA is the most commonly used example of bis-aldehydes with uses in microscopy, cytochemistry, leather tanning, enzyme technology and chemical sterilisation (Migneault *et al.* 2004). In this research, GA was used for the cross-linking of enzymes to amyloid fibrils.

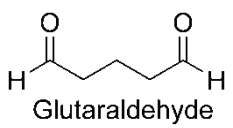

Figure 4.1 *Structure of glutaraldehyde (Whipple & Ruta 1974).*

GA is known to react with several functional groups of proteins, including, amine, thiol, phenol and imidazole moieties (Habeeb & Hiramoto 1968). The most reactive species towards GA are the ε-amino groups, followed by the α-amino groups, which correspond to the primary amino group present in lysine residues, and the N-terminal amino group present in proteins, respectively (Migneault *et al.* 2004). Lysine was the target for cross-linking using GA because it is reactive towards GA, and, is a common amino acid which is frequently located on the protein surface (Brady & Jordaan 2009). The mechanism by which GA reacts with the amino groups of proteins is still under debate. One possible mechanism is *via* the formation of a pyridinium cross-link, as shown in **Figure 4.2** (Hermanson 1996; Meade *et al.* 2003).

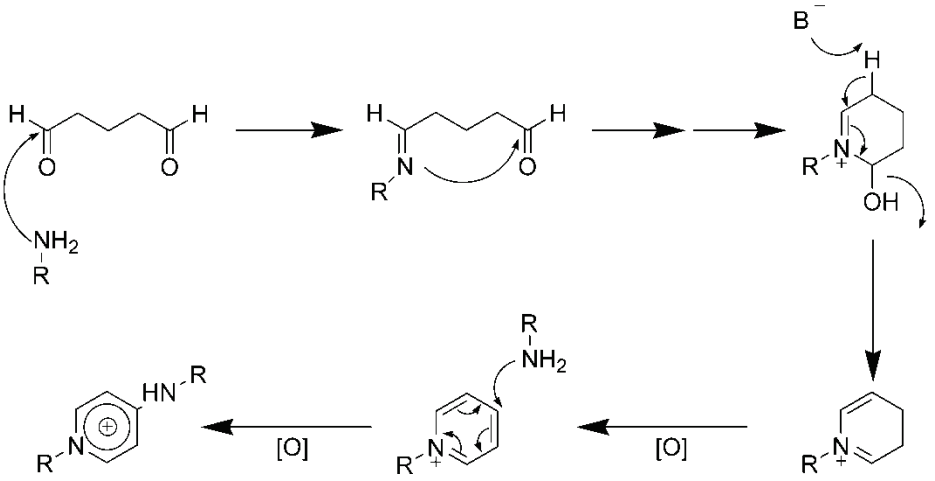

Figure 4.2 *Proposed mechanism for formation of pyridinium cross-links. Adapted from Meade et al. (2003).*

GA is one of the most commonly used and studied cross-linking agents for immobilising enzymes. Other typical bifunctional cross-linkers used include: dimethyl suberimidate, disuccinimidyl tartrate, disuccinimidyl carbonate (DSC), *N*-hydroxysuccinimide (NHS) and 1-ethyl-3-(3-dimethylaminopropryl) carbodiimide (EDC) (Moehlenbrock & Minteer 2011). GA was selected as the cross-linking agent for enzyme immobilisation in this research because it is simple to use, cheap, and highly reactive towards proteins. NHS in combination with EDC was also investigated as an alternative cross-linking method in preliminary studies, but the process was more difficult and did not produce cross-linked protein products as easily, therefore they were not used.

Because GA is extremely reactive towards proteins, there can be problems of creating large, often poorly defined protein aggregates if the reaction is not completed in a controlled way (Stratis 1969). When trying to cross-link two proteins using GA, the cross-linking targets are the same on both proteins, therefore, it can be very difficult to control the intra- and intermolecular cross-linking (Hermanson 1996). A two-step immobilisation protocol that first reacts the GA with one of the proteins, creating one activated protein, then adding the second protein, can be used to very good effect. This protocol limits the intramolecular cross-linking, and maximises the intermolecular cross-linking (Hermanson 1996). The concentration of GA present can also have a major influence on the cross-linking reaction, therefore, the procedure needs to be thoroughly investigated to achieve optimised conjugation. Although there are recognised shortcomings of homo-bifunctional cross-linkers, they work very well for many applications.

4.3 Organophosphate hydrolase immobilisation method development

OPH was recombinantly overexpressed and purified as outlined in chapter two. The immobilisation procedure to cross-link OPH to the amyloid fibrils used a two-step procedure. First, the GA was reacted with the amyloid fibrils to create an activated nanoscaffold, secondly, the OPH was added to create the functionalised amyloid fibrils. A two step procedure was used to limit OPH-OPH cross-linking and maximise the amount of OPH cross-linked to the amyloid fibrils. The specifics of the procedure required thorough investigation in preliminary experiments, to optimise the desired cross-linking.

Figure 4.3 shows the surface of the OPH and MBP crystal structures with the lysine residues highlighted in pink, to illustrate the lysine residues theoretically available for cross-linking with GA. There is no crystal structure of the OPH-MBP fusion protein, therefore the two structures are shown individually. Because it was shown in chapter two that the activity of the OPH-MBP fusion protein has very similar catalytic constants as the wild-type OPH, and because the MBP has many potential lysine residues available for cross-linking, it was initially decided to keep the MBP tag attached to the OPH.

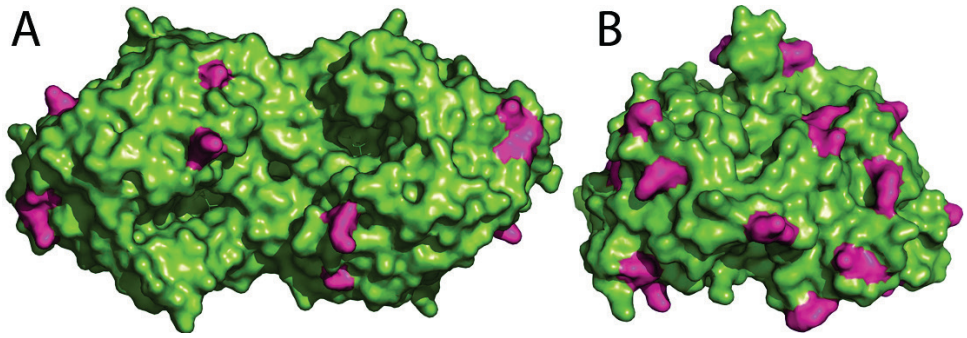

Figure 4.3 *Crystal structures of A – OPH (PDB 1EZ2) (Benning et al. 2000), and B – MBP (PDB 3MBP) (Quiocho et al. 1997) showing the surface with the lysine residues coloured in pink.*

OPH has previously been immobilised to a wide range of matrices including trityl agarose (Caldwell & Raushel 1991), polyurethane (Havens & Rase 1993), polyethylene glycol (Andreopoulos *et al.* 1999), silicone (Gill & Ballesteros 2000), carbon nanotubes (Borkar *et al.* 2010; Pedrosa *et al.* 2010) and gelatin pads (Kanugula *et al.* 2011). A variety of immobilisation techniques have been applied to OPH, for example, cross-linked enzyme aggregates (Laothanachareon *et al.* 2008), sol-gel encapsulation (Frančič *et al.* 2011), and self-assembly into hydrogels by fusion with an α-helical leucine zipper domain (Lu *et al.* 2010). The inspiration for the majority of research into OPH is for the creation of biosensors for detection of OP and/or chemical detoxification of OP. As stated in section 2.2, there is a need for a cheap, reliable, and reusable method for the bioremediation of OP and their chemical detoxification (Kanugula *et al.* 2011). Thus, immobilisation of OPH to an amyloid fibril nanoscaffold could provide a cheap and effective method to enhance the stability and reusability of OPH.

4.3.1 OPH cross-linking method development

Different concentrations of GA were initially investigated to determine what effect GA concentration had on the activity of OPH. A starting concentration of 7.6 mg/mL of OPH was used in the experiments because this was the concentration of the eluted protein after purification. At this protein concentration, the lysine concentration of the OPH-MBP fusion corresponds to 3.65 mM. **Table 4.1** shows with increasing concentrations of GA, there is a progressive drop in the activity of OPH when compared to an OPH sample with no GA.

Table 4.1 *Activity of OPH when cross-linked to another OPH molecule for 1 hour at 37 °C with different concentrations of GA. % Activity is the initial rate of reaction compared against the 0 mM GA sample. All reactions were carried out in triplicate and the error is the standard deviation of the mean.*

Final conc. of GA (mM)	% Activity	Error
0	100	± 12
2.5	83	± 7
3.75	79	± 11
5	82	± 5
10	51	± 5
15	40	± 2
20	35	± 2
25	35	± 6

The same samples were also investigated by SDS-PAGE (**Figure 4.4**), which shows that when using the lowest final concentration of 2.5 mM GA, almost all of the OPH has been cross-linked to another OPH molecule, because there is only a faint protein band at ~ 77 kDa compared to the control (lane 1). At final concentrations of 15 mM or higher, very large OPH aggregates had formed, which were unable to enter the polyacrylamide gel, shown by the lack of visible protein bands in the gel (lanes 6, 7 and 8). The presence of large aggregates corresponds well with the activity drop shown in **Table 4.1** suggesting that these aggregated structures are inactive. The inactivity could be caused by cross-linking of lysine 169 in the active site, which is known to bridge the two metal ions required for catalysis (Aubert *et al.* 2004), or by restriction of the active site binding pocket which would not allow the substrate to bind.

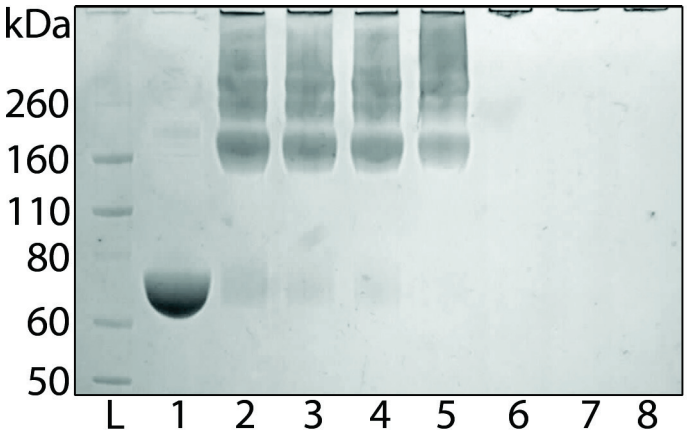

Figure 4.4 *SDS-PAGE gel of OPH cross-linked to itself using different final concentrations of GA for 1 hour at 37 °C. L – ladder, 1 – 0 mM GA, 2 – 2.5 mM GA, 3 – 3.75 mM GA, 4 – 5 mM GA, 5 – 10 mM GA, 6 – 15 mM GA, 7 – 20 mM GA, 8 – 25 mM GA.*

From the results in **Table 4.1** and **Figure 4.4**, 2.5 mM GA was selected as the final concentration cross-linker to use when cross-linking OPH. Using 2.5 mM GA with 7.6 mg/mL OPH means there are ~1.5 times more potential amino groups to react than there is GA, potentially therefore all of the GA will react with the OPH.

OPH was cross-linked to another OPH molecule over time to evaluate the time required for cross-linking to occur (**Figure 4.5).** As can be seen, at time 0 some cross-linking has already occurred, indicating that GA cross-linking occurs very quickly under the chosen conditions. 1 hour was selected as the time for the cross-linking reaction because at 60 mins a good amount of OPH-OPH cross-linking had occurred, whilst not creating many larger order aggregates.

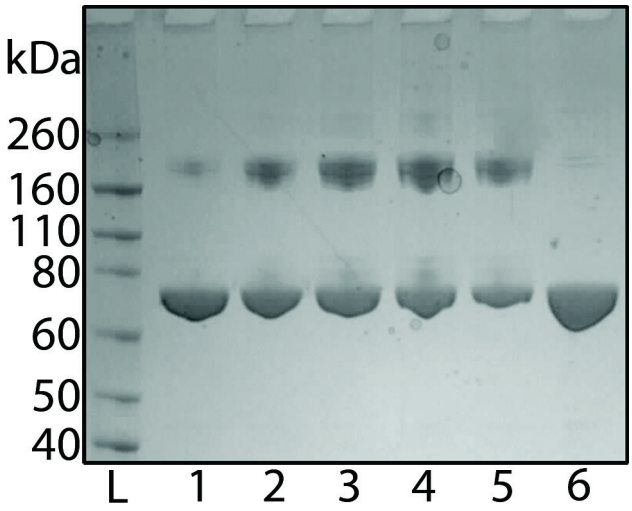

Figure 4.5 *SDS-PAGE gel of OPH cross-linked to itself using over time using 2.5 mM GA at 4 °C. L – ladder, 1 – 0 mins, 2 – 30 mins, 3 – 60 mins, 4 – 90 mins, 5 – 120 mins, 6 – no GA.*

Once the cross-linking time was selected, cross-linking temperature was investigated. As can be seen in **Figure 4.6**, 37 °C (lane 5) was the temperature that gave the most cross-linking, as judged by SDS-PAGE. The 37 °C cross-linked OPH was run on a size exclusion chromatography column (section 7.2.16) to detect the difference in elution volume compared to non-cross-linked OPH, and to recover the cross-linked OPH fractions for activity testing to investigate the effect of cross-linking on activity.

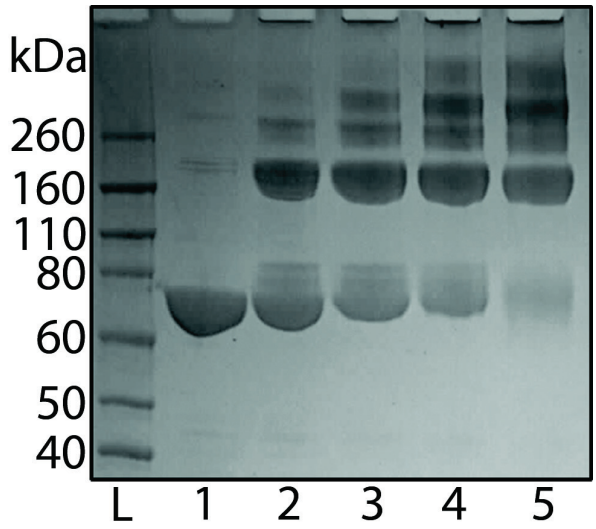

Figure 4.6 *SDS-PAGE gel of OPH cross-linked to itself at different temperatures using 2.5 mM GA. L- ladder, 1 – no GA, 2 – 1 °C, 3 – 4 °C, 4 – 25 °C, 5 – 37 °C.*

Figure 4.7 shows the difference in elution peaks between cross-linked and non-cross-linked OPH. The cross-linked OPH sample displays a new peak at ~11 mL, indicating the presence of larger OPH species. The cross-linked OPH peaks were collected and initial rates investigated (section 7.9.1) to explore if the cross-linked OPH had altered specific activity. The specific activity was 0.000138 and 0.000134 AUs^{-1}/mAU for the ~11 mL and ~ 13 mL peaks, respectively. This confirms that cross-linking does not hinder the activity of OPH significantly. This was a positive result for the potential immobilisation of OPH to insulin amyloid fibrils because OPH was predicted to retain activity when cross-linked to the amyloid fibrils.

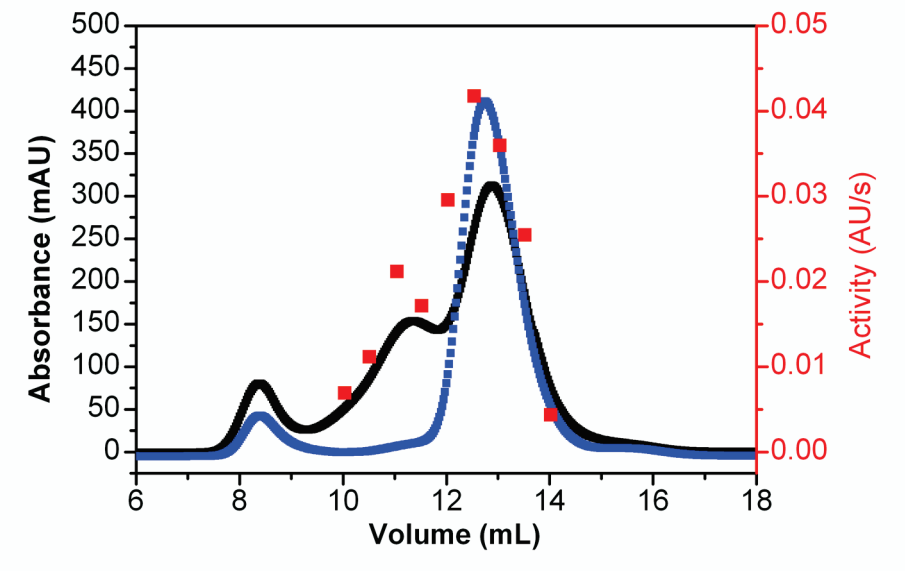

Figure 4.7 *Size exclusion chromatography showing OPH (■), and OPH cross-linked to itself using a final concentration of 2.5 mM GA, for 1 hour at 37 °C (■). The activity of different elution samples of the OPH cross-linked to itself sample is given by (■).*

From the experiments in this section it was decided to use a final concentration of 2.5 mM GA, for 1 hour, at 37 °C as the cross-linking conditions to immobilise OPH to the insulin amyloid fibrils. To stop the reaction from continuing after 1 hour, 2-amino-2-hydroxymethyl-propane-1,3-diol (tris) was added to quench any unreacted GA. Tris contains a primary amine and therefore can react with any unreacted GA.

4.3.2 Insulin amyloid fibril cross-linking method development

The effect of insulin amyloid fibrils in solution with the OPH and the consequence on activity (section 7.9.1) was first investigated. **Figure 4.8** shows that with increasing concentrations of insulin amyloid fibrils there is a decrease in OPH activity. This result was not ideal, but it was decided to use a starting concentration of 5.8 mg/mL (~1 mM) of the insulin amyloid fibrils because this is the concentration used to form the insulin amyloid fibrils *via* the in-house method. A starting concentration of 5.8 mg/mL insulin amyloid fibrils gives a final concentration of 1.9 mg/mL insulin fibrils in the immobilisation reaction because all parts of the reaction (GA, OPH, and fibrils) are added in a 1:1:1 v/v ratio. At a concentration of 1.9 mg/mL insulin amyloid fibrils, OPH retains the majority its activity, and from the FITC amine binding results (section 3.2.1), will provide ~0.3 mM amine groups for cross-linking with GA. There is no crystal structure of bovine insulin amyloid fibrils, it is therefore being assumed that some of the lysine residues and N-terminal residues are available on the surface of the amyloid fibrils for cross-linking because FITC was able to bind to them. The loss in OPH activity when incubated with insulin amyloid fibrils implies there could be an intrinsic association between OPH and the insulin amyloid fibrils. This interaction could have a positive benefit because there may not be the need for a cross-linking reagent.

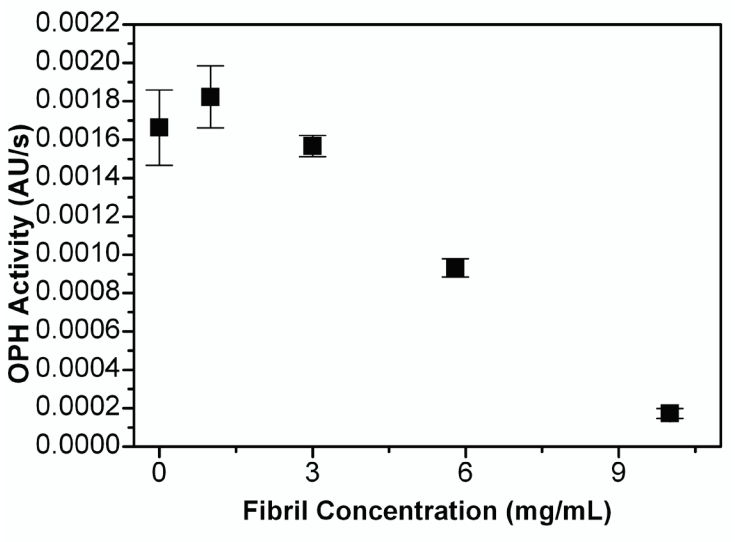

Figure 4.8 *Initial rates of OPH when incubated with different final concentrations of insulin amyloid fibrils. Each sample was measured in triplicate and the error bars represent the standard deviation of the mean.*

Insulin amyloid fibrils were then tested as an immobilisation scaffold for OPH by cross-linking with GA. After the cross-linking method development, the immobilisation conditions chosen were: a starting concentration of 5.8 mg/mL bovine insulin amyloid fibrils; with a starting concentration of 7.5 mM GA; and a starting concentration of 7.6 mg/mL OPH; incubated for 1 hour at 37 °C and quenched with an equal part of 100 mM tris (section 7.11.1). OPH was cross-linked to the insulin amyloid fibrils with GA and the sample, with controls, were evaluated with native PAGE. **Figure 4.9** shows that when OPH is immobilised to the insulin amyloid fibrils using GA (lane 5), the OPH bands, when compared to the OPH only control (lane 3) and OPH cross-linked to OPH with GA (lane 4), cannot be seen. This is due to insulin amyloid fibrils being large and insoluble, and therefore not able to enter the polyacrylamide gel, as shown by the insulin amyloid fibril controls (lanes 1 and 2). Thus, if OPH has been successfully immobilised to the insulin amyloid fibrils, the immobilised OPH cannot enter the polyacrylamide gel. The samples containing OPH were loaded with one lane between each sample, to minimise cross contamination. The native PAGE gel in **Figure 4.9**, therefore provides evidence that OPH can be immobilised to insulin amyloid fibrils using GA.

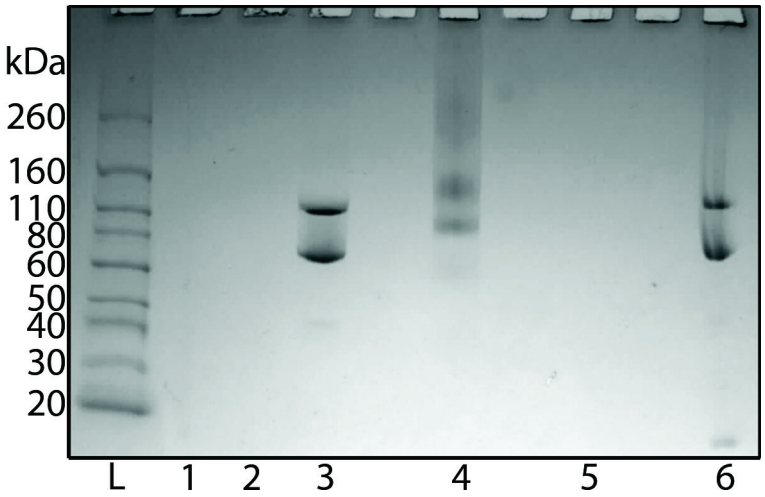

Figure 4.9 *Native PAGE gel of cross-linking OPH (7.6 mg/mL) to insulin amyloid fibril (5.8 mg/mL) samples. L – ladder, 1 – fibrils, 2 – fibrils + GA, 3 – OPH, 4 – OPH + GA, 5 – OPH + GA + fibrils, 6 – OPH + fibrils.*

The immobilised OPH samples were also investigated using SDS-PAGE (**Figure 4.10**). **Figure 4.10** shows the sample that contains OPH immobilised to the insulin amyloid fibrils with GA (lane 3), only has a very faint protein band present in the gel, compared to the controls, implying that the OPH has been successfully covalently immobilised to the insulin amyloid fibrils and cannot enter the gel.

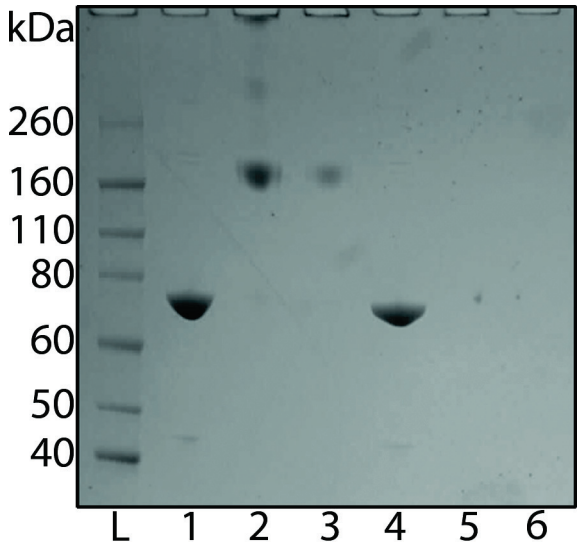

Figure 4.10 *SDS-PAGE gel of cross-linking OPH (7.6 mg/mL) to insulin amyloid fibril (5.8 mg/mL) samples. L – ladder, 1 – OPH, 2 – OPH + GA, 3 – OPH + GA + fibrils, 4 – OPH + fibrils, 5 – fibrils, 6 – fibrils + GA.*

ThT fluorescence (section 7.2.8) was used in combination with centrifugation to demonstrate that insulin amyloid fibrils could be collected using centrifugation. **Figure 4.11** shows that upon centrifugation the fluorescence of the supernatant compared to the initial fluorescence of the insulin amyloid fibril solution drops to about the level of the blank solution, containing ThT only. This confirms that centrifugation can be used to collect insulin amyloid fibrils.

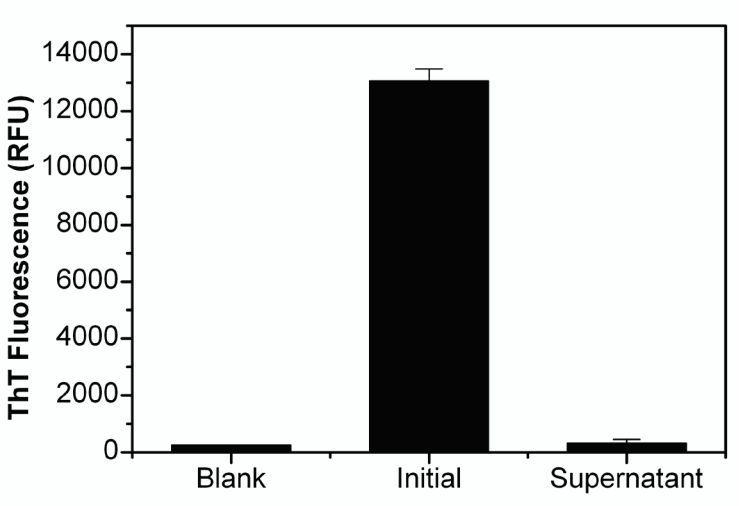

Figure 4.11 *ThT fluorescence of insulin amyloid fibril samples pre- (initial) and post-centrifugation (supernatant), compared against a blank solution containing ThT only. All measurements were carried out in triplicate and the errors bars represent the standard deviation of the mean.*

4.3.3 Crystallin amyloid fibril cross-linking method development

Crystallin proteins extracted from fish eye lenses were used in the manufacture of crystallin amyloid fibrils (section 7.10.5). Amyloid fibril formation was confirmed by TEM (section 3.2.2) (section 7.2.11). Initially OPH was cross-linked to the crystallin amyloid fibrils at a range of GA concentrations and pHs, and the samples analysed by SDS-PAGE (**Figure 4.12**). The ε-amino group of lysine has a pKa of > 9.5 (Migneault *et al.* 2004), and therefore a more alkaline pH results in more cross-linking occurring with GA due to the ε-amino groups being deprotonated. OPH runs as a single protein band at ~77 kDa in a SDS-PAGE gel. This protein band is only noticeably visible in lane 1 containing the lowest GA concentration (2.5 mM) and the lowest pH (7). Protein bands larger than ~77 kDa means that OPH has been cross-linked to one or more other OPH molecules. The trend of the gel is that with increased GA concentration and increasing pH, larger OPH species are formed. The gel showed very different results from when OPH was immobilised to insulin amyloid fibrils using GA (section 4.3.2), suggesting that no immobilisation to the crystallin amyloid fibrils was occurring, and that only OPH cross-linked to other OPH molecules was observed. The cross-linking results look similar to the results when OPH is cross-linked to another molecule of OPH in the absence of insulin amyloid fibrils, using GA (section 4.3.1).

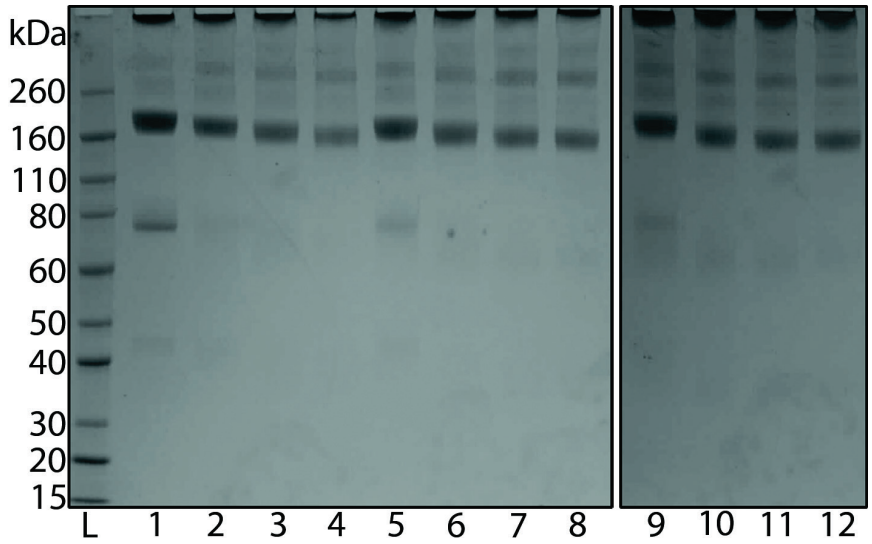

Figure 4.12 *SDS-PAGE gel of OPH cross-linked to crystallin amyloid fibrils (final concentration 1.9 mg/mL) at pHs 7, 8, and 9, and final concentrations of 2.5, 5, 10, and 20 mM GA. L – ladder, 1 – 2.5 mM GA, pH 7, 2 – 5 mM GA, pH 7, 3 – 10 mM GA, pH 7, 4 – 20 mM GA, pH 7, 5 - 2.5 mM GA, pH 8, 6 – 5 mM GA, pH 8, 7 – 10 mM GA, pH 8, 8 – 20 mM GA, pH 8, 9 – 2.5 mM GA, pH 9, 10 – 5 mM GA, pH 9, 11 – 10 mM GA, pH 9, 12 – 20 mM GA, pH 9.*

It was decided to use 2.5 mM GA, a cross-linking pH of 9, at 37 °C for 1 hour, because of the success of these parameters with insulin amyloid fibrils. The OPH immobilisation samples were analysed using SDS-PAGE, as shown in **Figure 4.13**. This gel confirms that no cross-linking of OPH to the crystallin amyloid fibrils was occurring. The sample containing OPH, GA and crystallin fibrils (lane 4) has very similar protein bands compared to the OPH and GA only (lane 2) sample, implying that OPH is not being covalently immobilised to the crystallin amyloid fibrils. In-house attempts to immobilise other enzymes to the crystallin amyloid fibrils using GA were tried, but successful immobilisation conditions could not be found (*Personal comm.* Roberts 2010). Initial in-house results have found the crystallin proteins that form the crystallin amyloid fibrils are glycosylated (*Personal comm.* Domigan 2012), which may be inhibiting the GA cross-linking reaction. Research to immobilisation biomolecules to crystallin amyloid fibrils was therefore discontinued, and more research is needed to be able to immobilise biomolecules to the crystallin amyloid fibrils.

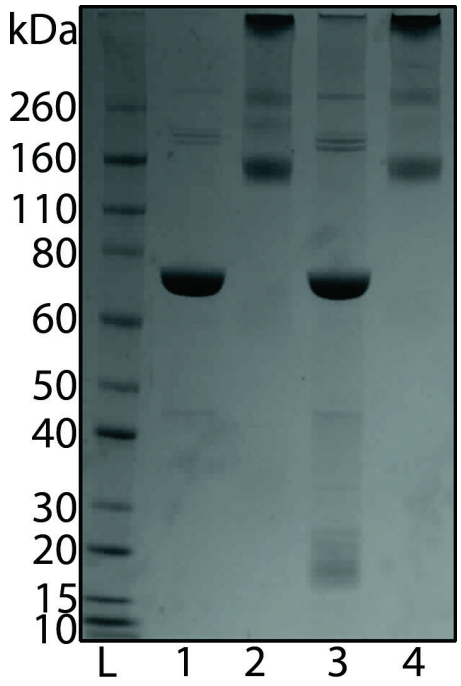

Figure 4.13 *SDS-PAGE gel of cross-linking OPH to crystallin amyloid fibril samples with the in-house method. L – ladder, 1 – OPH, 2 – OPH + GA, 3 – OPH + fibrils, 4 – OPH + GA + fibrils.*

4.4 Characterisation of OPH immobilised to insulin amyloid fibrils

Once reproducible conditions to immobilise OPH to the insulin amyloid fibrils were established (section 7.11.1), the immobilised OPH was investigated using the *p*-nitrophenol activity assay (section 7.9.1), centrifugation to assay the amount of OPH immobilised, thermostability assays, SDS-PAGE, and TEM.[1] It is known that by covalently immobilising enzymes to insoluble supports, an increase in the thermostability is common because of the buttressing effect imparted from the support and cross-linker (Sheldon 2007). This buttressing can also have negative effects on the activity of an enzyme because enzymes often require some flexibility for their catalytic activity and therefore any conformational restriction can impair the activity of the enzyme (Halling *et al.* 2005). Covalently immobilising multimeric enzymes like OPH can also cause problems because if only one of the monomers is covalently bound to the support, there is a chance that the other monomer could dissociate (Brady & Jordaan 2009).

OPH, despite being a multimeric enzyme, has the advantage of very high catalytic activity over other enzymes. OPH catalyses the reaction of paraoxon to form diethyl phosphate and *p*-nitrophenol with a k_{cat}/K_m value of 10^8 $M^{-1}s^{-1}$, which is close to the diffusion-controlled limit (Chen *et al.* 2007). This extreme efficiency suggests that if there is some loss in the activity of OPH when it is immobilised, it is likely to remain an efficient catalyst.

[1] This work was published in Biotechnology Progess (2011). Raynes, J. K., Pearce, F. G., Meade, S. J., Gerrard, J. A., 2011. Immobilization of organophosphate hydrolase on an amyloid fibril nanoscaffold: Towards bioremediation and chemical detoxification. *Biotechnology Progress*, 27(2), pp.360-367.

Initially, there were problems of OPH inactivation after the immobilisation reaction. This turned out to be a pH problem because of the low pH HCl buffer the amyloid fibrils are formed in. This was solved by increasing the OPH buffer concentration to offset the low pH. Another problem was the development of OPH initial rates that were higher when immobilised to the amyloid fibrils, than the non-immobilised OPH. Preliminary results looked very promising, but OPH is a metallo enzyme requiring Zn^{2+}, and bovine insulin natively has Zn^{2+} associated with it, therefore it was found there was not enough Zn^{2+} in the OPH buffer, and the Zn^{2+} from the insulin amyloid fibrils was activating apo-OPH. In this research the S5-OPH mutant was used, and as stated in section 2.2, this mutation stabilises the apo form of the protein, therefore, the use of S5-OPH could have created as excess of apo-OPH during the purification.

With these issues resolved, OPH was immobilised to the insulin amyloid fibrils using the established protocol, and the activity of the immobilised samples were investigated using the *p*-nitrophenol assay (section 7.9.1). **Figure 4.14** shows the initial rates of the immobilised OPH samples. When OPH is cross-linked to another molecule of OPH using GA, it loses some activity, as previously seen in section 4.3.1. OPH also loses some activity when in solution with insulin amyloid fibrils without any GA, as previously seen in section 4.3.2. The interesting result is that when OPH is immobilised to the insulin amyloid fibrils using GA, it loses about the same amount of activity as when OPH is cross-linked to another OPH molecule. This implies that either OPH has only been cross-linked to another OPH molecule, or that when OPH is immobilised to the insulin amyloid fibrils, it loses the same amount of activity because of the restriction on protein conformation from GA. To assess which process was occurring, centrifugation was used to investigate whether OPH activity was associated with the amyloid fibrils, or if OPH was only cross-linked to another molecule in solution.

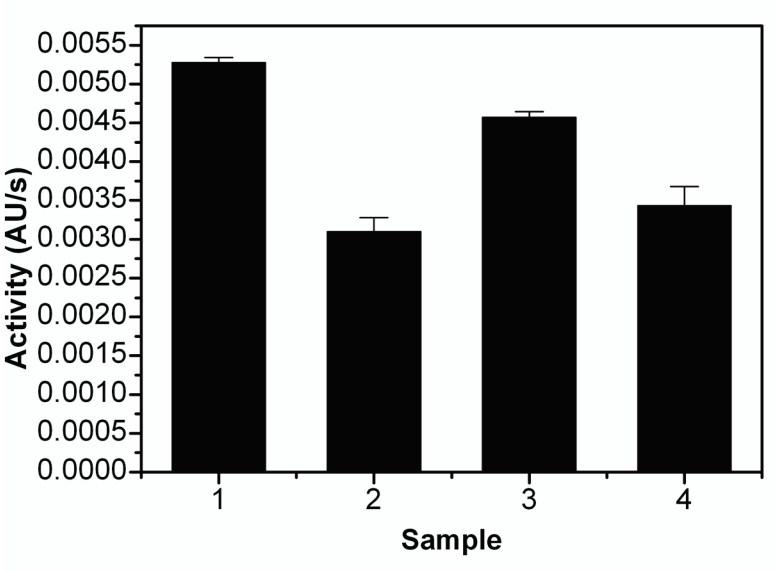

Figure 4.14 *Initial activity using the p-nitrophenol assay of immobilised OPH samples. 1 – OPH, 2 – OPH + GA, 3 – OPH + fibrils, 4 – OPH + GA + fibrils. All measurements were carried out in triplicate and the errors bars represent the standard deviation of the mean.*

To measure if and how much OPH was being immobilised to the insulin amyloid fibrils, activity testing was conducted on the immobilised OPH samples pre- and post-centrifugation. Testing the activity of the immobilised OPH solutions pre- and post-centrifugation gave the relative amount of OPH activity that was immobilised to the insulin amyloid fibrils. **Figure 4.15** shows the relative activity pre- and post-centrifugation of the immobilised OPH samples at pH 7. As can be seen, the sample which had the most OPH activity (~40 %) associated with the insulin amyloid fibrils was sample 4, containing OPH immobilised to insulin amyloid fibrils with GA. This provides good evidence that GA can be used to covalently immobilise OPH to insulin amyloid fibrils.

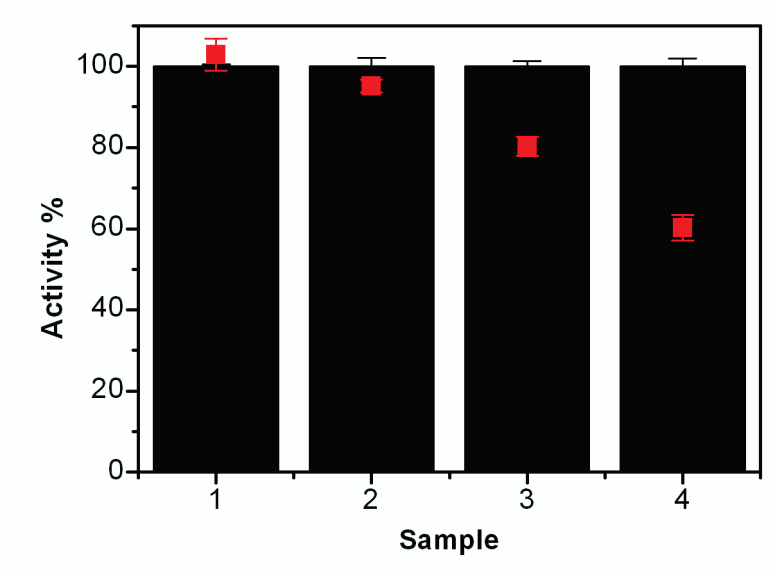

Figure 4.15 *Relative activity of OPH samples immobilised at pH 7 pre- (■) and post-centrifugation (■).1 – OPH, 2 – OPH + GA, 3 – OPH + fibrils, 4 – OPH + GA + fibrils. Each sample had three replicates and the error bars represent the standard deviation of the mean.*

Thermostability of enzymes is one of the major obstacles hindering their use in industry (Cao *et al.* 2003). OPH has a melting temperature of ~51.8 °C (section 2.2.2), which is comparatively low compared to other industrially relevant enzymes like glucose isomerase with an optimal temperature from 60-80 °C (Bhosale *et al.* 1996). As stated in section 1.5.5, covalent cross-linking of enzymes can result in an increase in stability due to restriction of enzyme movement from the buttressing effect from the cross-links (Spahn & Minteer 2008). The thermostability of the immobilised OPH was investigated to assess if the insulin amyloid nanoscaffold can impart extra stability to OPH.

Thermostability of the immobilised OPH samples was investigated at 30, 40, and 50 °C, and at cross-linking pHs of 7, 8, and 9. OPH was buffer exchanged into the desired buffer containing 100 mM HEPES pH 7, 8, or 9 for the cross-linking reaction. HEPES was chosen because of its wide (pH 6.8-8.2) buffering range, so that the each immobilisation sample contained the same chemical composition (Sigma-Aldrich 2012). pH 9 is slightly outside of the HEPES buffering range, but when OPH in 100 mM HEPES pH 9 was used in the cross-linking reaction, the reaction maintained a pH very close to 9. Once OPH had been immobilised to the insulin amyloid fibrils, samples were incubated at the appropriate temperature for a set amount of time before being place on ice, and the activity of the OPH sample tested. The activity of all individual samples at time zero were given an activity of 100 %, and subsequent measurements were compared relative to this measurement.

Figure 4.16 shows the relative activity of the immobilised OPH samples. There are two general trends present: At 40 and 50 °C, and all immobilisation pHs, the sample which retains the greatest relative activity during the thermostability experiment is the sample where OPH is covalently immobilised to the insulin amyloid fibrils using GA. The covalently immobilised OPH retains ~25 % of its relative activity, compared to 5-10 % for the OPH control. The samples containing OPH cross-linked to another molecule of OPH using GA retained about the same amount of activity as the OPH control, implying it is not the GA providing the increase in thermostability, and therefore, is most likely due to the OPH been covalently immobilised to the insulin amyloid fibrils. Interestingly, the samples which have OPH and insulin amyloid fibrils but no GA, also have an increase in thermostability, implying insulin amyloid fibrils bestow some gain in stability, probably due to OPH being adsorbed to the insulin amyloid fibrils. The second trend is that at 30 °C and all immobilisation pHs, the results are completely opposite to the 40 and 50 °C results. The OPH control samples actually show an increase in the relative activity after incubation for 3 days. The 30 °C thermostability experiment was repeated to ensure the result was reproducible. Therefore, it was decided to investigate the 30 °C results further by SDS-PAGE (appendix 1).

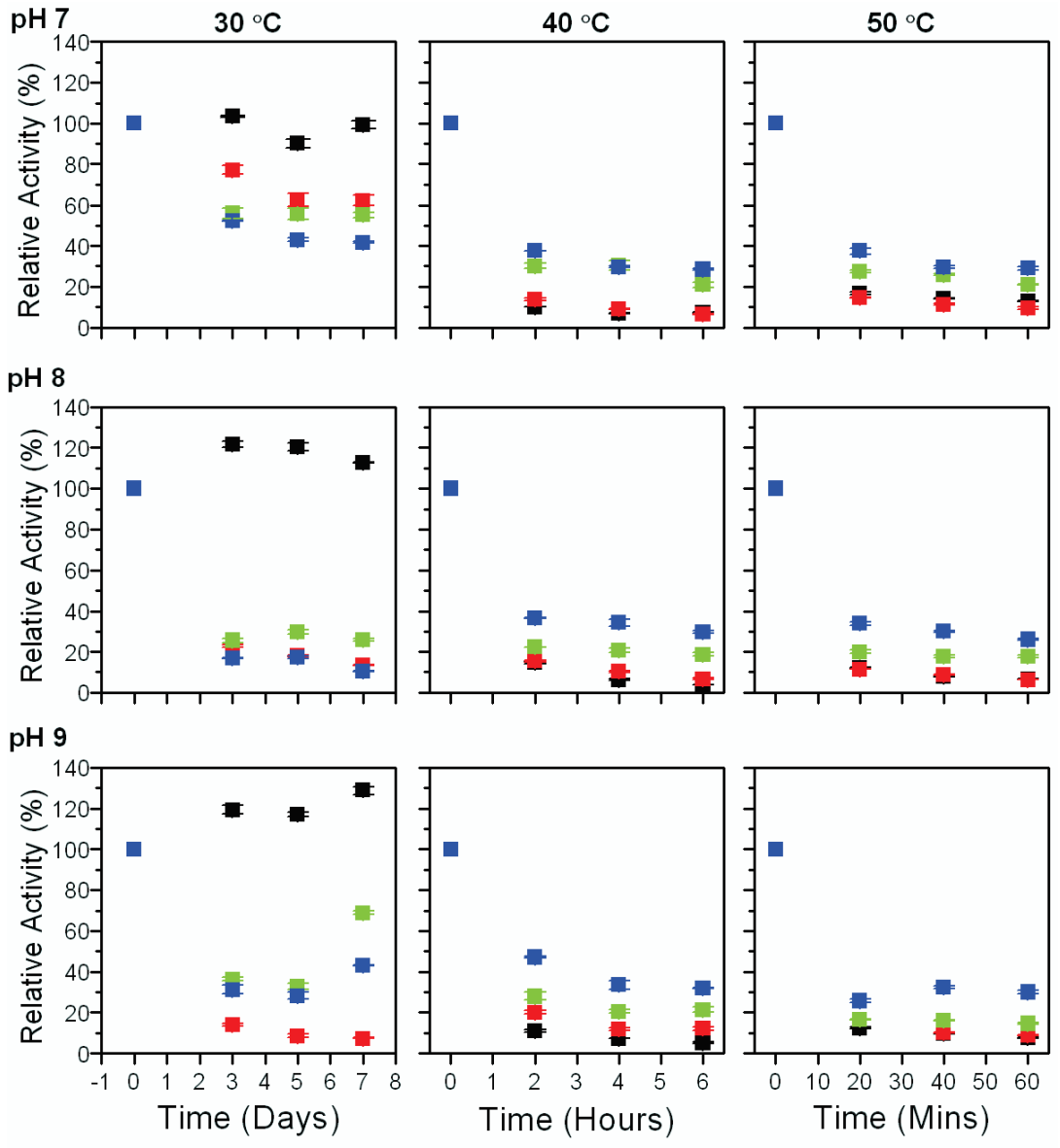

Figure 4.16 *Thermostability testing of immobilised OPH samples using relative activity from the p-nitrophenol assay. The relative activity was taken as 100 % activity from time zero for each sample, pH, and temperature. (■) – OPH, (■) – OPH + GA, (■) – OPH + insulin amyloid fibrils, (■) – OPH + GA + insulin amyloid fibrils. Each sample had three replicates and the error bars represent the standard deviation of the mean.*

Once OPH had been immobilised to the insulin amyloid fibrils, TEM was used to investigate the change in the morphology of the prepared amyloid fibrils. **Figure 4.17** shows that upon immobilisation of OPH to the insulin amyloid fibrils using GA the morphology of the amyloid fibrils appear wider (~10 nm) and less well defined. This could be due to the amyloid fibrils been covered with OPH, because the short side-to-side distance of OPH is ~5 nm, or because the amyloid fibrils have been cross-linked together. However, the large surface area nanoscaffold remained intact.

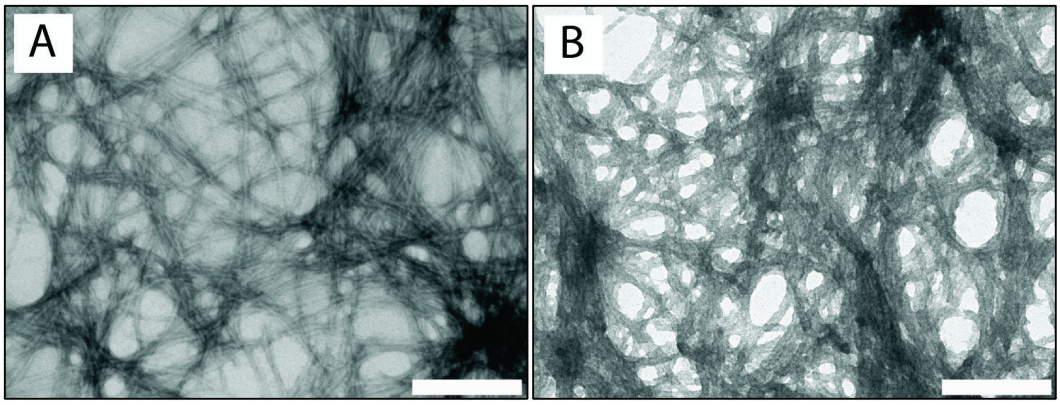

Figure 4.17 *TEM micrographs of A – insulin amyloid fibrils, B – OPH immobilised to insulin amyloid fibrils with GA. The scale bars = 200 nm. Each micrograph is representative of the overall sample.*

This section confirms that OPH can be immobilised to insulin amyloid fibrils using GA, and that insulin amyloid fibrils could potentially be used as a new type of nanoscaffold for enzyme immobilisation. Upon OPH immobilisation to the nanoscaffold, OPH loses ~35 % of its activity, which is equivalent to when OPH is cross-linked to another molecule of OPH using GA. The loss in activity is probably due to GA cross-linking hindering the natural movement of the enzyme, or due to diffusion effects, because OPH catalyses paraoxon near the limits of diffusion. A loss in activity due to diffusional effects with amyloid fibrils has been reported before with barnase and carbonic anhydrase, which are both also near-diffusion-limited enzymes (Baxa *et al.* 2002).

Covalently immobilised OPH showed a significant (~300 %) increase in the relative thermostability at 40 and 50 °C, compared to free OPH, and OPH cross-linked to itself using GA. The thermostability at 30 °C after three days free OPH started to show an increase in activity, compared to the immobilised OPH which lost activity. This was due to protease activity cleaving the MBP from the MBP-OPH fusion. OPH without the MBP has a higher catalytic efficiency and this caused the increase in activity to be seen (Refer appendix 1). Interestingly, there seems to be an intrinsic association between OPH and insulin amyloid fibrils, shown by a drop in activity when in solution together, centrifugation of some OPH activity when collecting the amyloid fibrils, and from the slight increase in thermostability at 40 and 50 °C. The morphology of the insulin amyloid fibrils changes to be wider and less well defined when OPH is immobilised to them using GA, which is consistent with OPH covering the surface of the amyloid fibrils.

4.5 Cytochrome $P450_{BM3}$ immobilisation method development

$P450_{BM3}$ was recombinantly overexpressed and purified as outlined in chapter two. The immobilisation procedure to cross-link $P450_{BM3}$ to the insulin amyloid fibrils used the same two-step protocol as used with OPH. **Figure 4.18** shows the crystal structure of the surface of $P450_{BM3}$ with the lysine residues highlighted in pink to show the theoretically available lysine residues for cross-linking using GA.

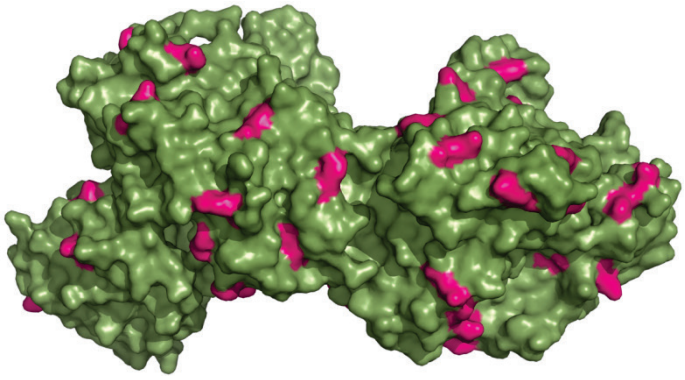

Figure 4.18 *Crystal structure of $P450_{BM3}$ (PDB 1BVY) (Sevrioukova et al. 1999) showing the surface with the lysine residues coloured in pink.*

Research into $P450_{BM3}$ immobilisation has used a number of methods and matrices including: entrapment in a sol-gel with the view to produce fine chemicals (Maurer *et al.* 2003), entrapment in polypyrrole for use as an electrochemical enzyme to bypass the need for NADPH (Holtmann *et al.* 2009), mesoporous silicates for an arachidonic acid biosensor (Weber *et al.* 2010; Giovannozzi *et al.* 2011), and DEAE-650S anion media entrapped in k-carrageenan to investigate the use of Zn/Co(III) as a cofactor instead of NADPH (Zhao *et al.* 2011).

The main area of interest in studying $P450_{BM3}$ is to use mutants of the enzyme to produce fine chemicals because of the potential reactions that it can catalyse (Whitehouse *et al.* 2012). $P450_{BM3}$ is a difficult enzyme to immobilise because of its reliance on NADPH co-factors from its reductase domain, which can be easily hindered with immobilisation (Weber *et al.* 2010). Therefore, immobilisation on an amyloid fibril nanoscaffold may provide a support that is beneficial towards $P450_{BM3}$ activity and stability.

4.5.1 $P450_{BM3}$ cross-linking method development

Based on the results obtained from the OPH cross-linking method development, final concentrations of 2.5, 5, and 7.5 mM GA were initially investigated to ascertain if $P450_{BM3}$ could be cross-linked to another molecule of $P450_{BM3}$, and what effect the cross-linking had on the activity of the enzyme. **Table 4.2** shows that <2.5 mM concentrations of GA, $P450_{BM3}$ is inactivated.

Table 4.2 *Initial rates of $P450_{BM3}$ when cross-linked intramolecularly for 1 hour at 4 °C with different concentrations of GA. - = rate was below measurable rates. All reactions were carried out in triplicate and the error is the standard deviation of the mean.*

Final conc. of GA (mM)	Rate (AU/s)	Error
0	0.0126	± 0.0015
2.5	-	-
5	-	-
7.5	-	-

Cross-linked $P450_{BM3}$ samples were analysed by CD spectroscopy (section 7.2.15) to determine if GA was altering the secondary structure of the enzyme, consequently inactivating it. **Figure 4.19** shows the CD spectra of the $P450_{BM3}$ cross-linked samples with different concentrations of GA. The result show GA is not affecting secondary structure, therefore, GA must be inactivating the enzyme by another means, possibly *via* interaction with arginine 47 at the mouth of the active site, which has been shown to play a significant role in the stabilisation of the lauric acid carboxylate group (Noble *et al.* 1999).

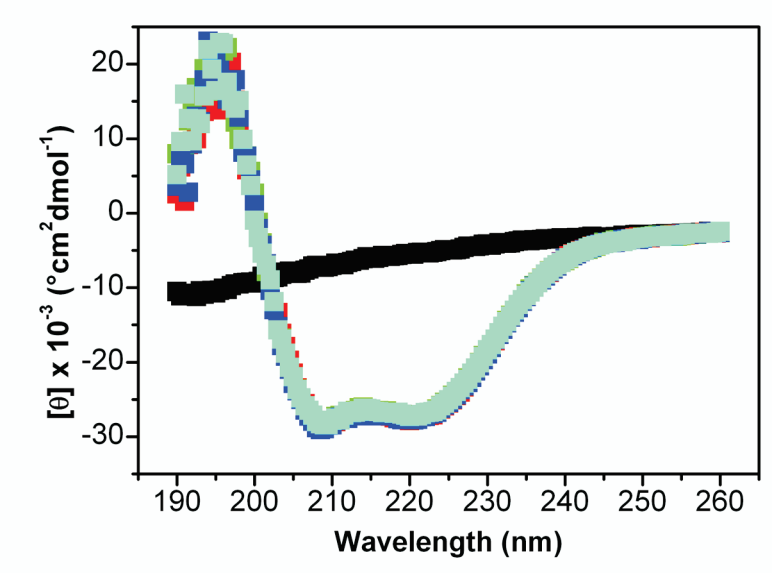

Figure 4.19 *CD spectroscopy of $P450_{BM3}$ (0.2 mg/mL) cross-linked using different concentrations of GA, at 37 °C for 1 hour. (■) – Buffer control, (■) – 2.5 mM GA, (■) – 5 mM, (■) – 7.5 mM GA, (■) – 10 mM GA. The measurements were the average of three scans of each sample.*

Figure 4.20 shows the interaction of $P450_{BM3}$ with 2.5 mM GA over time. As can be seen, there is a progressive loss in the activity of $P450_{BM3}$, confirming GA does inactivate the enzyme. Thus it was investigated whether $P450_{BM3}$ could be immobilised to insulin amyloid fibrils by physical adsorption without any cross-linker, to preserve the activity of the enzyme.

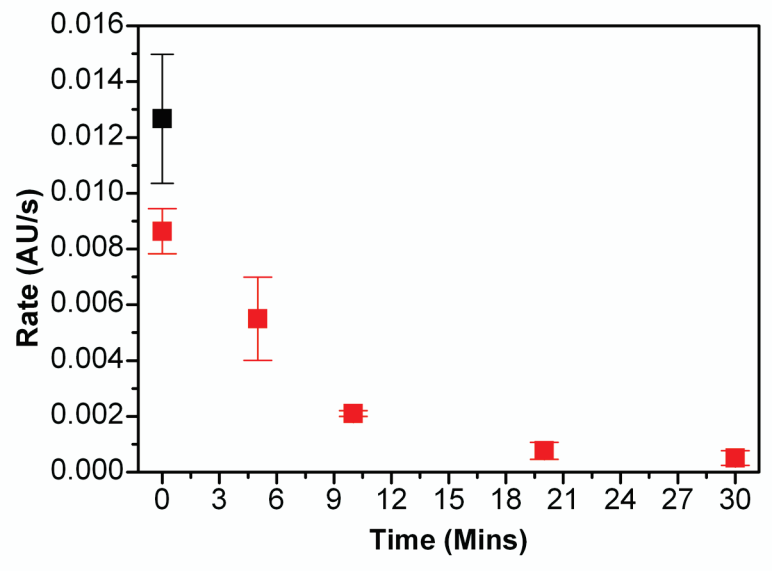

Figure 4.20 *Follow the initial rates of intramolecularly cross-linked $P450_{BM3}$ using 2.5 mM GA over time. (■) – Control with no GA, (■) – with 2.5 mM GA. Each sample had three replicates and the error bars represent the standard deviation of the mean.*

4.5.2 $P450_{BM3}$ cross-linking to insulin amyloid fibrils

From the results of immobilising OPH to the insulin amyloid fibrils, a starting concentration of 5.8 mg/mL insulin amyloid fibrils was used for the immobilisation of $P450_{BM3}$. Initially, the immobilised $P450_{BM3}$ samples were investigated to see what effect insulin amyloid fibrils had on the activity of the enzyme (section 7.11.3). **Table 4.3** indicates that when $P450_{BM3}$ is in solution with insulin amyloid fibrils without any cross-linker (sample 2) it loses ~80 % activity, when $P450_{BM3}$ is cross-linked to another molecule of $P450_{BM3}$ (sample 4) it loses ~98 % activity, and when $P450_{BM3}$ is cross-linked to the insulin amyloid fibrils using GA (sample 3) it loses activity.

Table 4.3 *Initial rates of immobilised $P450_{BM3}$ samples when cross-linked for 1 hour at 4 °C. N/A = rate was below measurable rates. All reactions were carried out in triplicate and the error is the standard deviation of the mean.*

Sample	Rate (AU/s)	Error
P450 only	0.013	± 0.001
P450 + fibrils	0.003	± 0.0003
P450 + GA + fibrils	-	-
P450 + GA	0.0003	0

An experiment to examine the interaction between the insulin amyloid fibrils and $P450_{BM3}$ over time was conducted. **Figure 4.21** confirms that when $P450_{BM3}$ is in solution with insulin amyloid fibrils it loses activity over time. This result implies there is a strong intrinsic association between $P450_{BM3}$ and the insulin amyloid fibrils. The association whilst strong, has negative consequences for the activity of the enzyme. The loss in activity could be from diffusional effects, the amyloid fibrils interacting or blocking the active site, an interaction between the substrate and the amyloid fibrils, or unfolding of the enzyme on the amyloid fibrils.

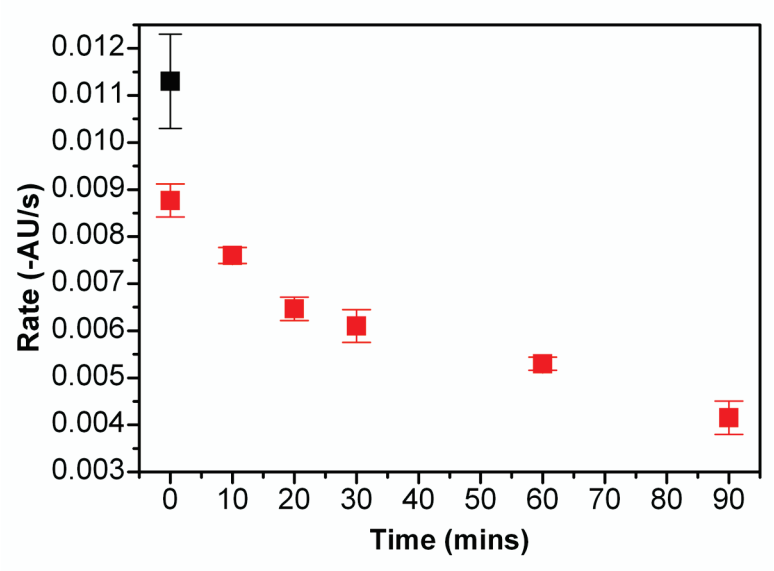

Figure 4.21 *Follow the initial rates of $P450_{BM3}$ in solution with insulin amyloid fibrils over time. (■) – Control with no fibrils, (■) – with fibrils. Each sample had three replicates and the error bars represent the standard deviation of the mean.*

The association between $P450_{BM3}$ and insulin amyloid fibrils was also investigated by SDS- and native PAGE (sections 7.2.3 and 7.2.4) to decipher the covalent and physical interactions occurring between $P450_{BM3}$ and the insulin amyloid fibrils. **Figure 4.22** shows the SDS- and native PAGE gels of the immobilised $P450_{BM3}$ samples. When $P450_{BM3}$ was covalently immobilised to the insulin amyloid fibrils using GA (lanes 3 and 7), the $P450_{BM3}$ protein bands completely disappear, implying all of the enzyme is immobilised to the insulin amyloid fibrils which are trapped in the top of the gel due to their size. Interestingly, when $P450_{BM3}$ was in solution with the insulin amyloid fibrils without any cross-linker (lanes 4 and 8), the $P450_{BM3}$ protein band is still visible in the SDS-PAGE gel but not in the native PAGE gel. This confirms that $P450_{BM3}$ does have a strong intrinsic interaction with the insulin amyloid fibrils, and that the interaction is a physical interaction that is lost upon the heating and denaturing conditions present in SDS-PAGE.

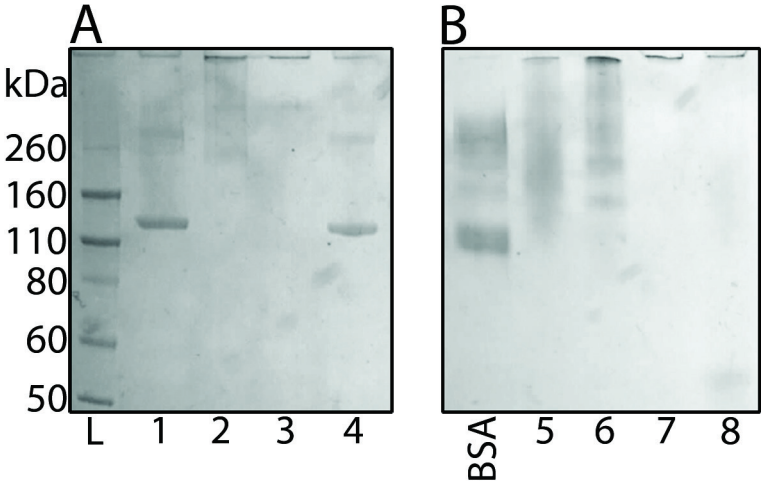

Figure 4.22 *SDS-PAGE (A) and native PAGE (B) gels of immobilised P450 $_{BM3}$ samples cross-linked for 1 hour at 4 °C. L – ladder, 1 – P450 $_{BM3}$, 2 – P450 $_{BM3}$ + GA, 3 – P450 $_{BM3}$ + GA + fibrils, 4 – P450 $_{BM3}$ + fibrils, BSA – bovine serum albumin, 5 – P450 $_{BM3}$, 6 – P450 $_{BM3}$ + GA, 7 – P450 $_{BM3}$ + GA + fibrils, 8 – P450 $_{BM3}$ + fibrils.*

The intrinsic association was also confirmed *via* centrifugation. $P450_{BM3}$ is a coloured protein due to the bound iron protoporphyrin (Meunier *et al.* 2004) and therefore, if there is an intrinsic association between $P450_{BM3}$ and the insulin amyloid fibrils, the colour (protein) would be pelleted with the amyloid fibrils. This is what is seen in **Figure 4.23**, which shows that only the samples with insulin amyloid fibrils can pellet the colour (protein).

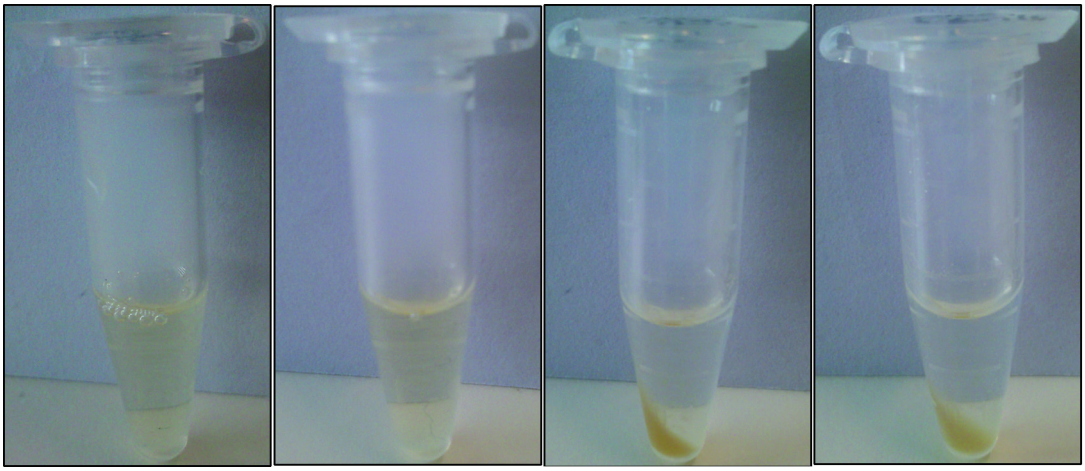

Figure 4.23 *Photos of the $P450_{BM3}$ immobilised samples post-centrifugation. The samples from left to right are: $P450_{BM3}$, $P450_{BM3}$ + GA, $P450_{BM3}$ + fibrils, $P450_{BM3}$ + GA + fibrils.*

Because of the near complete inactivation of $P450_{BM3}$ with GA and insulin amyloid fibrils, investigating the characteristics of the immobilised enzyme on the nanoscaffold was not carried out. Evidently not all proteins are able to be simply immobilised to the nanoscaffold. Previous research showed that $P450_{BM3}$ was not able to be immobilised to a number of commercial hydrophobic matrices, that covalent attachment to Eupergit (section 1.5.5) resulted in loss of activity, and anion exchanges immobilised $P450_{BM3}$, but they also bound the substrates and so were not suitable for immobilisation (Maurer *et al.* 2003). The problems encountered with immobilising $P450_{BM3}$ to a wide range of matrices, illustrates the difficulties in immobilising $P450_{BM3}$ whilst retaining activity. The loss in activity could be from diffusional effects, the amyloid fibrils interacting or blocking the active site, an interaction between the substrate and the amyloid fibrils, or most likely, the unfolding of the enzyme on the amyloid fibril surface.

4.6 Green fluorescent protein immobilisation

GFP was recombinantly overexpressed and purified as outlined in chapter two. **Figure 4.24** shows the crystal structure of GFP showing the surface of the protein with the lysine residues highlighted in pink, which are theoretically available for cross-linking with GA.

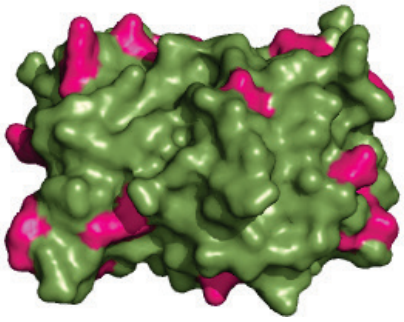

Figure 4.24 *Crystal structure of GFP (PDB 2Y0G) (Royant & Noirclerc-Savoye 2011) showing the surface with the lysine residues coloured in pink.*

GFP is one of the most widely used proteins in biochemistry and cell biology. Its uses can be split into two general categories, passive and active. The passive applications are its use as a reporter gene, cell marker, and most importantly as a fusion tag, where it is genetically fused to a host protein, to monitor the localisation and fate of the particular protein (Tsien 1998). As discussed in chapter one, GFP has previously been used as a fusion tag with a URE2 prion domain to create fluorescent amyloid fibrils (Baxa *et al.* 2002), but it had never been immobilised to the surface of amyloid fibrils using a cross-linker.

The active applications of GFP can be as a pH sensor, where GFP mutants are used as a sensor for cellular compartment pHs, but the most common active application uses fluorescent resonance energy transfer (FRET) between GFPs of two different colours. FRET works by having two fluorophores in close proximity (<100 Å apart), where the emission spectrum of one fluorophore, overlaps with the excitation spectrum of the second fluorophore (Stryer 1978). Therefore, if there is a change in distance between the two fluorophores, for example, from protease action, a change in the colour of the fluorescence is seen (Ross *et al.* 2011).

GFP has been immobilised to a range of scaffolds including: benzophenone-terminated boron-doped diamond (Marcon *et al.* 2009), polyethylene terephthalate SiO_2 composite (Katranidis *et al.* 2011) and patterned PEG hydrogels (Kolodziej *et al.* 2011). In all three examples, GFP was used to test new methods of surface protein immobilisation because of the high stability and fluorescence of the protein, allowing the use of confocal microscopy to detect if immobilisation was successful (Katranidis *et al.* 2011). GFP was used in this research because of its stability and intrinsic fluorescence, to fluorescently tag the insulin amyloid fibril nanoscaffold for visualisation.

4.6.1 GFP immobilisation method development

GFP immobilisation to the insulin amyloid fibrils used the same protocol (section 4.3) as used with OPH. GFP (~5 mg/mL) was immobilised to the insulin amyloid fibrils using a final concentration of 2.5 mM GA, a final concentration of 1.9 mg/mL insulin amyloid fibrils, for 1 hour at 37 °C (section 7.11.4). The resulting immobilised GFP samples were analysed by native PAGE (section 7.2.4). Native page was used because GFP could retain its intrinsic fluorescence and therefore allow the visualisation of the immobilised samples. **Figure 4.25** shows the native PAGE gel of the immobilised GFP samples when excited by UV light and photographed. As can be seen, GFP does retain fluorescence whilst in the gel, and when GFP is cross-linked to another molecule of GFP (lane 2), it still retains fluorescence. When GFP is immobilised to the insulin amyloid fibrils using GA (lane 4), most of the fluorescence is trapped in the top of the gel, indicating that it is covalently bound to the insulin amyloid fibrils, which cannot enter the gel due to their size. Lane 3 shows that GFP does not get physically adsorbed to the insulin amyloid fibrils without a cross-linker, because there is no fluorescence in the top of the gel and the protein band corresponding to native GFP is the same as the control (lane 1).

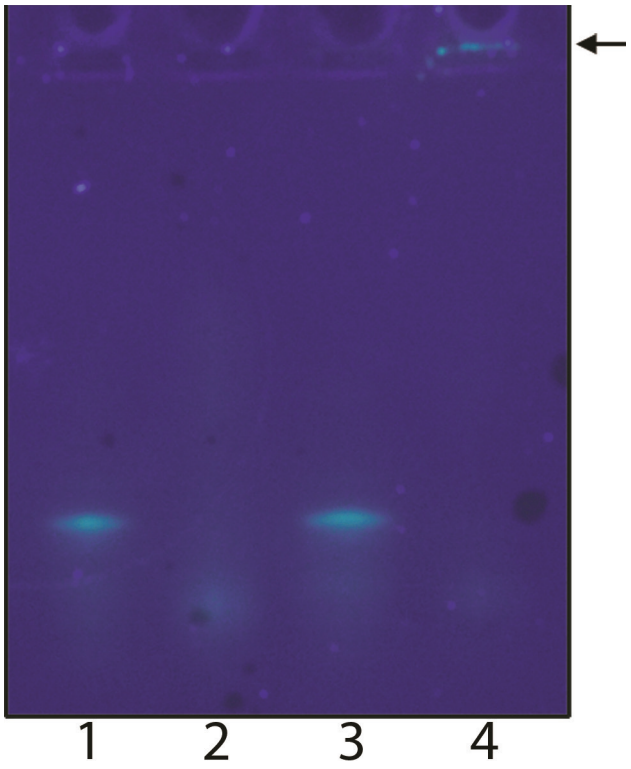

Figure 4.25 *Native PAGE gel of GFP samples. Lane 1 – GFP, lane 2 – GFP + GA, lane 3 – GFP + fibrils, lane 4 – GFP + GA + fibrils. The arrow is pointing to the GFP bound to the fibrils.*

The native PAGE gel provides very strong evidence that GFP can be covalently immobilised to insulin amyloid fibrils, and that it retains fluorescence upon immobilisation. GFP can therefore be utilised as a protein immobilisation tag to examine the covalent immobilisation ability of the insulin amyloid fibril nanoscaffold.

4.7 Tobacco etch virus protease

TEV protease was recombinantly overexpressed and purified as outlined in chapter two. **Figure 4.26** shows the surface of the protein in the crystal structure with the lysine residues highlighted in pink, which are theoretically available for cross-linking with GA. It has previously been predicted that of the 14 lysine residues in the TEV protease sequence, 12 of them are exposed and should be available for cross-linking (Puhl *et al.* 2009).

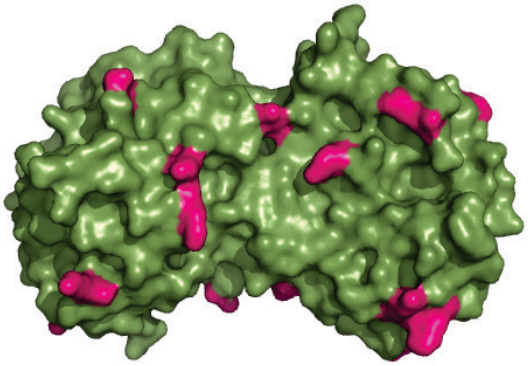

Figure 4.26 *Crystal structure of TEV protease (PDB 1LVM) (Phan 2002) showing the surface with the lysine residues coloured in pink.*

The main use of TEV protease is the cleavage of affinity tags used for purification of recombinantly expressed proteins. Tags are fused with proteins of interest, generally to assist with purification, but they can also act to increase yields, protect them from intracellular proteolysis and in the case of the maltose binding protein, aid in solubility (Fox & Waugh 2003; Waugh 2005). Whilst there are huge benefits of tags, their incorporation on a protein of interest can hinder the activity of the tagged protein. Therefore, it is generally advised to remove the tags (Tropea *et al.* 2009). The main advantage of TEV protease compared to other proteases, such as Factor Xa, and thrombin, is that it is extremely selective for its recognition site, thus its accuracy ensures the protein is not cleaved incorrectly, inactivating the protein (Jenny *et al.* 2003).

TEV protease is a prime candidate for immobilisation, because not only is it reasonably difficult to purify recombinantly (Puhl *et al.* 2009), but immobilisation will allow for the reuse of the protease (Cao *et al.* 2003). The general in-solution cleavage conditions for TEV protease are at ~1-100 w/w ratio of the target protein (Waugh 2010). Once the reaction has taken place, the TEV protease generally needs to be separated from the cleaved target protein. If using the poly-histidine tagged TEV protease, Ni-affinity chromatography can be used, but it requires removing DTT and EDTA (both are present in the TEV protease storage buffer) from the buffer, therefore the buffer would need to be dialysed first (Waugh 2010). Immobilisation could solve this problem, allowing for the simple separation of TEV protease from the target protein.

Waugh *et al.* (2010) stated "On-column (TEV protease) cleavage is possible but comparatively inefficient," and Puhl *et al.* (2009) covalently immobilised TEV protease to two insoluble supports, thiolsulfinate agarose and glutaraldehyde agarose, in which immobilised TEV protease only retained 0 or 30 % activity, respectively, compared to the enzyme in solution. The inactivation of the TEV protease was thought to be due to binding of the thiol group of a cysteine in the active site, and the GA interacting with lysine amino acid residues located near the substrate binding site. Recently, Miladi *et al.* (2012) immobilised TEV protease containing a Streptag II affinity sequence *via* affinity immobilisation on a strepavidin-agarose matrix, with a retained activity of ~81 %. This is a very good retention of activity, but examining their data closely the immobilised TEV protease has <10 % catalytic efficiency compared to the solution TEV protease. Immobilised TEV protease could prove to be extremely useful, but it is clearly a difficult protein to immobilise. Immobilising TEV protease to surface assembled insulin amyloid fibrils could provide a solution to the inactivation immobilisation problems and loss of catalytic efficiency seen with the other TEV protease immobilisation methods, because it could allow for a large enzyme loading and create a beneficial environment for TEV protease to remain active.

4.7.1 TEV protease functionalisation of surface assembled insulin amyloid fibrils

TEV protease immobilisation used the same protocol as used for OPH (section 4.3). TEV protease was immobilised at the concentration that it was purified at (1.2 mg/mL), with a final concentration of 2.5 mM GA, and a final concentration of 1.9 mg/mL insulin amyloid fibrils (section 7.11.5). The immobilised TEV protease samples were analysed by SDS- and native PAGE (sections 7.2.3 and 7.2.4) to establish if TEV protease was immobilised to the insulin amyloid fibrils. **Figure 4.27** shows when TEV protease is cross-linked to another molecule of TEV protease (lane 2) the protein band at ~27 kDa completely disappears compared to the control (lane 1) containing TEV protease only. This is also the result when TEV protease is immobilised to the insulin amyloid fibrils using GA (lane 3), suggesting either the TEV protease is covalently bound to the amyloid fibrils or it has created a large protein aggregate that could not enter the gel to be visible.

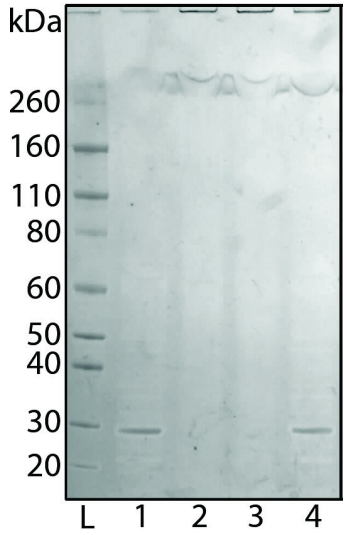

Figure 4.27 *SDS-PAGE gel of immobilised TEV protease samples. L – ladder, lane 1 – TEV protease, lane 2 – TEV protease + GA, lane 3 –TEV protease + GA + fibrils, lane 4 – TEV protease + fibrils.*

The same samples used in the SDS-PAGE were also analysed by native PAGE (**Figure 4.28**) The native PAGE gel shows very similar results to the SDS-PAGE gel. The TEV protease protein band in the TEV protease + fibrils sample (lane 4) appears to be slightly fainter than the control in lane 1, implying a small amount of TEV protease may bind to the insulin amyloid fibrils without any cross-linker.

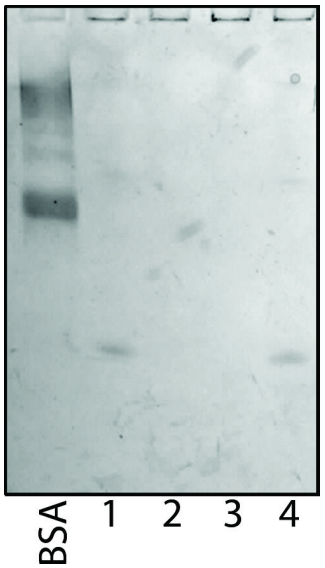

Figure 4.28 *Native PAGE gel of immobilised TEV protease samples. BSA – bovine serum albumin, lane 1 – TEV protease, lane 2 – TEV protease + GA, lane 3 –TEV protease + GA + fibrils, Lane 4 - TEV protease + fibrils.*

The immobilised TEV protease samples were tested for protease activity to examine any changes in activity arising from either GA or the insulin amyloid fibrils. 10 µL of the immobilised TEV protease samples (~0.03 mg/mL TEV protease) were mixed with 90 µL of 1 mg/mL dihydrodipicolinate synthase (Y107W mutant) known to contain a cleavable TEV protease recognition sequence between its poly-histidine purification tag and the enzyme. The samples were then left over night at 4 °C, and analysed for protease cleavage by SDS-PAGE. As can be seen in **Figure 4.29**, the samples containing cross-linking of TEV protease to another TEV protease molecule using GA (lane 3), and cross-linking TEV protease to insulin amyloid fibrils using GA (lane 5), showed a complete loss of protease activity to cleave the poly-histidine tag of the DHDPS. Only the TEV protease immobilised samples that did not contain GA (lanes 2 and 4) still showed the ability to cleave the DHDPS poly-histidine tag. The sample containing TEV protease and the insulin amyloid fibrils but no cross-linker (lane 4) showed slightly less cleavage of DHDPS as shown by the fainter protein band corresponding to the cleaved DHDPS. This suggests that TEV protease may be interacting with the insulin amyloid fibrils as seen in the native PAGE gel of **Figure 4.28**.

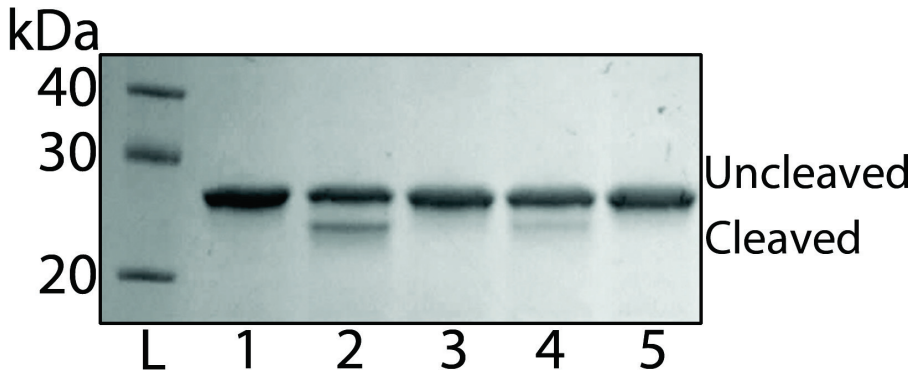

Figure 4.29 *Cleavage of E. coli DHDPS by TEV protease samples. L – Ladder, 1 – DHDPS only, 2 – DHDPS with TEV protease, 3 – DHDPS with TEV protease + GA, 4 – DHDPS with TEV protease + fibrils, 5 – DHDPS with TEV protease + GA + fibrils.*

The GA inactivation could be due to the cross-linker binding to the lysine residues K141, K147, K215 or K220, which are all located near the substrate binding site (Puhl *et al.* 2009). Because of the GA inactivation, and because of the possible intrinsic association between TEV protease and the insulin amyloid fibrils without any cross-linker, when it is attempted to immobilise TEV protease to the surface assembled insulin amyloid fibrils in chapter five, this intrinsic association will be optimised as the immobilisation technique.

4.8 Glucose oxidase immobilisation and characterisation

GOD was purchased commerically from Sigma Aldrich. **Figure 4.30** shows the crystal structure of GOD showing the surface of the enzyme with the lysine residues highlighted in pink. Previous research has shown that of the 24 lysine residues on the surface of the GOD dimer, 5 are potentially available for cross-linking due to the presence of glycosylation (Baszkin *et al.* 1997). The method to immobilise GOD to the insulin amyloid fibrils was based on the methods of (Pilkington *et al.* 2010), who showed that GOD can be covalently immobilised to insulin amyloid fibrils using GA.

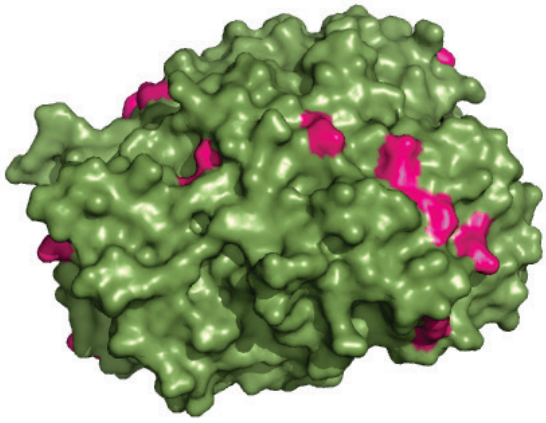

Figure 4.30 *Crystal structure of GOD (PDB 1CF3) (Wohlfahrt et al. 1999) showing the surface with the lysine residues coloured in pink.*

GOD is an extremely important enzyme, worth billions of dollars annually due to its commercial use in the chemical, food, beverage and biotechnology industries (Newman & Turner 2005; Bodade *et al.* 2010). The largest industrial use of GOD is as a glucose biosensor to monitor the concentration of blood glucose in people with diabetes (Cui *et al.* 2001), other uses include: the food and beverage industry to monitor, for example, the sucrose content in soybean grains, by using GOD in combination with an invertase enzyme (Teixeira *et al.* 2012); the production of gluconic acid, which can be used as an acidity regulator or bleach in food manufacturing (Bankar *et al.* 2009); as an anti-microbial, using the production of H_2O_2, in products such as tooth paste (Hannig *et al.* 2010), and anti-microbial wound dressings (Bang *et al.* 2003); or as a bleaching agent for cotton fabrics (Saravanan *et al.* 2012).

GOD has been immobilised to many different supports, some recent examples being a cellulose–tin oxide (SnO_2) hybrid nanocomposite (Mahadeva & Kim 2011), and multifunctional carbon nanotubes (Wang *et al.* 2011), as well as all manner of other possible supports. The large range of supports that GOD has been immobilised to, in conjunction with its enzyme stability, and high catalytic turnover rate (Bankar *et al.* 2009), make GOD an ideal model enzyme for immobilisation (Wilson & Turner 1992).

4.8.1 GOD immobilisation method development

GOD immobilisation was based on the methods of Pilkington *et al.* (2010) and used the two step protocol employed with OPH (section 4.3). The GOD (2 mg/mL) immobilised samples were cross-linked using a final concentration of 50 mM GA, with a final concentration of 1.9 mg/mL insulin amyloid fibrils for 1 hour at 25 °C (section 7.11.6). The samples were then investigated for covalent immobilisation by SDS-PAGE. **Figure 4.31** shows the GOD only sample (lane 1) runs as a ~55-60 kDa protein band, and when GOD is cross-linked to another molecule of GOD with GA (lane 2) there is a decrease in the protein band at ~55-60 kDa, and the appearance of a new larger protein band at ~160 kDa, indicating cross-linking. When GOD was immobilised to the insulin amyloid fibrils using GA (lane 3), there is a decrease in the protein band intensity at ~ 55-60 and ~160 kDa, compared to the controls (lanes 1 and 2). The lower band intensity is due to the GOD immobilised to the insulin amyloid fibrils, which cannot enter the gel due to their size. This provides evidence that some GOD has been successfully covalently immobilised to the amyloid fibrils.

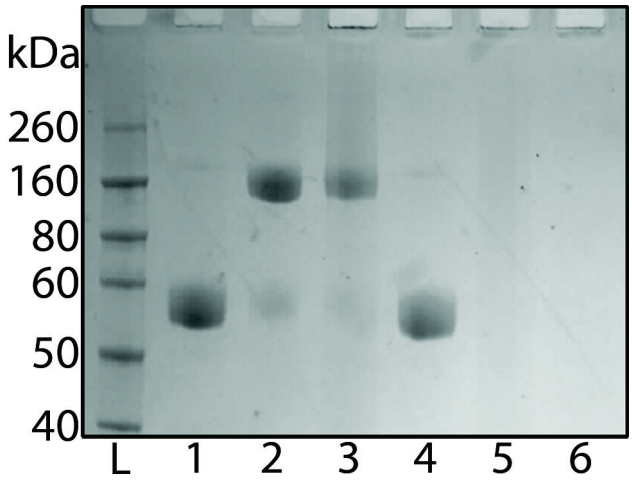

Figure 4.31 *SDS-PAGE gel of GOD immobilisation using GA. L – ladder, Lane 1 – GOD only, Lane 2 – GOD + GA, Lane 3 – GOD + GA + fibrils, Lane 4 – GOD + fibrils, Lane 5 – fibrils + GA, Lane 6 – fibrils only.*

To establish how much GOD activity was associated with the amyloid fibrils, the samples from **Figure 4.31** were assayed for initial activity using the Amplex red assay (sections 2.6.1 and 7.9.3). The samples were then centrifuged to collect the amyloid fibrils, and the supernatant retested for GOD activity. **Figure 4.32** shows that ~20 % of the GOD activity can be centrifuged down without any fibrils present. When GOD is immobilised to the insulin amyloid fibrils with GA, ~20 % more GOD activity is centrifuged with the insulin amyloid fibrils. This provides evidence that there is ~20 % of the GOD activity immobilised to the amyloid fibrils. This is in good agreement with the SDS PAGE gel of **Figure 4.31** that shows some GOD activity is immobilised to the amyloid fibrils. The results in **Figure 4.32** also demonstrate that when GOD is cross-linked to another molecule of GOD using GA, the activity of the enzyme is almost completely preserved, implying that GA does not inhibit activity. Although, considering that GA has a 100 M excess over GOD in the immobilisation reaction, the glycosylation of the enzyme must be having a significant impact on immobilisation.

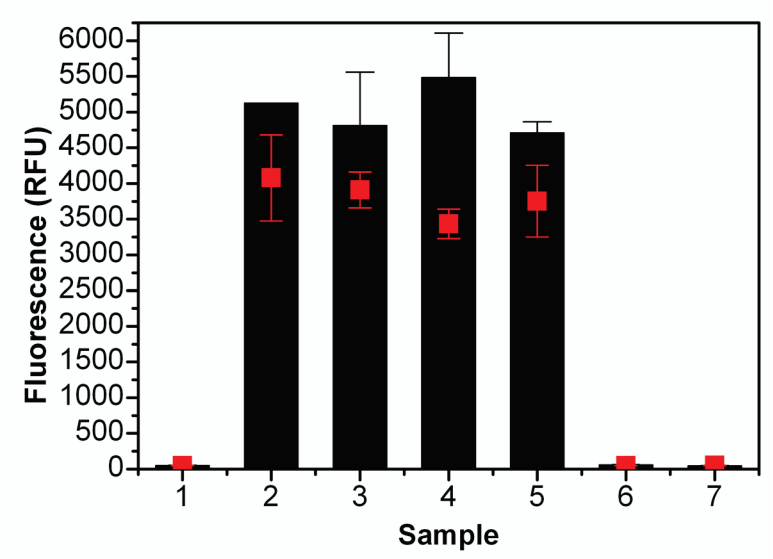

Figure 4.32 *Activity of immobilised GOD samples using the Amplex red assay. Black bars = initial GOD activity, red points = GOD activity in the supernatant after centrifugation. 1 – blank, 2 – GOD only, 3 – GOD + GA, 4 – GOD + GA + fibrils, 5 – GOD + fibrils, 6 – fibrils + GA, 7 – fibrils only. The average of 3 replicates of each sample was used and the error is the standard deviation of the mean.*

4.9 Summary

The immobilisation of a range of biomolecules that differ in size, tertiary structure, quaternary structure, catalytic activity, and substrate recognition, has shown insulin amyloid fibrils can act as a versatile nanoscaffold. The degree of immobilisation, and retained catalytic activity post-immobilisation differed between biomolecules, indicating immobilisation of individual biomolecules needs to be optimised.

OPH was for the first time successfully immobilised to the insulin amyloid fibril nanoscaffold and comprehensively characterised. The OPH immobilised to the insulin amyloid fibril nanoscaffold displayed a significantly higher thermostability. The OPH immobilisation results formed the basis of the protocols to immobilise all subsequent enzymes and proteins. Crystallin amyloid fibrils were not shown to be able to be functionalised with OPH using the established methods, and therefore require further investigation to be used as a nanoscaffold.

$P450_{BM3}$ was completely inactivated by GA, so physical adsorption was used to immobilise $P450_{BM3}$ to the insulin amyloid fibrils. The physical interaction was shown to be strong between the insulin amyloid fibrils and the enzyme, but physisorption caused almost complete inactivation. This was probably due to unfolding of $P450_{BM3}$ on the amyloid fibril surface. This result confirms that not any two enzymes share identical properties for immobilisation, and that a high starting catalytic activity helps tremendously when trying to immobilise enzymes to insoluble supports.

GFP was for the first time successfully covalently immobilised to the insulin amyloid fibril nanoscaffold, and showed the ability to retain its intrinsic fluorescence when immobilised. GFP provides a convenient method for tagging insulin amyloid fibrils allowing easy visualisation which can be exploited for future amyloid fibril research, for example by tagging amyloid fibrils to monitor their circulation post-injection in animal models for research into amyloid disease.

TEV protease has previously only been immobilised to three different supports, with varied success. TEV protease was for the first time immobilised to the insulin amyloid fibril nanoscaffold *via* physical adsorption. Physical adsorption was used because GA was shown to completely inactive the protease. Insulin amyloid fibrils provide a new nanosupport for the immobilisation of TEV protease, which could allow for the reuse of the enzyme, saving on production costs for recombinantly expressed poly-histidine tagged proteins.

The model immobilisation enzyme GOD was shown to be able to be covalently immobilised to the insulin amyloid fibril nanoscaffold and retain activity, as previously reported. Immobilisation of GOD to the solution insulin amyloid fibrils will provided the framework for testing the immobilisation of GOD to surface assembled insulin amyloid fibrils.

4.10 References

Andreopoulos, F.M., Roberts, M.J., Bentley, M.D., Harris, J.M., Beckman, E.J. & Russell, A.J., 1999. Photoimmobilization of organophosphorus hydrolase within a PEG-based hydrogel. *Biotechnology and Bioengineering*, 65(5), pp.579–588.

Aubert, S.D., Li, Y. & Raushel, F.M., 2004. Mechanism for the hydrolysis of organophosphates by the bacterial phosphotriesterase. *Biochemistry*, 43(19), pp.5707–5715.

Bang, L.M., Buntting, C. & Molan, P., 2003. The effect of dilution on the rate of hydrogen peroxide production in honey and its implications for wound healing. *Journal of Alternative and Complementary Medicine*, 9(2), pp.267–273.

Bankar, S.B., Bule, M.V., Singhal, R.S. & Ananthanarayan, L., 2009. Glucose oxidase-an overview. *Biotechnology Advances*, 27(4), pp.489–501.

Baszkin, Boissonnade, Rosilio, Kamyshny & Magdassi, 1997. Adsorption of hydrophobized glucose oxidase at solution/air interface. *Journal of Colloid and Interface Science*, 190(2), pp.313–317.

Baxa, U., Speransky, V., Steven, A.C. & Wickner, R.B., 2002. Mechanism of inactivation on prion conversion of the *Saccharomyces cerevisiae* Ure2 protein. *Proceedings of the National Academy of Sciences of the United States of America*, 99(8), pp.5253–5260.

Benning, M.M., Hong, S.-B., Raushel, F.M. & Holden, H.M., 2000. The binding of substrate analogs to phosphotriesterase. *Journal of Biological Chemistry*, 275(39), pp.30556–30560.

Bhosale, S.H., Rao, M.B. & Deshpande, V.V., 1996. Molecular and industrial aspects of glucose isomerase. *Microbiological Reviews*, 60(2), pp.280–300.

Bodade, R.G., Khobragade, C.N. & Arfeen, S., 2010. Optimization of culture conditions for glucose oxidase production by a *Penicillium chrysogenum* SRT 19 strain. *Engineering in Life Sciences*, 10(1), pp.35–39.

Borkar, I.V., Dinu, C.Z., Zhu, G., Kane, R.S. & Dordick, J.S., 2010. Bionanoconjugate-based composites for decontamination of nerve agents. *Biotechnology Progress*, 26(6), pp.1622–1628.

Brady, D. & Jordaan, J., 2009. Advances in enzyme immobilisation. *Biotechnology Letters*, 31, pp.1639–1650.

Caldwell, S.R. & Raushel, F.M., 1991. Detoxification of organophosphate pesticides using an immobilized phosphotriesterase from *Pseudomonas diminuta*. *Biotechnology and Bioengineering*, 37(2), pp.103–109.

Cao, L., Langen, L. van & Sheldon, R.A., 2003. Immobilised enzymes: Carrier-bound or carrier-free? *Current Opinion in Biotechnology*, 14(4), pp.387–394.

Chen, S.-L., Fang, W.-H. & Himo, F., 2007. Theoretical study of the phosphotriesterase reaction mechanism. *The Journal of Physical Chemistry B*, 111(6), pp.1253–1255.

Cui, Yoo, J.H., Woo, B.W., Kim, S.S., Cha, G.S. & Nam, H., 2001. Disposable amperometric glucose sensor electrode with enzyme-immobilized nitrocellulose strip. *Talanta*, 54(6), pp.1105–1111.

Fox, J.D. & Waugh, D.S., 2003. Maltose-binding protein as a solubility enhancer. *Methods in Molecular Biology*, 205, pp.99–117.

Frančič, N., Košak, A., Lyagin, I., Efremenko, E.N. & Lobnik, A., 2011. His_6-OPH enzyme-based bio-hybrid material for organophosphate detection. *Analytical and Bioanalytical Chemistry*, 401(8), pp.2631–2638.

Gill, I. & Ballesteros, A., 2000. Degradation of organophosphorous nerve agents by enzyme-polymer nanocomposites: Efficient biocatalytic materials for personal protection and large-scale detoxification. *Biotechnology and Bioengineering*, 70(4), pp.400–410.

Giovannozzi, A.M., Ferrero, V.E.V., Pennecchi, F., Sadeghi, S.J., Gilardi, G. & Rossi, A.M., 2011. P450-based porous silicon biosensor for arachidonic acid detection. *Biosensors and Bioelectronics*, 28(1), pp.320–325.

Habeeb, A.F.S.A. & Hiramoto, R., 1968. Reaction of proteins with glutaraldehyde. *Archives of Biochemistry and Biophysics*, 126(1), pp.16–26.

Halling, P.J., Ulijn, R.V. & Flitsch, S.L., 2005. Understanding enzyme action on immobilised substrates. *Current Opinion in Biotechnology*, 16(4), pp.385–392.

Hannig, C., Spitzmüller, B., Lux, H.C., Altenburger, M., Al-Ahmad, A. & Hannig, M., 2010. Efficacy of enzymatic toothpastes for immobilisation of protective enzymes in the *in situ* pellicle. *Archives of Oral Biology*, 55(7), pp.463–469.

Havens, P.L. & Rase, H.F., 1993. Reusable immobilized enzyme/polyurethane sponge for removal and detoxification of localized organophosphate pesticide spills. *Industrial and Engineering Chemistry Research*, 32(10), pp.2254–2258.

Hermanson, G.T., 1996. *Bioconjugate Techniques* 1st ed., Rockford, IL USA: Academic Press.

Holtmann, D., Mangold, K.-M. & Schrader, J., 2009. Entrapment of cytochrome P450 BM-3 in polypyrrole for electrochemically-driven biocatalysis. *Biotechnology Letters*, 31(5), pp.765–770.

Jenny, R.J., Mann, K.G. & Lundblad, R.L., 2003. A critical review of the methods for cleavage of fusion proteins with thrombin and factor Xa. *Protein Expression and Purification*, 31(1), pp.1–11.

Kanugula, A.K., Repalle, E.R., Pandey, J.P., Sripad, G., Mitra, C.K., Dubey, D.K. & Siddavattam, D., 2011. Immobilization of organophosphate hydrolase on biocompatible gelatin pads and its use in removal of organophosphate compounds and nerve agents. *Indian Journal of Biochemistry & Biophysics*, 48(1), pp.29–34.

Katranidis, A., Melachroinos, A., Karagiannidis, P.G., Lousinian, S., Papadopoulos, G., Logothetidis, S. & Choli-Papadopoulou, T., 2011. Biofunctionalization of PET/SIO_2 surfaces for single molecule experiments and medical applications. *NANO*, 6(3), pp.271–277.

Kolodziej, C.M., Chang, C.-W. & Maynard, H.D., 2011. Glutathione S-transferase as a general and reversible tag for surface immobilization of proteins. *Journal of Materials Chemistry*, 21(5), pp.1457–1461.

Laothanachareon, T., Champreda, V., Sritongkham, P., Somasundrum, M. & Surareungchai, W., 2008. Cross-linked enzyme crystals of organophosphate hydrolase for electrochemical detection of organophosphorus compounds. *World Journal of Microbiology and Biotechnology*, 24(12), pp.3049–3055.

Lu, H.D., Wheeldon, I.R. & Banta, S., 2010. Catalytic biomaterials: Engineering organophosphate hydrolase to form self-assembling enzymatic hydrogels. *Protein Engineering Design and Selection*, 23(7), pp.559–566.

Mahadeva, S.K. & Kim, J., 2011. Conductometric glucose biosensor made with cellulose and tin oxide hybrid nanocomposite. *Sensors and Actuators B: Chemical*, 157(1), pp.177–182.

Marcon, L., Wang, M., Coffinier, Y., Le Normand, F., Melnyk, O., Boukherroub, R. & Szunerits, S., 2009. Photochemical immobilization of proteins and peptides on benzophenone-terminated boron-doped diamond surfaces. *Langmuir*, 26(2), pp.1075–1080.

Maurer, S.C., Schulze, H., Schmid, R.D. & Urlacher, V., 2003. Immobilisation of P 450 BM-3 and an NADP cofactor recycling system: Towards technical application of hemecontaining monooxygenases in fine chemical synthesis. *Advanced Synthesis & Catalysis*, 345(6-7), pp.802–810.

Meade, S.J., Miller, A.G. & Gerrard, J.A., 2003. The role of dicarbonyl compounds in non-enzymatic crosslinking: A structure-activity study. *Bioorganic & Medicinal Chemistry*, 11(6), pp.853–862.

Meunier, B., de Visser, S.P. & Shaik, S., 2004. Mechanism of oxidation reactions catalyzed by cytochrome P450 enzymes. *Chemical Reviews*, 104(9), pp.3947–3980.

Migneault, I., Dartiguenave, C., Bertrand, M.J. & Waldron, K.C., 2004. Glutaraldehyde: Behavior in aqueous solution, reaction with proteins, and application to enzyme crosslinking. *BioTechniques*, 37(5), pp.790–802.

Miladi, B., Marjou, A.E., Boeuf, G., Bouallagui, H., Dufour, F., Di Martino, P. & Elm'selmi, A., 2012. Oriented immobilization of the tobacco etch virus protease for the cleavage of fusion proteins. *Journal of Biotechnology*, In press.

Moehlenbrock, M.. J. & Minteer, S.D., 2011. Introduction to the field of enzyme immobilization and stabilization. *Methods in Molecular Biology*, 679, pp.1–7.

Newman, J.D. & Turner, A.P.F., 2005. Home blood glucose biosensors: A commercial perspective. *Biosensors and Bioelectronics*, 20(12), pp.2435–2453.

Noble, M.A., Miles, C.S., Chapman, S.K., Lysek, D.A., MacKay, A.C., Reid, G.A., Hanzlik, R.P. & Munro, A.W., 1999. Roles of key active-site residues in flavocytochrome P450 BM3. *Biochemical Journal*, 339(2), pp.371–379.

Pedrosa, V.A., Paliwal, S., Balasubramanian, S., Nepal, D., Davis, V., Wild, J., Ramanculov, E. & Simonian, A., 2010. Enhanced stability of enzyme organophosphate hydrolase interfaced on the carbon nanotubes. *Colloids and Surfaces B: Biointerfaces*, 77(1), pp.69–74.

Phan, J., 2002. Structural Basis for the Substrate Specificity of Tobacco Etch Virus Protease. *Journal of Biological Chemistry*, 277(52), pp.50564–50572.

Pilkington, S.M., Roberts, S.J., Meade, S.J. & Gerrard, J.A., 2010. Amyloid fibrils as a nanoscaffold for enzyme immobilization. *Biotechnology Progress*, 26(1), pp.93–100.

Puhl, A.C., Giacomini, C., Irazoqui, G., Batista-Viera, F., Villarino, A. & Terenzi, H., 2009. Covalent immobilization of tobacco-etch-virus NIa protease: A useful tool for cleavage of the histidine tag of recombinant proteins. *Biotechnology and Applied Biochemistry*, 53(Pt 3), pp.165–174.

Quiocho, F.A., Spurlino, J.C. & Rodseth, L.E., 1997. Extensive features of tight oligosaccharide binding revealed in high-resolution structures of the maltodextrin transport/chemosensory receptor. *Structure (London, England: 1993)*, 5(8), pp.997–1015.

Ross, J.A., Gilmore, M.A., Williams, D., Aoki, K.R., Steward, L.E. & Jameson, D.M., 2011. Characterization of Förster resonance energy transfer in a botulinum neurotoxin protease assay. *Analytical Biochemistry*, 413(1), pp.43–49.

Royant, A. & Noirclerc-Savoye, M., 2011. Stabilizing role of glutamic acid 222 in the structure of Enhanced Green Fluorescent Protein. *Journal of Structural Biology*, 174(2), pp.385–390.

Saravanan, D., Sivasaravanan, S., Sudharshan Prabhu, M., Vasanthi, N.S., Senthil Raja, K., Das, A. & Ramachandran, T., 2012. One-step process for desizing and bleaching of cotton fabrics using the combination of amylase and glucose oxidase enzymes. *Journal of Applied Polymer Science*, 123, pp.2445–2450.

Sevrioukova, I.F., Li, H., Zhang, H., Peterson, J.A. & Poulos, T.L., 1999. Structure of a Cytochrome P450–redox Partner Electron-Transfer Complex. *Proceedings of the National Academy of Sciences*, 96(5), pp.1863–1868.

Sheldon, R.A., 2007. Enzyme immobilization: The quest for optimum performance. *Advanced Synthesis & Catalysis*, 349(8-9), pp.1289–1307.

Sigma-Aldrich, 2012. Buffer Reference Center. Available at: http://www.sigmaaldrich.com/life-science/core-bioreagents/biological-buffers/learning-center/buffer-reference-center.html.

Spahn, C. & Minteer, S.D., 2008. Enzyme immobilization in biotechnology. *Recent Patents on Engineering*, 2(3), pp.195–200.

Stratis, A., 1969. Coupling of enzymes to proteins with glutaraldehyde: Use of the conjugates for the detection of antigens and antibodies. *Immunochemistry*, 6(1), pp.43–52.

Stryer, L., 1978. Fluorescence energy transfer as a spectroscopic ruler. *Annual Review of Biochemistry*, 47, pp.819–846.

Teixeira, A.I., Ribeiro, L.F., Rezende, S.T., Barros, E.G. & Moreira, M.A., 2012. Development of a method to quantify sucrose in soybean grains. *Food Chemistry*, 130(4), pp.1134–1136.

Tropea, J.E., Cherry, S. & Waugh, D.S., 2009. Expression and purification of double his_6-tagged TEV protease. In *Methods in Molecular Biology: High Throughput Protein Expression and Purification*. Humana Press, pp.297–307.

Tsien, R.Y., 1998. The green fluorescent protein. *Annual Review of Biochemistry*, 67, pp.509–544.

Wang, Y., Liu, L., Li, M., Xu, S. & Gao, F., 2011. Multifunctional carbon nanotubes for direct electrochemistry of glucose oxidase and glucose bioassay. *Biosensors and Bioelectronics*, 30(1), pp.107–111.

Waugh, D.S., 2005. Making the most of affinity tags. *Trends in Biotechnology*, 23(6), pp.316–320.

Waugh, D.S., 2010. TEV Protease FAQ. Available at: mcl1.ncifcrf.gov/waugh_tech/faq/tev.pdf.

Weber, E., Sirim, D., Schreiber, T., Thomas, B., Pleiss, J., Hunger, M., Gläser, R. & Urlacher, V.B., 2010. Immobilization of P450 BM-3 monooxygenase on mesoporous molecular sieves with different pore diameters. *Journal of Molecular Catalysis B: Enzymatic*, 64(1–2), pp.29–37.

Whipple, E.B. & Ruta, M., 1974. Structure of aqueous glutaraldehyde. *The Journal of Organic Chemistry*, 39(12), pp.1666–1668.

Whitehouse, C.J.C., Bell, S.G. & Wong, L.-L., 2012. P450BM3 (CYP102A1): Connecting the dots. *Chemical Society Reviews*, Advanced Article.

Wilson, R. & Turner, A.P.F., 1992. Glucose oxidase: An ideal enzyme. *Biosensors and Bioelectronics*, 7(3), pp.165–185.

Wohlfahrt, G., Witt, S., Hendle, J., Schomburg, D., Kalisz, H.M. & Hecht, H.J., 1999. 1.8 and 1.9 A resolution structures of the Penicillium amagasakiense and Aspergillus niger glucose oxidases as a basis for modelling substrate complexes. *Acta Crystallographica. Section D, Biological Crystallography*, 55(Pt 5), pp.969–977.

Zhao, L., Güven, G., Li, Y. & Schwaneberg, U., 2011. First steps towards a Zn/Co(III)sep-driven P450 BM3 reactor. *Applied Microbiology and Biotechnology*, 91(4), pp.989–999.

Chapter Five

5 Amyloid fibrils as a surface assembled biomolecule nanoscaffold

5.1 Introduction

This chapter combines the experimental approaches of the previous two chapters to investigate the creation of materials with functionalised surface assembled insulin amyloid fibrils. Enzymes have been immobilised to many different surfaces (section 1.6) for a wide range of techniques including: surface plasmon resonance (SPR) (Homola 2008), protein microarrays (Rusmini *et al.* 2007), and quartz crystal microbalance (QCM) sensors. Enzymes have also been immobilised to surfaces to generate enzymatically active materials for the purposes of chemical decontamination (Havens & Rase 1993; Gill & Ballesteros 2000) and the manufacture of antimicrobial packaging (Vartiainen *et al.* 2005). GOD was recently immobilised to an electrospun nanofibrous PVOH extract for the production of a novel food packaging material to aid in food preservation (Ge *et al.* 2012), and lysozyme has been immobilised to cotton material to create an antimicrobial material with potential uses in wound dressings and antimicrobial wipes (Edwards *et al.* 2011).

In the above examples, the enzymes are immobilised directly to the surface, therefore an increase in surface area could prove beneficial for many immobilised enzyme applications. Increasing surface area enables a higher enzyme immobilisation capacity, which, if applied to techniques such as SPR, protein micro arrays, and QCM, could result in a device with greater sensitivity. Assembling amyloid fibrils on a surface leads to an increase in surface area because of their nanometre dimensions which afford a high surface to volume ratio (Gras *et al.* 2008). As stated in section 3.3, assembling amyloid fibrils on surfaces could also potentially allow for a bottom-up approach to functional bionanomaterial design (Scanlon & Aggeli 2008; Williams *et al.* 2010). The proteinaceous building blocks of the nanoscaffold may also offer a beneficial environment for protein immobilisation, resulting in an increase in stability and activity of the immobilised enzyme.

An overview of the process to create the functional self-assembling bionanomaterials is shown in **Figure 5.1**. First the material surface is derivatised to allow binding of the amyloid template, followed by self-assembly of the amyloid fibrils, then the surface assembled amyloid fibrils are functionalised with biomolecules. Two biomolecule immobilisation methods were used, physical adsorption, and covalent cross-linking, depending on which biomolecule was being immobilised. The immobilisation method adopted depended on whether the covalent cross-linker GA inhibited enzymatic activity, or if there was a strong physical adsorption of the biomolecule to the surface assembled amyloid fibrils.

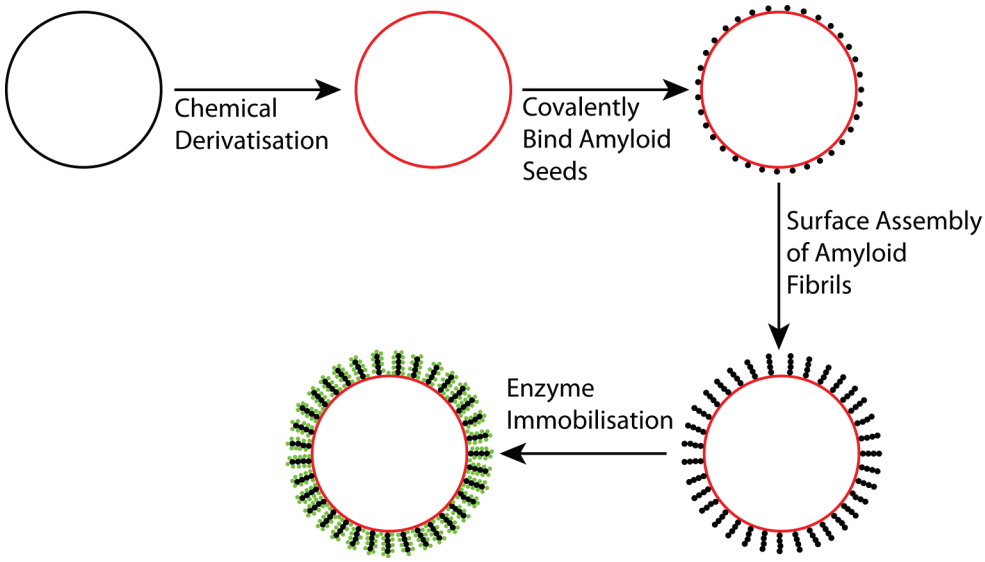

Figure 5.1 *Overview of the functional bionanomaterial manufacturing process. Firstly, glass beads or cellulose based materials are chemically derivatised with APTS and DSC to yield an activated surface that can then covalently bind amyloid seeds. Surface assembly of mature amyloid fibrils can then occur by immersion in native amyloid forming protein and heating at low pH. The surface assembled amyloid fibrils are then decorated with biomolecules by either physical adsorption or covalent coupling, depending on the biomolecule.*

Initially GOD was immobilised to the surface assembled insulin amyloid fibrils due to its stability and use as a model enzyme for immobilisation (Shi *et al.* 2011). GFP was immobilised as a fluorescent tag to aid in the visualisation of the surface assembled amyloid fibrils, and to try and establish the coverage of surface assembled insulin amyloid fibrils. TEV protease was immobilised to the surface assembled amyloid fibrils to create a reusable TEV protease nanomaterial bead system with potential commercial applications. Initial GFP immobilisation trials were investigated on cotton surface assembled insulin amyloid fibrils as a potential manufacturing route to create enzymatically functional cotton.

5.2 Glucose oxidase immobilisation

GOD was used as the model enzyme for immobilisation on to the surface assembled insulin amyloid fibrils because of its robustness, tolerating pHs between 2 and 8, and because it is still active at up to ~ 62 °C (Wilson & Turner 1992; Gouda *et al.* 2003). The Amplex red assay (sections 2.6.1 and 7.12.6) enables high throughput characterisation of GOD samples using a 96 well plate reader, allowing for optimisation of the immobilisation conditions on the surface assembled insulin amyloid fibrils. Optimising the surface immobilisation conditions first with GOD provided a starting protocol for the subsequent immobilisation of GFP and TEV protease.

5.2.1 Method development and characterisation of GOD functionalised surface assembled insulin amyloid fibrils

The method development for the immobilisation of GOD to the surface assembled insulin amyloid fibrils was based on in-house methodology developed by Roberts (2010), in which initial GOD immobilisation experiments were carried out on glass microscope slides. This initial work concluded that GA was not needed when immobilising GOD to surface assembled insulin amyloid fibrils, therefore GA was omitted from the immobilisation protocol (*Personal comm.* Roberts 2010). It is thought that GA is not needed because a physical interaction may be occurring between the glass surface, GOD, and the surface assembled insulin amyloid fibrils. This interaction could aid in the adsorption of the enzyme to the surface. The GOD immobilisation results produced with the glass slides were not very reproducible. Therefore GOD immobilisation to surface assembled insulin amyloid fibrils on glass beads was attempted to increase the reproducibility. Experimental reproducibility will allow a firm conclusion to be drawn on whether surface assembled insulin amyloid fibrils enable an increase in immobilised GOD.

Initial GOD immobilisation experiments investigated the requirement of the individual surface treatments outlined in **Figure 5.1**. The derivatisation of the glass beads, subsequent seeding of the surface, and self-assembly of the insulin amyloid fibrils was carried out, as described in section 3.4 (section 7.12.1 and 7.12.2). The bead samples were then immersed in a 1 mg/mL solution of GOD or GOD buffer and incubated for 1 hour at 37 °C (section 7.13.1). The samples were thoroughly washed in dH_2O before their activity and ThT fluorescence was measured. **Table 5.1** shows the amount of GOD activity of each immobilisation sample using the Amplex red assay (sections 2.6.1 and 7.12.6), and investigates the presence of amyloid fibril structures with ThT (section 7.12.5). The sample that showed the most GOD activity and highest ThT fluorescence is sample 17, which had all of the treatments. This result suggests the surface assembled amyloid fibrils enabled more GOD to be immobilised, but samples 9, 11, 19, and 20 also have relatively high GOD activity. This result indicates a strong interaction between GOD and the glass surface, because the ThT fluorescence of these samples is low, implying there are not amyloid structures present on the surface that are aiding in immobilisation.

Table 5.1 *Activity (RFU) of immobilised GOD glass bead samples using the Amplex red assay (Amp) and ThT) fluorescence (ThT) (RFU). APTS – APTS surface derivitisation, DSC – activation of surface, Seed – seeded with insulin fragments, Fibril – insulin amyloid fibrils assembled, GOD – GOD immobilised. Each sample had six replicated, three for the Amplex red assay, and three for the ThT assay. The errors represent the standard deviation of the mean.*

Sample	APTS	DSC	Seed	Fibril	GOD	Amp	A. Error	ThT	T. Error
1	-	-	+	+	+	8300	1700	600	200
2	-	-	+	-	+	1600	100	600	100
3	-	-	-	+	+	1000	200	400	200
4	-	-	-	-	+	1400	100	500	100
5	-	-	+	+	-	800	-	1100	200
6	-	-	+	-	-	800	-	500	-
7	-	-	-	+	-	700	-	500	100
8	-	-	-	-	-	800	-	600	200
9	+	-	+	+	+	10000	500	500	100
10	+	-	+	-	+	8000	2400	300	-
11	+	-	-	+	+	10500	900	300	-
12	+	-	-	-	+	8600	500	300	-
13	+	-	+	+	-	800	-	600	200
14	+	-	+	-	-	800	100	300	-
15	+	-	-	+	-	800	-	300	-
16	+	-	-	-	-	900	-	300	-
17	+	+	+	+	+	13000	800	1600	300
18	+	+	+	-	+	9000	400	300	-
19	+	+	-	+	+	10600	400	300	-
20	+	+	-	-	+	10700	300	300	-
21	+	+	+	+	-	900	-	1500	200
22	+	+	+	-	-	900	-	300	-
23	+	+	-	+	-	800	100	300	-
24	+	+	-	-	-	900	-	300	-

To try and impede the direct adhesion of GOD to the glass surface,, bovine serum albumin (BSA) was investigated as a blocking agent. Lowering the background GOD activity will enable the influence of the amyloid fibrils on the amount of GOD immobilised to be deciphered. BSA is a commonly used protein for blocking excess reactive sites on surfaces (Huang *et al.* 2003). For the glass beads, a 2 % BSA solution for 2 hours was used to block unreacted activated amino groups after the surface assembly of the insulin amyloid fibrils (section 7.12.4).

Shown in **Table 5.2** are the controls employing BSA as a blocking agent. Comparing the eight samples, four of which were blocked with BSA, and four which were not blocked, BSA blocking is lowering the amount of GOD being immobilised to all of the samples. As seen in **Table 5.1**, the beads with all of the treatment conditions have the highest GOD activity (samples 1 and 5). This could be due to the presence of the surface assembled insulin amyloid fibrils, but the background GOD activity of the controls is still relatively high, implying non-specific binding is still occurring. BSA is having an effect on the non-specific binding of GOD to the glass. Comparing samples 4 and 8, for which the glass surface is activated, but not seeded or amyloid fibrils assembled, the decrease in bound GOD activity is ~60 % less when BSA is used for blocking. This result is expected because the surface chemistry on the glass reacts with the same amine groups in both BSA, and the amyloid fragments.

Table 5.2 *Activity (RFU) using Amplex red fluorescence (Amp) of immobilised GOD glass bead samples. All of the glass beads had their surface derivatised by APTS and DSC. Seed – seeded with insulin fragments, Fibrils – insulin amyloid fibrils assembled, BSA – blocked with BSA for 2 hours, GOD – GOD immobilised. Each sample had three replicates. The error represents the standard deviation of the mean.*

Sample	APTS	DSC	Seed	Fibril	BSA	GOD	Amp	A. error
1	+	+	+	+	+	+	1873	153
2	+	+	+	-	+	+	1220	127
3	+	+	-	+	+	+	1488	361
4	+	+	-	-	+	+	1158	81
5	+	+	+	+	-	+	4377	621
6	+	+	+	-	-	+	2989	115
7	+	+	-	+	-	+	2667	74
8	+	+	-	-	-	+	3092	767

To try to lower the background GOD activity more, an extensive washing step was undertaken. The glass bead samples were placed in a small (~7 mm diameter) column with GOD buffer (50 mM sodium phosphate, pH 7.4) flowing over the beads for ~18 hours. Washing the beads for a long period of time will wash the loosely bound GOD, leaving only the strongly bound GOD. The bead samples were then analysed for GOD activity by the Amplex red assay, and the ThT assay to ensure the washing step did not remove any of the surface assembled insulin amyloid fibrils.

As can be seen in **Table 5.3**, the extensive washing step produced very similar results to samples 1-4 in **Table 5.2**, indicating that the GOD in all of the samples in strongly bound. The beads in sample 1 which have all of the treatment conditions have the highest GOD activity and the highest ThT fluorescence, again suggesting that the presence of the surface assembled insulin amyloid fibrils is allowing for more GOD to be immobilised. This suggests, for GOD immobilisation to activated glass beads, there is little advantage in using the nanoscaffold due to the high affinity of GOD to the glass surface.

Table 5.3 *Activity (RFU) of immobilised GOD glass bead samples using the Amplex red assay (Amp) and ThT fluorescence (ThT) (RFU). APTS – APTS surface derivitisation, DSC – activation of surface, Seed – seeded with insulin fragments, Fibril – insulin amyloid fibrils assembled, BSA – block with BSA for 2 hours, GOD – GOD immobilised. Each sample had six replicated, three for the Amplex red assay, and three for the ThT assay. The errors represent the standard deviation of the mean.*

Sample	APTS	DSC	Seed	Fibril	BSA	GOD	Amp	A. error	ThT	T. error
1	+	+	+	+	+	+	2251	73	1287	117
2	+	+	+	-	+	+	1407	142	402	85
3	+	+	-	+	+	+	1551	117	403	9
4	+	+	-	-	+	+	1384	73	364	14

Surface assembly of bovine insulin amyloid fibrils on glass beads, and subsequent immobilisation with GOD, revealed the presence of the nanoscaffold afforded little advantage when immobilising GOD. The high non-specific binding of GOD to the glass surface hinders any potentially positive effects of the nanoscaffold from being observed. ThT fluorescence demonstrated that amyloid fibril structures were present on the surface, thus the increases that were seen could be due to the amyloid fibril nanoscaffold. Although the increase in GOD activity was not as expected, the result, and the established immobilisation protocol, provided the framework to test the immobilisation of the other biomolecules, GFP and TEV protease.

5.3 Green fluorescent protein immobilisation

GFP was employed to fluorescently tag the surface assembled insulin amyloid fibrils, to analyse their coverage on the surface of the bead. Confocal laser scanning microscopy (CLSM) was used to assess the surface coverage of the GFP immobilisation because the microscope can excite GFP at 488 nm, inducing fluorescence, and capture images of the glass bead samples. The curvature of the glass bead surface creates problems with acquiring in-focus images of the entire surface by standard light microscope. CLSM offers a solution to curved surfaces, because it allows in-focus images to be acquired at multiple depths (Pawley 2006). The multiple images can be subsequently reconstructed, providing an in-focus image of an entire curved surface. The reconstructed images can be quantitatively analysed by pixel density calculations if the gain of the microscope is kept constant for all images (Piston *et al.* 1998). Quantitative pixel density calculations allow images to be directly compared by providing valuable information on the amount of fluorescence of each image.

5.3.1 GFP functionalisation and characterisation of surface assembled insulin amyloid fibrils

GFP surface immobilisation was based around the method developed for immobilising GFP to the solution insulin amyloid fibril (section 4.6.1). All of the bead samples were first immersed in a solution containing 2.5 mM GA for 1 hour, then washed thoroughly and placed in a 1 mg/mL solution of GFP for 1 hour, before being thoroughly washed again (section 7.13.2). The resulting immobilised GFP samples were investigated for fluorescence in a plate reader (section 7.12.7), and imaged using CLSM (section 7.2.13). As can be seen in **Figure 5.2**, the beads which were seeded, the amyloid fibrils assembled, and GFP immobilised (sample 4), had the highest GFP fluorescence detected in the plate reader. This confirms the presence of the surface assembled insulin amyloid fibrils enables more GFP to be immobilised to the glass surface. The background level of GFP absorption to the control glass beads is much lower than for GOD, presumably due to the different surface characteristics of each biomolecule.

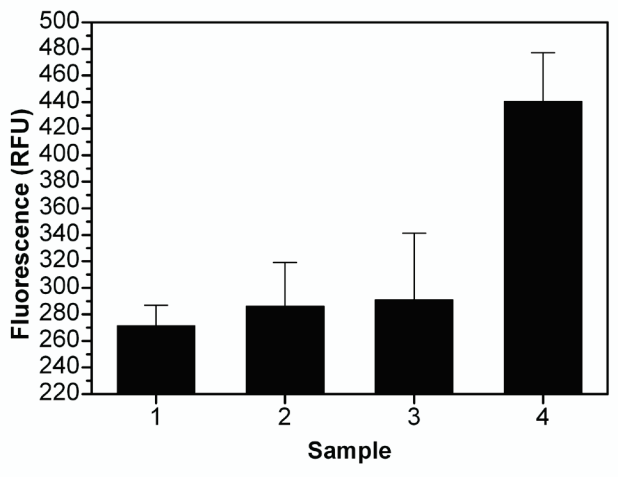

Figure 5.2 *GFP fluorescence in a 96 well plate fluorescence spectrophotomer using an excitation and emission of 488 nm and 509 nm, respectively. Sample 1 – bead not seeded, no fibrils, GFP immobilised, sample 2 – bead not seeded, fibrils assembled, GFP immobilised, sample 3 – bead seeded, no fibrils, GFP immobilised, sample 4 – bead seeded, fibrils assembled, GFP immobilised. Each sample had three replicates, and the error bars represent the standard deviation of the mean.*

The immobilised GFP samples were then analysed using CLSM. Each bead was mounted on a glass bottomed culture dish with ~200 µL of 50 mM NaPi, pH 7.4 buffer to hold the bead in position, and viewed using a 10 X objective lens (section 7.2.13). The lens was focused on the midpoint of the surface of the bead and 40 in-focus sections were imaged towards the halfway point of the bead. This technique allowed the entire surface of half the bead to be reconstructed by stacking the images on top of each other using the Leica LAS AF Lite 2.4.1 software. Quantitative analysis on the reconstructed images was undertaken to compare the amount of GFP immobilised to the different bead samples (section 7.2.14) (Piston *et al.* 1998). As can be seen in **Figure 5.3**, the mean pixel values of the glass beads which were seeded, insulin amyloid fibrils assembled, and then GFP immobilised gave the highest fluorescence (sample 4). This indicates that the presence of the amyloid fibrils on the surface of the beads allows for a higher loading of GFP, presumably because there is an increase in the available surface area for GFP immobilisation. The fluorescence of sample 3 was also relatively high, implying that there was some mature insulin amyloid fibrils physisorbed to the surface of the glass beads, even without seeds present. This result is very similar to the result seen in **Figure 5.2** using the plate reader fluorescent spectrophotomer.

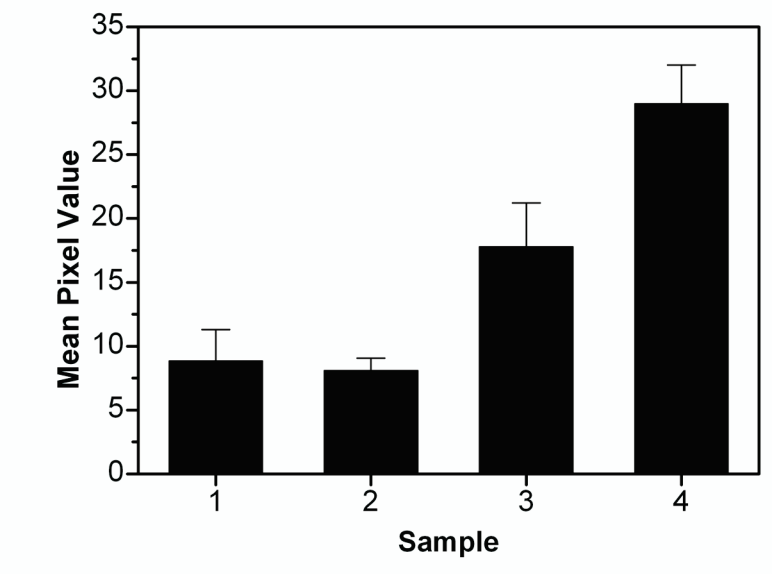

Figure 5.3 *Quantitative mean pixel value analysis of confocal images. Sample 1 – bead not seeded, no fibrils, GFP immobilised, sample 2 – bead not seeded, fibrils assembled, GFP immobilised, sample 3 – bead seeded, no fibrils, GFP immobilised, sample 4 – bead seeded, fibrils assembled, GFP immobilised. Each sample had six replicates, three from two independent experiments. The error bars represent the standard deviation of the mean.*

One representative image of each sample from **Figure 5.3** is shown in **Figure 5.4**. As can be seen, the mean pixel values correlate well to the images, with only samples 3 and 4 showing any significant fluorescence. The images confirm that when the beads are seeded, fibrils assembled and GFP immobilised (sample 4), the greatest amount of GFP is immobilised. The images show that the coverage of GFP functionalised amyloid fibrils on the bead surface was reasonably complete. Given that that the beads are handled extensively with tweezers throughout the immobilisation process, this is a testament to the resilience of the amyloid fibril nanoscaffold. Future work should investigate optimisation of the surface coverage using GFP fluorescence. Immobilising GFP to the surface assembled amyloid fibrils enabled visualisation of the functionalised amyloid fibrils by confocal microscopy, and investigation into the coverage of the amyloid fibril on the bead surfaces.

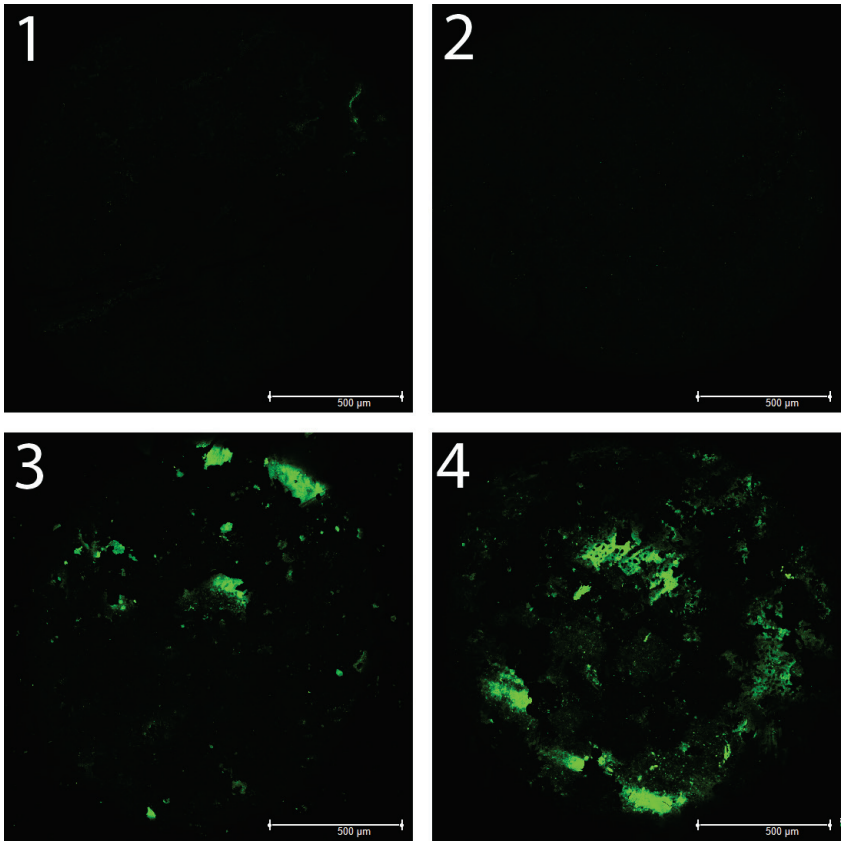

Figure 5.4 *Representative confocal images of GFP on bead samples. Sample 1 – bead not seeded, no fibrils, GFP immobilised, sample 2 – bead not seeded, fibrils assembled, GFP immobilised, sample 3 – bead seeded, no fibrils, GFP immobilised, sample 4 – bead seeded, fibrils assembled, GFP immobilised. The microscope gain was set at 400 for all of the samples. The scale bar = 500 µm.*

5.4 Tobacco etch virus protease

Following the successful immobilisation of TEV protease to the solution insulin amyloid fibrils (section 4.8.1), it was decided to try and create a reusable TEV protease bionanomaterial by immobilising TEV protease to the surface assembled insulin amyloid fibrils. By immobilising TEV protease to the surface assembled insulin amyloid fibrils, it was anticipated that the TEV protease-glass beads would be easily reused by simply washing the beads between cleavage reactions. As stated in section 4.8, TEV protease is not normally recoverable after it has completed its cleavage reaction. Therefore, if TEV protease can be immobilised to a solid support, whilst retaining activity, a reusable system will be created that saves on production costs.

TEV protease has recently been immobilised to a strepavidin-agarose matrix (Miladi *et al.* 2012) (section 4.8) The increase in surface area arising from the surface assembled insulin amyloid fibrils and the proteinaceous nature of the nanoscaffold could however, allow a higher TEV protease loading and better catalytic efficiency. It has already been shown that TEV protease can be physically adsorbed to insulin amyloid fibrils (section 4.81), and that in the immobilised form it retains protease activity, thus TEV protease was physically adsorbed to the surface assembled insulin amyloid fibrils.

5.4.1 TEV protease functionalisation and characterisation of surface assembled insulin amyloid fibrils

A similar method to immobilising TEV protease to the solution insulin amyloid fibrils was used for the immobilisation of TEV protease to the surface assembled insulin amyloid fibrils. The method assembled the insulin amyloid fibrils on the surface of glass beads, as described in sections 3.4.1 and 7.12.2. The beads were then immersed in a 1 mg/mL solution of TEV protease for 2 hours at 4 °C, and thoroughly washed (section 7.13.3). To assess the amount of TEV protease immobilised to the different bead samples, the pre-bead immersion and post-bead immersion TEV protease solutions were analysed by SDS-PAGE. This is due to the reduction in the amount of TEV protease in solution, if immobilisation is occurring. **Figure 5.5** shows the SDS-PAGE gel of the pre-bead immersion TEV protease solution (lane 1), and post-bead immersion TEV protease immobilised solutions, which clearly shows that some TEV protease is being immobilised to all of the bead samples, as evident by the fainter TEV protease protein bands. From the gel it appears that all bead samples, whether they have been seeded or not, or had amyloid fibrils assembled, immobilised about the same amount of TEV protease.

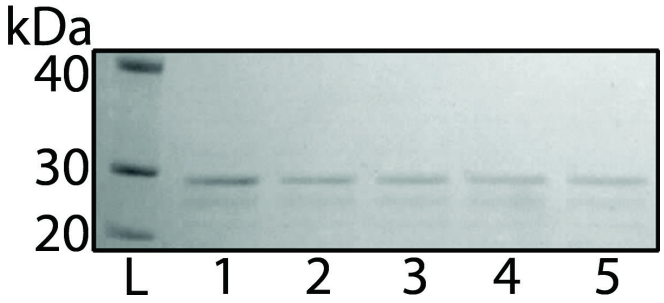

Figure 5.5 *SDS-PAGE gel showing the amount of TEV protease in the pre-bead immersion and post-bead immersion TEV protease solutions. L – ladder, 1 – pre-bead immersion, 2 – post-bead immersion with a bead that was seeded, no fibril assembled, and TEV protease immobilised, 3 – post-bead immersion with a bead that was seeded, fibril assembled, and TEV protease immobilised, 4 – post- immersion with a bead that was not seeded, no fibril assembled, and TEV protease immobilised, 5 – post-immersion with a bead that was not seeded, fibrils assembled, and TEV protease immobilised. The same amount of protein was loaded in each lane.*

The TEV protease functionalised surface assembled amyloid fibrils were initially tested for their ability to cleave the poly-histidine tag of wild-type *E. coli* DHDPS. The immobilised TEV protease bead samples were put in a 1 mg/mL solution of wild-type *E. coli* DHDPS, and were incubated for 18 hours at 4 °C (section 7.13.4). A fraction of each of the DHDPS solutions was carefully pipetted off without touching the glass beads, and the fractions analysed for poly-histidine tag cleavage by SDS-PAGE. As can be seen in **Figure 5.6**, all of the bead samples displayed the ability to cleave the poly-histidine tag of the DHDPS, but the immobilised TEV protease bead which showed the highest activity was the bead which was seeded, amyloid fibrils assembled, and TEV protease immobilised (lane 4). Furthermore, the bead sample from lane 4 actually showed as much activity as the control cleavage reaction (lane 3), verifying that the amyloid fibril immobilised TEV protease must retain most, if not all of its catalytic activity. The slight cleavage activity seen by the other bead samples could be due to the non-specific physisorption of TEV protease to the glass surface as seen in **Figure 5.5**, when investigating the amount of TEV protease being immobilised to the surface assembled amyloid fibrils. However, in contrast to the results with GOD, the nanoscaffold affords a clear advantage.

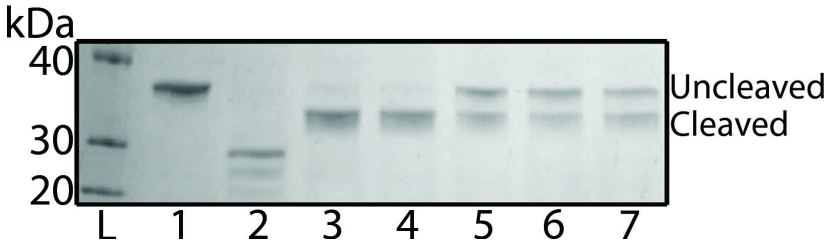

Figure 5.6 *SDS-PAGE gel of E. coli DHDPS cleavage by immobilised TEV bead samples. L – Ladder, 1 – DHDPS only control, 2 – TEV only control, 3 – solution TEV DHDPS cleavage control, 4 – bead (seeded + fibrils + TEV) DHDPS cleavage, 5 – bead (seeded + TEV) DHDPS cleavage, 6 – bead (fibrils + TEV) DHDPS cleavage, 7 – bead (TEV only) DHDPS cleavage.*

The TEV protease functionalised surface assembled amyloid fibrils were then tested for their ability to be reused sequentially, cleaving a different poly-histidine tagged protein on each day (section 7.13.4). It was decided to cleave a different protein each day, so that if there was any substantial contamination from a previous day's protein cleavage, a protein band corresponding to the previous days cleavage reaction would be visible on the SDS-PAGE gel. The cleavage reactions were setup as for **Figure 5.6**, but after each 18 hour cleavage reaction, the beads were thoroughly washed in dH_2O before being placed in the next cleavable protein solution. This procedure was repeated until immobilised TEV protease activity had ceased.

Figure 5.7 shows the sequential poly-histidine tag cleavage of *T. maritima* DHDPR, *A. thaliana* DHDPR, human peroxiredoxin 3 (PRX3), and *E. coli* DHDPS Y107W by TEV protease functionalised surface assembled amyloid fibril samples. On day one of the cleavage reactions, all of the bead samples showed some cleavage activity, with the SDS-PAGE gel showing very similar results as **Figure 5.6**. Again, the bead which was seeded, amyloid fibrils assembled, and TEV protease immobilised (lane 4) showed the highest TEV protease activity. The cleavage on day two had a very similar trend, but this time the amount of cleavage by the bead sample which was seeded, amyloid fibrils assembled, and TEV protease immobilised (lane 4), was much more pronounced compared to the other bead samples. By day three, the only bead sample retaining TEV protease activity was the bead sample which was seeded, amyloid fibrils assembled, and TEV protease immobilised (lane 4). This provides evidence that the presence of the surface assembled amyloid fibrils present protect TEV protease activity on the bead sample. By day four all of immobilised TEV bead samples showed no TEV protease activity. The control TEV protease reaction (lane 3) showed that the protein is cleavable, therefore the reason for no cleavage activity by the immobilised TEV protease beads samples could be due to inactivation of the immobilised TEV protease, or leaching of the immobilised TEV protease over time, which is known to be a problem when immobilising enzymes by physical adsorption (section 1.5.3).

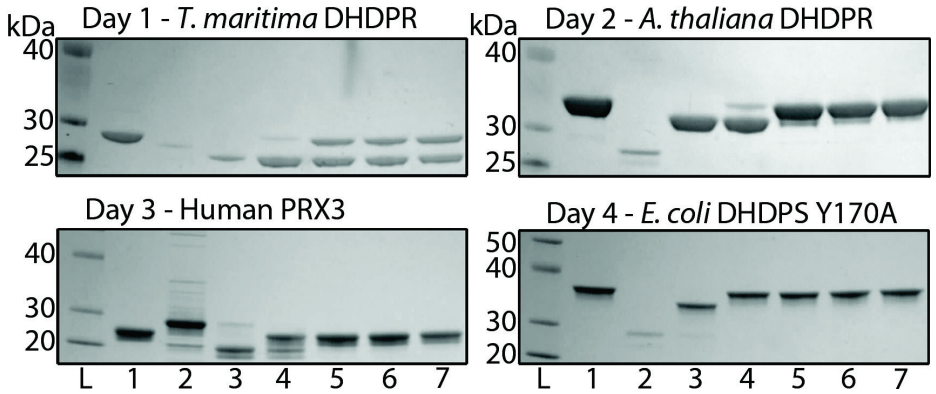

Figure 5.7 *SDS-PAGE gels of poly-histidine tag cleavage by TEV protease immobilised to bead samples. For all gels the lanes contain: L – Ladder, 1 – protein control, 2 – TEV protease only control, 3 – solution TEV protease protein cleavage control, 4 – bead (seeded + fibrils + TEV protease) protein cleavage, 5 – bead (seeded + TEV protease) protein cleavage, 6 – bead (fibrils + TEV protease) protein cleavage, 7 – bead (TEV protease only) protein cleavage.*

Functionalisation of the surface assembled insulin amyloid fibrils with TEV protease showed that the glass beads which were seeded and amyloid fibrils assembled, retained the most activity. This result was the similar to the results obtained when immobilising GOD and GFP, implying that the presence of the amyloid fibrils on the surface of the glass beads is allowing for a greater amount of enzyme to be immobilised. The catalytic activity of the immobilised TEV protease was preserved over three uses, with three different poly-histidine tagged proteins. Considering the immobilised TEV protease beads as a commercial proof-of-concept system, the results are promising taking into account that one 5 mm bead was used per reaction. Further optimisation of the surface amyloid fibril assembly and the enzyme immobilisation conditions could increase the enzymatic activity, reusability and storage life of the immobilised TEV protease bead system, and optimisation of this technology towards smaller micro glass beads packed into a column could potentially increase the specific enzyme activity exponentially.

5.5 Summary

This chapter has shown that surface assembled bovine insulin amyloid fibrils can be functionalised with a variety of biomolecules: GOD, GFP, and TEV protease. The evidence presented in this chapter shows that surface assembled insulin amyloid fibrils are providing a larger surface area and/or a biomolecule friendly environment that allows for a greater amount of biomolecule immobilisation or enhanced catalytic activity. In all cases of biomolecule immobilisation, the glass bead surface that was seeded, insulin amyloid fibrils assembled, and the particular biomolecule immobilised, had the greatest activity or fluorescence, although GOD immobilisation was confounded by the high affinity of the enzyme to the unmodified glass surface.

Improvements to the amount of biomolecule immobilisation could be gained by optimising the amyloid fibril surface coverage. GFP was shown to be an excellent tool for investigating surface coverage and immobilisation. Future optimisation of amyloid fibril surface assembly can use GFP immobilisation and subsequent analysis by CLSM to quantify increases in surface assembled insulin amyloid fibrils. The results illustrate that surface assembled insulin amyloid fibrils are a useful nanoscaffold, but their utility as a nanoscaffold depends on the biomolecule being immobilised.

Major steps have been taken in the characterisation and use of amyloid fibrils for bionanotechnology purposes, and a proof of principle reusable TEV protease-amyloid fibril bead system has been developed that has possible future commercial applications. This demonstrates the commercial potential of amyloid fibrils as a nanoscaffold. Initial research into the creation of GFP functionalised surface assembled insulin amyloid fibrils on cotton was commenced, but analysis of the cotton material proved more difficult than the glass beads, therefore future work is needed to transfer the technology to the cotton system.

5.6 References

Edwards, J.V., Prevost, N.T., Condon, B. & French, A., 2011. Covalent attachment of lysozyme to cotton/cellulose materials: Protein verses solid support activation. *Cellulose*, 18(5), pp.1239–1249.

Ge, L., Zhao, Y., Mo, T., Li, J. & Li, P., 2012. Immobilization of glucose oxidase in electrospun nanofibrous membranes for food preservation. *Food Control*, 26(1), pp.188–193.

Gill, I. & Ballesteros, A., 2000. Degradation of organophosphorous nerve agents by enzyme-polymer nanocomposites: Efficient biocatalytic materials for personal protection and large-scale detoxification. *Biotechnology and Bioengineering*, 70(4), pp.400–410.

Gouda, M.D., Sridevi, S.A., Appu, A.G.R., Thakur, M.S. & Karanth, N.G., 2003. Thermal inactivation of glucose oxidase: Mechanism and stabilization using additives. *Journal of Biological Chemistry*, pp.24324–24333.

Gras, S.L., Tickler, A.K., Squires, A.M., Devlin, G.L., Horton, M.A., Dobson, C.M. & MacPhee, C.E., 2008. Functionalised amyloid fibrils for roles in cell adhesion. *Biomaterials*, 29(11), pp.1553–1562.

Havens, P.L. & Rase, H.F., 1993. Reusable immobilized enzyme/polyurethane sponge for removal and detoxification of localized organophosphate pesticide spills. *Industrial and Engineering Chemistry Research*, 32(10), pp.2254–2258.

Homola, J., 2008. Surface plasmon resonance sensors for detection of chemical and biological species. *Chemical Reviews*, 108(2), pp.462–493.

Huang, T.T., Sturgis, J., Gomez, R., Geng, T., Bashir, R., Bhunia, A.K., Robinson, J.P. & Ladisch, M.R., 2003. Composite surface for blocking bacterial adsorption on protein biochips. *Biotechnology and Bioengineering*, 81(5), pp.618–624.

Miladi, B., Marjou, A.E., Boeuf, G., Bouallagui, H., Dufour, F., Di Martino, P. & Elm'selmi, A., 2012. Oriented immobilization of the tobacco etch virus protease for the cleavage of fusion proteins. *Journal of Biotechnology*, In press.

Pawley, J. ed., 2006. *Handbook of Biological Confocal Microscopy* 3rd ed., New York: Springer.

Piston, D.W., Patterson, G.H. & Knobel, S.M., 1998. Quantitative imaging of the green fluorescent protein (GFP). In K. F. Sullivan & S. A. Kay, eds. *Green Fluorescent Proteins*. Academic Press, pp. 31–48.

Rusmini, F., Zhong, Z. & Feijen, J., 2007. Protein immobilization strategies for protein biochips. *Biomacromolecules*, 8(6), pp.1775–1789.

Scanlon, S. & Aggeli, A., 2008. Self-assembling peptide nanotubes. *Nano Today*, 3(3-4), pp.22–30.

Shi, J., Claussen, J.C., McLamore, E.S., ul Haque, A., Jaroch, D., Diggs, A.R., Calvo-Marzal, P., Rickus, J.L. & Marshall Porterfield, D., 2011. A comparative study of enzyme immobilization strategies for multi-walled carbon nanotube glucose biosensors. *Nanotechnology*, 22(35), p.355502.

Vartiainen, J., Rättö, M. & Paulussen, S., 2005. Antimicrobial activity of glucose oxidase-immobilized plasma-activated polypropylene films. *Packaging Technology and Science*, 18(5), pp.243–251.

Williams, R.J., Mart, R.J. & Ulijn, R.V., 2010. Exploiting biocatalysis in peptide self-assembly. *Peptide Science*, 94(1), pp.107–117.

Wilson, R. & Turner, A.P.F., 1992. Glucose oxidase: An ideal enzyme. *Biosensors and Bioelectronics*, 7(3), pp.165–185.

Chapter Six

6 Summary and conclusions

6.1 Introduction

The aim of this research was to investigate amyloid fibrils as a nanoscaffold for the immobilisation of biomolecules with applications in biotechnology. This was achieved by immobilising a diverse range of biomolecules to insulin amyloid fibrils in solution, and subsequently characterising their immobilised forms. Insulin and crystallin amyloid fibrils were also assembled on the surface of glass beads, cotton, and microcrystalline cellulose, to increase their surface area. Active glass beads were then created by immobilising biomolecules to the surface assembled insulin amyloid fibrils on the glass beads.

With the advent of new technologies to create designer, stable enzymes (Quin & Schmidt-Dannert 2011), there is increasing interest in the industrial use of enzymes for a wide variety of applications. Enzymes are being pursued as a green chemistry alternative to traditional chemical catalysts, because they function in mild processing conditions such as low pressure, temperature, and aqueous media, whilst producing high yields, usually in a substrate specific, regio-specific, and stereo-specific manner. The use of enzymes in industrial settings is currently hampered by their instability outside of the cellular environment, and production costs. Immobilisation of enzymes has the ability to overcome these limitations by increasing their stability and reusability. As outlined in section 1.5.2, there are numerous immobilised enzymes currently in industrial use for the production of high value commodities. Immobilised enzymes also have uses in biosensing, for example, glucose oxidase is used to measure blood glucose concentration (Bankar *et al.* 2009), and chemical detoxification (Kanugula *et al.* 2011).

Recently there has been increased interest in utilising nanosupports to immobilise enzymes due to their large surface area, allowing for a higher specific activity, less diffusional resistance, and increases in stability by immobilisation on or in a support of similar dimensions to enzymes (Ansari & Husain 2012). Therefore, the potential uses of novel nanosupports such as amyloid fibrils have gathered interest. This is due their intrinsic ability to self-assemble, allowing a bottom-up approach to material design. They also have high surface to volume ratio, gained from their nanometre dimensions. Additionally, it is also possible to modify them with chemicals and biomolecules through amino acid side chain residues.

6.2 Characterisation of solution and surface assembled amyloid fibrils

Bovine insulin and crystallin amyloid fibrils were first formed in solution, and were found to have characteristic fibrillar morphology when viewed by TEM. The crystallin amyloid fibrils were ~6 nm wider, and considerably longer than the insulin amyloid fibrils. FITC was used to estimate the number of amino groups available for covalent biomolecule immobilisation on the bovine insulin amyloid fibrils. Bovine insulin has three amino groups for immobilisation of biomolecules. Derivitisation with FITC suggested ~1/3 of the amino groups in bovine insulin amyloid fibrils are available for biomolecule immobilisation. This result was subsequently used to ensure an excess of biomolecules was present in the immobilisation reaction to maximise immobilisation.

Insulin and crystallin amyloid fibrils were assembled on the surface of 5 mm glass beads. The surface assembly method used amyloid fragments as the template from which to assemble amyloid fibrils. By utilising fibril fragments instead of previously reported amyloid fibril seeds, a highly reproducible amyloid fibril surface assembly method was developed. This is the first time that crystallin amyloid fibrils have been assembled from a surface. Characterising the surface assembled crystallin amyloid fibrils by SEM revealed amyloid spherulite structures with a similar morphology to amyloid β fibril spherulites (Ban *et al.* 2006). Spherulites are thought to be a common architectural feature of amyloid fibrils (Ban *et al.* 2006), and this is the first observation of amyloid spherulite structure formation by crystallins on surfaces.

Insulin amyloid fibrils were assembled on the surface of cotton, and microcrystalline cellulose for the first time, and characterised by ThT and FTIR, respectively. The move from the model glass surface, to cellulose based materials represents a step towards realising the industrial potential of amyloid. Cellulose based materials are widely used in industry, and have been used in applications in which a range of enzymes have been immobilised to them. For example, lysozyme was recently immobilised on cotton to manufacture an antimicrobial material (Edwards *et al.* 2011). Surface assembly of amyloid fibrils could generate cellulose based materials with increased surface area allowing increased enzyme immobilisation, thus increasing the material's specific activity.

6.3 Immobilisation of biomolecules to solution amyloid fibrils

The biomolecules used for immobilisation ranged in size from ~27-175 kDa, and included a range of tertiary structures, monomeric and dimeric quaternary structures, and included a hydrolase, hydroxylase, oxido-reductase, a cysteine protease, and a fluorescent protein. By immobilising a diverse range of biomolecules, the generic versatility of amyloid fibrils as a nanoscaffold for biomolecule immobilisation was assessed.

OPH has potential applications in the decontamination and chemical detoxification of organophosphates such as VX, Sarin, Soman, and paraoxon (Mulchandani *et al.* 1998), but instability and productions costs inhibit its widespread use. Thus, OPH was covalently immobilised to insulin amyloid fibrils with GA. Immobilised OPH was shown to retain catalytic activity, and showed a ~300 % increase in relative thermostability at 40 and 50 °C. This result is promising for future implementation of OPH as a reusable immobilised biocatalyst. An example of an application of this technology could be in its use in a fixed bed reactor or filter, for the elimination of organophosphates from the environment, or in the creation of self protective materials, for decontamination in the event of a chemical attack.

Immobilisation of OPH was also attempted with the crystallin amyloid fibrils. It was predicted that more OPH would be immobilised due to increased length, and therefore larger surface-to-volume ratio. Methods to successfully immobilise OPH to the crystallin amyloid fibrils were not established, probably due to the glycosylation of the crystallins. Work is underway to develop new strategies to immobilise biomolecules on the crystallin amyloid fibril nanoscaffold. Two methods being investigated are the use of chemistry that is compatible with amino acids other than lysine residues, and the enzymatic deglycosylation of post-transcriptional modifications.

Collectively, cytochrome P450 enzymes catalyse a suite of chemical reactions, many of which are difficult to achieve by conventional chemical catalysis (Julsing *et al.* 2008). Like OPH, many cytochrome P450s are unstable outside their natural cellular environment, and therefore immobilisation has been used to increase their stability and reusability. $P450_{BM3}$ has been shown to have the greatest potential for industrial applications due to its catalytic self-sufficiency, affording it the highest known catalytic efficiency of the P450s; however, in the past it has proven difficult to immobilise. $P450_{BM3}$ was immobilised to insulin amyloid fibrils. Covalent immobilisation with GA was initially attempted, but the cross-linker was found to inactivate the enzyme, probably due to interaction with arginine 47. Physical adsorption was therefore used to immobilise $P450_{BM3}$. The physical interaction of $P450_{BM3}$ to the insulin amyloid fibrils was found to be very strong by native-PAGE and centrifugation experiments. However, the interaction with the amyloid fibrils caused an almost complete loss in enzymatic activity, possibly due to unfolding of the enzyme on the surface of the insulin amyloid fibrils. Further investigation is required to ascertain whether the lack of activity stems from unfavourable interactions of the enzyme or substrate/product with the nanoscaffold. Previous studies by Maurer *et al.* (2003) exhibited similar results, in that upon immobilisation of $P450_{BM3}$ to the anion exchanges DEAE and SuperQ, activity was lost.

GFP is extensively used in biochemistry and cell biology as a fluorescent reporter molecule for applications including: gene reporting, cell marking, and as a protein fusion tag (Tsien 1998). GFP was covalently immobilised to the insulin amyloid fibrils with GA to function as a fluorescent tag. GFP was shown to be immobilised to the insulin amyloid fibrils and retained fluorescence when characterised by native PAGE. This is the first time that GFP has been covalently immobilised to insulin amyloid fibrils, demonstrating a quick and convenient method for determining biomolecule immobilisation. GFP works well as a fluorescent tag because it does not rely on substrate binding for activity, but excitation at 495 nm. The lack of a chemical substrate enables functionality in non-natural conditions and it is therefore highly suited to immobilisation. GFP could be used to assess the immobilisation potential of other types of amyloid fibrils, allowing for optimisation of the immobilisation conditions by examining the degree of immobilised fluorescence. For example in the optimisation of biomolecule immobilisation to crystallin amyloid fibrils.

TEV protease in solution is a one-time use enzyme for poly-histidine tag cleavage that has low stability, and is therefore a good candidate for immobilisation. Initial GA immobilisation to the insulin amyloid fibrils showed the cross-linker inhibited TEV protease activity. Immobilisation to insulin amyloid fibrils therefore relied on physisorption. TEV protease displayed some physical interaction to the insulin amyloid fibrils as determined by native PAGE, and the immobilised TEV protease was shown to retain activity by cleaving a poly-histidine tag from his-tagged proteins. This is first time that TEV protease has been immobilised to insulin amyloid fibrils, or any protein based support, and represents a step in utilising this experimentally important protease in an immobilised form.

GOD is an industrially important enzyme with uses as a biosensor and antimicrobial agent. It is an extremely stable enzyme under a variety of conditions, thus is a typically used model enzyme for immobilisation. GOD was immobilised to insulin amyloid fibrils using GA, as previously described by Pilkington *et al.* (2010). The immobilised enzyme was shown to retain full activity. The immobilisation of GOD to the nanoscaffold in solution provided the framework for the immobilisation to the surface assembled amyloid fibril nanoscaffold.

By immobilising a range of biomolecules, insulin amyloid fibrils have been shown to be a versatile nanosupport that can impart significant increases in stability to some biomolecules. The degree of immobilisation, and retained activity differed between biomolecules. Whilst insulin amyloid fibrils proved to be a versatile nanoscaffold, individual biomolecule immobilisation needs optimisation to ensure activity post-immobilisation. Methods to immobilise biomolecules to crystallin amyloid fibrils were not established due to glycosylation. The immobilisation methods developed in this research can be used as a starting point for the immobilisation of any biomolecule to insulin, and possibly other types of amyloid fibrils for the creation of functional nanomaterials.

6.4 Creation of bionanomaterials with immobilised biomolecules

The successful assembly of bovine insulin amyloid fibrils on the surface of glass beads enabled immobilisation of GOD, GFP, and TEV protease. This method of first assembling the nanoscaffold on the surface of glass beads, followed by biomolecule immobilisation has not been investigated before. GOD was immobilised to the surface assembled insulin amyloid fibrils first, to establish immobilisation protocols for GFP and TEV protease. GOD was shown to be immobilised on the surface assembled insulin amyloid fibrils. The results of the experiments demonstrated that surface assembled insulin amyloid fibrils increased the surface area of the glass beads, enabling a small increase in net GOD activity. Only a small gain in immobilised GOD was observed due to the high non-specific binding of GOD to the unmodified glass surface. This could be improved by further optimisation of blocking and washing steps to help decrease the background non-specific adsorption.

GFP was successfully immobilised to surface assembled insulin amyloid using GA. The surface immobilised GFP samples were analysed for fluorescence in order to investigate the effect of the nanoscaffold on the surface of the glass beads. Fluorescence of the bead samples monitored in a plate reader showed that the glass beads with the surface assembled insulin amyloid fibrils had significantly more immobilised fluorescence. This result was also confirmed *via* quantitative imaging with CLSM. The images obtained by microscopy showed a reasonably complete surface coverage of the GFP functionalised surface assembled nanoscaffold. GFP was shown to be an excellent fluorescent tag for surface assembled amyloid fibrils, and in the future could be used in the optimisation of surface assembly of amyloid fibrils by enabling quantitative analysis of the amount of surface assembly.

TEV protease was successfully immobilised to surface assembled insulin amyloid fibrils by physical adsorption. The resulting functionalised glass beads successfully cleaved the poly-histidine tag of several proteins as efficiently as the solution TEV protease control cleavage reaction. This demonstrates that TEV protease is fully active when immobilised on the surface assembled insulin amyloid fibrils. Reusability testing of the surface immobilised TEV protease glass beads suggests this technology may provide a convenient and reusable protease system that may have commercial potential, as many labs utilise polyhistidine tags for recombinant protein purification. Testing additional TEV protease immobilisation conditions could yield increases in specific activity, whilst utilising micro beads with surface assembled amyloid fibrils in a fixed column could streamline protein purification.

This research has shown that insulin amyloid fibrils can act as a versatile nanoscaffold by increasing the surface area for biomolecule immobilisation. The intrinsic surface chemistry of the insulin amyloid fibrils enabled decoration with biomolecules by covalent and physical immobilisation. Functionalised surface assembled amyloid fibrils show promise as a novel nanosupport for the creation of functional bionanomaterials, for example, active surface coatings for the production of fine chemicals, chemical detoxification, or biosensing.

6.5 Future work

Due to their length and stability, crystallin amyloid fibrils may provide improved biomolecule immobilisation over insulin amyloid fibrils. Methods to optimise immobilisation of biomolecules to the crystallin amyloid fibrils are being actively explored. Deglycosylation of the crystallins may enable immobilisation chemistry to occur. This could be monitored using FITC binding. Amino acids other than lysine, for example cysteine, could be investigated as potential immobilisation targets.

Further optimisation of the surface assembly of amyloid fibrils to generate maximum surface coverage, and therefore overall surface area, could potentially enable for improved biomolecule immobilisation. The increases in surface coverage could be monitored by the immobilisation and subsequent quantification of GFP fluorescence.

Surface assembly and functionalisation of amyloid fibrils on other surfaces could lead to the creation of many new functional materials. For example, amyloid fibrils have been used as a nanocomposite and combining functional amyloid nanocomposites with functional surface assembled amyloid fibrils has the potential to produce highly active and unique materials.

6.6 References

Ansari, S.A. & Husain, Q., 2012. Potential applications of enzymes immobilized on/in nano materials: A review. *Biotechnology Advances*, 30(3), pp.512–523.

Ban, T., Morigaki, K., Yagi, H., Kawasaki, T., Kobayashi, A., Yuba, S., Naiki, H. & Goto, Y., 2006. Real-time and single fibril observation of the formation of amyloid β spherulitic structures. *Journal of Biological Chemistry*, 281(44), pp.33677–33683.

Bankar, S.B., Bule, M.V., Singhal, R.S. & Ananthanarayan, L., 2009. Glucose oxidase-an overview. *Biotechnology Advances*, 27(4), pp.489–501.

Edwards, J.V., Prevost, N.T., Condon, B. & French, A., 2011. Covalent attachment of lysozyme to cotton/cellulose materials: Protein verses solid support activation. *Cellulose*, 18(5), pp.1239–1249.

Julsing, M.K., Cornelissen, S., Bühler, B. & Schmid, A., 2008. Heme-iron oxygenases: Powerful industrial biocatalysts? *Current Opinion in Chemical Biology*, 12(2), pp.177–186.

Kanugula, A.K., Repalle, E.R., Pandey, J.P., Sripad, G., Mitra, C.K., Dubey, D.K. & Siddavattam, D., 2011. Immobilization of organophosphate hydrolase on biocompatible gelatin pads and its use in removal of organophosphate compounds and nerve agents. *Indian Journal of Biochemistry & Biophysics*, 48(1), pp.29–34.

Maurer, S.C., Schulze, H., Schmid, R.D. & Urlacher, V., 2003. Immobilisation of P 450 BM-3 and an NADP cofactor recycling system: Towards technical application of hemecontaining monooxygenases in fine chemical synthesis. *Advanced Synthesis & Catalysis*, 345(6-7), pp.802–810.

Mulchandani, A., Mulchandani, P. & Chen, W., 1998. Enzyme biosensor for determination of organophosphates. *Field Analytical Chemistry and Technology*, 2(6), pp.363–369.

Pilkington, S.M., Roberts, S.J., Meade, S.J. & Gerrard, J.A., 2010. Amyloid fibrils as a nanoscaffold for enzyme immobilization. *Biotechnology Progress*, 26(1), pp.93–100.

Quin, M.B. & Schmidt-Dannert, C., 2011. Engineering of biocatalysts: From evolution to creation. *Catalysis*, 1(9), pp.1017–1021.

Tsien, R.Y., 1998. The green fluorescent protein. *Annual review of biochemistry*, 67(1), pp.509–544.

Chapter Seven

7 Experimental

7.1 **Materials**

Unless otherwise stated, chemicals were purchased from Sigma-Aldrich or Invitrogen. Barracuda were purchased from the Lyttelton fish market, Christchurch, New Zealand.

7.2 **Biochemistry general methods**

Unless otherwise stated, enzymes were manipulated on ice or at 4 °C. pH measurements were made using a Denver Instrument Ultra Basic 10 benchtop meter fitted with a high performance tris electrode.

Centrifugation was performed in an Eppendorf 5810R on a small scale (< 2 mL) using an F-45-30-11. For medium and large scale centrifugation a Thermo Scientific Sorvall RC6 plus centrifuge was used with either a SS-34 or FiberLite F10-6x500y rotor, respectively.

Polyacrylamide gel electrophoresis was routinely run using a NuPAGE system from Invitrogen. Enzymes assays used an Agilent 8453 UV-visible spectrophotometer fitted with a circulating water bath, a Varian Cary 100 UV-vis spectrophotometer fitted with a Peltier temperature controller and a Peltier thermostattable multicell holder, or a Labtech FLUOstar OPTIMA plate reader.

7.2.1 **Standard Bradford assay for determining protein concentration**

This assay is based on the Bradford dye-binding procedure (Bradford 1976), and uses the Bio-Rad protein assay reagent. 800 µL of appropriately diluted protein solution was added to 200 µL of Bio-Rad protein assay reagent, mixed thoroughly and incubated at room temperature for 5 min exactly. The absorbance of the solutions was measured at 595 nm against a blank consisting of 800 µL of H_2O and 200 µL of Bio-Rad protein assay reagent. Protein concentrations were calculated from a standard curve prepared using BSA.

7.2.2 **NanoDrop protein determination**

Three µL of protein solution was pipetted onto a Thermo Fisher Scientific NanoDrop 1000 after being blanked against the appropriate buffer. Absorbance measurements were carried out at in triplicate at 280 nm. Proteins absorb light at 280 nm due to aromatic amino acids, such as tryptophan and tyrosine. The number of aromatic residues in a protein's sequence gives rise to the extinction coefficient of a protein, which was predicted using the web-based program "ExPASy" (Gasteiger *et al.* 2003). Using Beer's law, the known extinction coefficient, and the absorbance of the solution, the concentration of protein can be calculated.

7.2.3 **Sodium dodecyl sulfate polyacrylamide gel electrophoresis**

Electrophoresis tank buffer	50 mM MOPS
Coomassie Blue stain	1 % w/v Coomassie blue
	50 % v/v methanol
	10 % v/v glacial acetic acid
Destain	5 % v/v methanol
	10 % v/v glacial acetic acid
Sample buffer	Invitrogen NuPAGE® LDS Sample Buffer (4x)
Reducing agent	Invitrogen NuPAGE® Reducing Agent (10x)

Regular analysis of protein samples used precast Invitrogen NuPAGE® 4-12 % Bis-tris gels with 10, 1.0 mm wide wells. Samples were mixed with sample buffer and reducing agent to give a total of ~5 ng/μL of protein. Samples were then incubated at 90 °C for 4 min and then briefly centrifuged before being loaded into the gel. An Invitrogen Novex Sharp pre-stained protein standard was also loaded into the gel. Electrophoresis was carried out at room temperature at a constant voltage of 200 V for ~50 min. The gel was then immersed in stain and microwaved for ~30 sec before standing on a Bio-Rad Ultra Rocker for 10 min. The gel was then immersed in destain and microwaved for 1 min before the addition of 1 piece of tissue paper and place on the Bio-Rad Ultra Rocker until appropriately destained. The gel was viewed and photographed using a SYNGENE GelDoc.

7.2.4 **Native polyacrylamide gel electrophoresis**

Electrophoresis tank buffer	250 mM tris.base
	1.92 M glycine
Coomassie Blue stain	1 % w/v Coomassie blue
	50 % v/v methanol
	10 % v/v glacial acetic acid
Destain	5 % v/v methanol
	10 % v/v glacial acetic acid
Sample buffer (2x)	126 mM tris.HCl
	20 % glycerol
	0.005 % bromophenol blue

Regular analysis of protein samples used precast Invitrogen Novex® 10 % tris-glycine gels with 10, 1.5 mm wide wells. Samples were mixed with sample buffer and dH_2O to give a total of ~5 ng/µL of protein. Samples were then loaded into a 4 °C gel. Electrophoresis was carried out at 4 °C at a constant voltage of 135 V for ~120 min. The gel was then immersed in stain and microwaved for ~30 sec before standing on a Bio-Rad Ultra Rocker for 10 min. The gel was then immersed in destain and microwaved for 1 min before the addition of 1 piece of tissue paper and place on the Bio-Rad Ultra Rocker until appropriately destained. The gel was viewed and photographed using a SYNGENE GelDoc.

7.2.5 **Buffer exchange of proteins**

Desalting of proteins into the required buffers was routinely carried out using either a 5 mL HiTrap™ Desalting column or 12000 MWCO dialysis tubing stored in 0.1 % sodium azide. When using the desalting column, the column was first equilibrated with 4 column volumes of the desired buffer before loading of the sample. The sample was then eluted with desired buffer and fractions collected. The fractions containing the protein were then pooled. When using the dialysis tubing, the tubing was first thoroughly washed with dH_2O before the sample was placed in the tubing. The tubing was then placed in ~2 L of the desired buffer and left gently stirring at 4 °C over night.

7.2.6 **Sonication of cultured cells**

Cell disruption used a Sonics Vibracell Model CV33. The total running time was 5 min with the amplitude set at 100 %. The pulse was set for 3.0 sec on and 9.9 sec off. All samples were sonicated in a cooling bath of iced water.

7.2.7 **Differential scanning fluorimetry (DSF)**

Based on methods developed by Ericsson *et al.* (2006), protein melting temperature was investigated using a Bio-Rad® iQ5 real-time PCR machine. 80 µL of 0.5 mg/mL protein sample was mixed with 20 µL of 50x SYPRO® Orange dye. 25 µL of this protein/dye mix was placed into a 96-well thin-wall PCR plate (Bio-Rad) with triplicates of each sample being used. The plate was sealed with a Bio-Rad® Microseal® 'B' Film and heated from 20 °C to 80 °C in 0.5 °C increments with a dwell time of 10 seconds. The excitation and emission wavelengths were 490 and 575 nm, respectively. The melting temperature was determined as the point of maximum inflection of the -*d*RFU/*d*T curve.

7.2.8 **Plate reader Thioflavin T (ThT) assay**

ThT (2.5 mM) was made up in ThT buffer containing 50 mM tris-base, 100 mM NaCl, pH 7.5. This was filtered and stored in the dark for up to a maximum of two days. ThT fluorescence was measured using a BMG Labtech FLUOstar Optima plate reader with excitation/emission filters of 450 and 485 nm, respectively (LeVine III 1999). Samples had a total volume of 200 µL containing 25 µM ThT. Three replicates of each sample were measured.

7.2.9 **Surface Thioflavin T (ThT) assay**

Cotton samples were first immersed in a solution of 25 µM ThT in 50 mM tris-Base, 100 mM NaCl, pH 7.5 for 5 min before being rinsed 3 times in dH_2O. The cotton samples were then placed between two microscope cover slips and sellotaped together. The sample was then mounted on the sample holder with only the centre of the sample been viewed. ThT fluorescence was measured using a Fluorolog-3 spectrophotometer, model FL3-22, Horiba Jobin Yvon with 2 nm slits at an excitation of 450 nm with emission from 460-600 nm.

7.2.10 **Fourier transform infrared spectroscopy (FTIR)**

FTIR used a PerkinElmer® Spectrum One FT-IR spectrophotomer with diffuse reflectance sampling. Background measurements containing dry KBr only were used to blank the machine. Each sample was scanned 40 times at a resolution of 4 cm^{-1}. All samples were dried at 37 °C for at least 2 days before been analysed. Cotton samples were finely cut up and ground with KBr and placed in the sample holder. Cellulose powder was mixed with dry KBr and ground before being placed in the sample holder. Data were analysed using Spekwin32 (Menges 2010).

7.2.11 **Transmission electron microscopy (TEM)**

Insulin and crystallin amyloid fibrils (1.45 mg/mL) were negatively stained with filtered 1 % uranyl acetate on Formvar-coated copper grids (200 mesh) and washed twice with nanopure H_2O based on the method of Whittingham *et al.* (2002). Samples were viewed at 89,000 x magnification on a Morgagni 268D TEM (FEI Company, Oregon, USA) operating at 80 kV, fitted with a 40 μm objective aperture. Micrographs were representative of 3 images chosen as being an overall representation of the entire sample. Images were analysed using ImageTool (Wilcox *et al.* 2002).

7.2.12 **Scanning transmission electron microscopy (SEM)**

Air dried samples were first prepared by high vacuum evaporation with gold. The samples were then viewed using a JEOL JSM-7000F high resolution field emission scanning electron microscope.

7.2.13 **Confocal laser scanning microscopy**

Beads were mounted in small Petri dishes and viewed using a Leica Microsystems TCS SP5 confocal microscope with a Leica HCX PL 10x lens. An excitation of 488 nm and emission detection of 509 nm was used. The gain was adjusted to suit the most fluorescent sample and kept the same for all subsequent samples.

7.2.14 **Quantitative confocal Imaging**

Firstly, the confocal microscope gain was set to a level where the brightest sample was not being overexposed (section 7.2.13), then all the samples were imaged (Piston *et al.* 1998). The mean pixel value for each image was assessed using the Leica LAS AF Lite 2.4.1 software. The samples were always measured in triplicate.

7.2.15 **Circular dichroism spectroscopy**

CD spectra were recorded on a Jasco J-815 spectrophotomer in 20 mM phosphate buffer, pH 8.0 in a 2 mm pathlength quartz cell. The slit bandwidth used was 1 nm with a step size of 0.5 nm.

7.2.16 **Size exclusion chromatography**

Gel-filtration was performed using a pre-packed HiLoad Superdex 16/60 column (GE healthcare) connected to a UPC-900 ÄKTA FPLC from GE healthcare at 4 °C. The column was pre-equilibrated with 20 mM tris.HCl, 150 nM NaCl, pH 8.0. and samples were run on the column and collected.

7.3 **Molecular biology methods**

The pMAL-c2x/S5 and wild-type organophosphate hydrolase plasmids were a kind gift from Dan Tawfik, Weizmann Institute. The CYP450BM3 plasmid was a kind gift from Vlada Urlacher, Institute of Technical Biochemistry, University of Stuttgart. The *E. coli* DH5α eGFP containing bacterium was a kind gift from Arvind Varsani, University of Canterbury.

7.3.1 **Bacterial strains**

Three bacterial strains obtained from laboratory stocks were routinely used in this study:

- *E. coli* XL-1 Blue (genotype – recA1, endA1, gyrA96, thi-1, hsdR17, supE44, relA1, lac)
- *E. coli* BL21 (DE3) star (F-, ompT, hsdS_B, ($r_B^-m_B^-$), gal, dcm, rne131).
- *E. coli* DH5α (fhuA2 Δ(argF-lacZ)U169 phoA glnV44 Φ80 Δ(lacZ)M15 gyrA96 recA1 relA1 endA1 thi-1 hsdR17).

7.3.2 **Plasmid preparation by alkaline lysis**

Solution 1	50 mM glucose, 25 mM tris-HCl pH 8.0, 10 mM EDTA
Solution 2	1 % (w/v) SDS, 0.2 M NaOH
Solution 3	5 M potassium acetate, 11.5 % (v/v) glacial acetic acid

Plasmid preparation was based on the methods of Sambrook *et al.* (1989). 1.5 mL of an overnight culture produced from a single colony was placed in an Eppendorf tube, centrifuged (10000 rpm, 5 min, 4 °C), and the supernatant removed by aspiration. The pellet was resuspended in 300 µL solution 1 *via* vortexing and chilled on ice. After 5 min, 300 µL of solution 2 was added, mixed by gentle inversion, and chilled on ice. After 10 min, 300 µL of solution 3 was then added, mixed by gentle inversion until a white precipitate formed, and chilled on ice. The preparation was then centrifuged (10000 rpm, 5 min, 4 °C), the supernatant carefully transferred to a clean Eppendorf tube, and the pellets discarded.

The DNA was precipitated by addition of 650 µL isopropanol, mixed by inversion, and allowed to stand at room temperature for 2 min. After centrifugation (10000 rpm, 5 min, 4 °C) and discarding the supernatant, the pellet was rinsed with 1 mL 70 % ethanol, centrifuged (10000 rpm, 2 min, 4 °C), and the supernatant discarded. The pellet was allowed to dry for at least 10 mins, before resuspension in 80 µL dH_2O, and left at 37 °C for 30 min. The plasmids were identified by restriction digest (section 7.3.3) with agarose gel electrophoresis (section 7.3.10), and concentration determined at 280 nm by NanoDrop (section 7.2.2).

7.3.3 **Restriction digests of plasmids**

Restriction digests were performed in 10 µL volumes. Typically, ~1 µg of plasmid DNA (2.5 to 5 µL) was digested with the appropriate restriction enzyme and corresponding restriction buffer. Restriction products were then analysed by agarose gel electrophoresis (section 7.3.10).

7.3.4 **Transformation of *E. coli* XL-1 Blue**

The transformation protocol was based on the Stratagene XL-1 Blue competent cell manual (Stratagene 2004). A 100 μL aliquot of *E. coli* XL-1 Blue competent cells was thawed on ice, and 1 μL of DNA was added and incubated on ice for 30 min. The cells were then heat shocked at 42 °C for 45 seconds, and incubated on ice for 2 min. 900 μL of preheated (37 °C) SOC medium was added to the tube and incubated at 37 °C with shaking at 200 rpm for 1 hour. Less than or equal to 200 μL of the transformation mixture was then plated on LB agar containing the appropriate antibiotics (section 7.3.7). From these plates, 5-10 potential transformant colonies were selected and grown in 10 mL LB cultures containing the appropriate antibiotic and a glycerol stock culture was made and stored at -80 °C (section 7.3.9).

7.3.5 **Transformation of *E. coli* BL21 (DE3) Star**

The transformation protocol was based on the Stratagene BL21 (DE3) Star competent cell manual (Stratagene 2010). A 100 μL aliquot of *E. coli* BL21 (DE3) Star competent cells was thawed on ice, and 1 μL of DNA was added and incubated on ice for 30 min. The cells were then heat shocked at 42 °C for 45 seconds, and incubated on ice for 2 min. Preheated (37 °C) SOC (900 μL) medium was added to the tube and incubated at 37 °C with shaking at 200 rpm for 1 hour. ≤ 200 μL of the transformation mixture was then plated on LB agar containing the appropriate antibiotics (section 7.3.7). From these plates, 5-10 potential transformant colonies were selected and grown in 10 mL LB cultures containing the appropriate antibiotic and a glycerol stock culture was made and stored at -80 °C (section 7.3.9).

7.3.6 **Antibiotics**

Stock solutions of antibiotics were prepared and used at the appropriate concentrations as defined in **Table 7.1**. Stock solutions were made with the appropriate solvent, sterilised by passing through a 0.2 μm filter, and stored at -20 °C.

Table 7.1 *Antibiotic concentrations used for bacterial selection*

Antibiotic	Abbreviation	Solvent	[Stock] mg/mL	[Working] µg/mL
Ampicillin	Amp	dH_2O	100	100
Chloramphenicol	Cam	EtOH	30	30
Kanamycin	Kan	dH_2O	30	30

7.3.7 **Media and plate preparation**

Luria-Bertani medium (LB)

LB base was supplied in powered form. LB base (20 g) was added to 1 L of water, the pH was adjusted to 7.0 by the addition of NaOH, and the medium autoclaved.

ZYM-5052 auto-induction medium

The manufacture of ZYM-5052 media was based on the methods developed by Studier (2005). Tryptone (10 g) and 5 g yeast extract were added to 960 mL of water and autoclaved. After autoclaving, 20 mL 50 x 5052 stock (25 % glycerol, 2.5 % glucose, and 10 % lactose), 20 mL 50 x M stock (1.25 M Na_2HPO_4, 1.25 M KH_2PO_4, 2.5 M NH_4Cl, and 0.25 M Na_2SO_4), 1 mL 2 M $MgSO_4$, 200 µL trace metals (50 mM $FeCl_2$, 20 mM $CaCl_2$, 10 mM each of $MnCl_2$ and $ZnSO_4$, 2 mM each of $CoCl_2$, $CuCl_2$, $NiCl_2$, $NaMoO_4$, Na_2SeO_3, H_3BO_3 in ~60 mM HCl) solution and 1 mL antibiotics were added to give a final concentration of either 30 µg/mL kan or 100 µg/mL amp were added.

Super optimal broth (SOB) medium

To prepare SOB, 10 g tryptone, 2.5 yeast extract, and 0.25 g NaCl were dissolved in 480 mL dH_2O. Ten millilitres of 250 mM KCl was added and the solution pH adjusted to 7.0 with concentrated NaOH. The SOB was aliquoted and autoclaved. One molar glucose was added under sterile conditions just prior to use, giving a final concentration of 20 mM.

Agar plate preparation

LB base (20 g/L) and 15 g/L agar were added to water and autoclaved. This was stored at room temperature until required. The LB agar was melted in the microwave (~2 min for 100 mL) and allowed to cool to ~50 °C before being supplemented with antibiotics (30 μg/mL kan or 100 μg/mL amp), and poured into sterile Petri dishes in a biohazard flow hood. The plates were allowed to cool before use. Plates were stored sealed at 4 °C for up to 4 weeks.

7.3.8 **Bacterial cultures**

All equipment and media used for the culture of bacteria were sterilised by autoclaving at 121 °C for 20 min. Standard aseptic technique was maintained throughout the manipulation of bacterial cultures.

Agar plates containing appropriate selective antibiotics were streaked with a bacterial strain from a glycerol freezer stock, or a fresh single colony, using a flame-sterilised wire loop. The plates were incubated at 37 °C for ~12 hours, and a single colony selected using a flame-sterilised wire loop to inoculate a 10 mL culture medium containing appropriate selective antibiotics. These starter cultures were grown overnight at 37 °C, with shaking at 200 rpm, and subsequently used to inoculate larger cultures.

7.3.9 **Bacterial strain storage**

Glycerol freezer stocks were used to store all bacterial strains. The stocks were prepared by mixing 700 μL of an overnight culture grown from a single colony, with 300 μL of 50 % sterile glycerol in a sterile 1.5 mL screw-top cryo-storage tube, to give a final concentration of 15 % glycerol. The prepared glycerol stocks were then stored at -80 °C.

7.3.10 **Agarose gel electrophoresis**

Loading dye	Bioline Crystal 5x DNA loading buffer
TAE buffer	40 mM tris-acetate pH 8.0, 1 mM EDTA
Ladder	Bioline Hyperladder™

One % w/v agarose was mixed with 40 mL of TAE buffer and microwaved for 1 min. The agarose was left to cool to ~50 °C before 3 μL of 10000x concentrate Invitrogen SYBR® Safe DNA gel stain was added and poured into a gel casting tray. The gel was allowed to set for ~30 min before the well comb was removed and the casting tray transferred to a gel tank containing TAE buffer. The DNA samples in loading dye and the DNA ladder were then loaded. Electrophoresis was performed at 120 V for ~1 hour and visualised under UV light using a SYNGENE GelDoc.

7.4 **Overexpression and purification organophosphate hydrolase**

Lysis buffer	50 mM tris pH 8.5, 10 mM $NaHCO_3$, 5 mM $ZnCl_2$
Column buffer 1	50 mM tris pH 8.0, 0.25 M NaCl
Column buffer 2	50 mM tris pH 8.0, 0.25 M NaCl, 10 mM maltose

7.4.1 **Growth of *E. coli* BL21(DE3) star-pMAL-c2x/S5**

Plasmid pMAL-c2x/S5 was transformed into *E. coli* BL21 (DE3) star competent cells (section 7.3.5) for protein overexpression. The transformed cells where then used to inoculate solid LB-agar plates containing 100 μg/mL amp, which were grown overnight at 37 ºC.

A single colony was used to inoculate a 10 mL LB culture containing 100 μg/mL amp and grown overnight at 37 ºC, with shaking, at 250 rpm. 1 mL of the overnight culture was then used to inoculate 1 L of ZYM-5052 auto-induction media containing 100 μg/mL amp (Studier 2005). This was grown, with shaking, at 250 rpm at 37 ºC for 4 hours and then overnight at 30 ºC.

7.4.2 **Cell disruption and protein purification**

Protein purification took advantage of the C-terminal maltose binding protein as previously described Roodveldt & Tawfik (2005). Cells were harvested by centrifugation, resuspended in lysis buffer and disrupted by sonication (section 7.2.6). The cellular debris was centrifuged and the supernatant was passed through an amylose column (BioLabs®) equilibrated with column buffer 1, and the column subsequently washed with 5 column volumes of the same buffer. The fusion protein was eluted with column buffer 2, and fractions containing protein as evaluated with Bio-Rad protein assay reagent, were pooled.

The purified protein was then desalted (section 7.2.5) into the desired buffer containing either, 100 mM sodium phosphate, pH 8.0, or 100 mM HEPES pH 7, 8 or 9. The protein was purified to homogeneity with a band of expected size, ~76 kDa, as judged by SDS-PAGE (section 7.2.3). The concentration of the purified protein was verified using a NanoDrop ND1000 spectrometer (section 7.2.2), using an extinction coefficient of 0.8462. The yield for each purification was ~100 mg per litre of culture.

7.4.3 **Maltose binding protein cleavage**

Cleavage of the maltose binding protein from the OPH-MBP fusion protein exploited the serine protease cleavage site located between the MBP and the OPH. Factor Xa (Novagen®), a serine protease was added to the fusion protein at a concentration of one unit Factor Xa to 50 μg OPH-MBP fusion protein and incubated overnight at 4 ºC. Following cleavage, OPH was separated from MBP *via* an amylose column. Factor Xa was captured using Xarrest™ Agarose at a concentration of 100 μL (50 % slurry) resin per 4 U of enzyme. Non-cleaved and cleaved samples were analyzed using SDS-PAGE to verify cleavage had occurred, with cleaved mixtures showing the expected bands of 35 and 42 kDa for the OPH and MBP, respectively.

7.4.4 **OPH temperature stability assay**

OPH in either pH 7, 8, or 9, 100 mM HEPES underwent the immobilisation reaction (sections 7.11.1 and 7.11.2), and were diluted 1:50 in paraoxon assay buffer containing 5 mM $ZnCl_2$ for 1 hour to saturate the sample with zinc ions, known to be required for OPH activity (Vanhooke *et al.* 1996). Samples were incubated in temperature-controlled water baths for the appropriate time. The temperatures used were 30, 40, 45, and 50 °C. After preliminary range finding experiments, at 30 °C, readings were taken at time 0, 3, 5, and 7 days; at 40 °C, readings were taken at time 0, 2, 4, and 6 hours; at 45 °C, readings were taken at time 0, 5, 20, and 120 min; and at 50 °C, readings were taken at time 0, 20, 40, and 60 min. Samples were then stored on ice before testing the activity using the paraoxon assay. An initial activity reading was taken for each sample and this was used as the 100 % value. Subsequent activity readings were measured as a percentage of the initial reading.

7.5 **Overexpression and purification of cytochrome P450 BM3**

Buffer A	20 mM sodium phosphate pH 8.0, 0.5 M NaCl, 30 mM imidazole
Buffer B	20 mM sodium phosphate pH 8.0, 0.5 M NaCl, 300 mM imidazole

7.5.1 **Growth of *E. coli* BL21 (DE3) star-pET28-BM3**

Plasmid pET28-BM3 was transformed into *E. coli* BL21 (DE3) star competent cells for protein overexpression. The transformed cells were then used to inoculate solid LB-agar plates containing 30 μg/mL kan, which were grown overnight at 37 ºC. A single colony was used to inoculate a 10 mL LB broth containing 30 μg/mL kan and grown overnight at 37 ºC, with shaking, at 250 rpm. One millilitre of the overnight culture was then used to inoculate 1 L of ZYM-5052 auto-induction media containing 30 μg/mL kan (Studier 2005). This was grown, with shaking, at 250 rpm at 37 ºC for 4 hours then overnight at 30 ºC.

7.5.2 **Cell disruption and protein purification**

Protein purification took advantage of the N-terminal poly-6-histidine tag as previously described Pflug *et al.* (2007). Cells were harvested by centrifugation, resuspended in buffer A, and disrupted by sonication (section 7.2.6). The cellular debris was centrifuged and the supernatant was passed through a 5 mL HisTrap™ Fast Flow column previously equilibrated with buffer A. The column was then washed with 5 column volumes of buffer A. The protein was eluted with buffer B, and the fractions containing protein pooled, as determined by Bio-Rad protein assay reagent. The purified protein was then desalted (section 7.2.5) into 100 mM HEPES pH 8. The protein was purified to homogeneity with a band of expected size, ~119 kDa, as judged by SDS-PAGE (section 7.2.3). The concentration of the purified protein was verified using a NanoDrop ND1000 spectrometer (section 7.2.2), using an extinction coefficient of 1. The yield for each purification was ~40 mg per litre of culture.

7.6 **Overexpression and purification of enhanced green fluorescent protein**

Buffer A	50 mM tris pH 7.0
Buffer B	50 mM tris, 1 M NaCl pH 7.0

7.6.1 **Growth of *E. coli* DH5α eGFP**

The growth and purification of GFP was based around the methods of Yang *et al.* (1996). The *E. coli* DH5α bacterium routinely showed good eGFP protein expression levels therefore this bacterial strain was used for protein expression. 1 mL of culture containing *E. coli* DH5α eGFP was transferred to 1 L of LB media containing 100 μg/mL amp. This was grown overnight at 30 °C, with shaking at 250 rpm.

7.6.2 **Cell disruption and protein purification**

Cells were harvested by centrifugation, resuspended in buffer A and disrupted by sonication (section 7.2.6). The cellular debris was centrifuged and the supernatant was passed over a Superdex 16/10 high performance ion exchange column equilibrated with buffer A. The column was subsequently washed with 10 column volumes of buffer A. The proteins were eluted using a gradient of 0-100 % of buffer B over 35 min running at 2.5 mL/min. The fractions which fluoresced under UV light were pooled. The GFP was then buffer exchanged into 50 mM sodium phosphate pH 8.0 (section 7.2.5). The protein concentration was determined using the 96 well plate reader by using ε_{488} = 55000 $M^{-1}cm^{-1}$. The yield for each purification was ~7 mg per litre of culture.

7.7 **Overexpression and purification of tobacco etch virus protease**

Buffer A	50 mM sodium phosphate, 100 mM NaCl, 10 % glycerol, 25 mM imidazole, pH 8.0
Buffer B	50 mM sodium phosphate, 100 mM NaCl, 10 % glycerol, 200 mM imidazole, pH 8.0
Storage buffer	25 mM sodium phosphate, pH 8.0, 200 mM NaCl, 10 % glycerol, 2 mM EDTA, 10 mM DTT

7.7.1 **Growth of E. *coli* BL21-RIL pRK793**

The growth and purification of TEV MBP-His_7-pR_5 was based around the methods of Blommel & Fox (2007). One loop of culture was taken from the -80 °C glycerol stock culture, plated on a solid LB-agar plate containing 100 μg/mL amp and 30 μg/mL cam and grown overnight at 37 °C. A single colony was used to inoculate a 10 mL LB culture containing 100 μg/mL amp and 30 μg/mL cam and grown overnight at 37 ºC, with shaking, at 250 rpm. One millilitre of the overnight culture was then used to inoculate 1 L of ZYM-5052 auto-induction media containing 100 μg/mL amp and 30 μg/mL cam (Studier 2005). This was grown, with shaking, at 250 rpm at 37 ºC for 5 hours and then overnight at 26 ºC.

7.7.2 **Cell disruption and protein purification of BL21-RIL pRK793 MBP-His_7-pR_5**

Protein purification took advantage of the N-terminal poly-7-histidine tag. Cells were harvested by centrifugation, resuspended in buffer A and disrupted by sonication (section 7.2.6). The cellular debris was centrifuged and the supernatant was passed through a 5 mL HisTrap™ Fast Flow column equilibrated with buffer A. The column was then washed with 5 column volumes of buffer A. The protein was eluted with buffer B, the fractions containing protein as determined by Bio-Rad protein assay reagent. The pooled fractions were then allowed to stand at 4 °C for 2 hours to allow the self-cleavage of the N-terminal MBP. The protein was then diluted 10x with buffer A to lower the imidazole concentration. The diluted protein was then reapplied to the His column which had been equilibrated with buffer A. The column was washed with 5 column volumes of buffer A to wash the cleaved MBP. The protein was then eluted with buffer B, and the fractions containing protein as judged by Bio-Rad protein assay reagent, were pooled, and EDTA and DTT added to a final concentration of 1 mM. The purified protein was then desalted (section 7.2.5) into storage buffer, flash frozen with liquid nitrogen and stored at -80 ºC. The protein was purified to homogeneity with a band of expected size, ~28 kDa, as judged by SDS-PAGE (section 7.2.3). The concentration of the purified protein was verified using the standard Bradford method (section 7.2.1). The yield for each purification was ~10 mg per litre of culture.

7.8 **Glucose oxidase**

Lyophilised powdered (~75 %) GOD was purchased from Sigma-Aldrich. The powder contained 136000 U/g where 1 U will oxidise 1.0 μM of β-D-glucose to D-gluconolactone and H_2O_2 per min at pH 5.1 at 35 °C, equivalent to an O_2 uptake of 22.4 μL per min.

7.9 Enzymatic activity assays

7.9.1 OPH paraoxon assay

OPH initial rates assays were based on the methods of McLoughlin *et al.* (2005). Initial rates were calculated by monitoring the release of *p*-nitrophenol at 405 nm from the substrate paraoxon using an Agilent 8453 UV-visible spectrophotometer. Assays (1 mL) contained 100 mM MOPS, pH 7.0, 1 % MeOH, 0.1 mM paraoxon, and a final concentration of ~0.38 μg/mL OPH. Assays were initiated by the addition of paraoxon and kept at a constant temperature of 30 °C using a circulating water bath. All assays were repeated in triplicate and typically had an error of less than 5 % calculated using the standard deviation of the mean.

7.9.2 $CYP450_{BM3}$ sodium laurate assay

NADPH-dependent sodium laurate oxidation was based on the methods of (Munro *et al.* 1995). Initial rates were calculated by monitoring the decrease in NADPH at 340 nm. Assays (1 mL) contained 20 mM MOPS, 100 mM KCl, pH 7.4, 0.5 mM sodium laurate, 0.2 mM NADPH and a final concentration of ~5 μg/mL $P450_{BM3}$. Assays were initiated by the addition of sodium laurate and kept at a constant temperature of 30 °C using a circulating water bath. All assays were repeated in triplicate and typically had an error of less than 5 % calculated using the standard deviation of the mean.

7.9.3 **GOD Amplex red assay**

GOD activity was measure using an Amplex red assay from Invitrogen. The method was based on the method from Invitrogen (2006). In this coupled assay glucose oxidase reacts with D-glucose to form D-gluconolactone and H_2O_2. Because horseradish peroxidase (HRP) is also present in the reaction mixture, the H_2O_2 can then react with the Amplex red reagent in a 1:1 stoichiometry generating the fluorescent oxidation product resorufine. Samples for the assay contained 20 μM Amplex Red, 0.04 U HRP and 20 mM D-glucose in 50 mM sodium phosphate pH 7.4 buffer and were incubated for 4 min before fluorescence measurement. Fluorescence was measured with a Labtech FLUOstar OPTIMA plate reader using excitation at 560-10 nm and fluorescence detection at 590 nm with the gain set at 880.

7.10 **Amyloid fibril formation**

Bovine insulin obtained from Sigma-Aldrich, and barracuda crystallin proteins were used for the formation of amyloid fibrils.

7.10.1 **Insulin amyloid fibril formation**

Insulin amyloid fibrils were formed using in-house methods modified from Nielsen *et al.* (2001). Bovine insulin dissolved at a concentration of 5.8 mg/mL (1 mM) in amyloid fibril incubation buffer containing 25 mM HCl, 100 mM NaCl, pH 1.6. The insulin solution was then incubated at 60 ºC for at least 24 hours. Formation of insulin amyloid fibrils was assessed by the ThT assay and TEM (sections 7.2.8 and 7.2.11).

7.10.2 **Insulin fragment formation**

Bovine insulin amyloid fibrils were formed at 1 mg/mL (section 7.10.1). The mature amyloid fibrils were then frozen overnight to create amyloid fibril fragments. TEM (section 7.2.11) was used to confirm that fragments had been successfully produced. The fibril fragments were thawed, centrifuged at 14500 rpm using an Eppendorf MiniSpin plus centrifuge and resuspended in 50 mM HEPES pH 9.

7.10.3 **Insulin seed formation**

Bovine insulin (1 mg/mL) was incubated at 60 °C for 80 min. The sample was then tested for ThT fluorescence (section 7.2.8) to ensure amyloid formation had not occurred. The seeds were then dialysed (section 7.2.5) for ~ 15 hours into 50 mM HEPES pH 9.

7.10.4 **Fluorescein isothiocyanate immobilisation**

Fluorescein isothiocyanate (FITC) was dissolved in 100 mM HCO_3^- pH 9.0 at a concentration of 2.6 mM. 1 mg/mL insulin amyloid fibrils (section 7.10.1) were centrifuged, the supernatant discarded and replaced with 1 mL of FITC solution and incubated for 1 hour at 25 °C. The solution was then centrifuged, the pellet washed and resuspended in FITC buffer, followed by centrifugation at 14500 rpm using an Eppendorf MiniSpin plus centrifuge. The washing steps were done five times. The FITC concentration was then estimated using ε_{494} = 68000 $M^{-1}cm^{-1}$ at an emission wavelength of 525 nm.

7.10.5 **Crystallin amyloid fibril formation**

Crystallin amyloid fibrils were formed using in-house methods modified from Garvey *et al.* (2009). Crystallin proteins were extracted from barracuda eye lenses in a buffer containing 50 mM tris, pH 7.5, 1 mM DTT and 5 mM EDTA, using an IKA® Ultra Turrax® Tube disperser with Tube ST-20. After homogenisation was complete, the sample was centrifuged for 30 minutes at 12000 x *g*, the supernatant collected and protein concentration estimated using the NanoDrop (section 7.2.2) with an extinction coefficient of 1. Crude crystallin proteins were diluted to 5.8 mg/mL in preheated to 80 ºC, 10 % trifluoroethanol, pH 4 and then incubated at 80 ºC for 1 hour. The sample was then centrifuged at 12000 x *g* for 10 min and the supernatant collected and heated overnight at 80 ºC. The sample was then left at room temperature for at least two days for the amyloid fibrils to assemble. The samples were then analysed for amyloid fibrils using TEM (section 7.2.11).

7.10.6 **Crystallin amyloid fragment formation**

Formed crystallin amyloid fibrils (section 7.10.5) were first centrifuged and then buffer exchanged into 50 mM sodium phosphate pH 7.0 buffer before being subjected to sonication for a 0-60 sec pulse, amplitude 20 %, using a microtip. The fragments were verified using TEM (section 7.2.11).

7.11 Solution amyloid fibril enzyme immobilisation

OPH was the first enzyme to be immobilised to the insulin amyloid fibrils. The immobilisation methods developed OPH formed the basis of the immobilisation methods for all subsequent enzyme immobilisation. Two immobilisation methods were used, cross-linking with GA, and physical adsorption, depending whether GA inactivated the enzyme being immobilised. When GA was used, a two-step immobilisation protocol was implemented where the amyloid fibrils were first mixed with the GA, then the enzyme was added (Hermanson 1996). In all of the immobilisation reactions, the components of the immobilisation reaction were added in equal parts. A typical immobilisation reaction contained 50 μL of each component.

7.11.1 Organophosphate hydrolase immobilisation to insulin amyloid fibrils

Insulin amyloid fibrils (5.8 mg/mL) (section 7.10.1) were mixed with 7.5 mM GA and incubated for 5 min at room temperature to activate the lysine residues and N-terminal residues of the amyloid fibrils. OPH (7.6 mg/mL) (section 7.4) was then added and the reaction incubated at 37 °C for 1 hour. To quench the reaction 100 mM tris pH 8.0 was added to the immobilisation mixture.

7.11.2 Organophosphate hydrolase immobilisation to crystallin amyloid fibrils

Crystallin amyloid fibrils (5.8 mg/mL) (section 7.10.5) were mixed with 7.5 mM GA and incubated for 5 min at room temperature to activate the lysine residues and N-terminal residues of the amyloid fibrils. OPH (7.6 mg/mL) (section 7.4) was then added and the reaction incubated at 37 °C for 1 hour. To quench the reaction 100 mM tris pH 8.0 was added to the immobilisation mixture.

7.11.3 **Cytochrome $P450_{BM3}$ immobilisation to insulin amyloid fibrils**

Insulin amyloid fibrils (5.8 mg/mL) (section 7.10.1) were mixed with 7.5 mM GA and incubated for 5 min at room temperature to activate the lysine residues and N-terminal residues of the amyloid fibrils. P450 (section 7.5) (5 mg/mL) was then added and the reaction incubated at 4 °C for 1 hour. To quench the reaction 100 mM tris pH 8.0 was added to the immobilisation mixture.

7.11.4 **Green fluorescent protein immobilisation to insulin amyloid fibrils**

Insulin amyloid fibrils (5.8 mg/mL) (section 7.10.1) were mixed with 7.5 mM GA and incubated for 5 min at room temperature to activate the lysine residues and N-terminal residues of the amyloid fibrils. GFP (5 mg/mL) (section 7.6) was then added and the reaction incubated at 37 °C for 1 hour. To quench the reaction 100 mM tris pH 8.0 was added to the immobilisation mixture.

7.11.5 **Tobacco etch virus protease immobilisation to insulin amyloid fibrils**

Insulin amyloid fibrils (5.8 mg/mL) (section 7.10.1) were mixed with ~1 mg/mL TEV (section 7.7) and incubated for 1 hour at 4 °C. GA was not used because it deactivated the enzyme.

7.11.6 **Glucose oxidase immobilisation to insulin amyloid fibrils**

The immobilisation of GOD (section 7.8) was based on the methods of Pilkington *et al.* (2010). 5.8 mg/mL insulin amyloid fibrils (section 7.10.1) were mixed with 150 mM GA and incubated for 5 min at room temperature to activate the lysine residues and N-terminal residues of the amyloid fibrils. GOD (2 mg/mL) was then added and incubated for 1 hour at 25 °C. To quench the reaction 100 mM tris pH 8.0 was added to the immobilisation mixture.

7.12 Glass Beads

Five millimetre diameter borosilicate glass beads purchased from Sigma-Aldrich were used as a model surface for the template directed growth of insulin amyloid fibrils. The methods used were modified from Ha & Park (2005). Five millimetre glass beads were preferred over cut glass microscope slides because it allowed for the use of a 96 well plate spectrophotometer.

7.12.1 Glass bead surface activation

Glass beads were cleaned overnight in a piranha solution of 70 % H_2SO_4, 30 % H_2O_2 followed by rinsing in dH_2O. The beads were then treated with a 3 % APTS solution in ethanol/water (95:5 v/v) for 1 hour, immersed in 99.9 % ethanol and cured at 110 °C for 1 hour. The beads were allowed to cool then washed in 95 % ethanol followed by treatment with 20 mM DSC in a 50 mM $NaHCO_3$ pH 8.5 for 3 hours. The beads were then rinsed with dH_2O and left to dry prior to use.

7.12.2 Glass bead template directed insulin amyloid fibril assembly

Surface activated glass beads (section 7.12.1) were immersed in a solution of 1 mg/mL insulin fragments or seeds at room temperature (sections 7.10.2 and 7.10.3) for 30 min. The beads were then rinsed twice with dH_2O before being immersed in incubation buffer containing 1 mg/mL insulin for 5 hours at 50 °C. The beads were then rinsed twice in dH_2O.

7.12.3 Glass bead template directed crystallin amyloid fibril assembly

Surface activated glass beads (section 7.12.1) were immersed in a solution of 5.8 mg/mL crystallin fragments at room temperature (section 7.10.6) for 30 min. The beads were then rinsed twice with dH_2O before being immersed in incubation buffer containing 5.8 mg/mL crystallin for 24 hours at 80 °C. The beads were then left at room temperature for at least 2 days before rinsing twice in dH_2O.

7.12.4 **Glass bead blocking with BSA**

After surface assembly of insulin amyloid fibrils (section 7.12.2) the excess active groups on the surface of the beads were blocked with 2 % BSA in 50 mM sodium phosphate pH 7.4 for 2 hours. The beads were then rinsed trice in dH_2O.

7.12.5 **ThT assay on glass beads**

Each bead was placed into a well of a 96 well plate and immersed with 200 μL of ThT solution containing 25 μM ThT. ThT fluorescence was measured using a BMG Labtech FLUOstar Optima plate reader with excitation/emission filters of 450 and 485 nm, respectively (LeVine III 1999). All samples had three replicates.

7.12.6 **Amplex red assay on glass beads**

Glass bead immobilised GOD activity was measured with the Amplex red assay from Invitrogen. The method was based on the method from Invitrogen (2006). Each bead was placed into a well of a 96 well plate and immersed with 150 μL of 50 mM sodium phosphate, pH 7.4 containing 20 μM Amplex Red, 0.04 U HRP, 20 mM D-glucose, and incubated for 4 min, before fluorescence measurement. Fluorescence was measured with a Labtech FLUOstar OPTIMA plate reader using excitation at 560-10 nm and fluorescence detection at 590 nm with the gain set at 880. All samples had three replicates.

7.12.7 **Plate reader GFP assay**

GFP immobilised to glass beads (section 7.13.2) were immersed in 200 μL of 50 mM sodium phosphate pH 8.0, and fluorescence measured using a BMG Labtech FLUOstar Optima plate reader with excitation/emission filters of 495 and 525 nm, respectively (Chalfie *et al.* 1994). Three replicates of each sample were measured.

7.13 Surface assembled insulin amyloid fibril enzyme immobilisation

7.13.1 GOD immobilisation on surface assembled insulin amyloid fibrils

Glass beads with surface assembled insulin amyloid fibrils (section 7.12.2) were immersed in a solution containing 1 mg/mL GOD (section 7.8) for 1 hour at room temperature. The glass beads were then placed in a small ~7 mm diameter column, and 50 mM sodium phosphate, pH 7.4, flowed over the beads over night. This thorough washing was done to achieve a low background fluorescence, because of the strong physical adsorption of GOD to the glass surface.

7.13.2 GFP on surface assembled insulin amyloid fibrils

Glass beads with surface assembled insulin amyloid fibrils (section 7.12.2) were first immersed in a solution of 5 mM GA to activate the lysine residues and N-terminal residues of the amyloid fibrils before the addition of ~5 mg/mL GFP for 1 hour at room temperature. The beads were then rinsed 3 times in dH_2O. The GFP beads were stored at 4 °C. The beads were assessed for GFP fluorescence by either confocal microscopy (section 7.2.13) or in the BMG Labtech FLUOstar Optima plate reader (section 7.12.7)

7.13.3 TEV protease immobilisation on surface assembled insulin amyloid fibrils

TEV protease (section 7.7) from the -80 °C stock was thawed on ice before being used. Glass beads with surface assembled insulin amyloid fibrils (section 7.12.2) were immersed in the TEV protease for 2 hours before being rinsed 4 times with dH_2O. The beads were stored at 4 °C until needed.

7.13.4 **Surface immobilised TEV poly-histidine tagged enzyme cleavage**

Wild type *E. coli* DHDPS, Y107W *E. coli* DHDPS, wild type *T. maritima* DHDPR, wild type *A. Thaliana* DHDPR, and wild type human peroxiredoxin 3 were the cleavable poly-histidine tagged enzymes used in the cleavage experiments. All of the enzymes were obtained from purified frozen laboratory stocks. All of the enzymes were diluted to ~1 mg/mL with TEV storage buffer prior to use.

Glass beads with surface assembled amyloid fibrils and immobilised TEV protease (section 7.13.3) were covered with 150 μL of one of the poly-histidine tagged enzymes containing a TEV protease cleavage site. The cleavage reaction was carried out over night (~18 hours) at 4 °C to allow cleavage of the poly-histidine tags. The supernatant (20 μL) was carefully pipetted off and assessed for cleavage with SDS-PAGE (section 7.2.3). The beads where then washed 5 times in dH_2O ready for reuse, with another enzyme containing a cleavable poly-histidine tag.

7.14 **Cellulose based materials**

Unbleached, untreated, starched cotton was purchased from Haralds in Christchurch, New Zealand. 20 μm microcrystalline cellulose powder was purchased from Sigma-Aldrich.

7.14.1 **Cotton surface activation**

Cotton was cut into 25 mm^2 segments and boiled in dH_2O for 30 min to remove starch. The cotton was then rinsed 3 times in dH_2O. The cotton was then treated with a 3 % APTS solution in ethanol/water (95:5, v/v) for 1 hour, immersed in 99.9 % ethanol and cured at 110 °C for 1 hour. The cotton was allowed to cool, then washed in 95 % ethanol followed by treatment with 20 mM DSC in a 50 mM $NaHCO_3$ pH 8.5 for 3 hours. The cotton was then rinsed with dH_2O and left to dry prior to use.

7.14.2 **Cellulose surface activation**

Microcrystalline cellulose powder was treated with a 3 % APTS solution in ethanol/water (95:5 v/v) for 1 hour, immersed in 99.9 % ethanol and cured at 110 °C for 1 hour. The cellulose were allowed to cool then washed in 95 % ethanol followed by treatment with 20 mM DSC in a 50 mM $NaHCO_3$ pH 8.5 for 3 hours. The cellulose was then rinsed with dH_2O and left to dry prior to use.

7.14.3 **Cotton template directed insulin amyloid fibril assembly**

Surface activated cotton (section 7.14.1) was immersed in a solution of 1 mg/mL insulin fragments at room temperature (section 7.10.2) for 30 min. The cotton was then rinsed twice with dH_2O before being immersed in incubation buffer containing 1 mg/mL insulin for 5 hours at 50 °C. The cotton was then rinsed twice in dH_2O.

7.14.4 **Cellulose powder template directed insulin amyloid fibril assembly**

Surface activated cellulose powder (section 7.14.2) was immersed in a solution of 1 mg/mL insulin fragments at room temperature (section 7.10.2) for 30 min. The cellulose was then washed with dH_2O, collected with gentle (500 x g) centrifugation after which the supernatant was discarded. This process was repeated five times. The cellulose was then immersed in incubation buffer containing 1 mg/mL insulin for 5 hours at 50 °C. The cellulose was then washed with dH_2O and collected with gentle centrifugation and the supernatant discarded. This process was repeated five times. The cellulose was then allowed to dry.

7.15 **References**

Blommel, P.G. & Fox, B.G., 2007. A combined approach to improving large-scale production of tobacco etch virus protease. *Protein Expression and Purification*, 55(1), pp.53–68.

Bradford, M.M., 1976. A rapid and sensitive method for the quantitation of microgram quantities of protein utilizing the principle of protein-dye binding. *Analytical Biochemistry*, 72(1-2), pp.248–254.

Chalfie, M., Tu, Y., Euskirchen, G., Ward, W.W. & Prasher, D.C., 1994. Green fluorescent protein as a marker for gene expression. *Science*, 263(5148), pp.802–805.

Ericsson, U.B., Hallberg, B.M., Detitta, G.T., Dekker, N. & Nordlund, P., 2006. Thermofluor-based high-throughput stability optimization of proteins for structural studies. *Analytical Biochemistry*, 357(2), pp.289–298.

Garvey, M., Gras, S.L., Meehan, S., Meade, S.J., Carver, J.A. & Gerrard, J.A., 2009. Protein nanofibres of defined morphology prepared from mixtures of crude crystallins. *International Journal of Nanotechnology*, 6(3-4), pp.258–273.

Gasteiger, E., Gattiker, A., Hoogland, C., Ivanyi, I., Appel, R.D. & Bairoch, A., 2003. ExPASy: The proteomics server for in-depth protein knowledge and analysis. *Nucleic Acids Research*, 31(13), pp.3784–3788.

Ha, C. & Park, C.B., 2005. Template-directed self-assembly and growth of insulin amyloid fibrils. *Biotechnology and Bioengineering*, 90(7), pp.848–855.

Hermanson, G.T., 1996. *Bioconjugate Techniques* 1st ed., Rockford, IL USA: Academic Press.

Invitrogen, 2006. Amplex® red glucose/glucose oxidase assay kit. Available at: www.probes.invitrogen.com/media/pis/mp22189.pdf.

LeVine III, H., 1999. Quantification of β-sheet amyloid fibril structures with thioflavin T. *Methods in Enzymology*, 309, pp.274–284.

McLoughlin, S.Y., Jackson, C., Liu, J.-W. & Ollis, D., 2005. Increased expression of a bacterial phosphotriesterase in Escherichia coli through directed evolution. *Protein Expression and Purification*, 41(2), pp.433–440.

Menges, F., 2010. *Spekwin32: Free optical spectroscopy software*, Available at: http://www.effemm2.de/spekwin/. [Accessed October 25, 2011].

Munro, A.W., Lindsay, J.G., Coggins, J.R., Kelly, S.M. & Price, N.C., 1995. NADPH oxidase activity of cytochrome P-450 BM3 and its constituent reductase domain. *Biochimica et Biophysica Acta (BBA) - Bioenergetics*, 1231(3), pp.255–264.

Nielsen, L., Khurana, R., Coats, A., Frokjaer, S., Brange, J., Vyas, S., Uversky, V.N. & Fink, A.L., 2001. Effect of environmental factors on the kinetics of insulin fibril formation: Elucidation of the molecular mechanism. *Biochemistry*, 40(20), pp.6036–6046.

Pflug, S., Richter, S.M. & Urlacher, V.B., 2007. Development of a fed-batch process for the production of the cytochrome P450 monooxygenase CYP102A1 from *Bacillus megaterium* in *E. coli*. *Journal of Biotechnology*, 129(3), pp.481–488.

Pilkington, S.M., Roberts, S.J., Meade, S.J. & Gerrard, J.A., 2010. Amyloid fibrils as a nanoscaffold for enzyme immobilization. *Biotechnology Progress*, 26(1), pp.93–100.

Piston, D.W., Patterson, G.H. & Knobel, S.M., 1998. Quantitative imaging of the green fluorescent protein (GFP). In K. F. Sullivan & S. A. Kay, eds. *Green Fluorescent Proteins*. San Diego: Academic Press, pp.31–48.

Roodveldt, C. & Tawfik, D.S., 2005. Directed evolution of phosphotriesterase from *Pseudomonas diminuta* for heterologous expression in *Escherichia coli* results in stabilization of the metal-free state. *Protein Engineering, Design and Selection*, 18(1), pp.51–58.

Sambrook, J., Fritsch, E.F. & Maniatis, T., 1989. *Molecular cloning: a laboratory manual*, New York: Cold Spring Harbor Laboratory.

Stratagene, 2010. BL21 (DE3) competent cells, BL21 (DE3) pLusS competent cells, and BL21 competent cells. Available at: http://www.genomics.agilent.com/files/Manual/200133.pdf.

Stratagene, 2004. XL-1 Blue MR supercompetent cells. Available at: http://www.chem-agilent.com/pdf/strata/200249.pdf.

Studier, F.W., 2005. Protein production by auto-induction in high-density shaking cultures. *Protein Expression and Purification*, 41(1), pp.207–234.

Vanhooke, J.L., Benning, M.M., Raushel, F.M. & Holden, H.M., 1996. Three-dimensional structure of the zinc-containing phosphotriesterase with the bound substrate analog diethyl 4-methylbenzylphosphonate. *Biochemistry*, 35(19), pp.6020–6025.

Whittingham, J.L., Scott, D.J., Chance, K., Wilson, A., Finch, J., Brange, J. & Guy Dodson, G., 2002. Insulin at pH 2: Structural analysis of the conditions promoting insulin fibre formation. *Journal of Molecular Biology*, 318(2), pp.479–490.

Wilcox, D., Dove, B., McDavid, D. & Greer, D., 2002. *ImageTool*, The University of Texas Health Science Center at San Antonio. Available at: http://compdent.uthscsa.edu/dig/itdesc.html.

Yang, F., Moss, L.G. & Phillips, G.N., Jr, 1996. The molecular structure of green fluorescent protein. *Nature Biotechnology*, 14(10), pp.1246–1251.

Appendix 1

Analysis of thermostability of OPH-MBP at 30 °C

Figure 1 shows the SDS-PAGE results for the OPH control from the 30 °C thermostability experiment. As can be seen in days 3, 5, and 7 there is the appearance of two new protein bands (red box) in the gel at ~42 and ~35 kDa. These protein bands correspond to free MBP and free OPH, respectively, suggesting proteolysis of the OPH-MBP fusion protein. The melting temperature of free OPH (section 2.2.2) was found to be ~2 °C higher than OPH-MBP, and the K_{cat} (section 2.2.2) of free OPH was found to be ~1000 s^{-1} higher, therefore, if proteolysis of OPH-MBP was occurring, the corresponding free OPH would have a higher activity and thermostability, and the trends in **Figure 1** would be seen at 30 °C. The reason this trend is only seen at 30 °C could be that the protease cleaving OPH-MBP may not be active at higher temperatures, or there may not be sufficient time for proteolysis to occur at the higher temperatures.

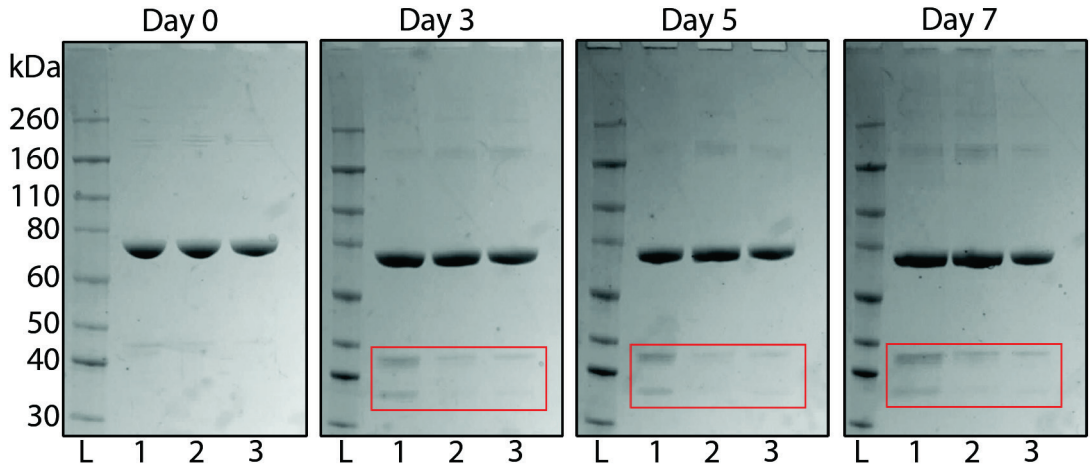

Figure 1 *SDS-PAGE gels of the OPH control sample in the 30 °C thermostability testing. In each gel L – ladder, lane 1 – pH 7 immobilisation, lane 2 – pH 8 immobilisation, lane 3 – pH 9 immobilisation. The red box shows the appearance of new protein bands.*